DIETARY MANIPULATION OF GLUCOSE AND FAT METABOLISM IN SKELETAL MUSCLES AND LIVER

SHAILEE BHAVAN JANI

A DISSERTATION SUBMITTED TO THE FACULTY OF GRADUATE STUDIES IN PARTIAL FULFILMENT OF THE REQUIREMENTS FOR THE DEGREE OF

DOCTOR OF PHILOSOPHY

GRADUATE PROGRAM IN KINESIOLOGY AND HEALTH SCIENCE
YORK UNIVERSITY
TORONTO, ONTARIO
MAY 2023

Abstract

This dissertation explores the role of intermediary lipid accumulation in the development of tissue specific and whole-body insulin resistance (IR). In this context, we investigated whether the intramyocellular lipid accumulation was sexually dimorphic, whether it differed between oxidative and glycolytic muscles, and how it correlated with high-fat sucrose-enriched (HFS) diet-induced skeletal muscle IR. To accomplish that, male and female Wistar rats were either fed a standard chow (SC) or a HFS diet for 8 weeks. Broadly, highly oxidative male muscles had impaired insulin sensitivity associated with the activation of PKCδ and θ isoforms in soleus (Sol, rich in type IA fibers), extensor digitorum longus (EDL, rich in type 2A fibers). In the highly glycolytic epitrochlearis (Epit, rich in type IIB fibers) muscles, impaired insulin sensitivity was associated with the upregulation of inflammatory mediators. In females, the HFS diet also led to a significant elevation in intramuscular DAG and TAG contents; however, without any alteration in ceramides levels in insulin-resistant female oxidative and glycolytic muscles. Moreover, a pro-inflammatory response was observed in skeletal muscles rich in type IIa and type IIb of female rats fed a HFS diet. Hence, based on my findings, all muscles from male and female rats fed the obesogenic diet developed IR, although the underlying associated mechanisms differed with respect to muscle fiber-type distribution in males and females.

Obesity has also been linked to severe intrahepatic triglycerides (IHTG) accumulation and the pathogenesis of non-alcoholic fatty liver disease (NAFLD). Unlike the conventional high-fat Western diet, the ketogenic diet has recently gained popularity as an effective non-pharmacological therapy for NAFLD. However, the underlying mechanisms are still unknown. In this context, we analysed the effects of a carbohydrate free ketogenic diet (KD) on livers from male Wistar rats. The KD indeed reduced intrahepatic glycerolipid content and PKCε

activity, but markedly increased liver ceramide content. The KD also enhanced the liver expression of key genes involved in mitochondrial biogenesis and fatty acid oxidation, suppressed inflammatory genes, and shifted substrate away from *de novo* lipogenesis. Thus, the KD induced anti-steatogenic and insulin-sensitizing effects in the liver.

Acknowledgements

Needless to say, science excited me but it was only with the help and guidance of my PhD supervisor that I understood its true powers and importance. I will forever be indebted to Dr. Rolando Ceddia for being such an extraordinary supervisor and mentor. You supported all my efforts, be it with experiment planning, execution and especially the writing. Thank you for steering me in the right direction and setting the right pace whenever you thought it was necessary. You have not only helped me with my professional development but have also allowed me to be a better human being, so thank you. In addition, I would like to my committee members for their passionate participation and expert input into my research work.

I also whole heartedly thank Daniel for going above and beyond his role as a lab mate and being an exceptional friend. You are a good listener, and an even better teacher. You know I wouldn't have been able to make it this far without you. Earnest thanks to Aris, Diane, Glen and Ishvinder for providing encouragement and insightful comments. I'd also like to thank the numerous contributions made by the lab's undergraduate students, Vanessa, Javid, and notably Mateja who willingly devoted their precious time involving long working hours. Also, thank you Mayoorey, John, Jessica, Veroni and George for always cheering me up and showing me the true meaning of friendship.

Lastly, my family, that deserves endless gratitude for being just the way they are: Thank you, Mom for being the positive one and having faith in me, Dad for being the watchful one and faking interest when I tried to talk science over dinner and Shivansh for being the calm one and helping me find humor in my work. Karan, thank you for always keeping me focused ($$$), listening to my rants, and helping me talk things out even if they made no sense to you. Thank you for all the sacrifices you have made and the support you showed throughout the tenure and particularly during the writing process.

Good judgement comes from experience...

Experience comes from bad judgement and persistence…

Table of Contents

List of Figures

List of Tables

List of Abbreviations

ACC	Acetyl-CoA carboxylase
ADP	Adenosine diphosphate
AMP	Adenosine monophosphate
AMPK	AMP-activated protein kinase
AS160	AKT substrate of 160 kDa
ATP	Adenosine triphosphate
βHB	Beta hydroxyl butarate
BAT	Brown adipose tissue
BSA	Bovine serum albumin
Ca2+	Calcium ion
cAMP	Cyclic AMP
CD36	Cluster of differentiation 36
CD40	Cluster of differentiation 40
CLAMS	Comprehensive laboratory animal monitoring system
CoA	Coenzyme A
CPT-1	Carnitine palmitoyltransferase-1
DAG	Diacylglycerol
DGAT	Diglyceride acyltransferase
DIO	Diet-induced obesity
EDL	Extensor digitorum longus
EE	Energy expenditure
EI	Energy intake
Epid	Epididymal
Epit	Epitrochlearis
ETC	Electron transport chain
FA	Fatty acid (used interchangeably with free FA (FFA) and NEFA)

FADH2	Flavin adenine dinucleotide
FAS	Fatty acid synthase
FGF21	Fibroblast growth factor 21
G6P	Glucose-6-phosphate
GAPDH	Glyceraldehyde-3-phosphate dehydrogenase
GLUT1/4	Glucose transporter isoform 1/4
GS	Glycogen synthase
GSK3	Glycogen synthase kinase 3
HF	High fat
HFS	High fat high sucrose
IR	Insulin resistance
IRS-1	Insulin receptor substrate-1
KRB	Krebs Ringer buffer
LCFA	Long chain fatty acid
LDH	Lactate dehydrogenase
Lpl	Lipoprotein lipase
MAG	Monoacylglycerol
MGAT	Monoacylglycerol acyltransferase
MyHC	Myosin heavy chain
NASH	Non-alcoholic steatohepatitis
NADH	Nicotinamide adenine dinucleotide
NAFLD	Non-alcoholic fatty liver disease
NEFA	Non-esterified fatty acid (used interchangeably with FA and FFA)
PDC	Pyruvate dehydrogenase complex
PDH	Pyruvate dehydrogenase
PDK-1	Phosphoinositide-dependent kinase-1
PEPCK	Phosphoenolpyruvate carboxykinase
PGC-1α	Peroxisome proliferator-activated receptor gamma coactivator-1 alpha

PIP3	Phosphatidylinositol 3,4,5-triphosphate
PIP2	Phosphatidylinositol 4,5-bisphosphate
PI3K	Phosphoinositide 3 kinase
PK	Pyruvate kinase
PKB	Protein kinase B (AKT)
PKC	Protein kinase C
PP1, PP2A	Protein phosphatase 1, protein phosphatase 2A
PPARα/γ	Peroxisome proliferator-activated receptor alpha/gamma
RER	Respiratory exchange ratio
Sc Ing	Subcutaneous inguinal
Sol	Soleus
SREBP-1c	Sterol regulatory element binding protein-1c
T2D	Type 2 diabetes mellitus
TAG	Triacylglyceride
TCA	Tricarboxylic acid (cycle)
TNFα	Tumor necrosis factor-alpha
TLR4	Toll-like receptor 4
VCO2	Carbon dioxide production
VO2	Oxygen consumption

Chapter 1 : Introduction

Obesity is a growing public health concern across the world, and it is one of the primary causes of morbidity and death from non-communicable illness. The epidemiological association between obesity and a wide range of metabolic illnesses is well established; however, the underlying pathophysiological processes are only poorly understood, and effective therapeutic choices are limited[1]. Skeletal muscle and the liver have increasingly become a focus of research aiming at understanding the reasons for decreased insulin action in obesity and its related metabolic consequences such as type 2 diabetes (T2D) and non-alcoholic fatty liver disease (NAFLD).

T2D is characterized by persistent hyperglycemia due to insulin resistance (IR) in peripheral tissues (*e.g.* skeletal muscle, adipose tissue, and liver) and the brain with insufficient compensating insulin secretion by pancreatic β-cells[2–4]. It is widely accepted that T2D is caused by a number of environmental factors such as high-calorie diets and sedentary lifestyle, which also promote the development of obesity[5]. Weight gain during adulthood, the degree of obesity, and the duration of obesity all independently and strongly predict the risk for developing T2D. In particular, fat deposition in the abdominal region aggravates insulin resistance and increases the risk for developing T2D[6]. Although obesity is not invariably associated with IR, the vast majority of overweight and/or obese individuals are IR. Obesity is, therefore, a major risk factor for the development of IR.

While, individuals with NAFLD often display poor glucose and lipid metabolism. It has been reported that the production of fat as well as glucose by the liver are elevated in these individuals, whereas oxidization/utilization of these substrates is impaired or insufficient. In its

later stages, NAFLD can progress to hepatocellular carcinoma and liver failure[7]. Therefore, treating this condition in its early stages is critical to prevent further health complications and possible mortality. Aside from bariatric surgery, which is limited almost exclusively to patients in the later stages of NAFLD or severe obesity, there are no therapeutic alternatives to treat fatty liver thus far. As such, healthcare professionals have turned to dietary interventions in conjunction with regular exercise as the primary means to reduce fat accumulation in the liver.

A growing body of evidence[8,9] points towards the composition of the diet as an important factor that determines fat accumulation and obesity development. This alternative view of the physiopathology of obesity is based on the premise that the ingestion of foods with elevated carbohydrate content increases insulin secretion, suppresses adipose tissue lipolysis, and favours fat accumulation[10]. Thus, dietary interventions that reduce energy intake and more so carbohydrate content of foods could potentially promote fat mobilization and lead to improvement in whole-body glucose homeostasis and the reversal of metabolic disregulation[11]. In this context, the work presented in this dissertation examines how diet-induced insulin resistance affects glucose and fatty acid metabolism in oxidative and glycolytic skeletal muscles in male and female rats. It also investigates whether an intervention that reduces dietary carbohydrate content can serve as a therapeutic approach to treat NAFLD and improve glycemic control.

Chapter 2 : Literature Review

2.1 Obesity and its association to Insulin Resistance

Obesity is a global crisis that is characterized by an increase in body weight (in particular adipose tissue) at an excessive magnitude to yield significant health complications[5]. Obesity is often attributed to an imbalance between the amount of energy taken in and the amount of energy spent[12,13]. Recent data from the World Health Organization (WHO) indicates that 1.6 billion adults globally are overweight (defined as a Body Mass Index (BMI) of 25-29.9 Kg/m^2) and 400 million are obese (defined as a BMI of ≥ 30 Kg/m^2)[14]. More importantly, obesity has become the most critical factor in the pathogenesis of metabolic diseases and also a major risk factor for the development of insulin resistance (IR)[2]. IR is characterized by a significant reduction in insulin-stimulated glucose transport and metabolism[15].

Weight gain during adulthood, degree of obesity, and duration of obesity all independently and strongly predict the risk for developing type 2 diabetes (T2D). The term “diabesity”, first described in the 1970s, refers to the strong linkage between T2D and obesity[16,17]. In particular, fat deposition in the abdominal region aggravates IR and increases the risk of developing T2D[6]. Causation of T2D has been linked to several environmental factors such as high-calorie diets and sedentary lifestyle, which also promote the development of obesity[5]. This explains why the rise in the numbers of people affected by T2D has essentially mirrored the escalation in the incidence of obesity worldwide[16]. Based on the CDC report from 2020, 34.2 million people in the USA have diabetes (i.e., approximately 10.5% of the US population). Of these, 26.8 million adults are diagnosed, whereas 7.3 million people remain undiagnosed[18]. By the year 2030, 366

million T2D cases are projected worldwide, making it both health as well as economic concern[19].

T2D is characterized by persistent hyperglycemia due to impaired insulin response in peripheral tissues (skeletal muscle, adipose tissue, and liver) as well as the brain, and/or by the failure of pancreatic β-cells to secrete sufficient amounts of insulin to overcome hyperglycemia[2–4]. T2D typically occurs later on in life (i.e. middle age), although it has become common in young individuals as a consequence of the growing incidence of obesity in children[16,20,21]. Disruption of insulin signaling and improper systemic glycemic control in T2D is directly linked to impaired ability of skeletal muscle, liver, and adipose tissue to respond to insulin. This is because skeletal muscles account for approximately 40% and 30% of total body mass in men and women, respectively, which is a major site for glucose disposal. In fact, it has been estimated that skeletal muscle is responsible for 85% of the insulin-stimulated glucose clearance that takes place after a meal[22,23].

Besides skeletal muscle, the liver also plays a major role in the regulation of whole-body glucose homeostasis. After a meal rich in carbohydrates, nearly 60% of the glucose entering the portal vein is retained by the liver, whereas 15% is taken up by muscle and adipose tissue in an insulin-dependent manner. The remaining 25% is used to meet the energy demands of the brain and other tissues where insulin is not necessary for glucose uptake[24,25]. Importantly, as glycemia increases subsequent to a meal, plasma insulin concentrations rise 3-10 fold above fasted conditions[26]. The elevated circulating insulin facilitates the uptake of glucose in skeletal muscle and adipose tissues where glucose is stored as glycogen and triglycerides, respectively. Insulin is not necessary for glucose uptake in the liver, but it is crucial to stimulate the storage of

glucose as glycogen inhibits glycogenolysis and gluconeogenesis in hepatocytes and suppresses hepatic glucose release.

2.2 Insulin signaling

Insulin signalling initiates with the binding of insulin to its receptor located on the plasma membrane. The insulin receptor comprises of two extracellular α-subunits and two transmembrane β-subunits that are linked by disulfide bonds[27]. Once insulin binds to its receptor, the α-subunit induces tyrosine autophosphorylation of the β-subunit causing a conformational change which then leads to tyrosine phosphorylation of insulin receptor substrates (IRS)[3]. A family of IRS proteins named IRS1-6 has been identified. These proteins display tissue-specific distribution and ability to engage with multiple substrates. Mammals express four IRS isoforms (IRS1-4), although in humans IRS3 is a pseudogene and the protein is absent[28,29]. With respect to metabolic regulation, IRS1 and IRS2 are the main isoforms involved in metabolic homeostasis[29–31]. IRS-1 has been shown to be important for insulin to regulate glucose metabolism in skeletal muscle, whereas IRS-2 seems crucial for insulin signaling and regulation of glucose metabolism in the liver[32,33]. IRS phosphorylation leads to the recruitment and activation of phosphatidylinositol-3-OH kinase (PI3K), which then phosphorylates the cell membrane lipid phosphatidylinositol 4,5-bisphosphate (PIP2) giving rise to phosphatidylinositol (3,4,5)-triphosphate (PIP3)[31,34]. The subsequent step involves recruitment and activation of PDK1, which occurs by the binding of its PH domain to PIP3 formed at the cell membrane[28,35]. In its activated state, PDK1 phosphorylates protein kinase B (PKB), also known as AKT or the master regulator. AKT is a serine-threonine kinase that exists

in three isoforms (AKT 1, 2 & 3), and it is able to influence multiple signaling networks, involving cellular metabolism, growth, cancer and neurodegeneration[36,37]. PDK1 promotes the phosphorylation of the Thr 308 site (AKT_{Thr308}) and partially activates it. Full AKT activation is attained by phosphorylation of its Ser 473 site (AKT_{Ser473}) by the mammalian target of rapamycin complex 2 (mTORC2)[28]. In its activated state, AKT covalently regulates the activity of the AKT substrate of 160 kDa (AS160), which releases Rab proteins and promote GLUT4 translocation towards the plasma membrane and facilitation of glucose uptake in skeletal muscle and adipocytes[38,39]. AKT also phosphorylates and deactivates glycogen synthase kinase-3 α/β (GSK3α/β) on serine residues 21 and 9, respectively[40,41]. AKT-mediated GSK3 inhibition enhances the activity of protein phosphatase-1 (PP1), an essential phosphatase responsible for dephosphorylating serine residues (640, 644, 648 and 652) on glycogen synthase (GS). Dephosphorylation of GS leads to its activation and stimulation of glycogen synthesis, particularly in myocytes and hepatocytes[40,42,43].

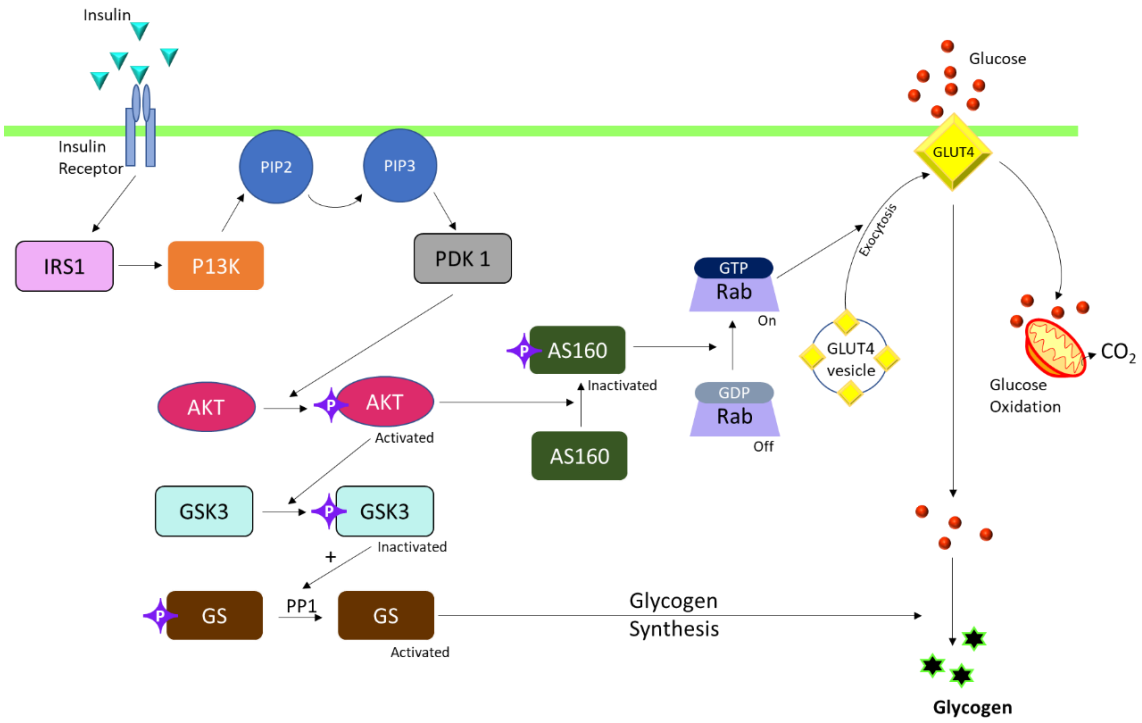

Figure 2.1: Schematic representation of insulin-mediated glycogen synthesis in skeletal muscle. Circulating insulin binds to its receptor on the plasma membrane leading to autophosphorylation of the receptor. This promotes the interaction of the insulin receptor with the insulin receptor substrate 1 (IRS1) which is then phosphorylated at its tyrosine residue. Subsequently, phosphatidylinositol 4,5-bisphosphate (PIP2) is converted to phosphatidylinositol (3,4,5) trisphosphate (PIP3) through phosphoinositide 3-kinase (P13K)-mediated phosphorylation. PIP3 activates phosphoinositide-dependent kinase-1 (PDK-1), which promotes the phosphorylation of AKT. In its phosphorylated/activated state, AKT phosphorylates AS160, causing the activation of Rab proteins and eventually the translocation of the GLUT4 vesicle towards the plasma membrane and enhanced glucose uptake. AKT phosphorylates glycogen synthase kinase 3αβ (GSK3) and inactivates the enzyme. GSK3 inactivation leads to increased activity of protein phosphatase-1 (PP1). Once activated, PP1 causes dephosphorylation and activation of glycogen synthase (GS), allowing it to actively convert glucose to glycogen.

2.2.1 Non-insulin dependent glucose uptake in skeletal muscle

In the absence of insulin stimulation glucose uptake can still occur through the activation of a heterotrimeric protein named AMP-activated protein kinase (AMPK). AMPK consists of an α catalytic subunit and two regulatory subunits (β and γ) [44]. Contraction in skeletal muscle leads to ATP depletion with a reduction of the intracellular AMP:ATP ratio. AMPK is activated when the AMP binds to cystathionine β-synthase sequence repeats (CBS domains) on its γ subunit. In addition, when AMP binds AMPK, a conformation change occurs that allows an upstream kinase, LKB1 to phosphorylate the α-catalytic subunit at the threonine (Thr) 172 residue and further enhancement of its kinase activity[44]. In its activated state, AMPK phosphorylates AS160 and removes the inhibitory effect on Rab proteins allowing GLUT4 translocation to the plasma membrane and increased uptake of glucose[45]. In the absence of insulin, the ubiquitously expressed transporter GLUT 1 also allows the influx of glucose through the plasma membrane. GLUT 1 is highly expressed in various tissues such as placenta, brain, epithelial cells of the mammary gland, transformed cells, and fetal tissues, but in relatively small concentration in skeletal muscle. GLUT1 does not need to be translocated as it is already present on the plasma membrane and facilitates the passive transport of glucose across the membrane[46].

2.3 Glucose Metabolism

2.3.1 Glycogen synthesis

The glycogen molecule is a highly branched polysaccharide formed by α1-4 and α1-6 glycosidic bonds and serves as an intracellular reservoir of energy. Glycogen is mobilized during intense physical activity or in response to conditions of stress such as fight or flight[47]. In the fed state, a

70 kg men stores about 400 g of glycogen, which provides about 1600 kcal of readily available energy[48]. Skeletal muscle and liver are the main sites of glycogen synthesis and play a major role in the maintenance of whole-body glucose homeostasis. Defects in the glycogen synthesis in skeletal muscle and liver impair the ability of peripheral tissues to clear glucose from the circulation and can lead to hyperglycemia. This is supported by reports that, rates of glycogen synthesis drop by approximately 50% in type 2 diabetic subjects in comparison to healthy subjects[49]. Hence, the ability of skeletal muscles and liver to store glycogen is crucial for proper whole-body glycemic control. The binding of insulin to its receptors in myocytes promotes glycogen synthesis by enhancing glucose uptake and also by activating the enzymatic machinery that diverts glycosyl units towards the pathway that expands glycogen content. In hepatocytes, insulin does not affect glucose uptake because these cells contain GLUT2, which is localized to the membrane and serves as a high-capacity glucose transporter. However, insulin is very important to divert glucose towards glycogen synthesis and to suppress hepatic glucose production[50]. Glycogen synthesis is initiated by the phosphorylation of glucose by hexokinase to form glucose-6-phosphate (G6P). If G6P accumulates in the cell, it can inhibit hexokinase activity and regulate the flow of substrate through pathways that process glucose intracellularly such as glycogen synthesis and glycolysis[51]. In addition, G6P allosterically activates GS, the rate limiting enzyme that controls the incorporation of glucose into glycogen. Thus, besides regulating the insulin-mediated influx of glucose into the cell, G6P also dictates the rate of glycogen synthesis[52,53]. Importantly, as the cellular content of glycogen increases, it down-regulates the activity of GS, imposing a limit to how much glycogen is stored in the cell[54,55].

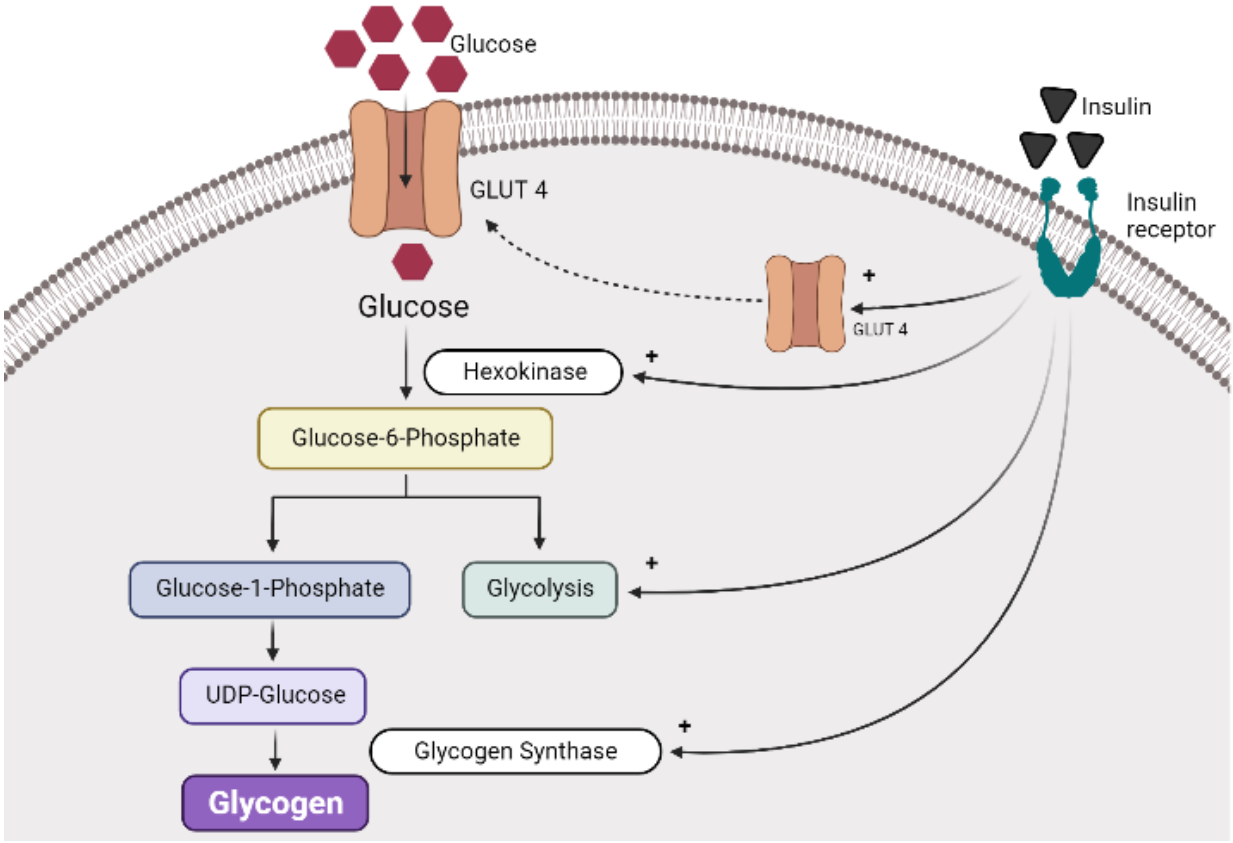

Figure 2.2: Role of insulin in the glycogen synthesis pathway. Upon entering skeletal muscle cells, glucose is phosphorylated by hexokinase. A fraction of glucose-6-phosphate can either be directed towards hexose biosynthesis or the pentose phosphate pathways. However, most of the glucose is used for energy production or incorporated into glycogen via the glycogen synthesis pathway. Impairment to any of the steps may lead to the development of insulin resistance. UDP-glucose = uridine diphosphoglucose. Image generated using BioRender.

2.3.2 Pyruvate dehydrogenase complex (PDC) and glucose oxidation

When not stored as glycogen, glucose catabolism majorly contributes towards ATP production in the skeletal muscle[56,57]. Briefly, through the glycolytic pathway, glucose is converted to pyruvate in the cytoplasm[58]. Then, in the mitochondria, the pyruvate dehydrogenase complex (PDC) mediates the irreversible oxidative decarboxylation of cytosolic pyruvate to form acetyl-CoA[59]. The structure of the PDC consists of several copies of the three main catalyst subunits, namely, pyruvate dehydrogenase (PDH), dihydrolipoyl transacetylase (DLATransferase), and dihydrolipoamide dehydrogenase (DLD), and five coenzymes forming the largest mammalian enzyme complex[60,61]. PDC is activated when PDH is phosphorylated by its kinase (PDK) or dephosphorylated by its phosphatase (PDP). Specifically, the action of PDK2 and PDK4 in skeletal muscle is known to regulate the rate of glucose oxidation, and therefore, are linked to impaired glucose tolerance and skeletal muscle IR[62]. This is supported by a study conducted by Pengfei Wu et al, in which gastrocnemius muscles of male Wistar rats exposed to starvation and diabetes had an increase in the expression of mitochondrial PDK4, which caused the complex to inactivate. Furthermore, it was reported that refeeding and insulin treatment increased PDK4 mRNA levels and reversed PDC complex inactivation[63]. It has also been reported that acute and chronic exercise increase PDP content and simultaneously reduce PDK4 transcription. These are effects of exercise that enhance PDC activity in skeletal muscles[64,65] and lead to an overall improvement in the rate of glucose oxidation[66]. More recently, Kristoffer Svensson et al. investigated the role of pyruvate dehydrogenase alpha 1 (*Pdha1*) in skeletal muscle on resting energy metabolism, exercise performance, and metabolic adaptations to diet. They found that, either under standard chow or HFS feeding conditions, ablation of PDHα did not alter energy expenditure, muscle contractile function, low-intensity exercise performance, muscle insulin

sensitivity, and body composition. However, mice lacking *Pdha1* displayed impaired ability to perform high-intensity exercise accompanied by significantly elevated concentrations of plasma lactate[66]. These findings suggest that skeletal muscle PDC does not affect basal energy expenditure or chronic low-intensity exercise performance, but it is essential for optimal performance during high-intensity exercise.

2.3.3 Lactate synthesis

As shown in **Figure 2.3**, glycolysis occurs in the cytoplasm of cells leading to the production of pyruvate. In skeletal muscle cells under resting conditions, pyruvate can easily diffuse into the mitochondria where it is converted into acetyl-CoA. The latter is processed in the citric acid cycle giving rise to reducing molecules such as NADH and FADH2. These reducing molecules are used in the Electron Transport Chain (ETC) to generate the proton gradient that ultimately drives ATP synthesis. However, under anaerobic conditions, oxidative phosphorylation is limited and pyruvate takes a distinct path that diverts pyruvate toward lactate production. Lactate dehydrogenase (LDH) converts pyruvate to lactate[67,68]. Although lactate is not always used directly by the cell as an energy source, its production enables for the regeneration of NAD+ from NADH. NAD+ is an oxidative component that is required to keep glucose flowing through glycolysis[69]. Lactic acid synthesis is used to provide energy in cells that cannot obtain all required energy through oxidative phosphorylation. The energy yield of glycolysis to lactate is much less (2 ATP) than through oxidation (32 ATP), but it provides for 100 times faster ATP generation than through oxidative phosphorylation in rapidly contracting skeletal muscle cells[70–72]. As lactate accumulates, it exits the muscle and reaches other tissues such as liver, heart, and kidney that are able to metabolize lactate. The flow of lactate across the plasma membrane

occurs through proton-linked monocarboxylate transporters (MCTs), which belong to the SLC16 gene family. Lactate transport is driven by both a transmembrane concentration gradient and local proton availability. MCTs 1–4 are the most described of the 14 known MCTs, serving major metabolic roles in most tissues, with MCT1 and MCT4 being the most important isoforms in skeletal muscle[73]. The precise molecular mechanisms governing MCT regulation are unknown, but they most likely entail both transcriptional and post-transcriptional control[67]. In fact, 75-80% of circulating lactate ions are used as metabolic sources of carbon by adjacent muscle cells itself, where they can either be oxidized or used to synthesize glycogen[68]. For example, during moderate exercise, glycolytic muscles can produce lactate, which is quickly utilized by neighboring oxidative muscles[74,75]. This makes skeletal muscles the largest tissue in the body with the highest capacity to generate and utilize lactate[76].

Lactate has been recognized as an important metabolic substrate in the skeletal muscle[77]. Furthermore, it has been reported that lactate enhances the expression of genes involved in oxidative metabolism in skeletal muscle, particularly mitochondria-related genes[78]. In fact, it has been demonstrated that the administration of sodium bicarbonate increased blood lactate levels, an effect that was accompanied by elevations in the expression of mitochondrial genes[79–81]. Conversely, lowering blood lactate levels with dichloroacetic acid inhibited the expression of mitochondrial genes[80]. Lactate administration has also been shown to improve not just oxidative metabolism signals, but also protein synthesis. Additionally, a recent study showed that daily lactate injection (1 g/kg body weight) prevented calorie restriction induced muscle atrophy by activating mammalian target of rapamycin (mTOR) signalling and enhanced mitochondrial function in plantaris and gastrocnemius muscles[82]. Hence, these findings suggest that lactate

serves as a key intermediate in many metabolic processes involving mitochondrial biogenesis, regulation of muscle mass, and modulation of the redox status within and between myocytes[83].

With respect to whole-body insulin resistance, elevated plasma lactate levels have been negatively associated with this variable[84], altough the underlying mechanism(s) is yet to be fully understood. In this context, hyperinsulinemic-euglycemic clamps were conducted in overnight-fasted rats infused with or without lactate for 6h[85]. In lactate-infused rats, insulin-stimulated glucose uptake and glycolysis was suppressed in soleus (highly oxidative), but not in epitrochlearis (highly glycolytic) muscles. Furthermore, lactate infusion did not change the ability of insulin to induce phosphorylation of its receptors, although it decreased the activation of downstream proteins like PI3K and AKT[85]. Another study (conducted in 11 healthy nonobese and 11 insulin-resistant obese women) found that lactate can cause defective insulin regulation in skeletal muscle and adipose tissue[86]. However, because adipose tissue mass is increased in obesity, lactate release from the adipose tissue may have contributed to the increased plasma lactate seen in insulin resistance and type 2 diabetes. Thus, in obese insulin-resistant subjects, it appears that it is the chronically elevated adipocyte-derived lactate instead of lactate transiently released from skeletal muscle that contributes to the genesis of diabetes. The mechanism by which glucose tolerance seem to be negatively affected by chronically elevated lactate seem to be associated with lowering both glucose uptake and insulin responsiveness in skeletal muscles.

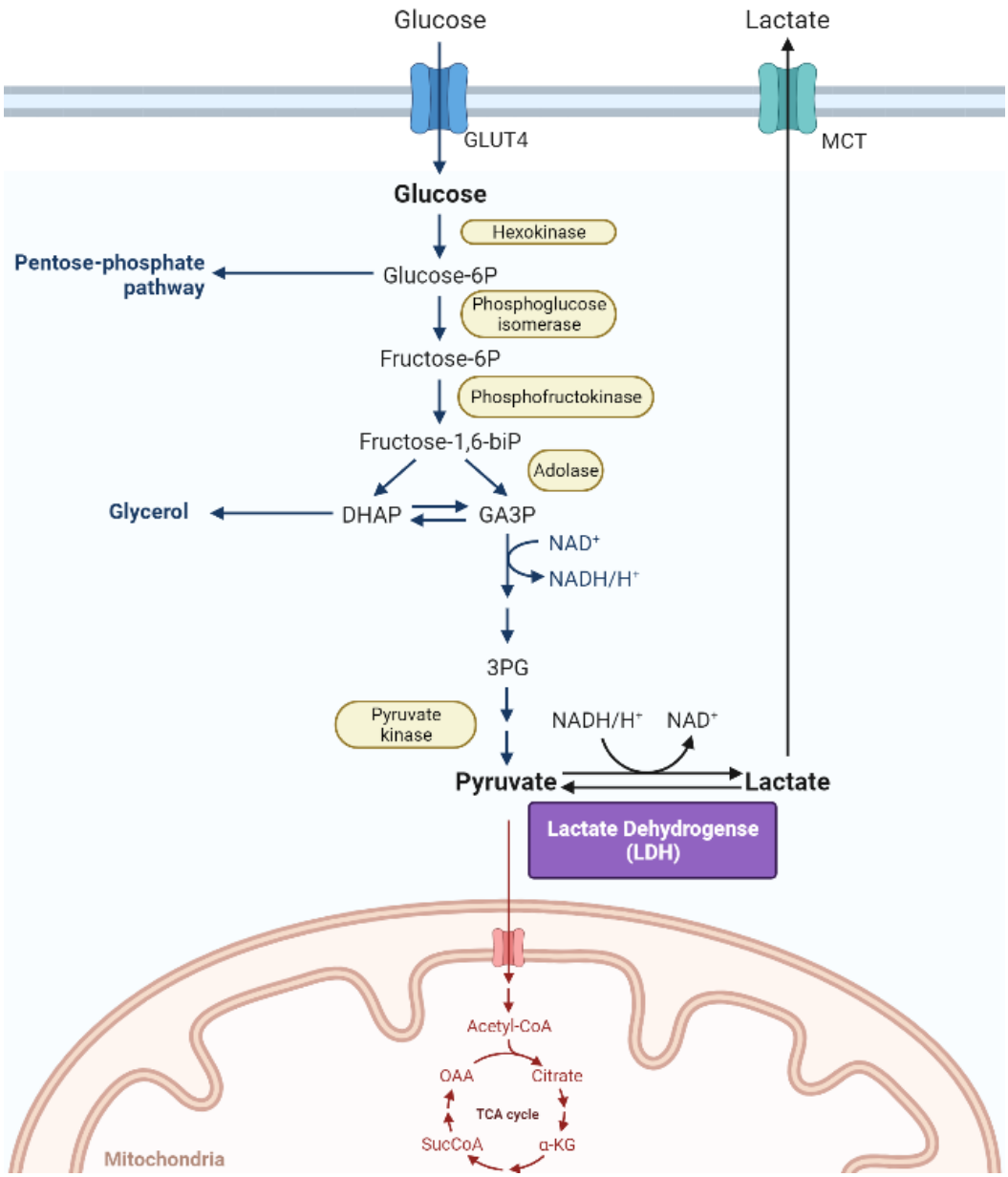

Figure 2.3: Lactic acid synthesis in skeletal muscle. Hexokinase catalyses the formation of glucose-6-phosphate (Glucose-6P), which is then isomerized to fructose-6-phosphate (Fructose-6P) by phosphoglucose isomerase. Subsequently, fructose-6P is phosphorylated by phosphofructokinase (PFK) to form fructose-1,6-bisphosphate (Fructose-1,6-biP). Aldolase breaks down Fructose-1,6-biP into two distinct sugar molecules: dihydroxyacetone phosphate (DHAP) and glyceraldehyde-3-phosphate (GA3P). DHAP is isomerized to form a second

molecule of GA3P that is phosphorylated by phosphoglycerate kinase to form 3-phosphoglycerat (3PG), in a reaction that uses NAD^+ as a cofactor. 3PG rearranges to form 2-phosphoglycerate and is dehydrated to produce phosphoenolpyruvate, which is eventually converted to pyruvate via pyruvate kinase enzyme. When deprived of oxygen, such as during contractions or during high intensity exercise, skeletal muscles convert pyruvate into lactate by LDH. The lactate generated is released into the circulation through specific monocarboxylate transporters (MCT). Image generated using BioRender.

2.4 Skeletal muscle and its role in glucose metabolism

Skeletal muscles are important for mobility, maintenance of posture, temperature regulation, soft tissue support, and regulation of whole-body energy metabolism. More importantly, skeletal muscle is critical for glucose clearance, accounting for more than 80% of postprandial glucose clearance after an oral glucose load[15,87]. Insulin resistance is induced by muscle desensitisation to insulin-stimulated glucose uptake, resulting in higher plasma blood glucose levels. Importantly, insulin resistance in skeletal muscles can occur decades before the onset of β-pancreatic cell failure[88]. This has been supported by observations that moderate skeletal muscle insulin resistance has been detected in lean non-diabetic normoglycemic subjects that are at a high risk of developing T2D (such as children with both diabetic parents)[88]. In fact, both the amount and timing of glucose absorption into skeletal muscles are affected when the ability of insulin to signal is impaired in this tissue[89,90]. This is consistent with observations that postprandial glucose uptake into muscle rises linearly with time in normal healthy individuals, whereas a delay in insulin action and blood glucose clearance is detected in skeletal muscles of

individuals with insulin resistance and T2D. Thus, as the predominant location of insulin-stimulated glucose clearance, skeletal muscle is thought to be the major driver of whole-body glycemic control.

Experiments using magnetic resonance spectroscopy (MRS) have been conducted to measure intracellular glucose transporter GLUT4 content as well as G6P levels to assess skeletal muscle insulin sensitivity[91,92]. Specifically, the ^{13}C MRS method was used to measure intracellular free glucose under hyperinsulinemic-hyperglycemic conditions[93]. It was reported that GLUT4 content in skeletal muscle cells was the rate-limiting step for insulin-stimulated glucose transport and glycogen synthesis in skeletal muscle[93]. Furthermore, it was found that intracellular G6P level was significantly lower in skeletal muscles of T2 diabetic patients than non-diabetics. Similar findings were made in lean insulin resistant offspring of type 2 diabetics[94], as well as in non-diabetic obese women[95]. These findings provided evidence that impairment in transport and/or phosphorylation of glucose underlie the inability of skeletal muscle to properly clear blood glucose in response to insulin[96] in obesity and type 2 diabetes.

2.4.1 Muscle Fiber Type Differences

Despite being referred to as a single organ, skeletal muscles are usually distinguished and studied on the basis of their fiber type composition[97]. Several categorization strategies distinguish fibres based on distinct myosin isoforms or physiologic characteristics. Mammalian skeletal muscles are made up of functional units called sarcomeres. Each sarcomere is made up of bundles of myofibrillar/contractile proteins, namely myosin and actin, that form muscle fibres. These muscle fibers can be classified on the basis of their histochemical and functional

characteristics[98]. The myosin protein complex, which is part of the molecular machinery that allows muscle contraction, is made up of 4 proteins (two heavy chains and two light chains) that are twisted around each other. Myosin Heavy Chains (MyHCs) are responsible for the power stroke action, which converts ATP into mechanical energy that drags the actin filament across the myosin filament. MyHCs are broadly classified into three categories: I, IIa, and IIb[9,99,100]. Human muscles do not express the fastest myosin heavy chain isoform (MyHCIIb), instead they express the MyHCIIx/d myosin heavy chain isoform, and therefore are often referred to as type IIx[101,102]. Hereon, MyHCIIx/d will be associated with histochemical characteristics of type IIB fibers. Muscle fibers rich in MyHC IIb are innervated by large motoneurons and display the fastest rate of contraction among all fiber types. However, type IIb fibers have low mitochondrial content, rely essentially on glycolysis for ATP generation, and fatigue quickly. Conversely, type I fibers are rich in MyHC I and are innervated by small motoneurons. These fibers display the slowest rate of contraction, are densely packed with mitochondria and highly oxidative, and fatigue resistant[103–105]. Type IIa fibers are intermediate and often referred to as fast-twitch oxidative because they exhibit features of both type I and type IIb fibers. Thus, type IIa fibers have the ability to adapt and become more specialized towards either a type I or a type IIb phenotype depending on the stimuli (e.g. endurance or resistant training, immobilization) that these fibers are exposed to[106,107].

From a metabolic perspective, type I fibres exhibit stronger insulin binding capacity, insulin receptor kinase activity, and autophosphorylation capacity when compared to fast twitch type II glycolytic fibres[108,109]. In this context, a relationship has been found between fibre type and insulin resistance[107]. In general, the metabolic characteristics of type IIb fibers include a reduced oxidative enzyme activity and an increased glycolytic enzyme activity when compared to

oxidative slow-twitch or oxidative fast-twitch muscle fibers[110,111]. Moreover, based on studies conducted in rodents, it has been postulated that muscle fibers follow an order of type I > type IIa > type IIb in regards to insulin sensitivity[105,112,113]. Thus, under conditions of insulin resistance, the reductions in oxidative enzyme activities, may be attributed to an increased proportion of type IIb and a decreased proportion of type I muscle fibers. This is consistent with observations that T2D patients have an increased number of glycolytic fibres, notably type IIb[114,115].

2.5 Obesity-induced inflammation and impaired insulin signalling in skeletal muscle.

2.5.1 Cytokines and other inflammatory molecules

The molecular linkages between obesity, insulin resistance, and T2D are unknown, although chronic low-grade inflammation in adipose tissue has been linked to impaired ability of many organs and tissues to respond to insulin[116,117]. It is currently recognized that besides serving as an energy storage compartment, the adipose organ also operates as a metabolic endocrine and paracrine tissue. In obesity, there is excessive expansion of adipose tissue mass, which is also often accompanied by the accumulation of fat in non-adipose tissues. Under these conditions, a large number of inflammatory adipokines/cytokines are produced and affect metabolism in various organs and tissues[118]. In this context, a link between chronic inflammation and skeletal muscle insulin resistance has been established. This is supported by the detection of elevated levels of inflammatory mediators in skeletal muscle, including tumor necrosis factor alfa (TNFα), interleukin-6 (IL-6), inducible nitric oxide synthase (iNOS), toll-like receptors (TLR), C-reactive protein (CRP), plasminogen activator inhibitor-1 (PAI-1), and sialic acid[119]. When

originated from skeletal muscle fibres, these inflammatory molecules are referred to as myokines[119].

2.5.1.1 Tumor necrosis factor-α (TNFα)

TNFα levels have been shown to be elevated in skeletal muscle tissue and in cultured skeletal muscle cells from humans and animals suffering from IR and/or diabetes[120,121]. In rodent models, high fructose diet-induced insulin resistance and hypertension are linked to elevated TNFα levels in skeletal muscle, but not in the adipose tissue[122,123]. Additionally, obesity-induced IR is preserved in mice missing TNFα and/or its receptor[124,125], and TNFα inhibition by anti-TNFα antibodies or TNFα converting enzyme inhibitors enhances insulin sensitivity in obese or nonobese insulin-resistant animals[125,126]. TNFα-induced IR has been attributed to the ability of this cytokine to increase IRS-1 serine phosphorylation[127], an effect that leads to impairment of the ability of insulin to promote IRS-1 tyrosine phosphorylation[128]. This is consistent with observations that infusion of anti-TNFα antibodies improves insulin receptor phosphorylation in skeletal muscle[129]. Bouzakri K et al. reported that TNFα inhibited AKT and AS160 signalling, and therefore, insulin-stimulated glucose uptake in skeletal muscle tissue[127].

2.5.1.2 Interleukin-6 (IL-6)

IL-6 is a myokine that affects immune response and has both pro- and anti-inflammatory properties. IL-6 may have insulin-sensitizing properties and help improve glucose metabolism and its disposal[130,131]. Similar to TNFα, IL-6 also induces a rapid and transient IRS-1 serine phosphorylation, resulting in enhanced IRS-1 ubiquitination/proteasomal degradation in skeletal muscle tissue[132]. Furthermore, in rats, acute IL-6 infusion causes abnormalities in IRS-1/PI3-kinase signal transduction and leads to impairment in insulin-stimulated skeletal muscle glucose

uptake[133]. It has been reported that elevated levels of circulating IL-6 have the ability to reduce insulin sensitivity and glucose transport in muscle, as well as impair hepatic insulin action and signalling[134].

Exercise has been shown to be effective in improving insulin sensitivity and counteracting dysfunctional metabolic alterations in obesity. Interestingly, exercise has also been demonstrated to release significant amounts of IL-6 from muscle, indicating that myocyte-derived IL-6 release may play an important role regulating skeletal muscle glucose metabolism[135]. This is consistent with reports that in healthy adults, acute IL-6 treatment did not exert any deleterious effect on muscle glucose uptake or whole-body glucose clearance[136]. Suggesting there is an apparent contradiction with respect to the pro- and anti-inflammatory effects of IL-6. This seems to derive from the fact that most human studies are essentially acute and limited to a few hours, whereas obesity is a chronic condition. In fact, it's chronic instead of acute exposure to IL-6 that has been associated with inhibitory changes in insulin action in 3T3L1 adipocytes[137,138]. However, in liver regeneration studies, it has been shown that short- (1–2 days) and long-term (5–7 days) exposure to IL-6 causes protective and deleterious effects, respectively[139]. Thus, time-dependent, and tissue-specific responses to be major factors determining the effects of IL-6.

2.5.1.3 Toll-like Receptor (TLR)

In mammals, TLRs comprise a family of at least 12 membrane proteins that play an important role in the innate immune response to bacterial infections and microbial compounds. TLR1–7 and TLR9 are mainly expressed in skeletal muscle cells and have been characterized; however, the precise molecular mechanisms responsible for insulin resistance still remain incompletely

understood[140]. TLR2 and TLR4 have been associated with diet-induced obesity, inflammation, insulin resistance, and diabetes[141]. In fact, TLR2 has been demonstrated to inhibit insulin receptor tyrosine phosphorylation and AKT phosphorylation in myotubules, whereas TLR4 activation impair insulin action through pro-inflammatory kinases and ROS[142]. This is consistent with observations that muscle biopsies from 7 lean, 8 obese, and 14 T2D subjects, revealed that obese and T2D subjects had significantly higher *Tlr4* gene expression and protein content in muscle than lean subjects. Moreover, TLR4 muscle protein content positively correlated with the severity of insulin resistance, which was also accompanied by elevated *Nf-κb* expression. The latter being a major transcription factor that promotes an inflammatory response[143]. In this context, it has also been reported that treating myotubes from lean, normal-glucose-tolerant subjects with palmitate increased TLR4 content and *Il-6* gene expression to levels similar to those found in muscles from insulin-resistant subjects[143]. Thus, because muscular *Tlr4* gene expression and protein content are elevated in insulin-resistant individuals and were reproduced by prolonged exposure to palmitate, it's been suggested that increased *Tlr4* expression/content is an acquired defect secondary to excess non-esterified fatty acids (NEFA) supply and or nutritional overload.

2.5.2 Reactive Oxygen Species (ROS) and glucocorticoids induced insulin resistance.

2.5.2.1 ROS

ROS are formed by the addition of an unpaired electron to a highly reactive oxygen[144] such as superoxide ($O2^-$), hydrogen peroxide (H_2O_2), and peroxynitrite ($ONOO^-$). Whenever ROS production overwhelms the antioxidant defences, oxidative stress ensues. Several lines of evidence suggest that oxidative stress plays a significant role in the development of obesity,

insulin resistance, and diabetes[145]. This is particularly true under conditions of nutrient overload (e.g. HFS diet) to the mitochondria that increases proton leak in the ETC, leading to increased ROS production[146]. This is supported by rodents studies reporting that increased HFS (45% to 60% kcal from fat) diet-induced adiposity coincided with elevated ROS production and reductions in glucose tolerance[147–149]. Oxidative stress causes cell damage and mitochondrial malfunction, which, in turn, leads to additional ROS production that operates in a vicious cycle of ROS-induced damage[150,151]. More recently, it has been proposed that mitochondrial failure is a consequence of lipotoxicity-induced oxidative stress in skeletal muscle[9], rather than an early event in the development of IR. In this model, elevated ROS levels causes mitochondrial dysfunction that culminates with extra fat buildup and eventually inhibition of insulin action[152–154]. In this context, interventions that shift lipid towards oxidation inside muscle cells (e.g., endurance exercise and calorie restriction) have the potential to attenuate oxidative in skeletal muscles and enhance whole-body glycemic control.

2.5.2.1 Glucocorticoids

Glucocorticoids are steroids that are naturally released by the adrenal cortex under the direction of the hypothalamic-pituitary-adrenal (HPA) axis. Cortisol secretion plays a role in tissue repair, immunological stability, and metabolic activities. Furthermore, during psychological and physiological stress or in response to fight or flight, cortisol production is increased in order to control whole-body glucose, lipid, and protein metabolism. However, elevations in cortisol levels cause a variety of negative health outcomes, ranging from depression to obesity and metabolic syndrome[155]. Glucocorticoids also derive from the conversion of cortisone into glucocorticoids in the muscles by the action of 11β-hydroxysteroid dehydrogenase type 1 (11β-

HSD1) enzyme[156,157]. The contribution of 11β-HSD1 activity to whole-body glycemic control has been demonstrated by the observations that mice lacking this enzyme displayed improvement in glycemia and lipid profile under conditions of obesity or stress[158,159].

Glucocorticoids are known as powerful antagonists of insulin action in skeletal muscles. This is consistent with previous reports that glucocorticoids reduce glucose uptake in skeletal muscles by inhibiting GLUT4 translocation[160]. Also, treatment with synthetic glucocorticoid, dexamethasone (DEX), reduced tyrosine phosphorylation of the insulin receptor in skeletal muscles, as well as AKT phosphorylation in rat muscles and in murine C_2C_{12} cells[161]. The impairment of AKT phosphorylation by DEX treatment further caused a reduction in GLUT4-mediated glucose uptake and glycogen storage[162–164]. Finally, due to its proteolytic effect, cortisol provides amino acids that serve as gluconeogenic substrates for hepatic glucose production[165], which may also contribute to elevate glycemia.

2.6 Fat metabolism in skeletal muscle

In addition to glucose, the body also uses fats for fuel. This is possible because dietary lipids previously stored as triglycerides in the adipose tissues can be hydrolyzed to release NEFAs into the bloodstream. These NEFAs can then be used as energy substrate in various tissues, including skeletal muscle and liver[166,167]. It has been widely accepted that skeletal muscle in lean, healthy individuals rely on lipid oxidation for the majority of resting energy production during fasting conditions[168,169]. Skeletal muscle has a high fractional extraction of fatty acids in the postabsorptive state, making it an essential location for fatty acid clearance[170]. Therefore, failure to properly regulate fatty acid delivery and disposition in skeletal muscle may result in the development of various obesity linked comorbidities such as insulin resistance[171]. There are

various metabolic factors that influence skeletal muscle's ability to use fatty acids. In animal studies, fatty acid utilization is fibre type-specific, with slow-twitch oxidative muscle fibres having a greater capacity for fatty acid uptake and oxidation than fast-twitch glycolytic muscle fibres. Malonyl-CoA, a powerful allosteric inhibitor of carnitine palmitoyl transferase I (CPT I) in skeletal muscle, was discovered to be elevated in obese animal models[172]. Other important variables such as distinct patterns of expression of fatty acid-binding proteins and the oxidation of fatty acids in the mitochondria for energy production[173] have also been associated with obesity. Importantly, several of these same skeletal muscle features are linked to insulin resistance, namely reduced oxidative capacity[174], higher content of glycolytic type II muscle fibres[174], and a higher malonyl-CoA concentration[172]. All these features being linked to lipid buildup in skeletal muscle and abnormal insulin sensitivity[175].

- *The role of Fatty acid transporters*

Four types of FA transporter proteins have been described: Fatty acid translocase (CD36), fatty acid transport protein (FATP), Fatty acid binding proteins (FABPs), and caveolae, all ubiquitously expressed[176].

2.6.1 Cluster of Differentiation 36 (CD36)

One of the major proteins involved in the transportation of FAs is the 88 kDa CD36 (FAT/CD36) protein. CD36 are ATP-dependent transporter proteins that show specificity for both long-chain fatty acids (LCFAs) and very long-chain fatty acids (VLCFAs). CD36 contains two transmembrane domains, that anchors a single extracellular loop and aids with the binding of various ligands, such as, collagen, thrombospondin, anionic phospholipids and most importantly fatty acids[177]. It was originally postulated that CD36 acts as an anion transporter

and aided in the transport of anionic aqueous unbound fatty acids[178]. However, this mechanism is not the primary mechanism because about 50% of fatty acids are unionized at a physiological pH[179]. CD36 promotes esterification of the FAs to aid with their transport across the membrane[180]. Further, research has pointed out that CD36 proteins are present on the plasma membrane as well as inside the mitochondria and other intercellular compartments. This makes it a unique fatty acid transporter[181] that may translocate from the intracellular organelles in the cytoplasm to the plasma membrane when triggered[182–184]. Often the translocation is induced by common physiological stimuli such as insulin or muscular contractions resembling the insulin-mediated translocation of GLUT4[185]. Ibrahim et al. showed that muscle-specific FAT/CD36 overexpression in mice led to increased fatty acid oxidation, reduced plasma triglycerides, and fatty acids, and elevated plasma glucose and insulin levels[179,186].

2.6.2 Fatty acid transport protein (FATP)

Six tissue-specific isoforms of FATP (FATP1-6) have been identified. FATPs exhibit some tissue specificity in terms of their distribution throughout the body. FATP-1 is predominantly found in the adipose tissue, heart, and skeletal muscles, whereas in the liver FATP-5 is the major isoform[187,188]. FATP isoforms are present in the luminal membrane of endothelial cells and bind specifically with LCFAs and VLCFAs, and are often referred to as LCFA receptors instead of transporters[189]. Based on the overexpression and or knockdown studies conducted on diverse cell types under various metabolic demands, the effectiveness among FATPs appears to differ substantially[190]. In obese insulin-resistant, Zucker rats identified an enhanced Fatp1 gene overexpression, leading to increased palmitate transport and oxidation (in soleus muscle), but not lipid accumulation[191]. FATP1 has also been found to be localized in mitochondria of the mouse gastrocnemius and peroneus muscles[192], indicating enhanced capacity to transport FA.

Furthermore, in FATP1 null mice, basal FA uptake in skeletal muscle remained unaltered, whereas insulin-stimulated FA uptake, Triglyceride (TAG) accumulation in skeletal muscle, and whole-body insulin resistance were significantly reduced[193,194].

2.6.3 Fatty acid-binding protein (FABP)

Membrane-associated FABPs are located on the outer surface of the plasma membrane where they bind to all FAs with great affinity and assist FAs to enter cells[191]. FABP transports FAs via two different mechanisms: 1) aqueous phase diffusion through the membrane, wherein cytosolic FABP-FA complexes move across the plasma membrane through passive diffusion, and 2) via collision transfer, where the FABP-FA complex transfers FA by connecting with the plasma membrane[195]. For the collision transfer to occur, the FABP consists of an arrangement with 10 anti-parallel beta-strands (β barrel) and 2 alpha-helices to form a secure structure that resembles a clam. This allows for an internal binding site to be formed that can protect and isolate the negatively charged fatty acid. The three-dimensional fatty acid-protein complexes are stabilized by electrostatic and hydrogen bond interactions of the hydrophobic fatty acid and the protein[196].

2.6.4 Caveolae

Caveolae are one of the most dynamic plasma membrane intercellular cavities (bulb-like pits) that have multiple functions in various types of mammalian cells. Work from several groups has identified three isoforms currently known: Caveolin-1 (CAV-1), Caveolin-2 (CAV-2), and Caveolin-3(CAV-3)[197]. A simplified structure of the caveolar pit is made up of two main proteins (caveolins and cavins) that unite on the plasma membrane by different mechanisms. Caveolins are membrane proteins that are formed in the endoplasmic reticulum and are then passed on via the Golgi body complex to the plasma membrane. On the plasma membrane, hair-

pin like caveolins meet other accessory proteins, such as cavins. The caveolae formed are typical charged intracellular vesicular structures that aid in molecular processes such as signal transduction via endo- and transcytosis[198,199]. Recently, Pohl et al. have demonstrated that amphipathic fatty acids are engulfed within the caveolae structure (bound to caveolin-1), forming a vesicle-like structure on the membrane which is then transported within the cell for further metabolism. However, how fatty acids are incorporated into the caveolae membrane remains unclear[197].

2.6.5 Fatty acid uptake into mitochondria and oxidation

In skeletal muscle cells, the majority of FAs undergo oxidation subsequent to uptake. This is because these cells have limited fat storage capacity, hence activated FAs are channeled towards oxidation in the mitochondria. Unlike short and medium-chain FA, long-chain fatty acids (LCFA) are first acylated and activated in the cytoplasm before entering the mitochondria (**Figure 2.4**). The mitochondrial mechanism to import LCFA is made up of three proteins: carnitine palmitoyltransferase I (CPT1), carnitine: acylcarnitine translocase (CACT), and carnitine palmitoyltransferase II (CPT2), each of which has a unique submitochondrial location. Acyl-CoAs produced by the enzymatic action of Long chain acyl-CoA synthetase (LCAS) in the mitochondrial outer membrane is transformed to acylcarnitines in the first step, and CPT1 catalyzes this transesterification[200]. Long-chain acylcarnitines produced by the process are subsequently translocated into the mitochondrial matrix via an exchange reaction mediated by CACT, an integral inner membrane protein. Further, CPT2, an enzyme associated with the inner leaflet of the mitochondrial inner membrane, facilitates the conversion of acetyl-coenzyme A (CoA) to fatty acyl-CoA[200,201].

Following, the entry of the fatty acyl-CoAs into the mitochondrial matrix, a major energy-producing metabolic pathway known as β-oxidation occurs. The process essentially breaks down FA into acetyl-CoA molecules by the enzymatic reactions that are regulated at both transcriptional and post-transcriptional levels[202]. The production of the number of acetyl-CoA molecules is directly dependent on the length of the carbon chain that was oxidized. The process is regulated by the action of acyl-CoA dehydrogenase, enoyl-CoA hydratase, hydroxyacyl-CoA dehydrogenase, and ketoacyl-CoA thiolase, generating two new molecules: acetyl-CoA and acyl-CoA at the end of one cycle[203]. In addition, during the process, NADH and $FADH_2$ are produced that are used by the electron transport chain to produce energy. Besides the enzymes mentioned, other auxiliary enzymes are required for the breakdown of unsaturated or odd-chain fatty acids. Odd-chain fatty acids upon oxidation result in one molecule of acetyl-CoA molecules and one molecule of propionyl-CoA each. Most often propionyl-CoA is metabolized into succinyl-CoA, which then enters the TCA cycle[204]. In nature, unsaturated fatty acids are more commonly found and require two additional auxiliary enzymes (enoyl-CoA isomerase and 2,4-dienoyl-CoA reductase) to completely oxidize polyunsaturated fatty acyl-CoAs[185,205].

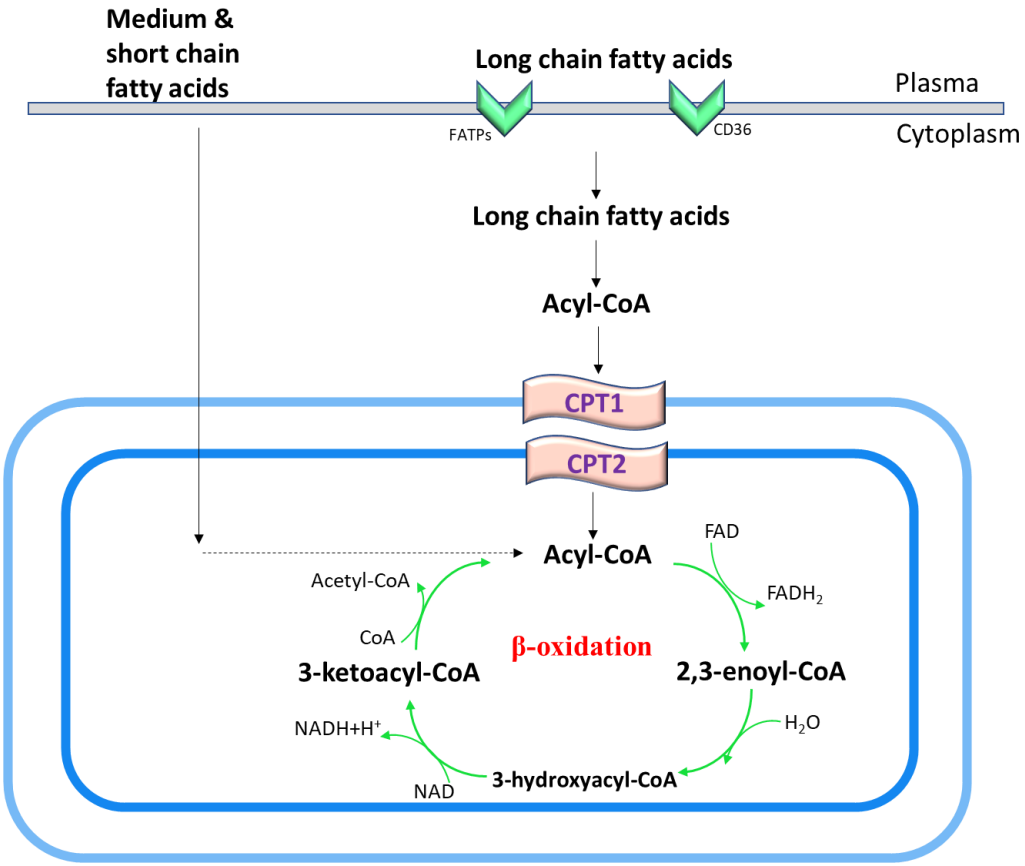

Figure 2.4: Fatty acid oxidation in the mitochondria. Short-and medium-chain fatty acids diffuse passively through the plasma membrane while long-chain fatty acids use membrane transporters. Long-chain fatty acids are first acylated in the cytoplasm the enter the mitochondria with the help of carnitine palmitoyltransferases (CPT1 and CPT2) and converted to acyl-CoA. β-oxidation of acyl-CoA takes place inside the mitochondrial matrix and is catalyzed by the mitochondrial trifunctional protein. At the end of each oxidation cycle, acetyl-CoA, nicotinamide adenine dinucleotide (NADH), and flavin adenine dinucleotide ($FADH_2$) are formed. NADH and FADH2 are used to generate ATP while acetyl-CoA is used in processes such as ketogenesis and TCA cycle[507]. Image generated using BioRender.

2.7 Regulation of fatty acid metabolism in skeletal muscles and its link to insulin resistance

Skeletal muscle IR has been associated with intramuscular lipid accumulation[206]. The original understanding was that an impairment in the ability of skeletal muscles to oxidize fat would lead to the formation and accumulation of lipid intermediates such as DAG and ceramides. This was supported by observations that obese individuals or individuals with T2D displayed low aerobic fitness and reduced number of muscle mitochondria[207,208]. In this context, the accumulation of lipid intermediates could interfere with normal insulin signaling and cause IR in the skeletal muscle. However, recent literature suggests that the rate of fatty acid oxidation, lipid accumulation, and insulin resistance are not related. For example, a study on obese Zucker rats revealed enhanced uptake and oxidation of fatty acids, as well as storage of triacylglycerols in red skeletal muscle[173]. Other studies have also reported that intramyocellular lipid accumulation and IR were not prevented in rodents fed a fat-rich diet, despite these animals exhibiting increased muscular mitochondrial protein content and enhanced oxidative capacity[209,210]. Interestingly, this inverse association between excess glycerolipid accumulation and IR is absent in endurance trained athletes and/or in conditions for efficient FA utilization. In fact, a parallel has been drawn between enhanced total IMCL accumulation and improved insulin sensitivity in individuals that perform chronic endurance exercise. This paradigm, is often referred to as the 'athletes paradox'[211–213]. Further analysis of the contradiction was conducted by Goodpaster's group, that looked at the deleterious effect of individual glycerolipids as opposed to the total accumulation. They found that participants that exercised had an increase in TAG content while a reduction in their DAG and ceramides content[214,215]. Where insulin sensitivity was found to be unaltered by a reduction of DAG but improved by reduction in ceramide content[216]. Making DAG and ceramides major lipid intermediates that are associated with skeletal muscle IR.

- *Mechanisms of DAG- and ceramides-induced insulin resistance*

2.7.1 DAG

Bioactive lipids such as DAG and ceramides are formed during the process of TAG synthesis[217]. As shown in **Figure 2.5**, TAG synthesis takes place in the Endoplasmic Reticulum (ER) via the monoacylglycerol (MAG) pathway[218]. The MAG-dependent pathway is exclusively found in animals and it plays an important role in dietary fat absorption in the small intestine, adipose tissue, and the liver[219,220]. MAG is first acylated to DAG by MGAT enzymes (MGAT 1/2/3) and then DAG is finally acylated to TAG by the enzyme DGAT (DGAT 1/2)[220]. DGAT1 inhibitors reduced plasma TAG levels, improved insulin response, and helped maintaining reduced body weight in obese and T2D patients. However, the patients in the study complained of severe adverse side effects such as nausea, diarrhea, and vomiting[221,222]. Suggesting a crucial role of DGAT towards synthesis of TAG and thereby fat metabolism and storage. In this context, excess accumulation of glycerolipids is said to contribute towards skeletal muscle IR genesis[215,223].

2.8.1.1 DAG induced PKC translocation and its involvement in IR

One of the primary downstream targets of DAG is protein kinase C and its role in impeding insulin signalling. The protein kinase C (PKC) family encompasses 10 isoforms that are classified based on their sequence homology and mechanisms of activation. Conventional PKCs (cPKC: α, β, and γ) are activated by Ca^{2+}, whereas novel PKCs (nPKCs: δ, θ, ε, and η) require DAG in addition to Ca^{2+} for complete activation[224]. A third group of atypical isoforms (aPKC) encompass PKC ζ and PKC ι/λ), which are neither dependent on DAG nor on Ca^{2+} for their activation. The conventional and novel isoforms are stimulated by G protein-coupled receptors

or receptor tyrosine kinases that induce hydrolysis of phosphatidylinositol 4,5-bisphosphate at the plasma membrane. This leads to the production of DAG and Ca^{2+} that trigger PKC translocation from the cytoplasm towards the cell membrane, leading to PKC activation.

In skeletal muscles, PKCθ and δ are the main isoforms activated by DAG[225]. In its activated state, PKC has been demonstrated to inhibit the kinase activity of the insulin receptor (InsR)[226], which then impairs all subsequent downstream steps of the intracellular signaling cascade causing IR. Indeed, in myocytes, PKCθ-induced phosphorylation of the Ser^{1101} residue on the IRS1 and impaired its tyrosine phosphorylation within the first 15 min of insulin stimulation[227]. This finding supported the idea that PKC-induced IRS1 Ser^{1101} phosphorylation acts as an acute negative feedback circuit that attenuates insulin action. Therefore, under conditions of fat abundance such as in obesity, the intramyocellular accumulation of DAG has been proposed to induce skeletal muscle IR through PKC activation[228]. However, the glycerolipid build-up does not always correlate with an increase in IR. This is the case with non-pharmacological approaches such as caloric restriction or exercise that enhance insulin sensitivity despite increasing DAG accumulation in skeletal muscles[214,229]. Additionally, we have recently, demonstrated that the HFS diet promoted DAG and ceramide buildup, PKC activation, and the stimulation of inflammatory pathways in a fibre type-specific manner. These findings assist to explain why oxidative and glycolytic muscles acquire insulin resistance in the same way, despite significant variations in their metabolic properties and sensitivity to dietary lipid abundance[230].

2.7.2 Ceramides

Ceramides are biomolecules known as lipid rafts that play an important role in cell membrane integrity and in the distribution of receptors and signaling molecules that reside in it[231]. Ceramides are synthesized in the endoplasmic reticulum and mainly dependent on the

availability of long- chain saturated fatty acids that may vary in chain lengths from 14 to 30 carbons[232].

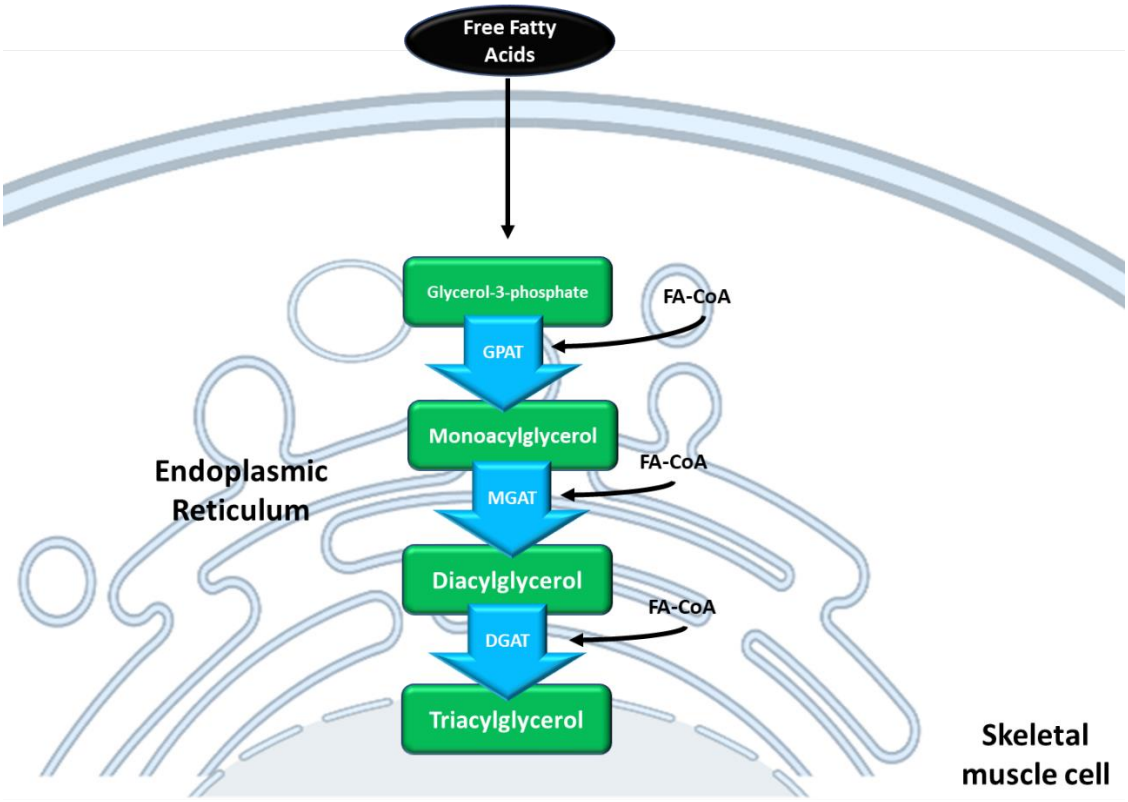

Figure 2.5: Schematic representation of triglyceride synthesis pathways, occurring predominantly in the endoplasmic reticulum bilayer membrane. DGAT enzymes catalyze the formation of an ester linkage between a fatty acyl CoA and the free hydroxyl group of diacylglycerol to synthesise the triacylglycerols (triglycerides); end-product of the multi-step pathway. GPAT, glycerol-phosphate acyltransferase and MGAT, acyl CoA:monoacylglycerol acyltransferase. Image generated using BioRender.

The *de novo* ceramides synthesis pathway is initiated by serine palmitoyl transferase (SPT) condensing serine and palmitoyl-CoA to produce 3-ketosphinganine. Next, the 3-ketosphinganine is reduced to sphinganine, which is acylated to dihydroceramide by six

ceramide synthase (CerS) enzymes (CerS1–6). Each of these enzymes synthesizes ceramides with distinct acyl chain lengths, which is finalized by dihydroceramide desaturase[233,234] (**Figure 2.6 & Table 2.1**). In fact, numerous studies have described the distribution of mammalian CerS in different tissues, and demonstrated that each tissue displays a distinct profile of CerS expression[235]. In addition, ceramides may also be hydrolysed from sphingomyelin (SM) by sphingomyelinases (SMases, neutral SMase and acidic SMase) via the stress-activated pathway. The breakdown of sphingomyelin to ceramide is usually triggered by upregulation of *TNFα*[236], *Fas ligand*[237], *Tlr4* activation[238], or oxidative stress[239,240]. Indicating a strong correlation between accumulation of ceramides to chronic low grade inflammation[241].

2.8.2.1 Role of Ceramides in causing Insulin Resistance, Diabetes and NAFLD

A study conducted over a period of 7-years including 1,557 adults[242] found that saturated C16 and C18 ceramides are linked to insulin resistance (when assessed by HOMA-IR), total body fat, and visceral adipose tissue content. Conversely, longer-chain polyunsaturated fatty acid ceramides C24:2, C30:10, and C32:11 were associated to better metabolic profiles[242]. Similarly increased plasma C16, C18, and C20 ceramides levels were observed in a large cohort subjects from Chinese origin in Singapore individuals with lower body mass index (BMI) and HOMA-IR [243]. Moreover, the C18/16 ratios were found to serve as a distinct measure for diabetes incidence risk[244]. Interestingly, this ratio fell in people who lost 5 percent or more of their body weight[244]. In type 1 diabetes patients, significant drops in blood levels of very long-chain ceramides (C20, C20:1, C22.1, C24, C26, C26:1) have also been linked to the onset of nephropathy[245].

With respect to NASH, levels of total serum and liver dihydroceramides (22:0 and 24:1) were significantly increased and strongly associated with whole body insulin resistance[246]. Additional

analysis also confirmed that sphingolipid species correlate with oxidative stress and liver inflammation[246]. In a prospective study of 31 children with NAFLD, Wasilewska et al. found a significant positive correlation between total serum concentrations of ceramides with insulin and HOMA-IR[247]. In addition, this study demonstrated that total ceramide concentrations and specific saturated fatty acyl subspecies of ceramides (C14, C16, C16:1, C18, and C18:1) were significantly higher in children with NAFLD than controls[247].

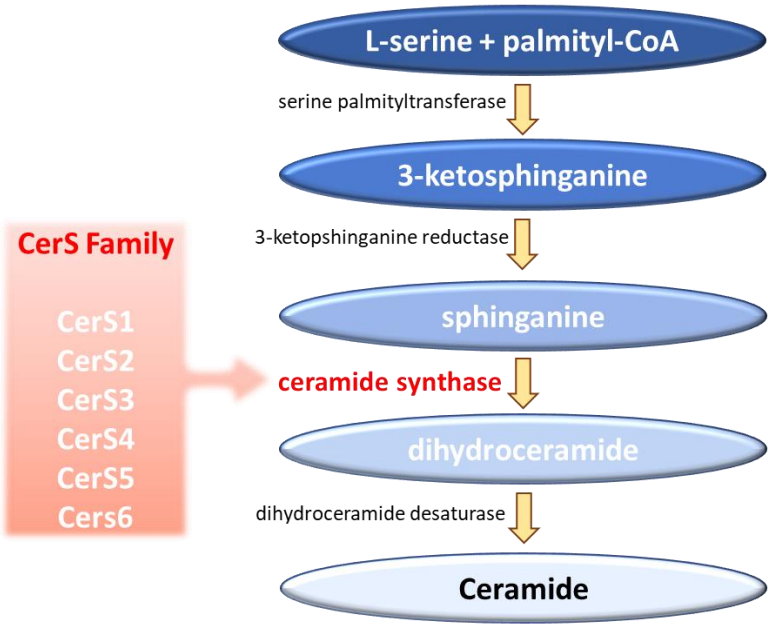

Figure 2.6: Ceramide synthases family acetylates sphinganine to dihydroceramide, which is eventually desaturated by dihydroceramide desaturase to form ceramides[248].

Table 2.1: *Ceramide synthase family, their expression sites and acyl-chain length.*

Ceramide Synthase	Tissue Expression	Acyl-chain length
CerS1	Brain, skeletal muscle, testis	C18
CerS2	Kidney, liver	C20-C26
CerS3	Testis, skin	C22-C26
CerS4	Low level of expression in various tissues	C18-C20
CerS5	Low level of expression in various tissues	C16
CerS6	Low level of expression in various tissues	C14 & C16

Higher levels of C18 ceramides produced by CerS1 have been associated with insulin resistance and inflammation in skeletal muscle[249]. In fact, C18 ceramides were found in increased levels in muscle tissue of C57BL/6N mice consuming an obesogenic diet[250], whereas the global ablation of CerS1 increased energy expenditure, reduced adiposity, and improved insulin and glucose tolerance in mice. The study also found that skeletal muscle CerS5 and CerS6 are dispensable for obesity-associated insulin resistance in knock-out mice models[250]. It has also been reported that low density lipoproteins (LPLs) with C16:0 and C24:0 ceramides decreased glucose uptake in cultured myotubes by obstructing insulin signalling and reducing the translocation of the GLUT4 glucose transporter[251]. Even though the involvement of muscular ceramides obesity development has been reported, the underlying molecular mechanism involved in the pathogenesis of IR and T2D remain yet to be elucidated[252,253].

2.8 Sexual Dimorphism

It has been well established that sex impacts the development and progression of various comorbidities, including metabolic disorders such as diabetes. Globally, diabetes is known to affect men more than women, especially middled aged men[16]. In this context, it is recognized that development of obesity, IR, and hyperglycemia are unique between sexes. These differences with respect to glycemic control appear to arise from distinct responses that men and

women display to diet[254]. Numerous aspects of energy balance, such as carbohydrate metabolism, lipid utilization and storage are believed to differ between sexes[255].

Also, men and women differ substantially in regards to their body composition, especially with respect to site-specific adipose tissue distribution[256,257]. In men and women, the predominant site for fat storage is the subcutaneous adipose tissue. However, men have more visceral (VC) adiposity and less subcutaneous adipose tissue (SC) in comparison to women[258]. Importantly, multiple studies have implicated the accumulation of VC adipose tissue in the development of IR and diabetes[259,260]. This has been, at least partially, attributed to the fact that VC adipocytes are more prone to lipolysis and less sensitive to insulin[261]. Moreover, increased VC adiposity is known to contribute to dyslipidemia, upregulation of gluconeogenesis, and IR[262]. Thus, it is the site-specific accumulation of fat instead of total fat mass that correlates with the higher prevalence of diabetes and abnormalities of glucose metabolism in men than in women[262].

It has also been reported that the susceptibility to fatty acid-induced peripheral IR is decreased in women[263]. In different rodent models of glucose intolerance, IR and diabetes, males show a stronger phenotype than females[264,265]. These sex-related differences in insulin sensitivity and adipose tissue development and function could be due to actions of oestrogen and testosterone hormones. For example, a link between decreased oestrogen levels, increased adiposity (Subcutaneous and Visceral fat) and increased IR have been observed in aging women[266]. Similarly, hormones such as dopamine, norepinephrine and epinephrine induce lipolysis leading to increased circulating free fatty acids, enhanced hepatic VLDL release and glucose production, as well as reduced insulin clearance. However, how hormone levels and insulin action differ

between males and females, and how these differences account for a sex-specific regulation of skeletal muscle glucose and fat metabolism and function remain largely unknown.

2.8.1 Sex differences in fiber-type composition

Women display 27%-35% higher number of type 1 muscle fiber type in vastus lateralis muscle when compared to age- and weight-matched men[267]. In addition, greater type I fiber type content and capillary density in women contribute to enhanced glucose and fat oxidation. Conversely, men displayed relatively higher proportion of type II A and type II X in comparison to women[268,269]. Immunohistochemical studies have also suggested lower transcriptional levels of myosin heavy chains I (MyHCI) in men than in women[270], whereas higher MyHCIIA and MyHCIIX mRNA expression has been reported in men than in women[271]. An association between insulin sensitivity and the amount of oxidative type I fibres has been proposed, with lower expression of type I fibres in the vastus lateralis muscle of insulin resistant and T2D subjects compared to healthy subjects[272,273]. Finally, the amount of type I fibres as well as capillary density were found to be highly correlated with insulin action during a hyperinsulinaemic-euglycaemic clamp in lean subjects and obese non-diabetic men[274]. Another recent study looked at age matched and weight matched men and women and confirmed higher type II X fibers in men than in women. But more importantly found a positive correlation between higher proportion of type II X fibers and the development of T2D[275]. A study of non-diabetic men reported an association between type 1 fibers and insulin sensitivity during hyperinsulinaemic euglycaemic clamps[276]. To add to it, a correlation between the oxidative capacity of the muscle and increased cell mass (obesity) was established. It was found that in muscles with higher type I fibers had a higher oxidative capacity and infact had an enhanced tyrosine kinase activity of the insulin receptor. Suggesting that enhanced blood flow can be

considered a limiting factor in the pathogenesis of obesity and other metabolic dysfunctionalities[276].

2.8.2 Sex differences in circulating fatty acids.

Plasma FA concentration has been reported to be significantly higher in women (median 517 vs. 434 μmol/l) than in men[277]. Additionally, in healthy men and women fasted for 48 h, plasma FA concentration was 30% higher in women than in men[278], and when the length of fasting was increased to 72 h, serum FA was reported to be 81% higher in women than men[279]. Similarly, in lean and obese subjects exposed to four consecutive days of isocaloric feeding, women displayed ~40% higher postabsorptive FA release and resting energy expenditure than men[280]. Altogether, these findings demonstrate that women have higher FA concentrations, in particular in the fasted state, and thereby a higher FA availability per unit of their lean body mass, as a result of their higher fat mass than men[167].

2.8.3. Sex differences in FA transport in skeletal muscle

Irrespective of training status, a higher gene as well as protein expression of FAT/CD36 has been reported in women than men, [280]. Gene expression of FABP (plasma membrane)[280] and FATP1[281] have also been reported to be higher in lean women compared to lean men. Women also display higher FABP (cytoplasm) mRNA expression than men[282,283]. However, at the protein level, only FAT/CD36 has been demonstrated to be higher in women than men. Thus, it is possible that higher FAT/CD36 protein in women increase their capacity for FA transport into skeletal muscles. Moreover, higher plasma FA availability[284] coupled with higher amount of FAT/CD36 in skeletal muscle could lead to higher intramuscular triglyceride (IMTG) concentrations in skeletal muscle of women. However, a higher amount of type I muscle fibers

in women is a factor to consider since IMTG content is reported to be 2.8-fold higher in type I fibers compared to type II fibers[103]. Notably, IMTG concentrations are often negatively correlated to whole-body insulin sensitivity in men, with the exception of athletes[211,285]. It can be questioned why this relationship is different in women? Tarnopolsky et al. found that IMTG in women is localized in a higher number of smaller lipid droplets compared to men using electron microscopy[286]. Interestingly, these smaller lipid droplets in women were found to be located closer to mitochondria[287], a location which may increase susceptibility to oxidation. The phospholipid surface of lipid droplets is covered with a number of proteins involved in lipid metabolism and trafficking of the lipid droplets. It has been demonstrated in men and women, matched for age, BMI and VO_2-peak/kg LBM, that skeletal muscle protein expression of perilipin 3 and 5 is 1.5- to 2-fold higher in women[288]. Perilipin 3 and 5 mediates an interaction between lipid droplets and mitochondria[288,289]. Taken together, perhaps smaller lipid droplets and increased expression of perilipins in women are likely to increase the lipolytic turnover of IMTG. However, as mentioned earlier that IMTG concentration *per se* is not an important determinant of insulin sensitivity in skeletal muscle. Instead, accumulation of lipid metabolites, such as DAG or ceramides, has been suggested to play a role, and it could be speculated whether there are sex differences in each of the glycerolipid intermediates. Studies in this area are scarce, and further studies are required to exclude a differential influence of lipid metabolites and related lipotoxicity in men and women.

2.9 The role of the Liver in glucose and lipid homeostasis

As blood glucose rises after a meal, β-pancreatic cells sense it and release insulin. In hepatocytes, insulin stimulates glycogen synthesis and inhibits gluconeogenesis and glycogenolysis[25]. The liver receives diet-derived glucose via the portal vein at a concentration

that is 3-10 fold higher than the rest of the body[24]. Nearly 60% of diet-derived glucose is stored as glycogen in the liver, whereas 15% of the glucose that escapes the liver is used up by skeletal muscles and adipose tissues[290]. The remaining circulating glucose is taken up by organs such as the brain and other peripheral tissues (e.g., erythrocytes, kidneys, etc.) to meet their energy demands[25]. The molecular steps by which insulin stimulates glycogen synthesis in the liver are similar to what has been previously described in skeletal muscle (**Figure 2.1**). Conversely, under conditions of prolonged fasting and/or deprivation of dietary carbohydrates, gluconeogenesis and glycogenolysis are activated in the liver to produce glucose and release it in the circulation. Glycogenolysis is an important process that accounts for ~75% of the glucose in circulation in the absence of incoming dietary glucose[24]. As hepatic glycogen is depleted, gluconeogenesis is activated and it can start as early as just 4 to 6 hours of fasting[291,292]. Lactate, pyruvate, amino acids, and glycerol are substrates used by the liver for gluconeogenesis. In the fasted state and/or under prolonged exercise conditions, insulinemia is reduced, whereas glucagon and epinephrine are upregulated. Together, glucagon and epinephrine coordinate a hepatic response that maintains glycemia tightly regulated at all times.

2.10 Lipid metabolism in the Liver

2.10.1 De novo Lipogenesis (DNL)

In hepatocytes, DNL is a critical biosynthetic pathway leading to (NAFLD)[293]. The DNL pathway is regulated in two ways: 1) transcriptionally by altering the expression of enzymes involved in FA synthesis and 2) through the modification of acetyl-CoA carboxylase (ACC) activity. The transcriptional factors sterol regulatory element binding protein 1c (SREBP1c) and carbohydrate response element binding protein (ChREBP) are activated under conditions of

increased insulin and glucose concentrations, both of which are caused by overnutrition[294]. SREBP regulates over 30 genes (*e.g.* Ac1, Acc, Scd1, as well as glyceraldehyde-3-phosphate acyltransferase and NADPH producing genes)[24] that are involved in lipid metabolism and the physiopathology of T2D, hepatosteatosis, and atherosclerosis[295]. In the context of DNL, insulin increases SREBP1c activity by proteolytically releasing the active form of SREBP1c from the Golgi membrane, where the membrane-bound immature form resides. This allows SREBP1c to translocate to the nucleus and promote the transcription of lipogenic genes, including FAS and ACC. SREBP1c regulates fatty acid synthesis and energy storage in the liver, whereas the SREBP2 isoform is involved in the regulation of whole-body cholesterol levels[296]. In mice overexpressing nSREBP-1c, liver triglyceride and cholesterol levels increased and these mice displayed NAFLD[297].

In contrast to SREBP1c, ChREBP is activated by a postprandial increase in glucose delivery to hepatocytes. The rate of glycolysis in hepatocytes increases as a result of the rapid influx of glucose via GLUT2[298]. The activation of ChREBP appears to be triggered by a number of metabolites produced during glycolysis, though the exact mechanism is unknown. In this context, glucose-6P and fructose-2,6-bisphosphate have been proposed to regulate ChREBP activity in hepatocytes[299]. ChREBP appears to predominantly bind to glucose and trigger the activation of the carbohydrate response element (ChoRE) which eventually activates genes such as FAS, ACC, and also cytosolic liver-type pyruvate kinase (L-PK). Systemic deletion of ChREBP inhibits glycolysis and hepatic lipogenesis, which in turn results in glucose to be converted to glycogen as observed in the liver of ChREBP-null mice[300]. Similarly, genetic deletion of ChREBP or liver-specific inhibition of ChREBP lowers hepatic lipogenesis and steatosis in ob/ob mice[301,302].

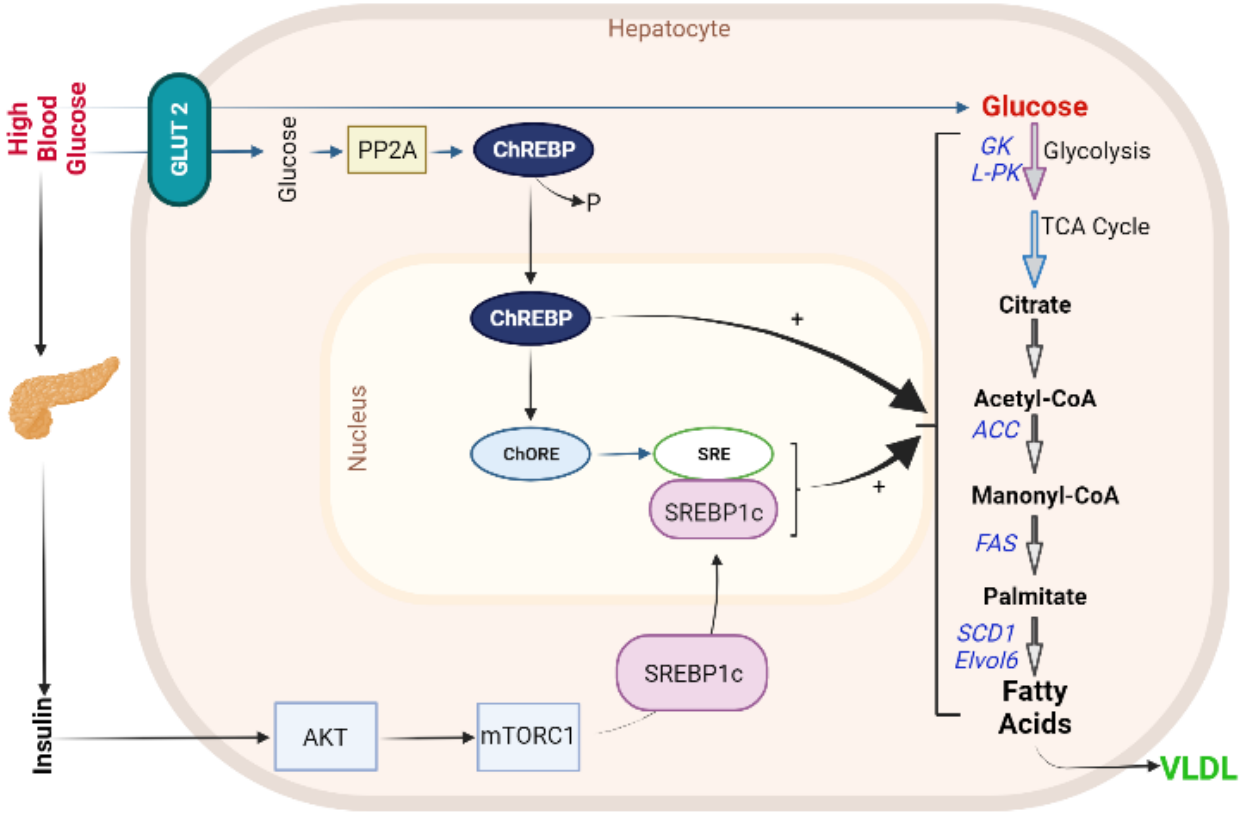

Figure 2.7: *Glucose metabolism in the liver.* In the presence of high levels of glucose and insulin, carbohydrate responsive element-binding protein (ChREBP) and sterol regulatory element-binding protein (SREBP-1c) are activated via two different pathways in the hepatocytes, which then promote de novo lipogenesis (DNL). DNL involves a series of steps in which glucose undergoes glycolysis to generate pyruvate that is utilized by various metabolic processes such as the Krebs (TCA) cycle. Further the fructolytic pathway feeds into the glycolytic pathway and allows for the production of acetyl-CoA from glucose/fructose to continue without regulation by insulin, and hence promote lipogenesis, and subsequent triglyceride (TG) synthesis from the acyl-coenzyme A (CoA) product. The TGs produced are packed into very low density lipoproteins(VLDLs) for export from the liver, or are stored within hepatocytes. Image generated using BioRender.

2.11 NAFLD

Hepatic steatosis characterizes NAFLD, which is determined by histological section and imaging. Excessive alcohol consumption, steatogenic medical prescriptions, or congenital metabolic disorders are well-known for causing NAFLD[303,304]. However, a spectrum disease ranging from benign mild steatosis (macro vesicular steatosis) to fibrotic hepatic inflammation known as non-alcoholic steatohepatitis (NASH) can evolve to cirrhosis and hepatocellular carcinoma (HCC)[305]. Obesity and T2D are conditions that lead to elevated lipid accumulation in the liver and set the stage for the development of NAFLD[306]. This is supported by reports that 85% individuals with pre-diabetes or T2D had NAFLD, whereas this condition was observed only in 30% of controls[307]. Furthermore, patients with T2D displayed on average 80% more liver fat than control subjects. A positive correlation was also found between increased waist circumference and elevated lipid deposition in the liver[308]. Highlighting the correlation between NAFLD and metabolic conditions like obesity.

2.12.1 Development and progression of NAFLD

The exact cause and progression of NAFLD are poorly understood. The theory frequently presented for the clinical progression of NAFLD is the ‘Multiple-hit’ theory. This theory is based on the idea that an energy imbalance caused by the abundance of dietary carbohydrates and fats leads to the IR. The latter condition then leads to an increased uptake and synthesis of fatty acids and their storage as TAG in the liver, resulting in steatosis[309]. In addition, the abundance of fat causes adipose tissue dysfunction an leads to an increase in the secretion of numerous inflammatory mediators such as TNFα, IL-6, and NF-kB[310]. TNFα has been shown to also promote serine phosphorylation of IRS-1 in the liver, which inhibits the insulin-mediated

tyrosine phosphorylation of IRS1[310]. Consequently, this leads to inhibition of all downstream insulin-signaling steps in hepatocytes, an effect that has been shown to be averted in TNFα-KO mice[130]. Similarly, primary hepatocytes treated with IL-6 displayed less phosphorylation of AKT and a 75% reduction in glycogen synthesis[309]. Along the same lines, activation of the NF-kB pathway and increased hepatic expression of TLR-2, -4 and -9 contributed to NASH in Sprague Dawley rats[311]. Thus, it is the combination of these various factors that is known as the 'second hit', which gradually drives the progression from macro vesicular steatosis to NASH. The pathogenesis includes uncontrolled apoptosis in the liver, hepatocyte inflammation, and fibrogenesis. Finally, hepato-fibrosis further progresses to hepatocellular carcinoma (HCC) and eventually liver failure[312,313].

2.11.2 Other plausible mechanisms for the pathogenesis of NAFLD

IR inhibits the anti-lipolytic action of insulin and leads to an increased release of NEFA into the blood. Other sources of fats derived from hepatic DNL and abundant dietary fatty acids also play an important role in the pathogenesis of NAFLD[314,315], although an elevation of lipogenic transcription factors and enzymes including SREBP-1c and FAS[316] have also been reported. These factors further increase DNL in an already steatotic liver[297,317,318]. Therefore, an overabundance of dietary fats in combination with increased lipolysis and elevated DNL are believed to eventually promote hepatic inflammation and further liver damage[319].

2.12 Lipid induced insulin resistance in the Liver

In addition to TAG, glycerolipids such as DAG and ceramides also accumulate in the liver. This is attributed to various factors such as high content of fat or sugar in the diet and reduced fat storage capacity in adipocytes, leading to elevated levels of NEFAs in the circulation[320,321]

and/or increased oxidative stress[322,323]. The synthesis of DAG is initiated by MAG in the endoplasmic reticulum or in the mitochondria. MAG is first acylated to DAG by MGAT 1/2/3, and then DAG is finally acylated to TAG by DGAT 1/2[220]. MGAT has been shown to prefer FAs with C18:2 and C18:3 in the sn-2 position for DAG synthesis[219,324]. In patients with IR and NAFLD, the expression of liver MGAT is elevated[325]. Also, *ob/ob* mice fed a HFS diet had elevated expression of peroxisome proliferator-activated receptor (PPAR) γ, a transcription factor known to regulate the MGAT1 promoter in the liver. As expected, these mice displayed increased levels of MGAT1 expression, which is the dominant murine MGAT isoform[326]. Conversely, when fed a HF/high fructose/high cholesterol diet, *Mgat1* knockdown mice had decreased MGAT activity, enhanced hepatic insulin signalling, reduced DAG content, improved whole-body insulin response, and reduced weight gain[327]. Similarly, MGAT2 expression is elevated in obese individuals suffering from NAFLD and reduced in patients that have undergone gastric bypass surgery[328]. In humans, intestine, and liver also express MGAT3, but its exact role in lipid-induced IR is unknown. Interestingly, all three MGAT isoforms share sequence homology with DGAT2 (expressed in the liver), but not DGAT1 (mainly expressed in adipose tissue and small intestine)[219]. In this context, promising results have been obtained with DGAT1 inhibitors with respect to maintaining whole-body glucose homeostasis and reducing postprandial serum TAG content in obese patients. These findings provided evidence for a critical role of DGAT1 in lipid synthesis and storage in humans[221,222]. Unfortunately, the effects of these inhibitors were not sustained for prolonged period of time because the patients complained of nausea, diarrhea, vomiting and general discomfort. Therefore, despite showing apparent therapeutic benefits, with respect to improved insulin sensitivity and reduced TAG

accumulation, DGAT1 inhibitors may not be an ideal treatment for metabolic disorders such as obesity, IR, dyslipidemia, and hepatic steatosis[329].

2.12.1 The link of hepatic DAG content with impaired insulin sensitivity

There is increasing evidence correlating intrahepatic triglyceride (IHTG) accumulation with reduced hepatic insulin sensitivity[226,330–333]. Analysis of various lipid metabolites in liver samples from obese non-diabetic individuals revealed that only total hepatic DAG content was associated with IR[334]. Other factors such as BMI, LCFA content, markers of endoplasmic reticulum stress, and inflammatory cytokine content seemed to have no effect on the homeostasis model assessment of insulin resistance (HOMA-IR)[334]. This was consistent with other reports of a strong correlation between hepatic DAG accumulation and whole-body IR[335]. Further investigation of 5 DAG species by Luukkonen et al. revealed that 4 of them were involved in NAFLD pathogenesis and significantly correlated with HOMA-IR[336]. In fact, analysis of liver biopsies from 133 obese individuals revealed that hepatic cytosolic DAG content, not hepatic ceramide content, was increased in subjects with hepatic IR[337]. Moreover, a strong association was found between DAG accumulation and PKCε translocation to the plasma membrane[337]. These findings provide evidence for a mechanism linking hepatic glycerolipid accumulation to the pathogenesis of NAFLD-associated hepatic IR in humans[330,338,339].

The proposed mechanism of DAG-mediated lipid induced hepatic IR involves the activation of the aforementioned PKC protein. The most abundantly expressed PKC isoform in the liver is the epsilon (PKCε)[320], which has been shown to become prominent after feeding rats a HFS diet for 3 days. In fact, Pkce$^{-/-}$ mice are protected from diet-induced IR following 1 week of HFS feeding, despite increases in intrahepatic triglyceride (IHTG) accumulation[340]. Recently,

Petersen et al. (2016) reported that the phosphorylation of the insulin receptor on the Thr_{1160} residue is critical for deactivation of the insulin signalling cascade in the liver. They used a threonine-to-alanine mutation at the homologous residue Thr_{1160} (T1160A) mutant and found that its activation was not altered by PKCε in vitro. Furthermore, hyperinsulinemic clamp studies revealed that the mutant mice also displayed enhanced insulin sensitivity, suppressed gluconeogenesis, and increased hepatic glycogen synthesis in comparison to wild type controls[341] (**Figure 2.8**). These data support a model of hepatic IR caused by DAG-mediated activation of PKCε and impairment of insulin activation. Such that DAG accumulation causes the activation of PKCε that results in phosphorylation of the insulin receptor threonine 1160, which in turn leads to disruption of the insulin receptor tyrosine kinase activity. This mechanism for lipid-induced hepatic IR has also been reported in humans as indicated in **Figure 2.8**.

Kumashiro et al. (2011) studied determinants of IR in people undergoing bariatric surgery. As expected, hepatic DAG content and PKCε migration to the plasma membrane were the strongest predictors of hepatic IR in individuals with NAFLD[342]. Consistent with these results, Luukkonen et al. (2016) and ter Horst et al. (2017) have shown that liver DAG content, specific lipid metabolites (species of fatty acids, ceramides, and TAGs), and increased PKCε activity are related to hepatic insulin sensitivity in obese individuals undergoing bariatric surgery[336,339]. Finally, Lyu et al. (2020) found that liver plasma membrane sn-1,2-DAG content increased and phosphorylation on insulin receptor T1160 residue were increased in individuals with hepatic IR and/or NAFLD[330].

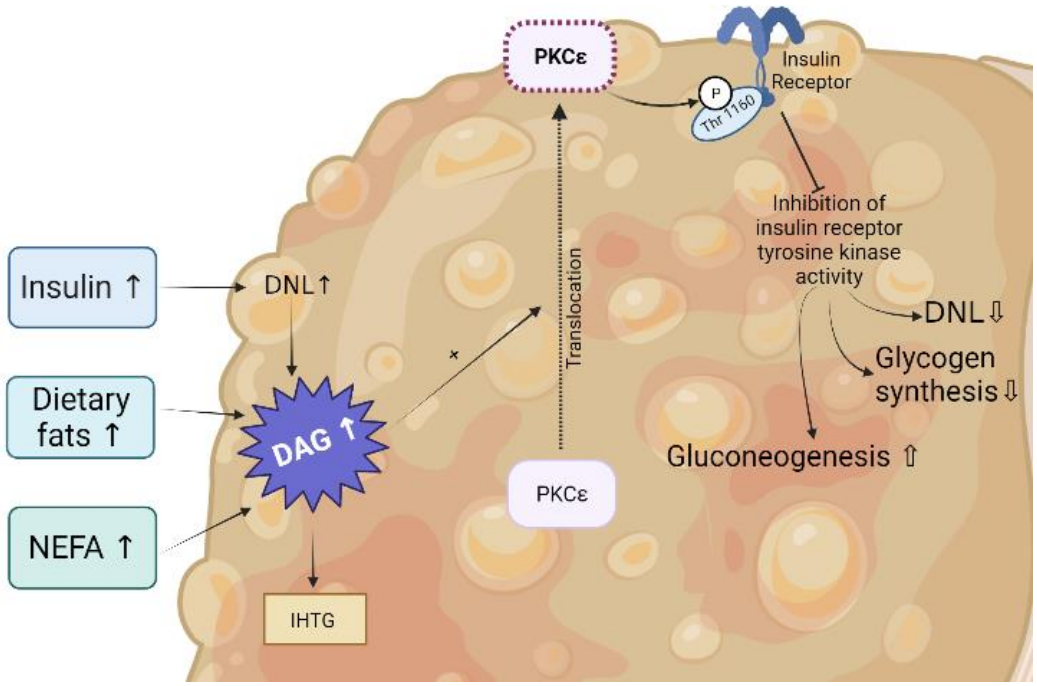

Figure 2.8: Postulated action of diacylglycerol (DAG) on Protein Kinase C epsilon (PKCε) in lipid-induced hepatic insulin resistance. Excessive calorie intake is a major factor in causing obesity and, consequently, insulin resistance. Insulin resistance causes NAFLD directly by increasing de novo lipogenesis and indirectly by increasing FFA flux to the liver by decreasing inhibition of lipolysis. As a result of all these factors, the synthesis of intrahepatic triglycerides (IHTG) is increased, and as a result DAG accumulation also increased. DAG further activates PKCε and causes it to translocate from the cytoplasm to the plasma membrane. The translocated PKCε phosphorylates the Threonine 1160 residue on the insulin receptor inhibits its tyrosine kinase activity and leads to impairment of downstream insulin signalling, reduction in glycogen synthesis, and upregulation of DNL and gluconeogenic genes[459]. Image generated using BioRender.

2.12.2 Mechanisms linking ceramide and impaired insulin signaling

The role of ceramides in hepatic insulin signaling has been controversial and evolving. This is because studies on obese non-diabetic humans have failed to show a correlation between ceramide content and IR assessed by HOMA-IR[334] or insulin suppression of hepatic glucose production[339]. Also, in mice fed a HFS diet for 8-12 weeks no alteration in total hepatic ceramide content was found[253,343,344]. Similarly, in Sprague Dawley rats, 3 days of HFS feeding neither induce IR in the liver nor increase total hepatic ceramide content[345]. Finally, studies that have successfully reversed steatosis have shown a correlation between reduced DAG content and improved insulin sensitivity, but no association with ceramide content[330,331,338,346,347]. Conversely, studies in mice indicated that DGAT2 overexpression was linked to IR, increased total hepatic ceramides, as well as to DAG and TAG accumulation[348]. Wistar rats also displayed elevated ceramide content and hepatic DAG accumulation along with IR[349]. Thus, due to inconsistencies in studies on total hepatic ceramide content in rodent models of hepatic steatosis and IR, researchers turned their attention to the potential role of specific ceramide species instead of their total content. However, it was only recently that research has attempted to address the role of specific ceramides in hepatic IR[350–352]. In C57BL/6 mice fed a HFS diet for 7-21 days, hepatic IR was accompanied by hepatic steatosis and varying contents of ceramide species between days 7 and 21[353]. Also in C57BL/6N mice, 14 weeks of HFS feeding resulted in increases of 14:0, 16:0, 18:0, 20:0, and 24:1 ceramide species that correlated with impaired insulin sensitivity in the liver[350].

Initial work in the field had proposed two main mechanisms by which the action of AKT is impaired by ceramides: 1) increased protein phosphatase-2A (PP2A), and 2) PKCζ activation[354–357]. However, when Galbo et. al (date) inhibited PP2A in rats by using cantharidin and LB1, they found that inhibition of PP2A resulted in an acute worsening of IR, indicating that PP2A activity is actually required for insulin-stimulated glycogen synthesis. Similarly, other studies that increased hepatic PP2A activity confirmed that this phosphatase dephosphorylates sites on ChREBP, such as Ser$^{(196)}$, Thr$^{(666)}$ and Ser$^{(568)}$, which in turn promote the transcription of the lipogenic enzymes genes, such as ACC and FAS[358], and in fact worsened hepatic IR[359].

Alternatively, activation of CD36 via PKCζ has been proposed as a mechanism for ceramide-induced hepatic steatosis[360]. It is postulated that the upregulation of the fatty acid transporter promotes hepatic lipid accumulation. Alternatively links between ceramides, PKCζ activation, and activation of the NLRP3 inflammasome have been reported in the liver. Activation of the NLRP3 inflammasome has been linked to several inflammatory disorders and upregulation of other inflammatory markers such as ROS, TNFα and IL-8. However, the mechanism linking ceramides-NLRP3 are yet to be identified[361]. Thus, current understanding has been inconclusive and has failed to identify a clear molecular mechanism by which ceramides might be involved in the impairment of insulin action in hepatocytes.

2.13 Ketogenic diet (KD)

The KD is a dietary intervention designed to elevate and maintain blood ketone levels within 0.5 to 3 mg/dl[362–364]. This is achieved by drastically reducing dietary carbohydrate and by increasing the fat content while maintaining appropriate levels of protein in the diet. In this context, a

typical KD provides 5-10% of its energy from carbohydrates (usually 20-50 g of carbohydrates per day), 20% from protein (~1-1.5 g/kg/day), and the remaining 70-80% of its energy content from fat[365,366].

There are three ketone bodies synthesised by the hepatocytes, namely β-hydroxybutyrate (βHB), acetoacetate (AcAc) and acetone[24,367](**Figure 2.9**). Condensation of two acetyl-CoA molecules leads to the formation of AcAc, which is then released in the blood stream[368,369]. Further reduction of AcAc produces βHB, the most abundantly found ketone in the body[370,371]. Typical serum βHB levels range between 25-150 μM in a fed state and after fasting for 12-16 hours they rise up to 150-900 μM range[372,373]. Two days of fasting can elevate plasma ketone levels to 1-2 mM, whereas prolonged starvation can result in 6-8 mM circulating βHB levels[373,374]. Interestingly, infants are known to maintain serum βHB levels of 0.5-2.5 mM with just 8-10 h of fasting. In adults, similar βHB levels can be achieved after 90 min of intense exercise or by adopting a KD[373]. Once AcAc and βHB reach extra hepatic tissues, they are reversed back to acetyl-CoA, which is processed in the TCA cycle culminating in the production of energy (~22 ATP molecules) [375]. Acetone is a volatile product formed via decarboxylation of acetyl-CoA that can be eliminated from the body by breathing it out or via urination. In fact, the "fruity odour" in the breathe that some people experiment after consuming a KD may be attributed to acetone being released as a result of ketosis[368,376]. In addition, it should be noted that the threshold for entering a ketogenic state is subjective. The production of ketone bodies is orchestrated by a sophisticated and well-integrated biochemical and hormonal complex and may vary based on how intense and prolonged the ketogenic stimulus is, sometimes reaching pathologic levels such as diabetic ketoacidosis[364,377].

2.13.1 Ketone synthesis, transport, and utilization

Ketogenesis mainly occurs in the liver and only to a small extent in other tissues in the body[378]. Ketogenesis is initiated by the condensation of two acetyl-CoA molecules via a reversible reaction that is catalyzed by acetoacetyl-CoA thiolase (AcAcT) to form acetoacetyl-CoA[379]. The latter condenses with another acetyl-CoA to form β-Hydroxy β-methylglutaryl-CoA (HMG-CoA)[378]. Finally, AcAc is formed by cleaving off the acetyl-CoA from HMG-CoA by the lysis action of HMG-CoA lyase (HMGCL). Further βHB is formed by the enzymatic action of β-hydroxybutyrate dehydrogenase (BDH1) on AcAc[380]. Both, βHB and a small fraction of AcAc are then transported out of the liver into the blood stream via the monocarboxylate transporter SLC16A6[380,381]. Similar monocarboxylate transporters (MCT1 and MCT2) exist on the surfaces for the brain and peripheral tissues to aid with the uptake of the ketones from the blood[378,379].

Ketone bodies are broken down in non-hepatocellular cells, especially in the heart, brain, and skeletal muscle via a process called ketolysis[368,378]. In the first step of ketolysis, βHB is oxidised back to AcAc by BDH1. Subsequently, 3-ketoacid coenzyme A transferase (OXCT1) catalyzes the donation of CoA to AcAc from succinyl-CoA to form acetoacetyl-CoA[378,382]. The absence of OXCT1 is responsible for preventing a futile cycle for the production and utilization of ketone bodies by the liver, making them available to be transported to other tissues in the body[368]. Finally, acetoacetyl-CoA and a free CoA are converted into two molecules of acetyl-CoA by AcAcT. Acetyl-CoA is used in the TCA cycle to produce ATP[378,382]. Interestingly, the catalytic action of AcAcT is down regulated when AcAc levels in circulation are higher than 5 mM, forming a feedback loop that is able to control the breakdown of ketone bodies[380].

2.14 Whole-body effects of a KD

The KD leads to effective weight loss and changes in body composition, making it an effective dietary intervention to target obesity and other related metabolic disorders. In fact, a 12-week study by Garbow et al. (2011) revealed that a KD attenuated weight gain and lean mass loss in C57BL/6J mice in comparison to chow-fed counterparts[313]. The KD diet used in the study comprised of 95.1% of calories from fat, 4.5% from protein, and negligible calories from carbohydrates[313]. Serum glucose levels were reduced and HOMA-IR and the quantitative insulin sensitivity check index (QUICKI) both showed lowered circulating insulin under fasted conditions. These findings suggested an improvement in insulin sensitivity in KD-fed mice[383,384].

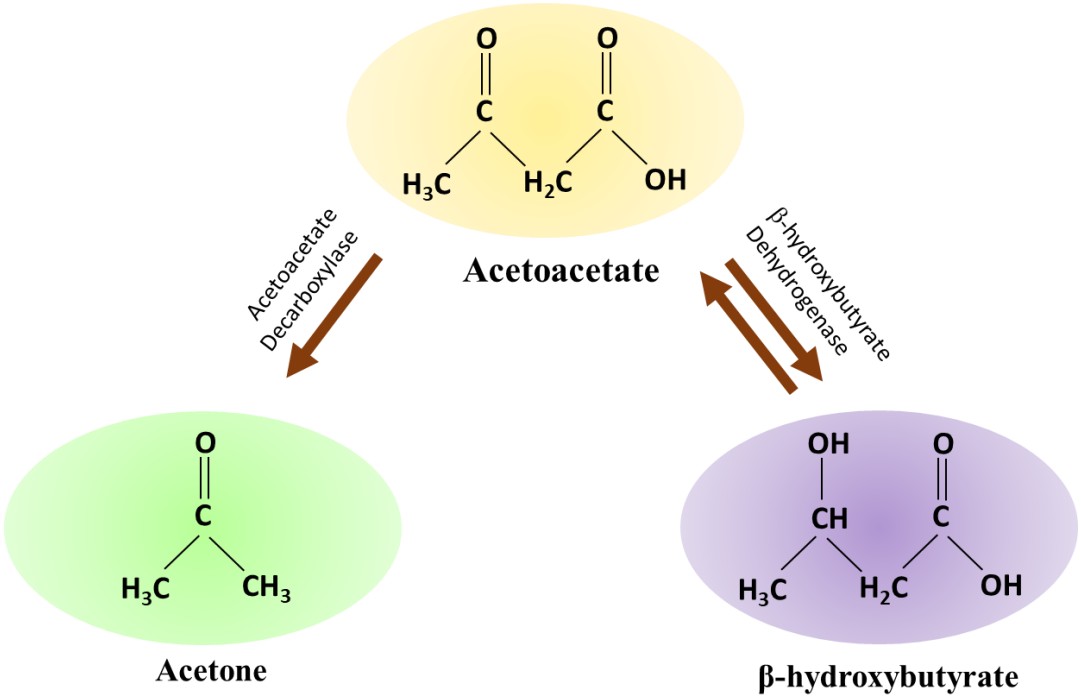

Figure 2.9: The chemical structure of ketone bodies. Acetoacetate (AcAc) is produced and utilized during intermediary metabolism and other ketone bodies are derived from it. Acetone is

produced by the spontaneous decarboxylation, whereas β-Hydroxybutyrate (βHB) is produced via the reduction of AcAc.

In mice fed the KD for a span of 80 weeks, weight loss occurred in the first 18 weeks of the study and then reached a plateau. However, in the end, KD-fed mice gained less weight and had reduced lean and fat masses. Moreover, these mice had increased energy expenditure and lowered insulin levels, which was indicative of improved insulin sensitivity[385]. In another study, sedentary and exercised (resisted voluntary wheel running) Sprague Dawley rats were fed a KD for 6 weeks and both groups of animals displayed lower body mass, plasma insulin, serum glucose, triglycerides, and total cholesterol levels[386]. In order to further understand the metabolic implications of a KD in the liver, hyperinsulinemic-euglycemic clamps were performed. It was found that despite being lighter and displaying increased whole-body energy expenditure, KD animals developed acute hepatic IR. Further investigation found that hepatic DAG content was also upregulated (3.5-fold) in KD fed animals, indicating the association between DAG accumulation causing PKCε activation followed by decreased phosphorylation of the insulin receptor substrate[387]. However, further research is required on specific organs and their adaptations to the diet, in order to make conclusive recommendations regarding the consumption of KD.

Chapter 3 Objectives and Hypothesis

Skeletal muscle, the body's biggest tissue, is essential for movement, glucose uptake, and its utilisation, as well as mediating the body's sensitivity to insulin. In fact, poor glucose metabolism and glycogen accumulation in skeletal muscle are the primary causes of the loss in insulin sensitivity that occurs decades before the onset of type 2 diabetes. Interestingly, ectopic lipid accumulation in the skeletal muscle has been linked to weakened insulin signaling, contributing to the reduced glucose uptake and insulin resistance in the tissue. Therefore, in the context of cellular lipid overload, a number of intermediates of incomplete fatty acid oxidation such as diacylglycerol (DAG), ceramides, have been identified as drivers of insulin resistance. Conversely, some findings have shown an increased lipid accumulation in endurance trained athletes suggesting that there was no connection between DAG or ceramides and insulin resistance [285]. As a result, it is currently unclear whether certain lipid species found in skeletal muscle cause insulin resistance. Further, skeletal muscles are made up of a variety of fibre types that exhibit fiber-type-specific adaptation responses to various physiological inputs. Slow-twitch type I fibres with many mitochondria have an oxidative metabolism, are resistant to fatigue, and

can be recognised by the expression of type I myosin heavy chain. In contrast, fast twitch type IIa, IIx/d, and IIb myofibers are characterised by the expression of fast myosin heavy chain isoforms, with a tendency to fatigue quickly, fewer mitochondria, and undergo glycolytic metabolism[104]. Thus, the distribution of fibre types in skeletal muscles may therefore have a significant influence in defining the tissue's vulnerability to insulin resistance. Furthermore, as most research has long been male-dominated, the role of biological sex on diet induced insulin resistance is unknown.

Another organ strongly associated with glucose clearance from the blood is the liver. Therefore, cases with excessive hepatic glucose production and compensatory hyperinsulinemia have been linked to the most common chronic liver disease, non-alcoholic fatty liver disease (NAFLD). Under conditions of overfeeding, increased insulin fails to suppress lipolysis in the adipose tissues, which leads to increased hepatic delivery of non-esterified fatty acids (NEFA), the main substrate for synthesis of intrahepatic triglycerides (IHTG)[388]. The increased insulin secretion stimulates re-esterification and DNL of fatty acids, which increases the IHTG content leading to advancement of NAFLD and pathogenesis of T2D. Recently, research has concentrated on a number of potential therapies due to the worrying rise in the prevalence of this disorder. Altering energy metabolism has been proposed as a possible treatment option. In particular, a very high-fat and extremely low-carbohydrate diet, known as the ketogenic diet. Essentially, the body becomes deprived of dietary sugar and starch, and reacts by reducing insulin secretion and switching to primarily burning fat for fuel. However, despite the potential benefits of KD on weight loss, and insulin sensitivity, the benefits of KD for liver stay controversial. There have been some contradictory reports suggesting KD could actually induce hepatic insulin resistance mediated by DAG activation of PKCε[389,390]. Therefore, the overall objective of this document is

to elucidate how manipulation of macronutrient content can alter glucose and lipid metabolism in oxidative and glycolytic skeletal muscles, and the liver.

Objectives:

1. To investigate whether the consumption of a HFS diet leads to enhanced fatty acid oxidation and if it affects intramyocellular content of lipid intermediates.
2. To assess how the intramyocellular accumulation of DAG, TAG and ceramides is altered in oxidative and glycolytic muscles of male rats fed a high-fat sucrose enriched diet, and how it affects the activation of specific PKC isoforms and insulin signaling in oxidative and glycolytic muscles.
3. To investigate whether the mechanisms underlying the development of skeletal muscle insulin resistance in rats fed a high-fat-high sucrose diet differs between males and females.
4. To assess if inflammation is similarly induced in oxidative and glycolytic muscles under conditions of diet-induced obesity.
5. To investigate whether the chronic consumption of high-fat diet devoid of carbohydrate can induces a metabolic shift that affects the liver content of DAG and ceramides, alters PKC activity, and maintains the ability of the liver to properly regulate whole-body glucose homeostasis.

Hypotheses:

1. Due to their high oxidative capacity, skeletal muscles rich in type I fibers will oxidize more fat and reduce the availability of substrate to form lipid intermediates. Conversely, skeletal muscles that are rich in type IIb/x fibers and have limited capacity to oxidate fat

will be more susceptible to lipotoxicity under conditions of elevated fatty acid abundance.

2. Because the accumulation of intramyocellular DAG, TAG, and ceramides would be reduced in oxidative as compared to glycolytic muscles in diet-induced obesity, the activation of DAG-sensing PKCs (PKCθ/δ) would also be lower in oxidative than glycolytic muscles.
3. Existing literature suggests that females display a higher number of type 1 muscle fiber type when compared to age- and weight-matched males. Because the amount of oxidative type I fibres has been associated to insulin sensitivity, we hypothesized that female skeletal muscles would be less susceptible to the development of insulin resistance than male skeletal muscles when exposed to an obesogenic diet.
4. Because lipotoxicity is associated with inflammation in skeletal muscles, we hypothesized that Sol and EDL muscles that are highly oxidative would display lower levels of inflammatory mediators, whereas the highly glycolytic Epit muscle would display upregulation of inflammatory mediators.
5. Because the KD lowers insulinemia and shifts metabolism towards fatty acid oxidation, we hypothesize that despite providing an abundant source of dietary fat, DAG and ceramides accumulation in the liver would be reduced and prevent cause a protective effect against insulin resistance and the development of hepatic steatosis.

Chapter 4

Distinct mechanisms involving diacylglycerol, ceramides, and inflammation underlie insulin resistance in oxidative and glycolytic muscles from high fat-fed rats

Authors: Shailee Jani[1], Daniel Da Eira[1], Ishvinder Hadday[1], George Bikopoulos[1], Arta Mohasses[1], Ricardo A. de Pinho[2], and Rolando B. Ceddia[1]

[1]Muscle Health Research Center – School of Kinesiology and Health Science, York University, North York, ON, Canada. [2]Graduate Program in Health Sciences, School of Medicine, Pontifícia Universidade Católica Do Paraná, Curitiba, Paraná, Brazil.

Abbreviated title: Insulin resistance in oxidative and glycolytic muscles

Key words: PKC, obesity, insulin resistance, cortisol, TNFα, TLR4, IL-6

A version of this manuscript has been published in Scientific Reports on 27th September 2021. (*The copyright policy of the journal automatically grants permission for authors to reproduce whole published articles without charge in dissertations and post to thesis repositories.)*

Jani, S., Da Eira, D. and Ceddia, R. Distinct mechanisms involving diacylglycerol, ceramides, and inflammation underlie insulin resistance in oxidative and glycolytic muscles from high fat-fed rats. *Scientific Reports*, (2021). https://doi.org/10.1038/s41598-021-98819-7.

Statement of Labour

The majority of the research experiments were conducted by Shailee Jani (SJ), including the administration of the high-fat sucrose-enriched diet (HFS), collection of blood samples, extraction of tissues, RNA extraction, real time PCR analysis, and metabolic assays. SJ was also responsible for conducting all western blots, data analysis, interpretation of results for DAG and ceramide content, preparation of figures, and manuscript preparation. Due to the logistics of this study, Daniel Da Eira assisted with administration of the HFS diet, collection, and extraction of tissues, as well as revising the manuscript. Ishvinder Hadday, George Bikopoulos, Ricardo A. de Pinho, and Arta Mohasses helped collecting whole-body parameters such as RER and circulation IL-6, NEFA and TNFα. The research was supervised by Dr. Rolando Ceddia and was funded by a Discovery Grant from NSERC and by infrastructure grants from the Canada Foundation for Innovation and the Ontario Research Fund.

4.1 Abstract

This study investigated whether oxidative and glycolytic rat skeletal muscles respond differently to a high-fat high-sucrose (HFS) enriched diet with respect to diacylglycerol (DAG) and ceramides accumulation, protein kinase C (PKC) activation, glucose metabolism, and the expression of inflammatory genes. HFS diet (8 weeks) suppressed insulin-stimulated glycogen synthesis and glucose oxidation in soleus (Sol), extensor digitorum longus (EDL) and epitrochlearis (Epit) muscles. However, DAG and ceramides levels increased in Sol and EDL, but not in Epit muscles of HFS-fed rats. Additionally, membrane-bound PKCδ and PKCθ increased in Sol and EDL, whereas in Epit muscles both PKC isoforms were reduced by HFS diet. In Epit muscles, HFS diet also increased the expression of tumor necrosis factor-α (TNFα) receptors (CD40 and FAS), toll-like receptor 4 (TLR4), and nuclear factor kappa light polypeptide gene enhancer in B cells (NF-kB), whereas in Sol and EDL muscles the expression of these inflammatory genes remained unchanged upon HFS feeding. In conclusion, HFS diet caused DAG and ceramides accumulation, PKC activation, and the induction of inflammatory pathways in a fiber type-specific manner. These findings help explain why oxidative and glycolytic muscles similarly develop insulin resistance, despite major differences in their metabolic characteristics and responsiveness to dietary lipid abundance.

4.2 Introduction

Besides encompassing a large proportion of total body mass[391], skeletal muscles have the capacity to store up to 1 to 2% of their weight in glycogen[392], accounting for the majority of whole-body glucose uptake and virtually the entire non-oxidative glucose metabolism[23]. In type 2 diabetes (T2D) patients, the insulin-mediated glucose disposal is reduced to about 50% of the

values of non-diabetic control subjects. Such reduction in glucose disposal is mainly due to impaired skeletal muscle glycogen synthesis[393]. Therefore, proper regulation of whole-body glucose homeostasis is dependent on the preserved ability of skeletal muscles to synthesize and store glycogen in response to insulin.

Several mechanisms have been proposed to explain the pathogenesis of obesity-induced insulin resistance in skeletal muscles. These include excessive intracellular accumulation of lipids[89,394,395], mitochondrial dysfunction and reduced oxidative capacity[396–398], elevated levels of inflammatory cytokines[89,399], and increased oxidative stress[153,154]. Although all of these have been associated with impaired insulin signalling and glucose metabolism, no single mechanism seems to explain how skeletal muscles with different metabolic characteristics develop insulin resistance under conditions of obesity[400]. From the perspective of lipotoxicity, the accumulation of lipid intermediates like DAG and ceramides and the activation of PKC have been implicated in insulin resistance by triggering pathways that lead to serine phosphorylation of IRS-1, thereby suppressing insulin-stimulated glucose metabolism[89,395]. Also, the activation of proinflammatory pathways by elevated production of reactive oxygen species (ROS) has been proposed as a mechanism by which increased oxidation of non-esterified fatty acids (NEFAs) leads to insulin resistance in skeletal muscles[154,399]. However, it has been reported that PKC content and activation, as well as ROS production associated with NEFA oxidation in rat skeletal muscles display fiber type-specific patterns[36,401]. In fact, the amount of PKCθ was 2.5 times higher in the white tensor fascia latae muscle compared with the red Sol muscle, with the mixed muscles vastus intermedius and plantaris having intermediate levels of this kinase[36]. It has also been reported that H_2O_2 emission rates in red Sol were much lower than in the mixed EDL and the white Epit muscles[401]. In this context, it is plausible that the mechanisms governing diet-induced

insulin resistance vary depending on the fiber type composition of various skeletal muscles. This is particularly relevant if one considers that in diet-induced obesity, insulin resistance develops in all muscles, despite their variability in fiber type distribution. Thus, it may be that, under obesogenic conditions, DAG-mediated PKC activation leads to impaired insulin signalling and glucose metabolism in oxidative muscles, whereas the presence of elevated circulating inflammatory cytokines and the ability to respond to them and to other endocrine/metabolic factors could be the main determinants of insulin resistance in glycolytic muscles.

Obesity is indeed characterized by a state of low-grade inflammation in which TNFα, interleukin-1β (IL-1β), and interleukin-6 (IL-6)[399] are chronically elevated. Furthermore, insulin resistance has been associated with hyperactivity of the hypothalamic-pituitary adrenal axis and excess circulating glucocorticoids in animal models of obesity[402–404], whereas treatment of rats with an anti-glucocorticoid drug ameliorated HFS diet-induced skeletal muscle insulin resistance[405]. These observations provide support to the idea that circulating factors (e.g., inflammatory cytokines and hormones) and altered intramuscular lipid metabolism, either independently or in combination, determine the pathophysiology of obesity-induced skeletal muscle insulin resistance. To test this hypothesis, we measured insulin-stimulated glycogen synthesis and glucose oxidation, DAG and ceramides content, membrane-associated PKCδ and PKCθ levels, and the expression of inflammatory genes in slow- and fast-twitch skeletal muscles extracted from rats exposed for 8 weeks to a HFS diet. This study provides evidence that the accumulation of DAG and ceramides, PKCδ and PKCθ activation, as well as the expression of inflammatory genes and glucocorticoid receptor (GR) differ significantly between highly oxidative and highly glycolytic skeletal muscles under conditions of HFS diet-induced

obesity. The findings support that HFS feeding causes impairment of glucose metabolism in predominately slow- or fast-twitch rat muscles through distinct mechanisms.

4.3 Materials and Methods

Reagents – Fatty acid (FA)-free bovine serum albumin (BSA), glycogen, and palmitic acid were obtained from Sigma (St. Louis, MO, USA). Diolein was from Nu-check (Elysian, MN, USA). Human insulin (Humulin R) was purchased from Eli Lilly Inc. (Toronto, ON, Canada). The insulin ELISA kit was from Millipore (Billerica, MA, USA). The Corticosterone RIA kit was from ALPCO Diagnostics (Salem, NH, USA). The TNF-α and IL-6 ELISA kits were from Invitrogen (Montreal, QC, Canada). The NEFA kit was from Wako Chemicals (Richmond, VA, USA). N-Acetyl-D-sphingosine was from Sigma. The RNeasy Kit was from Qiagen Inc. (Toronto, ON, Canada) and the DNase from Thermo Fisher (Toronto, ON, Canada). D-[U-^{14}C] glucose and [1-^{14}C] palmitic acid were from GE Healthcare Radiochemicals (Quebec City, QC, Canada). The reverse phase column (C18 5 μm 250 x 4.6 mm) was from Restek (Bellefonte, PA, USA). The subcellular protein fractionation Kit was from Thermo Fisher (Cambridge, MA, USA). The PKCθ (cat # 13643), PKCδ (cat # 9616), Na,K-ATPase (cat # 3010), and the GAPDH (cat # 2118) antibodies were from Cell Signalling Technology Inc. (Beverly, MA, USA).

Animals – Male albino rats from the Wistar strain (Charles River Laboratories, Montreal, QC, Canada) weighing 200 – 250 g (initial weight) were maintained in a constant-temperature (23 ^{o}C), with a fixed 12-h light/12-h dark cycle and fed for 8 weeks *ad libitum* either a standard rat chow (Control, 27.0 %, 13.0 %, and 60.0 % of calories provided by protein, fat, and carbohydrates, respectively, energy density 3.43 kcal/g) or a HFS diet (20.0 %, 60.0 %, and 20.0

% of calories provided by protein [casein], fat [lard/soybean oil], and carbohydrates [sucrose], respectively, energy density 5.24 kcal/g)[401]. The control diet (standard rat chow, catalog # 5012) was purchased from TestDiet (Richmond, IN, USA). The HFS diet (catalog # D12492) was purchased from Research Diets Inc. (New Jersey, NJ, USA).

Ethics approval – The protocol containing all animal procedures described in this study was specifically approved by the Committee on the Ethics of Animal Experiments of York University (York University Animal Care Committee, YUACC, permit number: 2021-03) and performed strictly in accordance with the YUACC guidelines. All tissue extraction procedures were performed under ketamine/xylazine anesthesia, and all efforts were made to minimize suffering[401]. All experiments in this study were carried out in compliance with the ARRIVE guidelines[406].

Determination of corticosterone, TNFα, IL-6, and NEFAs in the serum – Blood from all animals was collected in the fed state between 09:00 and 10:00 by saphenous vein bleeding and the serum was used to determine plasma corticosterone, TNFα, IL-6, and NEFAs using commercially available kits listed in the reagents section. All procedures were performed according to instructions provided by the manufacturers of the kits.

Whole-body fat oxidation – At the end of the 8-week-diet-intervention period, all animals were placed in the comprehensive laboratory animal monitoring system (CLAMS) as previously described [407]. The CLAMS from Columbus Instruments (Columbus, OH, USA) perform automated *in vivo* determinations of oxygen consumption (VO_2), carbon dioxide production (VCO_2), and respiratory exchange ratio (RER). The animals were placed in the CLAMS at 12:00 and the first hour of data collected in the CLAMS was discarded, since it is the time

required for the rats to fully acclimatize to the cage environment [407]. The rats were monitored for a 24 h period encompassing the light (07:00 – 19:00 h) and dark (19:00 – 07:00 h) cycles.

Muscle isolation and incubation – All animals were anesthetized with a single intraperitoneal injection of ketamine/xylazine (90 mg and 10 mg/100 g B.W., respectively). Subsequently, Sol, EDL, and Epit muscles were quickly extracted. These muscles were chosen because of their wide range of reported fiber-type distributions with distinct mitochondrial contents and oxidative capacities. The percentages of type I, type IIa, and type IIb in Sol, EDL, and Epit muscles are 84/16/0, 3/57/40 [408], and 15/20/65 [409], respectively. Three sets of muscle strips (18 – 22 mg) were mounted onto thin stainless steel wire clips to maintain optimal resting length, and immediately placed in plastic scintillation vials containing 2 ml of pre-gassed [30 min with O_2:CO_2-95:5 % (vol/vol)] Krebs-Ringer bicarbonate (KRB) buffer containing 4 % fat-free BSA and 6 mM glucose. The vials were sealed with rubber stoppers and gasification was continued for the entire 1h pre-incubation period. One set of muscles was then transferred to vials containing 2 ml of the same KRB buffer plus D-[U-^{14}C]glucose (0.2 µCi/ml) and incubated under continuous gasification for one additional hour either in the absence (basal) or presence of insulin (100 nM) for the determination of glycogen synthesis [410]. For the assessment of glucose oxidation, a centered isolated well containing a loosely folded piece of filter paper moistened with 0.2 ml of 2-phenylethylamine/methanol (1:1, vol/vol) was inserted into the flasks where the muscles were incubated. After the 1h incubation period, the muscles were removed, and the media were acidified with 0.2 ml of H_2SO_4 (5N). The flasks were maintained sealed at 37 °C for an additional 1h for collection of the $^{14}CO_2$ released. Subsequently, the filter papers were carefully removed and transferred to scintillation vials for radioactivity counting.

Measurement of glycogen synthesis in isolated muscles – Glycogen synthesis was assessed by measuring the incorporation of D-[U-^{14}C]glucose into glycogen as previously described [410]. Briefly, immediately after incubation, muscle strips were quickly washed in ice-cold PBS, blotted on filter paper, frozen (N_2), and digested in 0.5 ml of KOH 1M at 70 ^{o}C for 1h. Of the digested muscle solution, aliquots were taken for the determination of glycogen synthesis. Glycogen was precipitated overnight (-20 ^{o}C) with 100 % ethanol, resuspended in 0.5 ml of water, and its radioactivity was determined using a scintillation counter.

Measurement of palmitate oxidation in isolated muscles – Palmitate oxidation was measured by assessing the production of $^{14}CO_2$ from [1-^{14}C] palmitic acid. The flasks where muscle strips were incubated contained 2 ml of KRB buffer plus 0.2 mM of cold palmitic acid previously complexed with FA free BSA and [1-^{14}C] palmitic acid (0.2 µCi/ml). The muscles were incubated under continuous gasification for 1h and the vials had a centered isolated well containing a loosely folded piece of filter paper moistened with 0.2 ml of 2-phenylethylamine/methanol (1:1, vol/vol). After the 1h-incubation period, the muscles were quickly removed and the media were acidified with 0.2 ml of H_2SO_4 (5N), and the flasks were maintained sealed at 37 °C for an additional 1h for collection of the $^{14}CO_2$ released. Subsequently, the filter papers were carefully removed and transferred to scintillation vials for radioactivity counting [411].

Determination of DAG and ceramides contents* in *Sol, EDL, and Epit muscles – The ultra-high-pressure liquid chromatography system (UHPLC-UV, Nexera X2, Shimadzu, Kyoto, Japan) was used to measure total amounts of DAG in lipid samples extracted from Sol, EDL, and Epit muscles using the Folch's method [412]. Briefly, 150 mg of muscle tissue were

homogenized in 200 µl of chloroform:methanol (MeOH) [2:1 vol/vol], dried overnight under nitrogen gas, and resuspended in 100 µl of 2-propanol-hexane (ProHex, 5:4 vol/vol) prior to chromatographic analysis. Quantification was performed using the UHPLC-UV detection machine. Sample volumes (50 µl) were injected automatically into a reverse phase column (C18 5 µm 250 x 4.6 mm). The chromatography conditions were set to 40 °C for 20 min using a gradient of MeOH and ProHex:100% of MeOH from 0 to 10 min, followed by 50% of MeOH and 50% of ProHex for 10 min, maintained with isocratic elution for 10 min. Diolein (0.25 µg/µl) were also dissolved in ProHex and quantified to obtain a standard curve [413]. To analyse total ceramide content, a small volume of the lipid extract obtained after chloroform extraction was transferred into new pre-weighed eppendorfs as previously described [414]. The organic phase was hydrolyzed in 1M KOH at 90 °C for 60 min. The sphingosine liberated from ceramides was analyzed by means of UHPLC by mixing it with 15µl OPA reagent and allowing it to derivatize for 20 min at room temperature. The calibration curve was prepared using N-Acetyl-D-sphingosine as a standard. The samples were reconstituted in 100 µl of chloroform-methanol-acetic acid-water (50:37.5:3.5:2 vol/vol/vol/vol) and run through a porous silica column (ARC-18 1.8 µm 100 x 2.1 mm). Elution was conducted with heptane-isopropyl ether-acetic acid (60:40:3 vol/vol/vol) at a gradient from 0 to 10 % in 30 min at a flow rate of 0.8 ml/min followed by isocratic elution with acetonitrile: deionized distilled water (90:10, vol/vol) and a flow rate of 1 ml/min [240]. Subsequently, the column was equilibrated with chloroform-methanol-acetic acid-water (50:37.5:3.5:2 vol/vol/vol/vol) for 10 min at the same flow rate.

Tissue fractionation and Western blotting analysis of PKCδ and PKCθ content and cellular localization in Sol, EDL, and Epit muscles – PKCδ and PKCθ protein levels were determined

in the cytosolic and membrane fractions by immunoblotting with each respective PKC-specific antibody. Muscle homogenates (50 mg) were used to attain the cytoplasmic and membrane protein fractions using a fractionation kit. The separated fractions were then collected, and respective aliquots were used to measure the protein content by the Bradford method. Samples were then diluted 1:1 (vol/vol) with 2x Laemmli sample buffer, heated to 95 °C for 5 min, and subjected to SDS-PAGE. PKCδ and PKCθ-specific antibodies (1:2,000 dilution) were used determine the subcellular localization of these proteins.

Quantitative PCR analysis **–** Total RNA was isolated from skeletal muscles using the RNeasy kit, followed by DNase treatment in order to remove genomic DNA carry-over. Primers were designed using the software PrimerQuest (IDT) based on probe sequences available at the Affymetrix database (NetAffix Analysis Center, http://www.affymetrix.com/analysis) for each given gene. Real-time PCR reactions were carried out at amplification conditions as follows: 95°C (3 min); 40 cycles of 95°C (10 s), 65 °C (15 s), 72 °C (20 s); 95 °C (15 s), 60 °C (15 s), 95 °C (15 s). Quantitative PCR was performed using the CFX96 Real-time system from Bio-Rad. All genes were normalized to the control gene TBP, and values are expressed as fold increases relative to control. Primers sequences utilized are shown in Table 4.1.

Table 4.1**:** *Primer sequences used for qPCR analysis*

Gene	Forward	Reverse
Fas	TGGCTGTGTTCTGGACTTAAA	GTATCCCTGCTCATGATGTCTAC
Cd40	AGATTATCCCGGTCACAACAC	CTGAGATGCGACTCTCTTTACC
Tlr4	ACCTAAGGAGAGGAGGCTAAG	GGTAACTGCAGCACACTACA
Nf-κb	TCCAGCTGCTATTGGATTACAC	GGGACTGCGATACCTTAATGAC

Gr	GAAGGGAACTCCAGTCAGAAC	AATGTCTGGAAGCAGTAGGTAAG
11β-Hsd1	CTCCACTTCTGCTTGGGAAT	CTCAGGAGTTCCTAGTTGCTTAC
Tbp	TACAGGTGGCAGCATGAAGTGACA	AACCAACAATCACCAGCAGCAGTG

Statistical Analyses – Data were expressed as Mean ± SE. Statistical analyses were performed by using Two-way ANOVA with Tukey-Kramer multiple comparison post-hoc test or *t*-tests as indicated in the figure legends. Parametric tests selected for statistical significance were based on normality tests performed on the data. The GraphPad Prism software version 9.1.12 was used for all statistical analyses and for the preparation of all graphs. The level of significance was set to $p<0.05$.

4.4 Results

Body weight and NEFAs – Both groups of animals progressively increased body weight during the study-period, although the rate of weight gain was significantly higher in HFS-fed than control rats. In fact, HFS-fed rats weighed 6.6 % and 8.2 % more than controls after 4 and 8 weeks of diet intervention, respectively (Table 4.2). Time-course analysis of circulating NEFAs in the fed state revealed that this parameter did not differ between control and HFS rats (Table 4.2).

Table 4.2: *Time-course alterations in body weight and circulating NEFAs in SC and HFS-fed rats.*

		Duration of the study (Weeks)			
		0	2	4	8
Body weight (g)	SC	231.89 ± 2.98	290.63 ± 4.02	383.26 ± 5.87	501.80 ± 11.46
	HFS	233.95 ± 3.84	298.21 ± 4.51	408.37 ± 5.94*	543.08 ± 7.43$^{\#}$
NEFAs (mM)	SC	0.343 ± 0.037	0.309 ± 0.017	0.376 ± 0.028	0.414 ± 0.052
	HFS	0.372 ± 0.032	0.373 ± 0.025	0.418 ± 0.036	0.483 ± 0.041

*P<0.05 vs. SC 4 weeks; $^{\#}$p<0.05 vs. SC on 8 weeks. n=10

IL-6, TNFα, and corticosterone – At week 8 of the dietary intervention, HFS-fed rats also had circulating IL-6, TNF-α, and corticosterone elevated by 2.75-fold (Figure 4.1 A), 4-fold (Figure 4.1 B), and 2.8-fold (Figure 4.1 C), respectively, when compared to control SC-fed rats.

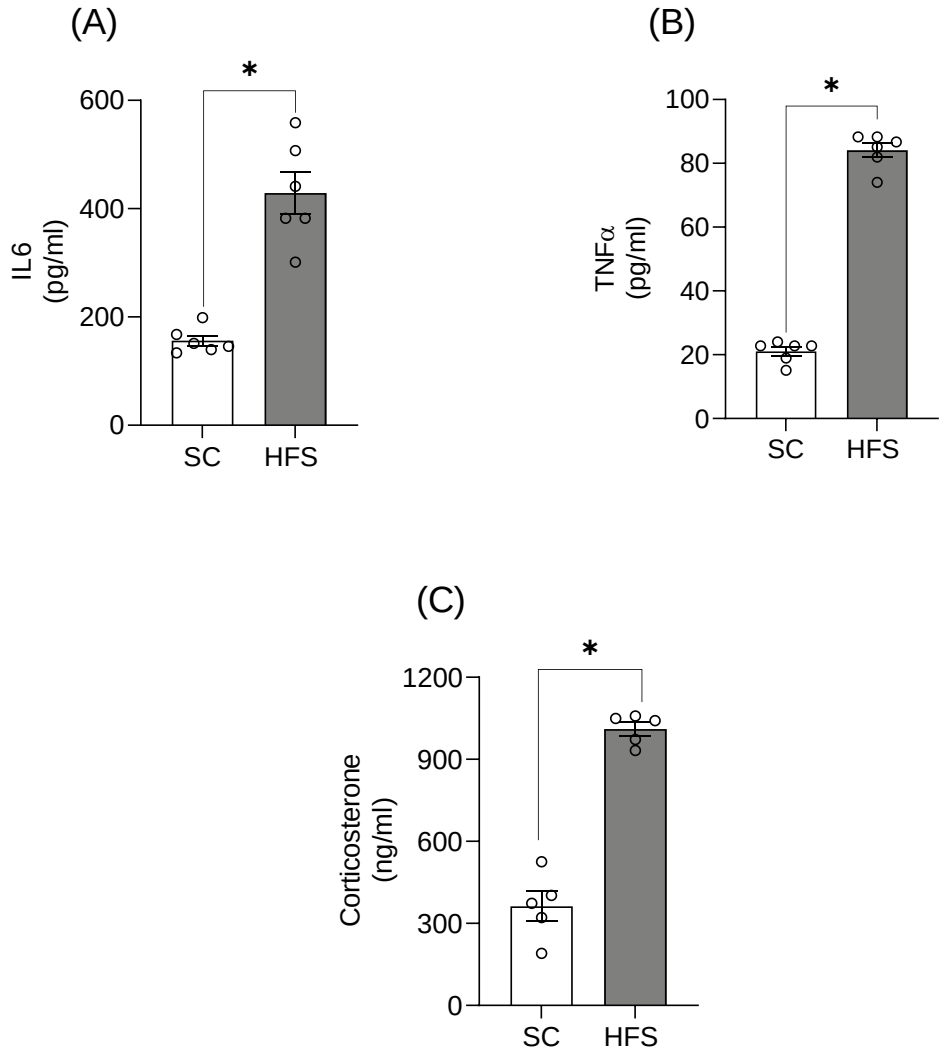

Figure 4.1: Circulating IL-6 (A), TNF-alpha (B), and corticosterone (C) are increased after 8 weeks of HFS feeding in comparison SC feeding. *p<0.05 vs. SC, t-test, n=5-6.

Glycogen synthesis and glucose oxidation in Sol, EDL, and Epit muscles – Glycogen synthesis was similar in Sol and Epit muscles of control and HF-fed rats under basal conditions. In contrast, EDL muscles from HFS rats showed lower rates of glycogen synthesis under basal conditions when compared to controls. As expected, insulin-stimulated rates of glycogen synthesis increased by 3.68-fold in Sol (Figure 4.2 A), 1.75-fold in EDL (Figure 4.2 B), and 1.97-fold in Epit (Figure 4.2 C) muscles of control rats; however, this variable was significantly reduced in all three muscles of HFS rats. In the presence of insulin, glucose oxidation was also increased by 1.41-fold in Sol (Figure 4.2 D), 1.57-fold in EDL (Figure 4.2 E), and 1.57-fold in Epit (Figure 4.2 F) muscles of SC rats, whereas in all three muscles from HFS rats, insulin-stimulated glucose oxidation was potently suppressed. These findings indicate that Sol, EDL, and Epit muscles similarly developed impaired insulin-stimulated glucose metabolism upon HFS feeding.

RER and palmitate oxidation – RER averaged 0.955 ± 0.003 and 0.824 ± 0.009 for control and HFS rats, respectively (Figure 4.3 A), indicating that the latter significantly increased whole-body fat oxidation. Also, as expected, rates of palmitate oxidation in SC-fed rats were much higher in soleus and EDL than Epit muscles (Figure 4.3 B). In HFS-fed rats, rates of palmitate oxidation followed a similar pattern and significantly increased in all muscles, reaching values 1.66-, 1.83-, and 1.59-fold higher than Sol, EDL, and Epit muscles from SC-fed rats, respectively (Figure 4.3 B). Thus, our findings indicate that energy substrate partitioning was shifted towards fatty acid oxidation in HFS-fed rats.

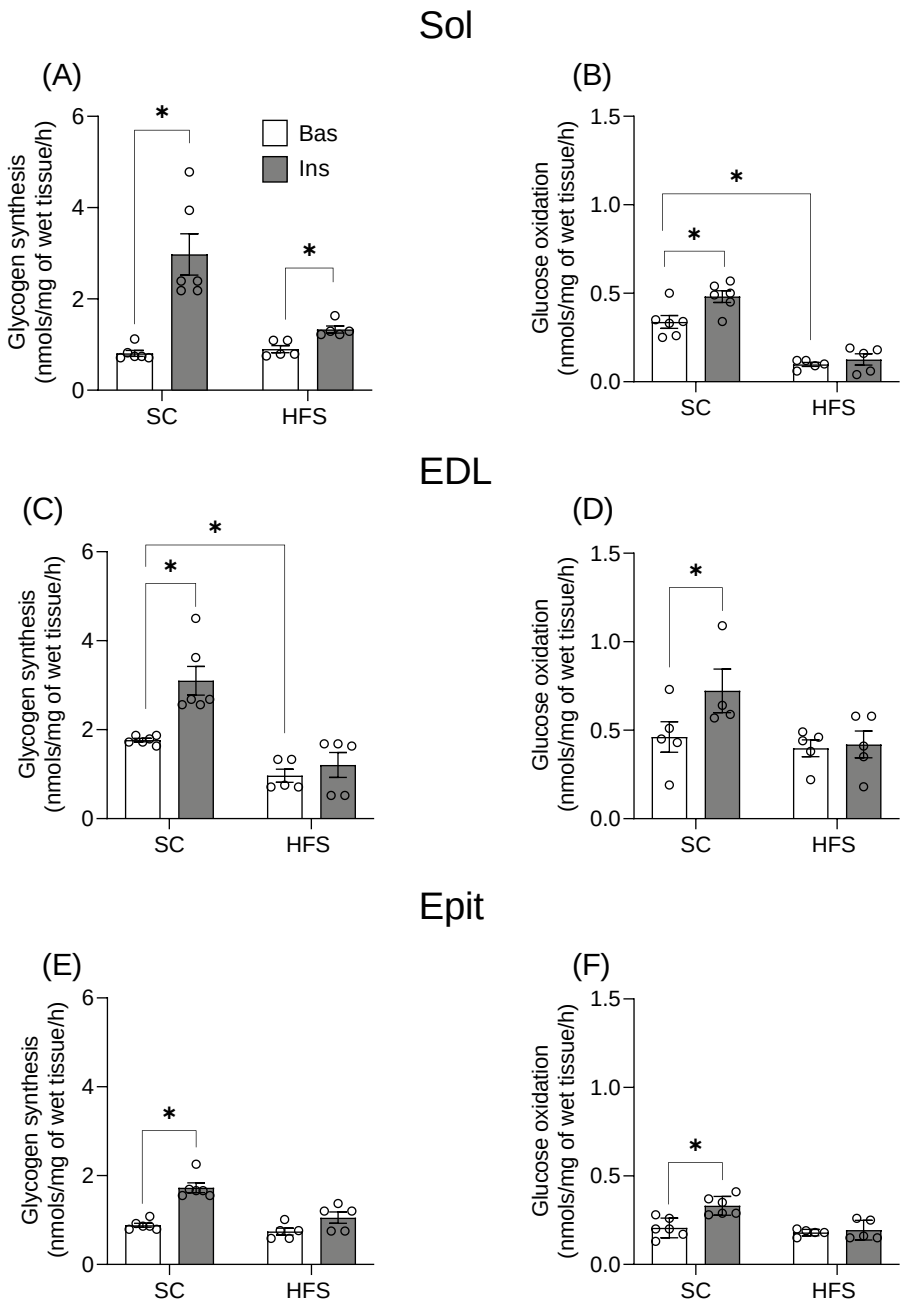

Figure 4.2: HFS diet inhibits insulin-stimulated glycogen synthesis (A, C, and E) and glucose oxidation (B, D, and F) in Sol, EDL, Epit rat muscles. Distinct letters denote statistical significance ($p<0.05$), Two-way ANOVA, n=5-6.

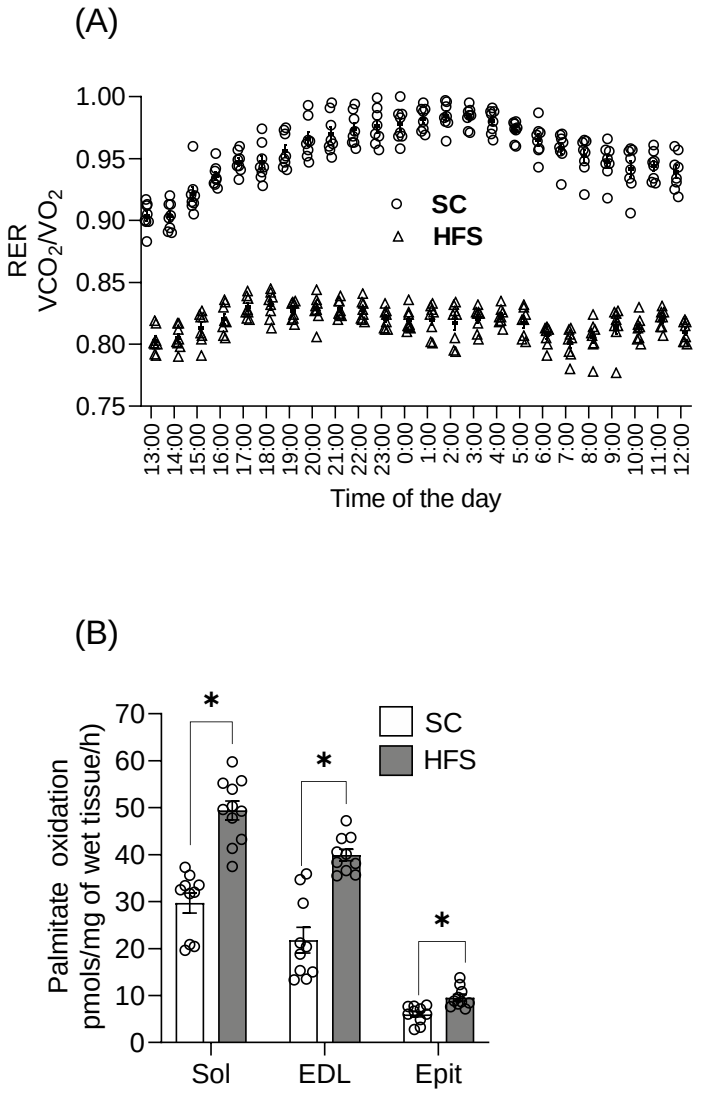

Figure 4.3: HFS diet increases whole-body (A) and skeletal muscle (B) fat oxidation. Strips of Sol, EDL, and Epit muscles from SC and HFS-fed rats were assayed for 14CO2 production from 14C-palmitic acid at week 8 of the study. Twenty four-hour RER was measured at week 8 of the study. Palmitate oxidation and RER are presented as average ± SEM. Distinct letters denote statistical significance ($p<0.05$), Two-way ANOVA, n=8-11.

DAG and ceramides contents in Sol, EDL, and Epit muscles – In SC-fed rats, DAG content was highest in EDL (1.63 ± 0.23 μg/mg of tissue) followed by Sol (1.06 ± 0.12 μg/mg of tissue) and Epit (0.24 ± 0.03 μg/mg of tissue) muscles (Figure 4.4 A). HFS feeding significantly increased DAG content by 1.74- and 1.93-fold in EDL and Sol, respectively, whereas in Epit muscles this variable did not significantly differ between SC and HFS animals (Figure 4.4 A). In SC-fed rats, ceramides content was also highest in EDL (0.26 ± 0.08 μg/mg of tissue), although no significant differences were found between Sol (0.14 ± 0.05 μg/mg of tissue) and Epit (0.10 ± 0.03 μg/mg of tissue) muscles (Figure 4.4 B). Upon HFS feeding, ceramides content in EDL and Sol muscles significantly increased by 3.66- and 4.46-fold, respectively. In Epit muscles from HFS-fed rats, ceramides content was 2.67-fold higher than in Epit muscles from SC-fed rats, however, it did not reach statistical significance (Figure 4.4 B). These findings indicate that muscles displaying higher rates of fatty acid oxidation not only were richer in DAG and ceramides, but also accumulated higher amounts of these intermediary lipids upon HFS feeding.

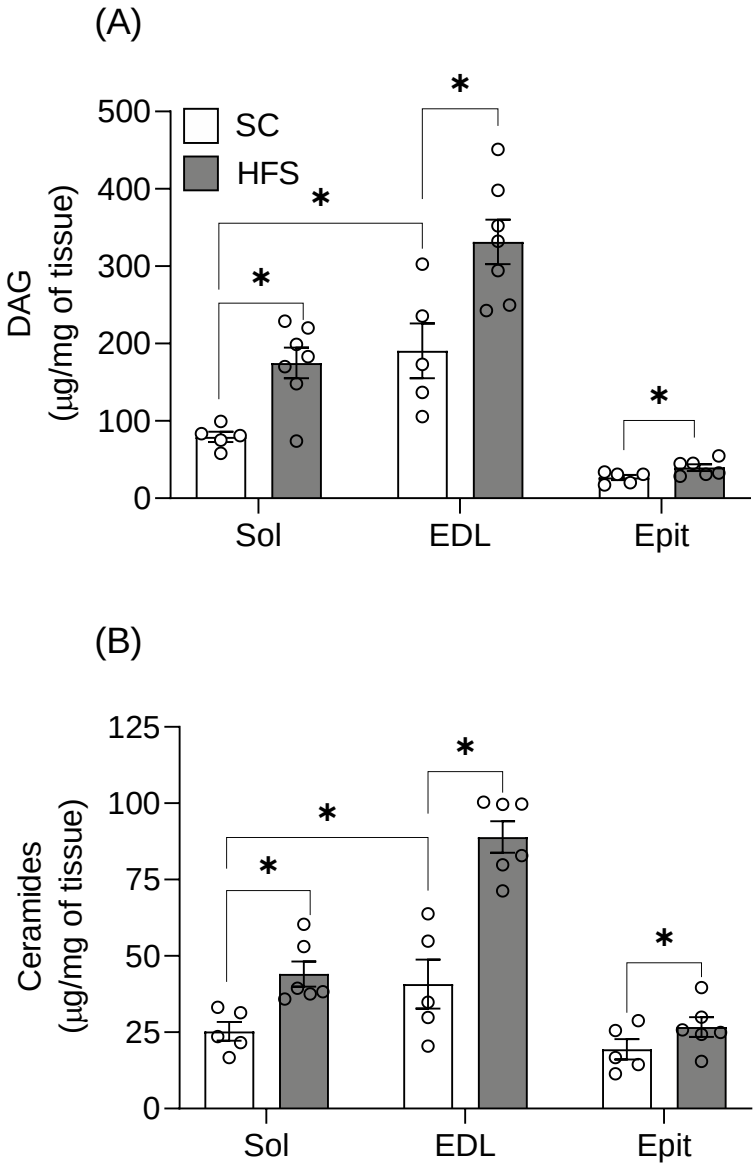

Figure 4.4: DAG (A) and ceramides (B) levels increase in Sol and EDL, but not in Epit rat muscles after 8 weeks of feeding a HFS diet. Distinct letters denote statistical significance ($p<0.05$), Two-way ANOVA, n=5-6.

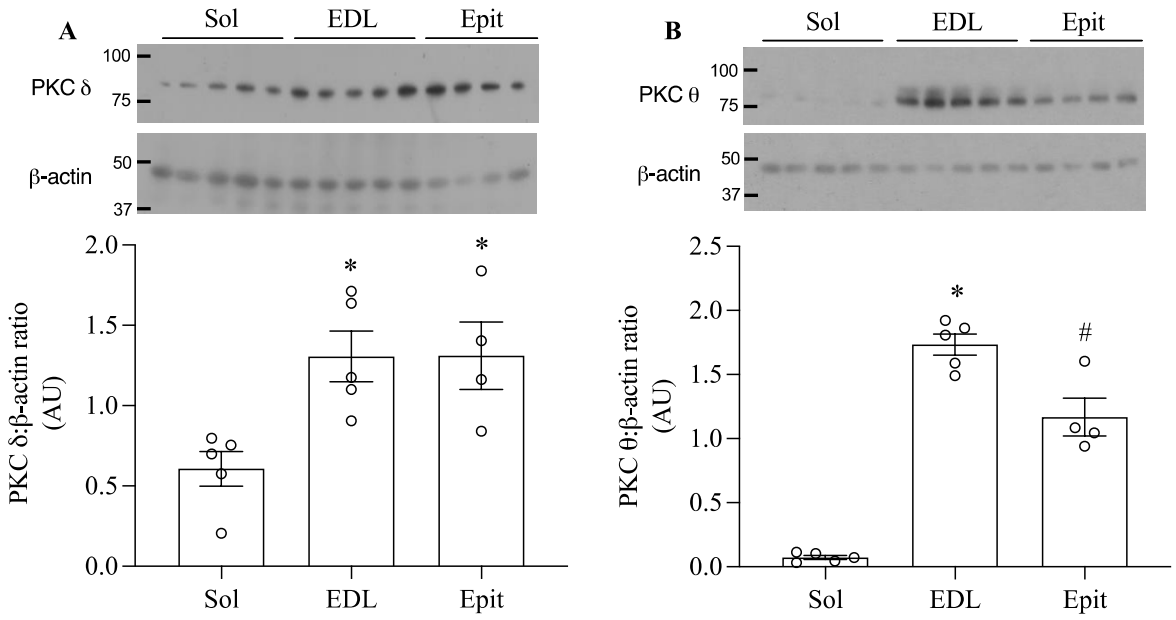

Figure 4.5: Higher levels of PKCδ (A) and PKCθ (B) in EDL and Epit than in Sol muscles. Densitometric analyses show arbitrary units (AU) for PKCδ and PKCθ levels divided by β-actin. *$p<0.05$ vs. Sol, #$p<0.05$ vs. Sol and EDL, One-way ANOVA, n= 4-5.

PKCδ and PKCθ content and localization in Sol, EDL, and Epit muscles – PKCθ is recognized as the dominant isoform of DAG-sensing PKCs in skeletal muscles [415]. However, PKCδ displays the highest sequence similarity (67 %) to PKCθ [416] and it has been shown to translocate to the membrane [417] and regulate insulin sensitivity and skeletal muscle metabolism [418]. Thus, in this study we measured levels of these two PKC isoforms in Sol, EDL, and Epit muscles. We found that PKCδ levels were similar between EDL and Epit, whereas in Sol its levels were approximately half of those of EDL and Epit muscles (Figure 4.6 A). These differences were even bigger for PKCθ, with its levels in Sol muscles being only 4 % and 6 % of those of EDL and Epit muscles, respectively (Figure 4.6 B). Translocation of PKCδ and PKCθ from cytosol to plasma membrane, reflecting PKC activation, was determined by

measuring the membrane/cytoplasm ratios of both PKC isoforms. First, the densitometric values of the PKC membrane and cytoplasm blots were normalized by the densitometric values of Na,K-ATPase and GAPDH, respectively. The normalized values for the membrane fractions were then divided by their respective normalized cytoplasm fractions. In HFS-fed Sol and EDL muscles, the membrane/cytoplasm ratios for PKCδ were significantly increased by 26.9- and 2.77-fold, respectively (Figure 4.6 A and B), whereas for PKCθ, only the HFS-fed Sol muscle had the membrane/cytoplasm ratio significantly elevated (1.68-fold) in comparison to SC-fed muscles (Figure 4.6 D and E). Conversely, Epit muscles from HFS-fed rats displayed 34 % and 24 % lower membrane/cytoplasm ratios than SC muscles for PKCδ and PKCθ, respectively (Figure 4.6C and F). These findings indicate that HFS diet increased PKC activity in Sol and EDL muscles and reduced the activity of this kinase in Epit muscles.

mRNA expression of inflammatory mediators, glucocorticoid receptor (GR), and 11β-hydrohysteroid dehydrogenase type 1 (11β-HSD1) – Quantitative PCR analysis revealed that the mRNA levels of *Cd40* and *Fas, Tlr4, and Nf-κb* were not altered in Sol and EDL muscles of HFS rats (Figure 4.7 A and B). Only the mRNA expression of the *GR* was significantly increased (~2.5-fold) in EDL muscles of HFS rats when compared to SC-fed controls (Figure 4.7B). However, in Epit muscles form HFS rats, the mRNA expression of *Cd40*, *Fas, Tlr, GR,* and *11β-HSD1* significantly increased by 1.8-fold, 2.1-fold, 2.6-fold, 2.0-fold, 3.6-fold, and 3.7-fold, respectively (Figure 4.7 C). Thus, a clear distinct fiber-type pattern of expression for inflammatory markers and *GR* was detected upon HFS feeding.

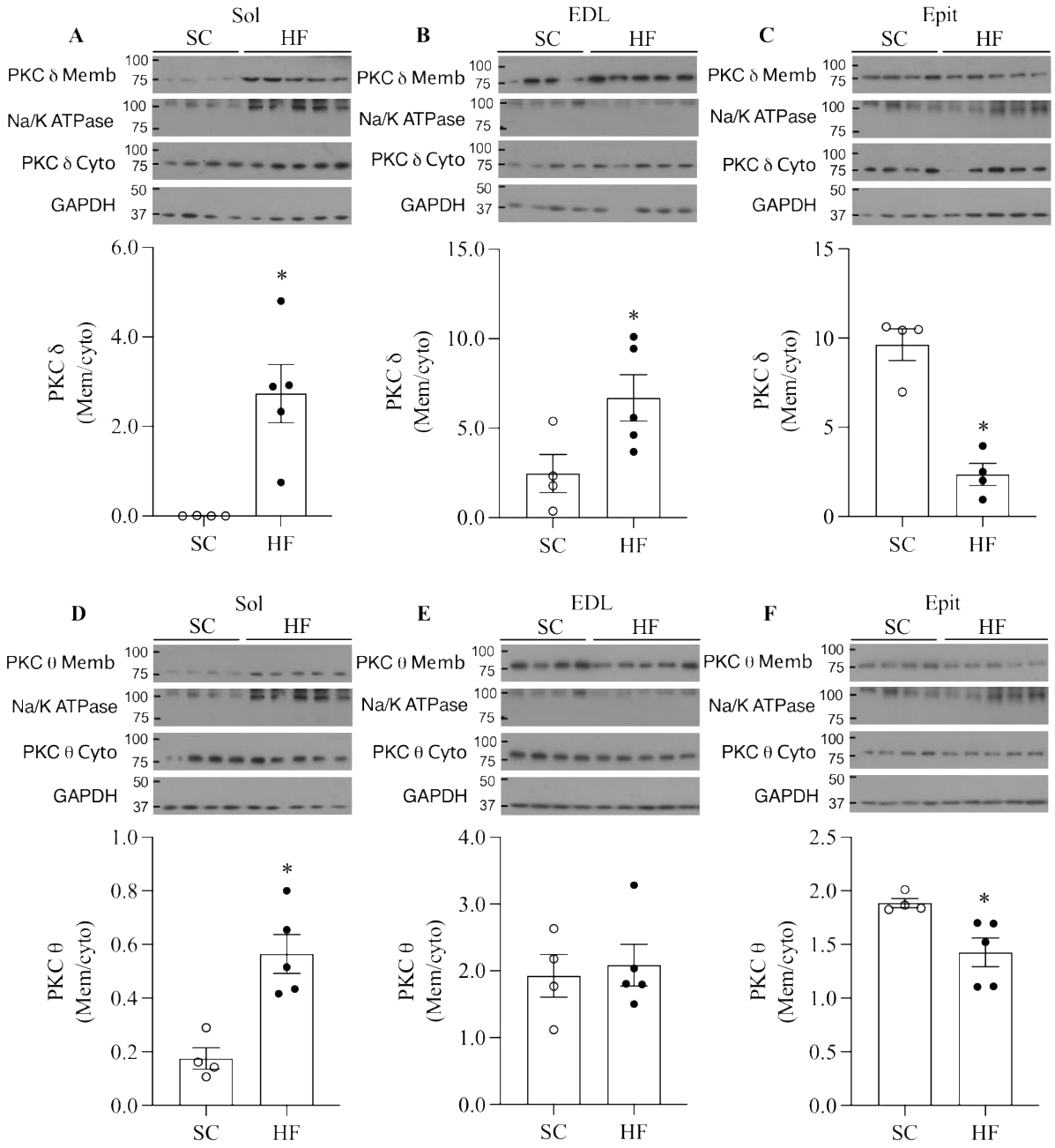

Figure 4.6: Distinct effects HFS diet on PKC translocation towards the membrane in Sol, EDL, and Epit muscles. Representative blots and densitometric analyses of PKCδ normalized by Na, K-ATPase, and GAPDH (A, B, and C) and PKCθ normalized by Na,K-ATPase, and GAPDH (D, E, and F) levels in membrane (Mem) and cytoplasmic (Cyto) cellular fractions.

Densitometric analyses show PKC δ and θ ratios (mem/cyto) as an index of activation. *p<0.05, t-test, n= 4-5.

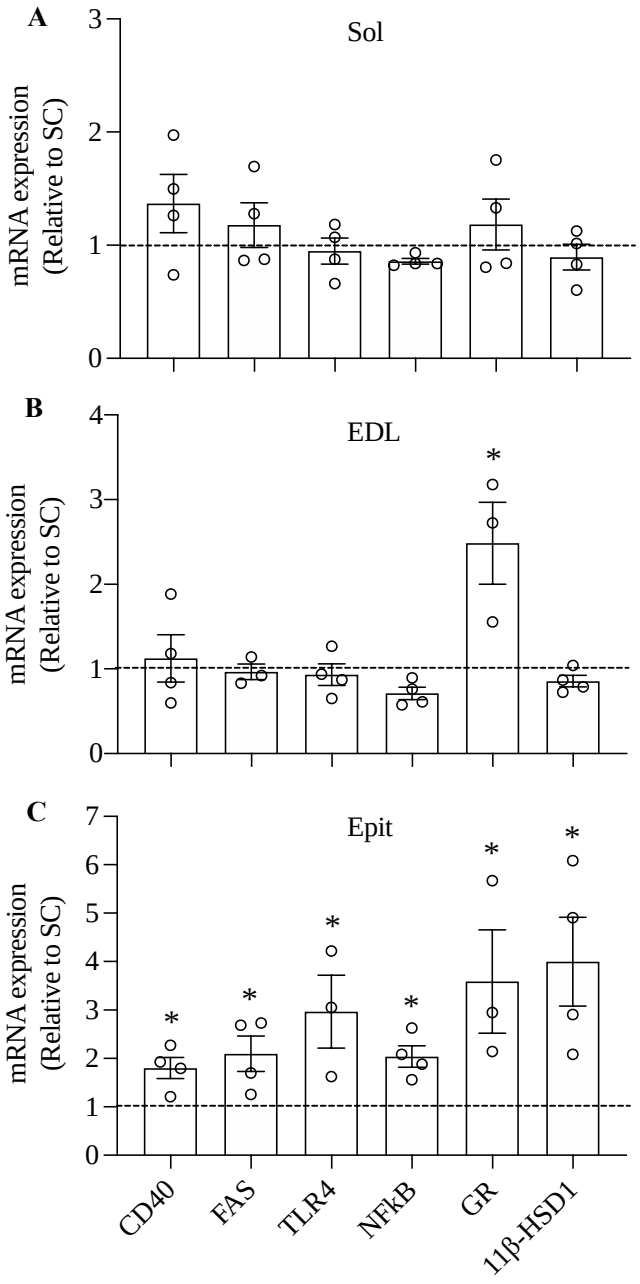

Figure 4.7: The expression of receptors for inflammatory mediators and glucocorticoids is up-regulated in a fiber type-specific manner by HFS diet. mRNA expression of *Tnf* receptors (*Cd40* and *Fas*), *Tlr4*, *Nf-κb*, *GR*, and *11β-HSD1* was measured in Sol, EDL, and Epit muscles. Data

presented relative to SC-fed rats (dashed lines). Average ± SEM. *p<0.05 vs. control, t-test, n=3-4.

4.5 Discussion

Here, we provide evidence of a muscle fiber type-specific adaptation with regards to the accumulation of DAG and ceramides, PKC activation, and the expression of receptors involved in inflammatory cytokines and glucocorticoid signalling in response to chronic exposure to a high fat and sucrose enriched diet. Insulin is well known for its ability to potently stimulate glucose uptake and glycogen synthesis in skeletal muscles, and conditions that limit glycogen synthesis in this tissue are associated with hyperglycemia and other metabolic disorders typically found in T2D patients[392]. Here, we show that Sol, EDL, and Epit muscles of HFS rats had blunted insulin-stimulated glycogen synthesis and glucose oxidation rates, indicating that regardless of their fibre type distribution and capacity to oxidize fat, all muscles developed insulin resistance. Our original hypothesis was that, under conditions of chronic HFS feeding, muscles such as Sol and EDL that are rich in type I and type IIA fibers would accumulate lower levels of DAG and ceramides in comparison to the Epit muscle rich in type IIB fibers. This would occur because more fatty acids would be oxidized in type I and IIB fibers leaving fewer to be diverted towards the formation of DAG and ceramides. This hypothesis was consistent with previous reports that PKCθ, considered the dominant isoform of DAG-sensing PKCs in skeletal muscle[419,420], was more abundant in white than red rat muscles, and that insulin resistance was accompanied by DAG-mediated increase in PKCθ only in the membrane fraction of white muscles [36]. Indeed, we found that the total contents of PKCδ and PKCθ were much lower in Sol than in EDL and Epit muscles. However, analysis of the cytosolic and membrane

fractions, revealed that the translocation of both PKCδ and PKCθ were markedly elevated in Sol muscles, whereas in EDL, only PKCδ translocation was increased by HFS diet. Conversely, in Epit muscles, translocation of both PKC isoforms was reduced. These findings were consistent with the fact that HFS feeding increased DAG and ceramides in Sol and EDL, but not in Epit muscles. Thus, contrary to our original hypothesis, high rates of fatty acid oxidation did not prevent DAG and ceramides accumulation and the induction of PKC translocation toward the membrane. Furthermore, our findings suggested that distinct mechanisms dictate insulin resistance under diet-induced obesity in red, white, and mixed muscles. In this context, we tested whether the expression of inflammatory mediators could also follow a distinct pattern among these muscles. Indeed, we found that even though circulating *TNFα* and *Il-6* were significantly increased in HFS rats, only Epit muscles displayed an enhanced expression of major molecules that mediate inflammatory responses such as *Cd40, Fas, Tlr4*, and *Nf-κb* in these animals. *Tlr4* has been reported to selectively increase sphingolipid levels within the cell, suggesting that ceramides may be an important mediator of insulin resistance induced by *Tlr4* signalling. In fact, in order to induce insulin resistance in mice, the proinflammatory *Tlr4* has been shown to require the biosynthesis of ceramides[421]. Interestingly, in this study we found ceramides to be significantly elevated in Sol and EDL, but not in Epit muscles upon HFS feeding. Thus, it appears that in Sol and EDL muscles the intracellular accumulation of DAG and ceramides contributed to the development of insulin resistance in these muscles, whereas in Epit muscles the signalling of inflammatory cytokines such as *TNFα* and *Il-6* through *Cd40* and *Fas, Tlr4*, and *Nf-κb* likely played a more relevant role in HFS diet-induced insulin resistance.

Besides directly affecting insulin signalling and glucose metabolism in peripheral tissues, *TNFα* and *Il-6* have been shown to activate the hypothalamic-pituitary-adrenal axis (HPA) and stimulate adrenocorticotropic hormone (ACTH) and cortisol production[422]. Increased levels of glucocorticoids lead to dysfunctional alterations in glucose and lipid metabolism[161,404,423]. In fact, animal models with genetic predispositions to obesity and T2D such as the *ob/ob* mouse[424] and the Zucker fatty rat[403], as well as the HFS diet-induced insulin resistance rat model[425] show HPA hyperactivity. Additionally, treatment with dexamethasone has been reported to induce insulin resistance in oxidative and glycolytic rat skeletal muscles[161,423], and severe hyperglycemia has also been recently described in HF-fed rats receiving exogenous corticosterone[426]. Conversely, adrenalectomy has been shown to reverse many of the metabolic abnormalities found in genetic models of obesity and insulin resistance[404,427] and HFS diet-induced insulin resistance in skeletal muscles was ameliorated in rats treated with an anti-glucocorticoid drug[405]. These previous observations are in line with our findings that skeletal muscle insulin resistance was accompanied by increased circulating corticosterone levels and also with upregulation of *GR* mRNA expression in EDL and Epit muscles in HFS-fed rats. Furthermore, we found that the mRNA expression of *11β-HSD1*, the enzyme that catalyses the intracellular conversion of circulating 11-dehydrocorticosterone into corticosterone in rodents[158], was upregulated in Epit muscles from HFS rats. Even though the mRNA expression of receptors for inflammatory cytokines, *Nf-κb*, *GR*, and *11β-HSD1* were unaltered in Sol and EDL muscles of rats fed a HFS diet, we cannot discard the possibility that elevated circulating *TNFα, Il-6,* and corticosterone may have also contributed to some extent to the development of insulin resistance in these muscles.

Altogether, our findings provide evidence that the activation of PKCδ and PKCθ and pathways by which inflammatory cytokines and glucocorticoids signal in skeletal muscles are regulated by HFS feeding in a muscle fiber type-specific manner. These findings could also explain why insulin resistance similarly develops in oxidative and glycolytic muscles of rats fed an obesogenic diet, despite major differences in the ability of these muscles to oxidize fat. Thus, the accumulation of DAG and ceramides appear to be important factors leading to PKC activation and disruption of insulin signalling and glucose metabolism in oxidative muscles under diet induced obesity conditions. However, because in highly glycolytic muscles DAG and ceramides were not significantly elevated and membrane-bound PKC was not altered, the activation of inflammatory pathways and upregulation of glucocorticoid signalling were more likely associated with HFS diet-induced insulin resistance in these muscles.

Authors Contribution: *Shailee Jani*: Acquisition or analysis or interpretation of data for the work; Drafting the work or revising it critically for important intellectual content; Final approval of the version to be published; Agreement to be accountable for all aspects of the work. *Daniel Da Eira*: Acquisition or analysis or interpretation of data for the work; Drafting the work or revising it critically for important intellectual content; Final approval of the version to be published; Agreement to be accountable for all aspects of the work. *Ishvinder Hadday, George Bikopoulos, and Arta Mohasses*: Acquisition or analysis or interpretation of data for the work; Final approval of the version to be published; Agreement to be accountable for all aspects of the work. *Rolando Ceddia*: Conception or design of the work; Acquisition or analysis or interpretation of data for the work; Drafting the work or revising it critically for important intellectual content; Final approval of the version to be published; Agreement to be accountable for all aspects of the work.

Grants: This research was funded by a Discovery Grant from the Natural Science and Engineering Research Council of Canada (NSERC) and by infrastructure grants from the Canada Foundation for Innovation (CFI) and the Ontario Research Fund (ORF) awarded to RBC. RBC is also a recipient of the Canadian Institutes of Health Research (CIHR) New Investigator Award and the Early Research Award from the Ontario Ministry of Research and Innovation.

DISCLOSURES: The authors state no conflict or duality of interest with regards to this work.

Data Availability Statement: All data supporting the results are included within the figures revealing their range and distribution.

Chapter 5

Insulin-resistant female rat skeletal muscles display diacylglycerol-mediated PKC activation and inflammation without ceramides accumulation.

Authors: Shailee Jani[1], Daniel Da Eira[1], Mateja Stefanovic[1], Rolando B. Ceddia[1]

[1]Muscle Health Research Center – School of Kinesiology and Health Science, York University, North York, ON, Canada.

Abbreviated title: Insulin resistance in oxidative and glycolytic female skeletal muscles

Keywords: Glycogen synthesis, glucose oxidation, obesity, lipid oxidation, intramyocellular lipids, TAG.

A version of this manuscript has been published in The Journal of Physiology on March 11th 2023. (*The copyright policy of the journal automatically grants permission for authors to reproduce whole published articles without charge in dissertations and post to thesis repositories.)*

Jani, S., Da Eira, D. and Ceddia, R.B. (2023), Insulin-resistant female rat skeletal muscles display diacylglycerol-mediated PKC activation and inflammation without ceramides accumulation. *Journal of Physiology*, (2023). https://doi.org/10.1113/JP284324

Statement of Labour

The majority of the experiments were conducted by Shailee Jani (SJ), including breeding of rats, administration of the high-fat sucrose enriched diet (HFS), extraction of tissues, and conduction of all metabolic assays. SJ was also responsible for conducting all western blots, real-time PCR, HPLC experiments, analyzing DAG and ceramide contents in tissues, interpreting all results, preparing the figures, and revising the manuscript. Daniel Da Eira and Mateja Stefanovic assisted with the feeding and extraction of tissues. The research was designed and supervised by Dr. Rolando Ceddia and was funded by a Discovery Grant from NSERC and by infrastructure grants from the Canada Foundation for Innovation and the Ontario Research Fund.

5.1 Abstract

This study investigated the role of diacylglycerol (DAG)-mediated protein kinase C (PKC) activation, ceramides accumulation, and inflammation in insulin-resistant female oxidative and glycolytic skeletal muscles induced by an obesogenic high-fat sucrose-enriched (HFS) diet. The HFS diet impaired insulin-stimulated AKT_{Thr308} phosphorylation and glycogen synthesis, whereas rates of fatty acid oxidation and basal lactate production were significantly elevated in soleus (Sol), extensor digitorum longus (EDL), and epitrochlearis (Epit) muscles. Insulin resistance was accompanied by increases in triacylglycerol (TAG), and DAG contents in Sol and EDL, whereas in Epit muscles only TAG content and markers of inflammation were associated with HFS diet-induced insulin resistance. Analysis of membrane/cytoplasm-bound PKC fractions revealed that the HFS diet promoted activation/translocation of PKCδ and θ isoforms in Sol, EDL, and Epit muscles. However, none of these muscles displayed alterations in ceramides contents in response to HFS feeding. This could be explained by a significant increase in *Dgat2* mRNA expression in Sol, EDL, and Epit muscles, which likely diverted most of the intramyocellular acyl-CoAs toward TAG synthesis instead of ceramides. Overall, this study helps elucidate the molecular mechanisms underlying insulin resistance caused by diet-induced obesity in female skeletal muscles with distinct fiber type compositions.

5.2 Introduction

Skeletal muscles account for ~30% and 40% of body mass in women and men, respectively[391]. Given the large mass and its capacity to take up relatively high amounts of glucose from the circulation, the skeletal muscle compartment plays a significant role in the maintenance of whole-body glucose homeostasis[428]. Interestingly, even though women have approximately two-third the skeletal muscle mass and twice the adipose mass of their male counterparts, impaired fasting glucose has been reported to be higher in men (17%) than in women (13%)[429]. Furthermore, the rate of blood glucose clearance during an intravenous glucose tolerance test has been reported to be 15% higher in women than men[430]. Even in rodent models of glucose intolerance, insulin resistance, and diabetes, males show a stronger phenotype than females[264,265]. These observations indicate that in addition to major body composition differences between males and females, sex has a profound impact on glucose and fat metabolism, conferring women a favourable effect on insulin sensitivity.

At the whole-body level, insulin sensitivity is regulated by the ability of several organs and tissues such as liver, adipose tissue, and skeletal muscles to metabolize glucose. In this context, as the capacity of the adipose tissue to store fat reaches its maximum (*e.g.* obesity), lipotoxicity resultant from ectopic lipid deposition causes insulin resistance in peripheral organs[89,431], including liver and skeletal muscle. It could be that because men have lower fat mass than women, the susceptibility to dysfunctional metabolic alterations caused by lipotoxicity could be higher in the former than the latter. Indeed, it has been reported that women are less prone to fatty acid-induced peripheral insulin resistance than men[264]. This was based on the observation that acutely increased levels of circulating non-esterified fatty acids (NEFA) inhibited peripheral tissue insulin sensitivity in men, but not in women[264]. However, no distinction has been reported

regarding the contribution of specific peripheral organs (*e.g.*, liver, and skeletal muscle) to NEFA-induced insulin resistance in men versus women.

One of the proposed mechanisms by which excess intracellular fat accumulation causes insulin resistance involves the accumulation of lipid intermediates such as diacylglycerol (DAG) and ceramides in myocytes[178]. According to this model, elevated levels of the bioactive signaling lipids DAG or ceramides, formed during the process of triacylglycerol (TAG) synthesis and storage in skeletal muscles, activate protein kinase C (PKC, mainly the θ and δ isoforms in skeletal muscles). In its activated state, PKC has been demonstrated to inhibit the kinase activity of the insulin receptor[226], which then impairs all subsequent steps of the intracellular insulin signaling cascade and glucose metabolism in skeletal muscles. Similarly, it has been proposed that ceramides promote the activation of atypical PKC isoforms (PKCζ/λ), which also impairs insulin-stimulated AKT phosphorylation and its downstream signaling steps[432]. Recent work from our lab[433] confirmed that male Wistar rats fed for 8 weeks an obesogenic high-fat sucrose-enriched (HFS) diet increased DAG and ceramides contents in Sol (highly oxidative muscle rich in Type 1 fibers)[408] and EDL (mixed muscle, rich in Type I and IIa fibers)[408], whereas in Epit muscles (highly glycolytic, rich in Type IIa and IIb fibers)[409] neither DAG nor ceramides were significantly elevated by the HFS diet. Moreover, whereas membrane-bound PKCδ and PKCθ was increased in Sol and EDL, both PKC isoforms were reduced in Epit muscle from obese rats[433]. Hence, data from our previous studies provide evidence that glycerolipid and ceramide accumulation, as well as DAG-induced PKC activation follow a fiber type-dependent pattern under conditions of diet-induced obesity. Also, that distinct mechanisms drive insulin resistance in oxidative and glycolytic muscles from male rats fed an obesogenic diet[433]. Whether this is also the case in female skeletal muscles remains to be determined. Furthermore, it has been

shown that despite having 47% more TAG content, lean moderately trained women displayed 29% higher skeletal muscle insulin sensitivity than matched men[434]. It could be that a higher capacity to store intramuscular TAG prevented DAG and ceramides accumulation in female skeletal muscles and consequently led to a lower induction of PKC activation. This could be one of the potential mechanisms underlying higher peripheral insulin sensitivity in females than males. To address this hypothesis, in this study we provide a detailed analysis of glycerolipid and ceramides content, PKC activation, as well as rates of basal and insulin-stimulated AKT phosphorylation, glycogen synthesis and glucose oxidation in oxidative and glycolytic muscles from female rats fed an obesogenic diet for 8 weeks.

5.3 Materials and Methods

Reagents – Fatty acid (FA)-free bovine serum albumin (BSA), glycogen, and palmitic acid were obtained from Sigma (St. Louis, MO, USA). Human insulin (Humulin R) was purchased from Eli Lilly Inc. (Toronto, Ontario, Canada). D-[U-^{14}C] glucose was ordered from American Radiolabelled Chemicals (St. Louis, MO, USA) and [1-^{14}C] palmitic acid was ordered from PerkinElmer, Inc. (Waltham, Massachusetts, USA). N-Acetyl-D-sphingosine was from Sigma. The reverse phase column (C18 5 µm 250 x 4.6 mm) was from Restek (Bellefonte, PA, USA). The subcellular protein fractionation Kit was from Thermo Fisher (Cambridge, MA, USA). The lactate colorimetric assay kit was obtained from BioVision (San Francisco, CA, USA). The AKT (cat # 9272), P-AKT$_{Thr308}$ (cat # 9275) PKCθ (cat # 13643) and PKCδ (cat # 9616) antibodies were from Cell Signalling Technology Inc. (Beverly, MA, USA).

Animals – Wistar strain Female albino rats ordered from Envigo (Indianapolis, IN, USA) weighing 150-200g (initial weight) were maintained in a constant-temperature (23^{o}C), with a

fixed (12h/12h) light and dark cycles and fed for 8 weeks *ad libitum.* The diet was either a standard rat chow (SC) providing 27.0%, 13.0%, and 60.0% of calories from protein, fat, and carbohydrates, respectively (energy density = 3.43 kcal/g) or a high-fat sucrose-enriched (HFS) diet purchased from Research Diets (catalog # D12492) providing 20.0%, 60.0%, and 20.0% of calories from protein, fat, and carbohydrates, respectively (energy density = 5.24 kcal/g).

Ethics approval – The protocol containing all animal procedures described in this study was specifically approved by the Committee on the Ethics of Animal Experiments of York University (York University Animal Care Committee, YUACC, permit number: 2021-03 and performed strictly in accordance with the YUACC guidelines. All tissue extraction procedures were performed under ketamine/xylazine anesthesia (90 mg and 10 mg/100g B.W.), and all efforts were made to minimize suffering. All experiments in this study were carried out in compliance with the ARRIVE guidelines. The investigators understand the ethical principles under which the journal operates and that their work complies with this animal ethics checklist.

Glucose monitoring and glucose tolerance test (GTT) – Rats were bled from the saphenous vein to assess glycemia and insulinemia in the fed state after 8 weeks of dietary intervention. Plasma glucose was determined by using the OneTouch UltraMini blood glucose monitoring system from LifeScan Canada Ltd (BC, Canada). Insulin measurements were conducted using an ELISA kit purchased from Millipore-Sigma (Burlington, MA, USA). For the GTT, the animals were fasted overnight and had their basal glucose measured. Subsequently, each animal received an intraperitoneal (i.p.) injection of 1.75 g of glucose/kg of B.W. (30% glucose solution in saline). Blood was then collected after 15, 30, 60, 90, and 120 min for the determination of serum glucose and insulin concentrations[435].

Muscle isolation and incubation for measurement of glucose oxidation, glycogen synthesis and lactate production – After anesthetizing with Ketamine/Xylazine (90 mg and 10 mg/100g B.W.) tissue samples were immediately extracted. Muscles chosen were based on their wide range of reported fiber-type distributions with distinct mitochondrial contents and oxidative capacities. The percentages of type I, type IIa, and type IIb in Sol, EDL, and Epit muscles are 84/16/0, 3/57/40[408], and 15/20/65[409], respectively. Upon extraction, muscle strips (18 – 22 mg) were mounted onto thin stainless steel wire clips to maintain optimal resting length, and then quickly added to 2 ml of pre-gassed [30 min with O_2:CO_2 95:5% (vol/vol)] Krebs-Ringer bicarbonate (KRB) buffer containing 4% fat-free BSA and 6 mM glucose in scintillation vials. Subsequently, the vials were sealed and continuously gasified for the entire 1h-pre-incubation period. Muscle strips were then transferred to vials containing 2 ml of the same KRB buffer plus D-[U-^{14}C]glucose (0.2 μCi/ml) and incubated for one additional hour under continuous gasification either in the absence (basal) or presence of insulin (100 nM) for the determination of glucose oxidation, glycogen synthesis and lactate production [410]. To assess glucose oxidation, a small eppendorf containing a loosely folded piece of filter paper moistened with 0.2 ml of 2-phenylethylamine/methanol (1:1, vol/vol) was inserted into the scintillation vial with the muscles. After the 1h-incubation period, the muscles were removed to measure glycogen synthesis and samples (100 μl) of the incubation media were collected for lactate production. The remaining media were acidified with 0.2 ml of H_2SO_4 (5N) at 37°C for an additional 1h to collect $^{14}CO_2$ released. Subsequently, the filter papers were carefully removed and processed for radioactivity counting to assess glucose oxidation. Immediately after incubation, muscle strips were quickly washed in ice-cold PBS, blotted on filter paper, snap frozen with liquid nitrogen (N_2), and digested in 0.5 ml of 1mol/l KOH at 70°C for 45 min. To the digested muscle,

glycogen carrier was added and allowed to precipitate overnight in 100% ethanol at -20ºC. Next morning, samples were centrifuged (5000 rpm), the supernatant was discarded, and 0.5 ml of water was added to each precipitate to count radioactivity and determine rates of glycogen synthesis. For lactate production, the media aliquots were first deproteinated using 10 kDa filters (centrifuged at 13,000 rpm for 15 min at 4ºC) and then assayed using a colorimetric assay kit following manufacturer's instructions.

Measurement of palmitate oxidation in isolated muscles – After extraction, muscle strips were mounted onto thin stainless steel wire clips and then quickly added to 2 ml of pre-gassed [30 min with O_2:CO_2 95:5% (vol/vol)] KRB buffer containing 4% fat-free BSA and 6 mM glucose in scintillation vials. Subsequently, the pre-incubated muscle strips were gasified and incubated in 2 ml of KRB buffer plus 0.2 mM of cold palmitic acid previously complexed with fatty acid-free BSA and [1-^{14}C] palmitic acid (0.2 µCi/ml) for one more hour. A tube with a loosely folded filter paper was moistened with 0.2 ml of 2-phenylethylamine/methanol (1:1, vol/vol) was added inside the scintillation vial. After the 1h-incubation period, the muscles were removed and the media was sealed and acidified with 0.2 ml of H_2SO_4 (5N), at 37 °C for an additional 1h for collection of the $^{14}CO_2$ released. Finally, the filter papers extracted and processed for radioactivity counting[411].

Determination of AKT phosphorylation, total PKCδ and PKCθ contents, as well as their cytoplasmic and membrane fractions in Sol, EDL, and Epit muscles – Samples of Sol, EDL, and Epit muscles were homogenized in a buffer containing 25 mmol/l Tris-HCl and 25 mmol/l NaCl (pH 7.4), 1 mmol/l MgCl2, 2.7 mmol/l KCl, 1% Triton-X, and protease and phosphatase inhibitors (0.5 mmol/l Na_3VO_4, 1 mmol/l NaF, 1 µmol/l leupeptin, 1 µmol/l pepstatin, and 20 mmol/l PMSF). Subsequently, muscle homogenates were centrifuged, and the supernatants were

collected and used for the determination of total protein content. For fractionation of cytoplasmic and membrane fractions, a protein fractionation kit from Thermo Fisher was then used for each muscle. The Bradford assay was used to measure protein in samples of fractionated muscle tissue. An aliquot of each subcellular fraction was diluted 1:1 (vol/vol) with 2 x Laemmli sample buffer, heated to 95°C for 5 min, and subjected to SDS-PAGE. Primary antibodies for PKCδ and PKCθ were used in a dilution of 1:2,000. β-actin were used as loading control for total PKCδ and PKCθ, while Na,K-ATPase was used as a loading control for the membrane fractions of PKCδ and PKCθ, and GAPDH was used as loading control for cytoplasmic fractions of PKCδ and PKCθ.

Determination of TAG, DAG and ceramides contents in Sol, EDL, and Epit muscles – DAG, TAG and ceramides content was quantified using the ultra-high-pressure liquid chromatography system (UHPLC-UV, Nexera X2, Shimadzu, Kyoto, Japan) as described earlier [433]. Briefly, lipid samples were extracted from Sol, EDL, and Epit muscles using the Folch's method [412]. About 100 mg of muscle tissue were homogenized in 200 µl of chloroform:methanol (MeOH) [2:1 vol/vol], dried overnight under nitrogen gas (N_2), and resuspended in 100 µl of elution media of 2-propanol-hexane (ProHex, 5:4 vol/vol). 50 µl of the sample was injected automatically into a reverse phase column (C18 5 µm 250 x 4.6 mm). The chromatography conditions were set to 40°C for 20 min using a gradient of MeOH and ProHex:100% of MeOH from 0 to 10 min, followed by 50% of MeOH and 50% of ProHex for 10 min, maintained with isocratic elution for 10 min. Diolein and Triolein (0.25 µg/µl) were used obtain a standard curve[413]. Quantification was performed using the UHPLC-UV detection machine. In order to analyse total ceramide content, a small volume of the lipid extract obtained after Folch's extraction was transferred into new pre-weighed eppendorfs as previously described[414]. The

organic phase was hydrolyzed in 1M KOH at 90°C for 60 min. The sphingosine liberated from ceramides was analyzed by means of UHPLC by mixing it with 15µl OPA reagent and allowing it to derivatize for 20 min at room temperature. Subsequently, the samples were reconstituted in 100 µl of chloroform-methanol-acetic acid-water (50:37.5:3.5:2 vol/vol/vol/vol) and run through a porous silica column (ARC-18 1.8 µm 100 x 2.1 mm). Elution was conducted with heptane-isopropyl ether-acetic acid (60:40:3 vol/vol/vol) at a gradient from 0 to 100 % in 30 min at a flow rate of 0.8 ml/min followed by isocratic elution with acetonitrile: deionized distilled water (90:10, vol/vol) and a flow rate of 1 ml/min[240]. The calibration curve was prepared using N-Acetyl-D-sphingosine as a standard. The column was then equilibrated with chloroform-methanol-acetic acid-water (50:37.5:3.5:2 vol/vol/vol/vol) for 10 min at the same flow rate. Due to limited amount of tissue obtained from Epit muscles, two muscles from animals from the same treatment group were combined to be able to run all assays in duplicates. Therefore, for some experiments the graph data shows n=4 for Epit. For Sol and EDL, this was not the case because these muscles are much larger and provide enough material to run all assays without combining material.

Quantitative analysis of mRNA expression changes in skeletal muscle with HFS diet – Primers were designed using the software PrimerQuest (IDT) and the Affymetrix database (NetAffx™ Analysis Center, http://www.affymetrix.com/analysis) for each given gene. RNA was isolated from Sol, EDL and Epit using the RNeasy kit, followed by DNase treatment to remove genomic DNA carry-over. RT-PCR reactions were carried out at amplification conditions as follows: 95ºC (10 min); 40 cycles of 95ºC (15 s), 60ºC (60 s). Quantitative PCR was performed using the CFX96 Real-time system from Bio-Rad (Mississauga, ON, Canada).

All genes were normalized to the control gene TBP, and values are expressed as fold changes relative to SC. Primers sequences used are shown in Table 5.1.

Table 5.1:*Primer sequences used for qPCR analysis.*

Genes	Forward	Reverse
Cd40	AGATTATCCCGGTCACAACAC	TGAGATGCGACTCTCTTTACC
Dgat1	TAGAAGAGGACGAGGTGCGAGAC	GGGCTTCATGGAGTTCTGGATAGT
Dgat2	AGACCAAATTCGGCCTTCCAGAGA	TTTGCAGTCATTCCTTCCAGGAGC
Fas	AAGGCATCACCATAGCTACAGCCT	TATGCTTCTCACAGTGGCCACACA
Il-6	TGGCAACCTTAGTGCTCATT	TGTCTGCTCCAGCTTGTTAC
Nf-κb	TCCAGCTGCTATTGGATTACAC	GGGATGCGATACCTTAATGAC
Tbp	TACAGGTGGCAGCATGAATGACA	AACCAACAATCACCAGCAGCAGTG
Tlr4	ACCTAAGGAGAGGAGGCTAAG	GGTAACTGCAGCACACTACA

Statistical Analyses – Statistical analyses were performed by using two-way ANOVA with Holm-Bonferroni comparison post-hoc test or *t*-tests as indicated in the figure legends. Normality was evaluated using the Kolmogorov-Smirnov normality test. Data are presented as means ± SD. The level of significance was set to $P<0.05$.

5.4 Results

Energy intake, body weight, adiposity, and muscle weight – Despite having similar total energy intake during the feeding period amongst the groups, at the end of the 8-week dietary intervention period, the HFS-fed group gained significantly more body weight (BW) than SC-fed rats (Table 2). HFS-fed rats also had significantly higher weight of Sol, EDL, and Epit

muscles in comparison to control SC rats. In addition, HFS-fed rats displayed significantly elevated blood glucose and insulin levels in comparison to SC-fed rats (Table 5.2).

Table 5.2: Body weight, fat mass, muscle mass, and glycemia in female Wistar rats after 8 weeks of either feeding a SC or a HFS diet.

	SC	HFS
Food intake (kcal/rat/week)	472.45 ± 29.59	514.14 ± 42.99
Body Weight (g)	335.75 ± 3.95	382.51 ± 17.12 *
Sc Ing fat (g)	5.37 ± 0.63	13.02 ± 0.99 *
PO fat (g)	5.29 ± 0.60	15.09 ± 0.93 *
Soleus (mg)	295.54 ± 4.89	336.67 ± 12.79 *
EDL (mg)	301.36 ± 5.68	321.56 ± 12.23 *
Epit (mg)	106.00 ± 3.59	122.23 ± 3.12*
Plasma Glucose (mmol/L)	6.4 ± 0.16	7.38 ± r0.34 *
Plasma Insulin (ng/ml)	1.20 ± 0.08	2.05 ± 0.25 *

Data presented as Mean ± SD. For all variables n=9-11. *p<0.05 vs. SC (t-test). PO = periovarian; Sc Ing = subcutaneous inguinal.

Insulin-induced phosphorylation of AKT_{Thr308} and rates of glycogen synthesis in Sol, EDL, and Epit muscles – As expected, AKT_{Thr308} phosphorylation increased robustly in Sol, EDL, and Epit muscles of SC-fed rats upon insulin stimulation (Figure 5.1 A-C). However, in all muscles from HFS rats insulin-stimulated AKT_{Thr308} phosphorylation was significantly impaired (Figure 5.1 A-C). Under basal conditions, glycogen synthesis rates were similar in all three muscles when comparing SC- and HFS-fed rats. Also, rates of insulin-stimulated glycogen synthesis increased by 1.5-fold in Sol (Figure 5.1 D), 1.57-fold in EDL (Figure 5.1 E), and 1.42-fold in Epit (Figure 5.1 F) in SC-fed rats. In contrast, all muscles from HFS-fed rats displayed a

stunted glycogen synthesis response when stimulated with insulin (Figure 5.1 F). These findings clearly show that insulin signalling is defective in skeletal muscles of rats fed a HFS diet, which is consistent with the reduction in insulin-stimulated glycogen synthesis in oxidative and glycolytic muscles of these animals.

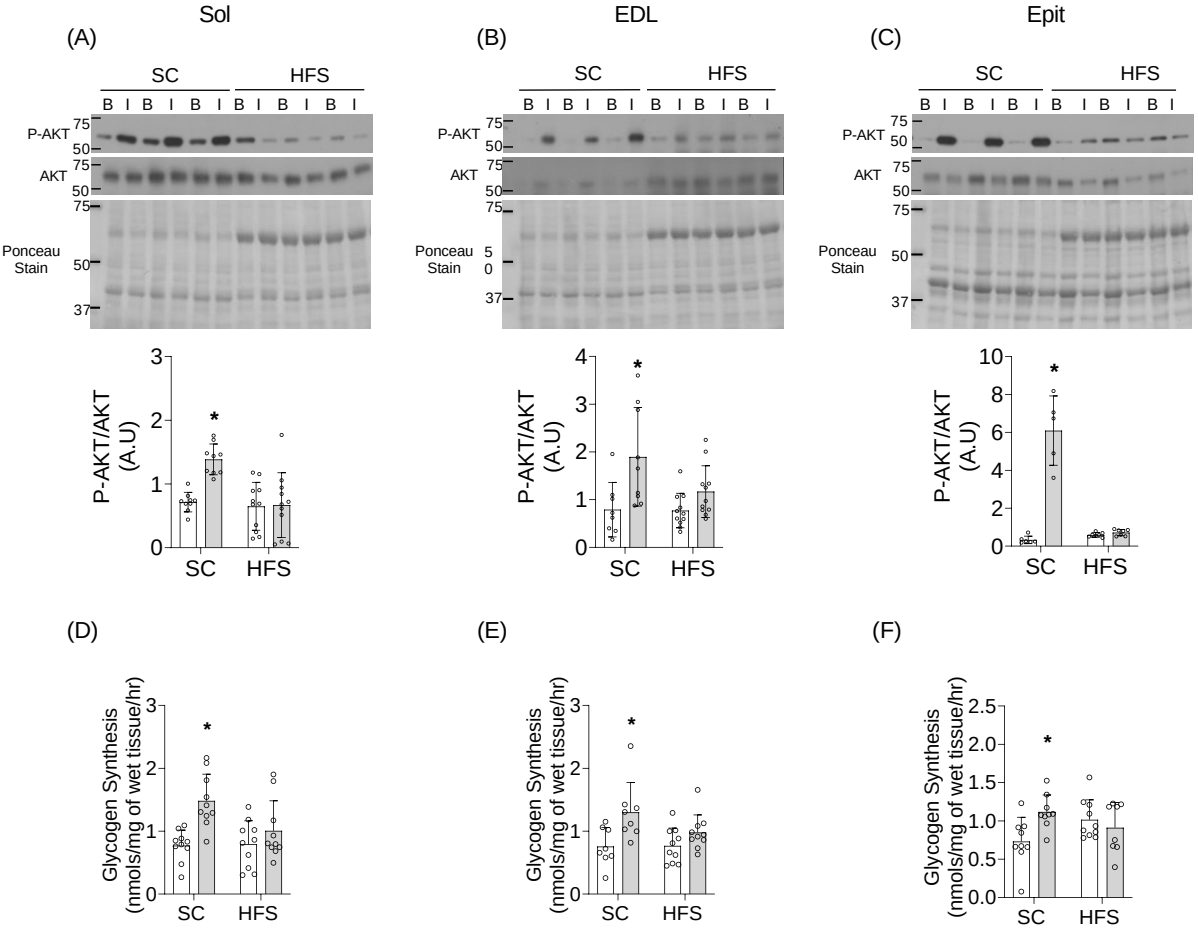

Figure 5.1: HFS diet causes impairment of insulin-induced AKT_{Thr308} phosphorylation and glycogen synthesis in oxidative and glycolytic muscles. AKT phosphorylation (A-C) and glycogen synthesis (D-F) in Sol, EDL, and Epit, respectively. *p<0.05 versus SC basal, Two-way ANOVA, n=6-11 for AKT phosphorylation and n=8-10 for glycogen synthesis. Mean ± SD.

Insulin-stimulated lactate production and glucose oxidation in Sol, EDL, and Epit muscles – All three muscles from rats fed a HFS diet had a higher basal rate of lactate production than SC-fed muscles (Figure 5.2 A-C). In fact, HFS diet significantly increased basal lactate production by 2.88-, 2.56-, and 3.8-fold in Sol, EDL, and Epit muscles, respectively, in comparison to the SC diet. However, the production of lactate in response to insulin by muscles from rats fed a HFS diet was stunted. Similarly, in the presence of insulin, glucose oxidation was significantly increased by 1.43-fold in Sol (Figure 5.2 D), 1.28-fold in EDL (Figure 5.2 E), and 1.58-fold in Epit (Figure 5.2 F) muscles of SC rats, whereas in HFS-fed rats insulin-stimulated glucose oxidation was potently suppressed in all three muscles (Figure 5.2 D-F).

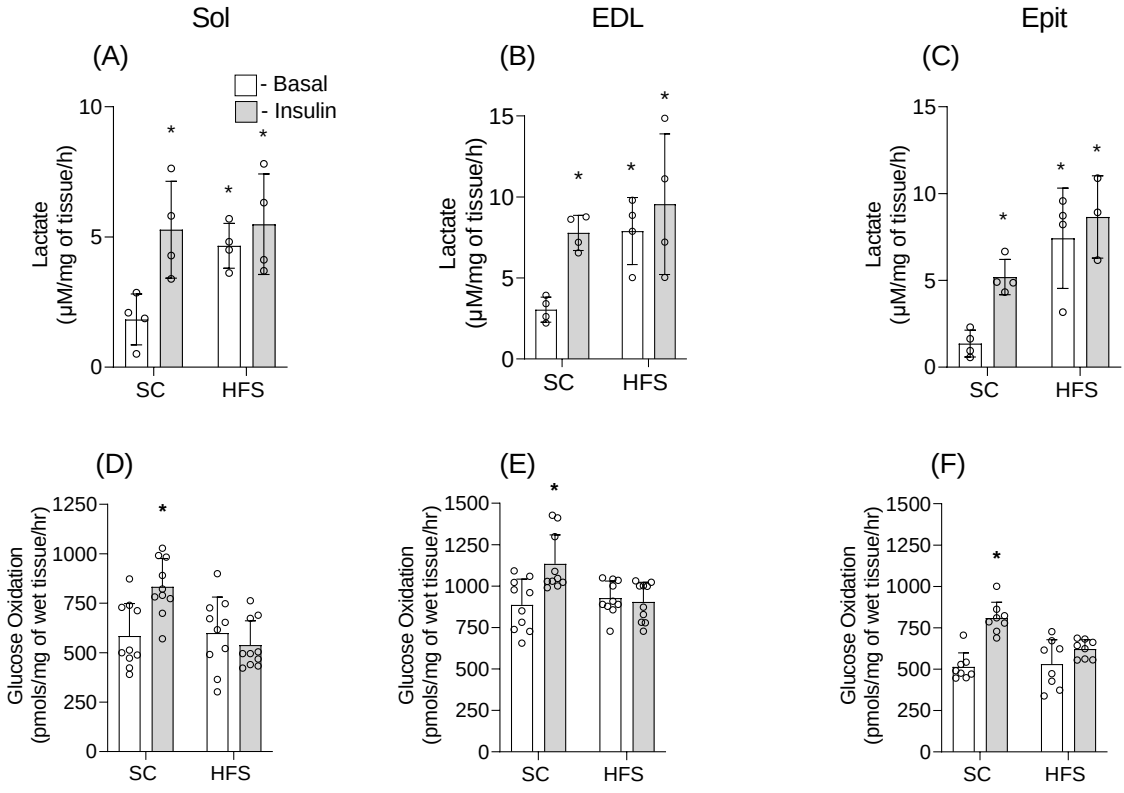

Figure 5.2: The HFS diet increases basal and insulin-stimulated lactate production and reduces rates of glucose oxidation in oxidative and glycolytic muscles. Basal and insulin-stimulated

lactate production (A-C) and glucose oxidation (D-F) in Sol, EDL, and Epit muscles, respectively. *p<0.05 versus SC basal for panels A-C and versus all other conditions for panels D-F, Two-way ANOVA, n = 4 for lactate assay and n=8-10 for glucose oxidation. Mean ± SD.

Palmitate oxidation and TAG accumulation in Sol, EDL, and Epit muscles – Rates of palmitate oxidation in Sol, EDL, and Epit muscles (Figure 5.3 A-C) were significantly elevated with a HFS diet by ~1.4-fold in all three muscles. Similarly, TAG accumulation was increased by 1.78-, 1.71-, and 2.56-fold in Sol, EDL, and Epit muscles, respectively by the HFS diet (Figure 5.3 D-F).

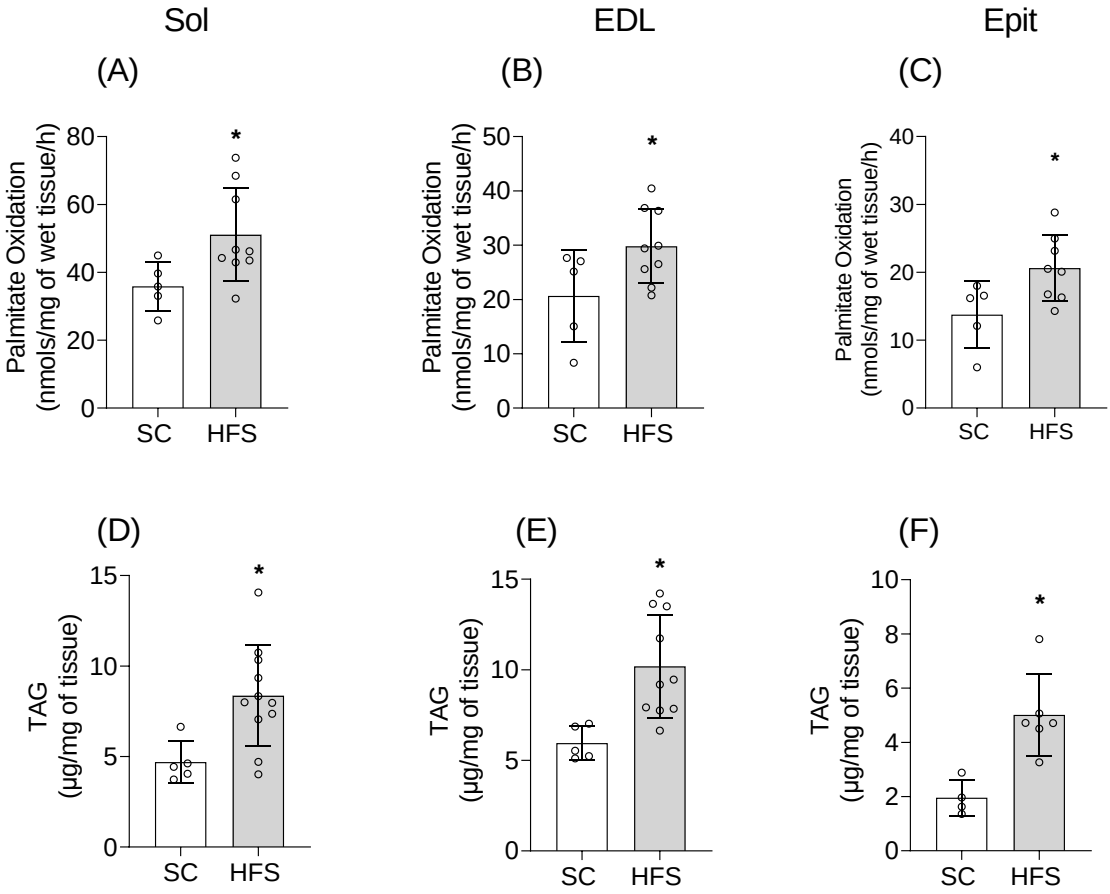

Figure 5.3: The HFS diet increases palmitate oxidation and TAG accumulation in oxidative and glycolytic muscles. Palmitate oxidation (A-C) and TAG accumulation (D-F) in Sol, EDL, and Epit muscles, respectively. *p<0.05 vs. SC, t-test, n = 5-9 for palmitate oxidation and n = 5-11 for TAG content. Mean ± SD.

DAG and ceramides contents and mRNA expression of IMCL in Sol, EDL, and Epit muscles – In SC-fed rats, DAG content was highest in EDL (5.63 ± 1.08 µg/mg of tissue) followed by Sol (2.4 ± 0.2 µg/mg of tissue) and Epit (1.3 ± 0.016 µg/mg of tissue) muscles (Figure 5.4 A-C). HFS feeding significantly increased DAG content by 2.33-, 2.01-, and 1.76-fold in Sol, EDL

and Epit, respectively. In SC-fed rats, ceramides content was also highest in EDL (0.36 ± 0.18 µg/mg of tissue), followed by Epit (0.12±0.046 µg/mg of tissue), and the least in Sol (0.058 ± 0.0093 µg/mg of tissue) muscles (Figure 5.4 D-F). Upon HFS feeding, ceramides content in Sol, EDL, and Epit muscles remained unaltered. These findings indicate that despite fiber-type differences, DAG accumulation increased in all three muscles, whereas the ceramide content was not affected by the obesogenic HFS diet. Quantitative PCR analysis revealed that the mRNA levels of *Dgat1* in Sol, EDL, and Epit muscles did not differ between SC- and HFS-fed rats (Figure 5.5 G-I). However, *Dgat2* mRNA levels were 4.37-fold higher in Sol, 2.61-fold higher in EDL, and 4.41-fold higher in Epit muscles of HFS than SC-fed rats (Figure 5.5 G-I).

PKCθ and PKCδ content and localization in Sol, EDL, and Epit muscles – PKCθ and PKCδ are the most abundant isoforms of these kinases in skeletal muscle [415,416]. In this context, we found that total PKCδ levels remained unaltered in Sol, EDL, and Epit muscles, whereas total PKCθ levels were significantly reduced in Sol and EDL, but not in Epit muscle from rats fed a HFS diet (Figure 5.6 A-C). We then determined the activation of PKCθ and PKCδ by measuring its content in the membrane and cytoplasmic fractions in Sol, EDL, and Epit [417,418,436]. With chronic HFS feeding Sol membrane/cytoplasm ratios for PKCδ and PKCθ were significantly increased by 1.26- and 1.51-fold (Figure 5.6 A and D). In EDL muscles, HFS diet increased by 1.8-fold the PKCθ membrane/cytoplasm ratio, whereas PKCδ remained unchanged (Figure 5.6 B and E). Densitometric values of cytoplasm and membrane fractions from Epit PKCθ and PKCδ were unaltered by the HFS diet (Figure 5.6 C and F). These findings indicate that HFS diet increased PKCθ membrane/cytoplasm ratio in Sol and EDL, but not in Epit muscles that did not display a significant increase in the activity of both PKC isoforms.

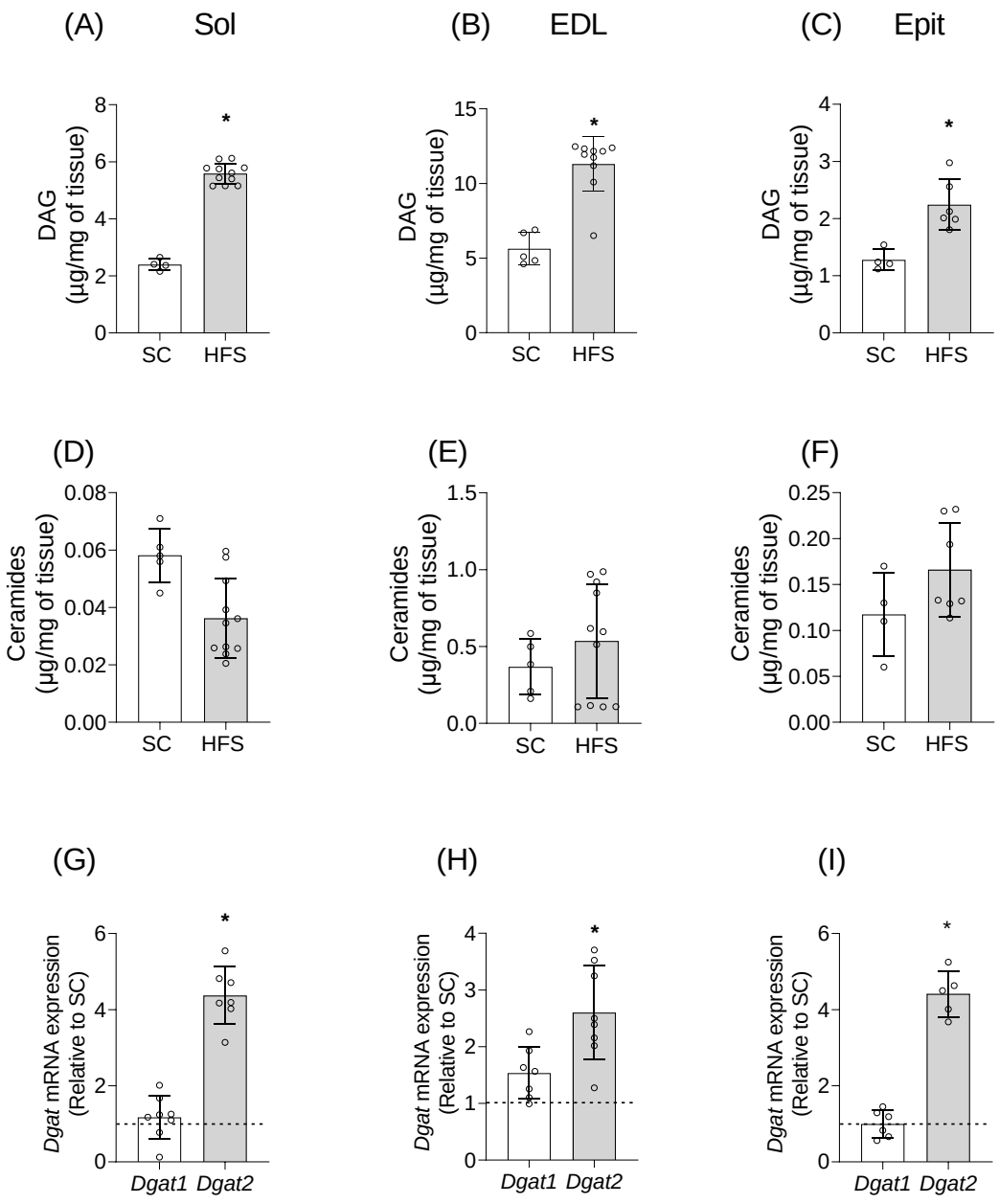

Figure 5.4: The HFS diet increases DAG content and the mRNA expression of diacylglycerol Acyltransferase 2 (Dgat2) but does not affect ceramide accumulation in oxidative and glycolytic muscles. DAG content (A-C), ceramides (D-F), and *Dgat 1* and *2* mRNA expression (G-I) in Sol, EDL, and Epit muscles. Dashed line refers to standard chow (SC). For panels A-F, *p<0.05 denotes statistical significance compared to SC values. For panels G-I, *p<0.05 denotes

statistical significance for Dgat1 and 2 mRNA expression relative to SC as a control. n = 5-11. Mean ± SD.

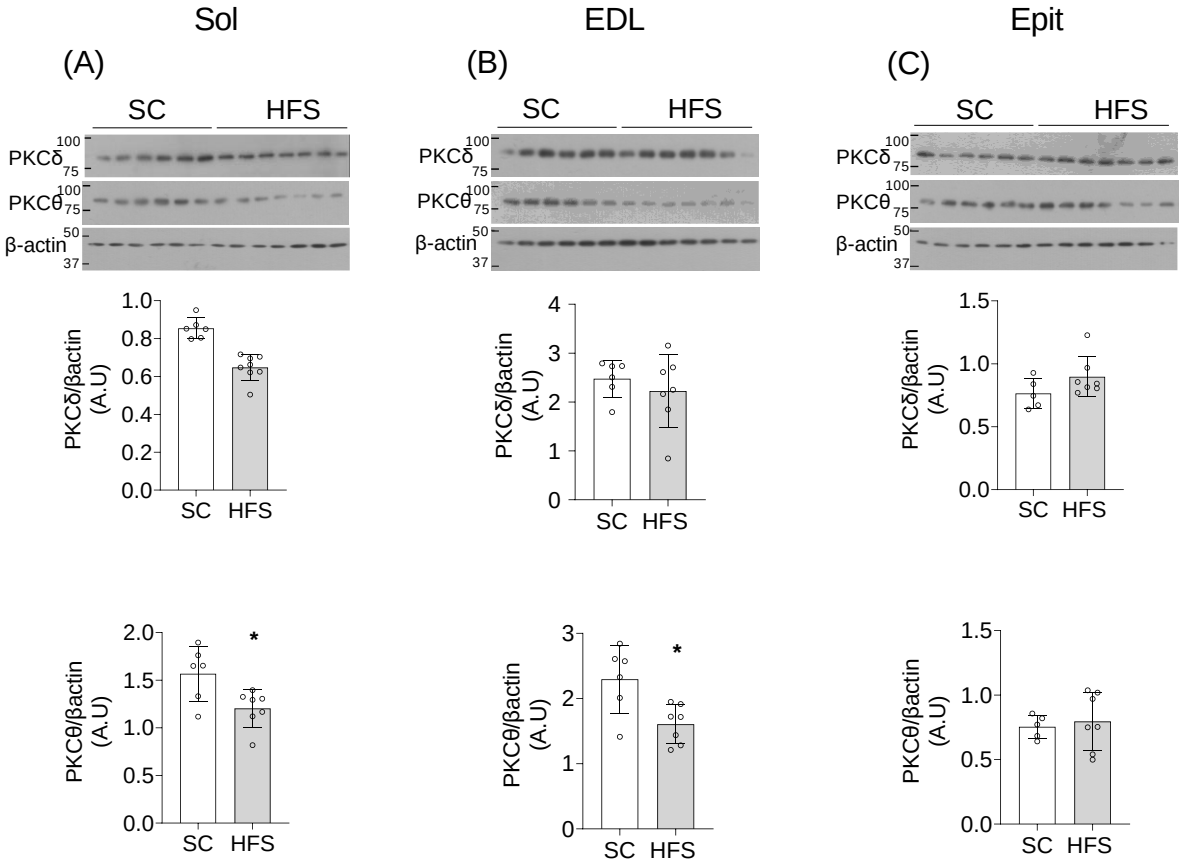

Figure 5.5: The HFS diet does not alter total PKCδ and PKCθ protein levels in oxidative and glycolytic muscles. PKCδ and PKCθ normalized by β-actin in Sol(A), EDL(B) and Epit(C). *p<0.05 vs. SC (t-test), n = 6-7. Mean ± SD.

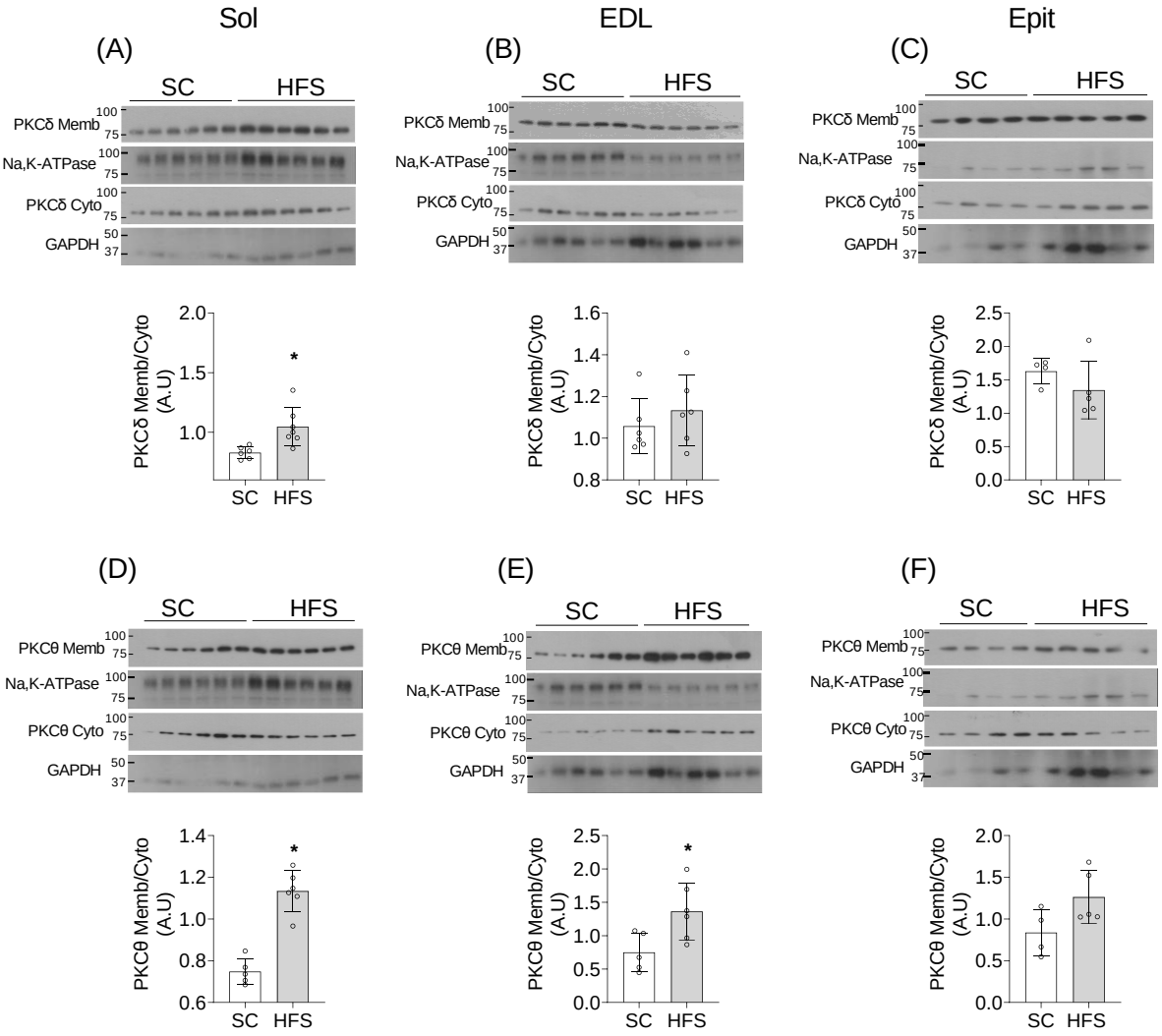

Figure 5.6: The HFS diet distinctly affects membrane-bound PKC levels in oxidative and glycolytic muscles. Representative blots and densitometric analyses of PKCδ (A-C) and PKCθ (D-F) levels in membrane (Mem) and cytoplasmic (Cyto) cellular fractions in Sol, EDL, and Epit muscles, respectively. *p<0.05 vs. SC, t-test, n=6 for Sol and EDL, n=4 and 5 for Epit. Mean ± SD.

mRNA expression of inflammatory mediators – With HFS feeding, *Tlr4, Cd40, Il-6* and *Fas* expression were elevated in Sol (1.5-fold, 1.4-fold, 1.5-fold, and 1.5-fold respectively) while a reduction of 5% in *Nf-κb* expression was seen (Figure 5.7 A). In EDL muscles of HFS rats, the mRNA expression of *Tlr4, Il-6,* and *Nf-κb* were significantly increased when compared to SC-fed controls (Figure 5.7 B). In Epit muscles from HFS rats, the mRNA expression of *Tlr4, Cd40, Il-6, Nf-κb* and *Fas* significantly increased by 4.9-fold, 4.7-fold, 4.4-fold, 3.2-fold, and 3.9-fold, respectively (Figure 5.7 C). Thus, a clear distinct fiber-type pattern of gene expression for glycerolipid synthesis enzymes and inflammatory markers was induced by HFS feeding.

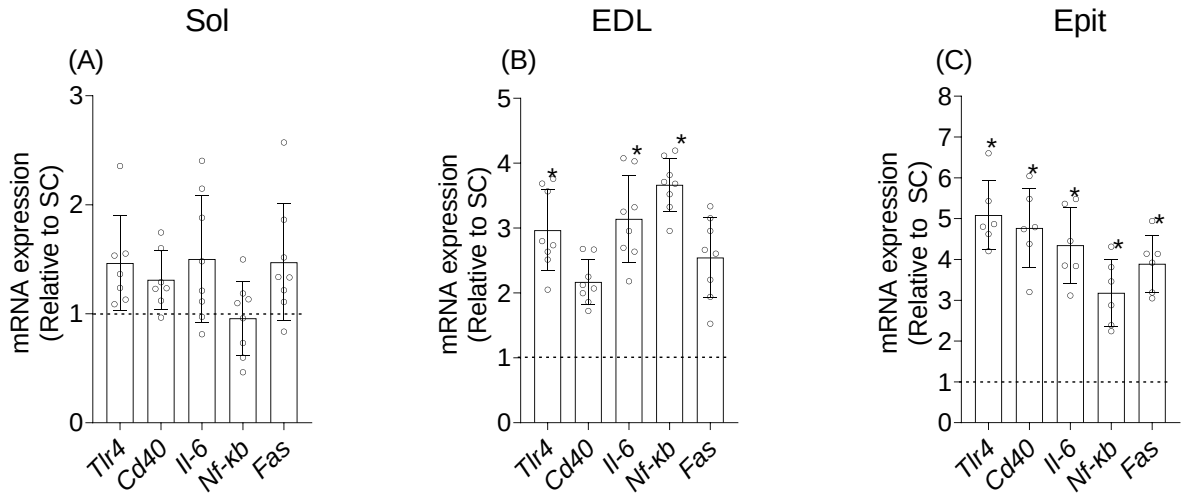

Figure 5.7: The mRNA expression of inflammatory mediators and genes regulating glycerolipid synthesis are altered in a fiber type-specific manner following a high-fat diet. mRNA expression of toll-like receptor 4 (Tlr4), Cluster of differentiation 40 (*Cd40*), interleukin 6 receptor (*Il-6*), nuclear factor kappa light polypeptide gene enhancer in B-cells (*Nf-κb*), and Fas receptor (*Fas*) in soleus (A), EDL (B), and epitrochelaris (C) muscles of HFS-fed rats. Dashed lines denote control levels. *$p<0.05$ vs. control, n=8. Mean ± SD.

5.5 Discussion

The main findings of this study were that HFS diet-induced obesity led to a significant elevation in intramuscular DAG and TAG contents without any alteration in ceramides levels in insulin-resistant female oxidative and glycolytic muscles. Moreover, a pro-inflammatory response was observed in skeletal muscles of rats fed a HFS diet, although this occurred in a fiber type-specific pattern. In fact, muscles rich in type IIa and type IIb fibers (EDL and Epit) [408,409] displayed a marked increase in the mRNA expression of *Tlr4*, *Il-6*, *Nf-κb,* and *Fas*, whereas in Sol muscles (rich in type I fibers) these markers of inflammation did not differ from SC-fed rats. Despite these fiber type-specific alterations in the expression of inflammatory mediators, all muscles from female rats fed the obesogenic HFS diet significantly enhanced their rates of fatty acid oxidation and displayed marked impairments in insulin-stimulated AKT_{Thr308} phosphorylation, glycogen synthesis, and glucose oxidation. These effects, also previously reported in male rats[433], were accompanied by elevated glycemia and insulinemia, which are consistent with whole-body insulin resistance in female rats fed a HFS diet. We have also observed that despite similar energy intake between SC- and HFS-fed rats, adiposity was significantly higher in the latter than the former group of animals. The apparent disproportional increase in adipose tissue growth in HFS-fed rats in comparison to SC-fed rats could be at least partially attributed to reduced energy expenditure in HFS-fed rats. This is supported by our previous observations that rats fed a HFS diet for 8 weeks displayed ~30% lower ambulatory activity[407,437,438]. Moreover, we have recently provided evidence that the HFS diet causes whitening of the brown adipose tissue in rats[439], an effect that likely attenuated diet-induced thermogenesis and favored adipose tissue growth in these animals. This is also consistent with enhanced energy efficiency we have reported in rats fed a HFS diet [437]. One of the mechanisms

associated with skeletal muscle insulin resistance in diet-induced obesity involves the activation of PKC by elevated DAG levels in myocytes[392]. Here, we investigated the activation of the two most prominent PKC isoforms (PKCδ and PKCθ) in skeletal muscles[419,440]. We observed that the total levels of PKCδ in all muscles studied were not affected by feeding the HFS diet; however, total PKCθ content was significantly reduced in Sol and EDL, whereas in Epit muscles it remained unaltered. Importantly, analysis of the cytosolic versus membrane fractions revealed that in Sol and EDL female muscles the translocation of PKCθ was significantly elevated by the HFS diet. This latter finding was similar to what we had previously reported for male Sol and EDL muscles in which insulin resistance was accompanied by elevated PKCδ and PKCθ translocation upon HFS feeding[433]. However, in female Epit both PKC isoforms were reduced by HFS feeding. Thus, in both males[433] and females the mechanism underlying HFS diet-induced insulin resistance in Epit muscles appears to be independent of DAG-induced PKC activation. This is consistent with observations that subcellular glycerolipid distribution in skeletal muscle does not explain sex differences that exist in obese humans with respect to insulin sensitivity[441]. Thus, even though females have been reported to accumulate higher amounts of TAG than males in skeletal muscles[434], it did not protect against DAG-induced PKC activation and the development of insulin resistance in both oxidative and glycolytic female muscles under conditions of HFS diet-induced obesity. In this context, both male[433] and female Epit muscle elicited a significant pro-inflammatory response under obesogenic conditions, which likely played a preponderant role in driving insulin resistance in this glycolytic muscle chronically exposed to the HFS diet.

Because *Tlr4* has been reported to selectively increase sphingolipid levels within the cell[240,421] and the HFS diet caused a marked increase in *Tlr4* expression in female EDL and Epit muscles,

one would expect that this would be followed by an increase in ceramides in both muscles. Surprisingly, despite increased *Tlr4* mRNA expression, we found that ceramides remained unaltered by the HFS diet in all female muscles studied. This differs from our previous observations that in male rats Sol and EDL muscles displayed an increase in ceramides content, whereas in Epit it remained unaltered by feeding a HFS diet[433]. In this scenario, our findings support that DAG-induced PKC activation was a key factor in promoting insulin resistance in EDL and Epit muscles of female rats fed a HFS diet. Furthermore, our qPCR analysis revealed that the mRNA levels of *Dgat2* were also elevated in Sol, EDL, and Epit muscles, whereas *Dgat1* remained unaltered in muscles of female rats fed the HFS diet in comparison to SC-fed animals. DGAT catalyzes the conversion of DAG into TAG and both *Dgat1* and *Dgat2* mRNA expressions can be regulated transcriptionally, although evidence exists that the activity of these enzymes can also be regulated post-translationally[442], but the exact mechanisms remain poorly understood. Thus, our finding that *Dgat2* mRNA expression was elevated in all three female muscles could signify that the majority of the intramyocellular acyl-CoAs were directed towards TAG formation rather than being used for ceramide synthesis in these muscles.

Besides DAG-induced PKC activation, it is also possible that alterations in other parameters of lipid metabolism not measured in this study (*e.g.* accumulation of muscle acylcarnitines) [441] could explain obesity-induced muscle insulin resistance in female muscles. In this context, here we show that muscles from HFS-fed female rats displayed enhancement (~40%) in rates of fatty acid oxidation, which is lower than what we had previously reported (60-80%) for male rats of the same strain (Wistars) and age after 8 weeks of HFS feeding[433]. Thus, lower capacity to enhance fatty acid oxidation compared to males under conditions of dietary lipid abundance likely led to a metabolic shift that contributed to DAG-induced PKC activation and insulin

resistance. This is compatible with our findings that insulin-stimulated glucose oxidation was impaired, whereas basal lactate production was markedly increased in all three muscles from female rats fed the HFS diet. These findings are consistent with previous observations that PKC-induced impairment of insulin signaling also causes suppression of glycogen synthesis[89,395], the pathway essentially responsible for the entire non-oxidative glucose metabolism in skeletal muscles[431]. Under such conditions, even though insulin resistance limited glucose uptake, the impairment of glycogen synthesis likely led to a diversion of intramyocyte glucose toward lactate synthesis in rats fed a HFS diet. Interestingly, lactate has been shown to suppress glycolysis in rats[85,443], whereas lactate-induced IRS-1_{Ser636} phosphorylation, which has been associated with impairment of insulin signaling in human skeletal muscle[444]. Thus, increased lactate production itself could be contributing to aggravating insulin resistance in skeletal muscles of HFS-fed rats. It is possible that substrate competition also contributed to enhance lactate formation, given that fatty acid oxidation was significantly increased in all muscles from female rats fed the HFS diet. This would be consistent with the tenets of the metabolic inflexibility hypothesis[445] and the Randle cycle[446]. However, more recent studies in muscles of insulin resistant HF-fed male rats and obese insulin resistant humans[447] provided evidence that the physiopathology of muscle insulin resistance is dissociated from alterations in mitochondrial substrate preference. This was supported by findings that the ratio of mitochondrial pyruvate oxidation (V_{PDH}) to rates of mitochondrial citrate synthase (V_{CS}) flux did not differ between insulin-sensitive and insulin-resistant Sol and quadriceps rat muscles[447]. Importantly, these V_{PDH}/V_{CS} data were from male Sprague-Dawley rats fed a HF diet for 3 weeks, whereas in our study we used female Wistar rats fed a HFS diet for 8 weeks. Thus, potential metabolic differences regarding rat strain, length of feeding, and sex should be considered and further

explored with respect to the role of diet-induced obesity and insulin resistance in mitochondrial function in future studies.

In summary, by looking at muscles with different fiber type compositions we were able to assess distinct metabolic pathways to integrate insulin signaling responses with the accumulation of lipid intermediates (*e.g.* DAG and ceramides), isoform-specific PKC activation, lactate production, and inflammatory markers. Thus, through a more integrative approach, our female rat studies allowed us to identify important meaningful pathways that lead to impairment in skeletal muscle metabolism and insulin sensitivity. In fact, our data from female rats provide evidence that DAG-induced PKC activation along with inflammation are the main drivers of insulin resistance in oxidative and glycolytic skeletal muscles under conditions of HFS diet-induced obesity. This was supported by impairments in insulin-stimulated AKT phosphorylation and glycogen synthesis, whereas rates of fatty acid oxidation and basal lactate production were significantly elevated. We also found that, despite developing insulin resistance and increasing *Tlr4* expression in response to HFS feeding, none of the muscles studied displayed alterations in ceramides contents. This could be explained by a significant increase in *Dgat2* mRNA expression in all three female muscles studied. In this context, upregulation of *Dgat2* likely diverted the majority of the intramyocellular acyl-CoAs to TAG synthesis instead of ceramides. These findings differ from what we had previously reported for male rats in which insulin resistance was accompanied by increases in both DAG and ceramides in Sol and EDL muscles. However, for Epit muscles, DAG accumulation and inflammation were associated with insulin resistance, since in both males[433] and females ceramides remained unaltered in Epit from HFS-fed rats. Thus, regardless of sex, we identified that multiple fiber type-specific mechanisms determine insulin resistance in skeletal muscles. Overall, this study helps elucidate the sexual

dimorphism in molecular mechanisms controlling insulin resistance in the skeletal muscles under conditions of diet-induced obesity.

Authors Contribution: *Shailee Jani*: Acquisition or analysis or interpretation of data for the work; Drafting the work or revising it critically for important intellectual content; Final approval of the version to be published; Agreement to be accountable for all aspects of the work. *Daniel Da Eira*: Acquisition or analysis or interpretation of data for the work; Drafting the work or revising it critically for important intellectual content; Final approval of the version to be published; Agreement to be accountable for all aspects of the work. *Rolando Ceddia*: Conception or design of the work; Acquisition or analysis or interpretation of data for the work; Drafting the work or revising it critically for important intellectual content; Final approval of the version to be published; Agreement to be accountable for all aspects of the work.

Grants: This research was funded by a Discovery Grant from the Natural Science and Engineering Research Council of Canada (NSERC) and by infrastructure grants from the Canada Foundation for Innovation (CFI) and the Ontario Research Fund (ORF) awarded to RBC. RBC is also a recipient of the Canadian Institutes of Health Research (CIHR) New Investigator Award and the Early Research Award from the Ontario Ministry of Research and Innovation.

DISCLOSURES: The authors state no conflict or duality of interest with regards to this work.

Data Availability Statement: All data supporting the results are included within the figures revealing their range and distribution.

Chapter 6

The ketogenic diet prevents steatosis and insulin resistance by reducing lipogenesis, diacylglycerol accumulation, and PKC activity in male rat liver.

Authors: Shailee Jani[1], Daniel Da Eira[1], Mateja Stefanovic[1], Rolando B. Ceddia[1]

[1]Muscle Health Research Center – School of Kinesiology and Health Science, York University, North York, ON, Canada.

Abbreviated title: Effects of a ketogenic diet on hepatic steatosis and insulin signaling.

Key words: Obesity, ceramides, TAG, NAFLD, glycogen, type 2 diabetes, AKT.

A version of this manuscript has been published in The Journal of Physiology on 16th August 2022. (*The copyright policy of the journal automatically grants permission for authors to reproduce whole published articles without charge in dissertations and post to thesis repositories.)*

Jani, S., Da Eira, D., Stefanovic, M. *et al.* The ketogenic diet prevents steatosis and insulin resistance by reducing lipogenesis, diacylglycerol accumulation and protein kinase C activity in male rat liver *Journal of Physiology*, (2022). https://doi.org/10.1113/JP283552.

Statement of Labour

The majority of the experiments were conducted by Shailee Jani (SJ), including breeding of rats, administration of the high-fat sucrose enriched diet (HFS), extraction of tissues, and conduction of all metabolic assays. SJ was also responsible for conducting all western blots, real-time PCR, HPLC experiments, analyzing DAG and ceramide contents in tissues, interpreting all results, preparing the figures, and revising the manuscript. Daniel Da Eira and Mateja Stefanovic assisted with the feeding and extraction of tissues. The research was designed and supervised by Dr. Rolando Ceddia and was funded by a Discovery Grant from NSERC and by infrastructure grants from the Canada Foundation for Innovation and the Ontario Research Fund.

6.1 Abstract

Obesity-associated insulin resistance plays a major role in the pathogenesis of nonalcoholic fatty liver disease (NAFLD). The accumulation of diacylglycerol (DAG), ceramides and inflammation are key factors that cause NAFLD. In recent years, the ketogenic diet (KD) has emerged as an effective non-pharmacological intervention for the treatment of NAFLD and other obesity-related metabolic disorders. What remains undetermined is how the KD affects DAG and ceramides content and insulin sensitivity in the liver. Thus, this research was designed to assess these variables, as well as glucose and fat metabolism and markers of inflammation in livers of rats exposed for 8 weeks to one of the following diets: standard chow (SC), obesogenic high-fat, sucrose-enriched diet (HFS), or a KD. Despite having a higher fat content than the HFS diet, the KD did not cause steatosis and preserved hepatic insulin signaling. The KD reduced DAG content and protein kinase C epsilon (PKCε) activity, but markedly increased liver ceramides content. However, whereas the KD increased ceramide synthase 2 (*CerS2)* expression, it suppressed *CerS6* expression, an effect that promoted the production of beneficial very long-chain ceramides instead of harmful long-chain ceramides. The KD also enhanced the liver expression of key genes involved in mitochondrial biogenesis and fatty acid oxidation (*Pgc-1α* and *Fgf21*), suppressed inflammatory genes *(Tnfα, Nf-kb, Tlr4, and Il-6)*, and shifted substrate away from *de-novo* lipogenesis. Thus, through multiple mechanisms the KD exerted anti-steatogenic and insulin-sensitizing effects in the liver, which supports the use of this dietary intervention to treat NAFLD.

6.2 Introduction

Nonalcoholic fatty liver disease (NAFLD) is characterized by hepatic fat accumulation in the absence of significant alcohol intake. Obesity-associated insulin resistance plays a major role in the pathogenesis of NAFLD and worsens with disease progression. In fact, it is estimated that 70% of patients with type 2 diabetes (T2D) and 90% of obese individuals display NAFLD[448–450]. Under conditions of obesity and insulin resistance, accelerated adipose tissue lipolysis, especially in visceral fat[451], delivers an abundant supply of non-esterified fatty acids (NEFAs) to the liver. This effect is compounded by the release of NEFAs by subcutaneous fat as its capacity to store fat is exceeded[390]. In total, it has been estimated that ~60% of liver Triacylglycerol (TAG) originates from circulating NEFAs, ~26% from fatty acids produced via the activation of *de novo* lipogenesis (DNL), and ~15% arise from dietary fat sources in obese NAFLD patients [452]. Through DNL, the liver is capable of synthesizing fatty acids from acetyl-CoA arising from the oxidation of multiple substrates (*e.g.* glucose and NEFAs) in the Krebs cycle[450]. Additionally, the regular consumption of a carbohydrate-rich diet has been associated with the development of NAFLD[453]. Of particular relevance is fructose, a monosaccharide that is cleared by the liver from the portal vein and almost entirely diverted to the pathway of DNL, as it cannot be processed in the glycolytic pathway[300]. Two key transcription factors, sterol regulatory element-binding protein 1c (SREBP1c, activated by insulin and liver X receptor α) and carbohydrate regulatory element-binding protein (ChREBP, activated by carbohydrates)[450], essentially regulate DNL. When activated, SREBP1c and ChREBP promote the expression of lipogenic genes including fatty acid synthase (FAS), acetyl-CoA carboxylase (ACC), and lipin 1[454]. This helps to explain why a diet rich in carbohydrates can lead to TAG overproduction and the development of NAFLD.

Importantly, the TAG synthesis pathway generates diacylglycerol (DAG) as an intermediate lipid[390,455]. DAG has been shown to activate protein kinase C (PKC), particularly the epsilon (PKCε) isoform that predominates in the liver[390,456]. In its activated state, PKC inhibits tyrosine kinase activity of the insulin receptor[226], which then impairs all subsequent steps of the intracellular insulin signaling cascade causing insulin resistance. This is supported by observations that reduced PKCε expression protected rats from lipid-induced hepatic insulin resistance, despite not altering liver DAG and TAG contents[457]. In line with this, mice lacking *Prkce* did not develop insulin resistance after feeding on a high-fat diet, even though the content of fat in the liver of these animals increased[458]. Another class of lipids, namely ceramides, have also been associated with the development of hepatic steatosis and insulin resistance in obesity[459,460]. The mechanisms by which ceramides cause this effect are not well established. However, it appears to involve the activation of PKCζ and protein phosphatase 2A (PP2A) that lead to impairment of AKT translocation to the plasma membrane and dephosphorylation/inactivation of AKT, respectively[459]. Additionally, ceramides have been implicated in the inhibition of β-oxidation and activation of the nucleotide-binding domain, leucine-rich-containing family, pyrin domain containing 3 (NLRP3) inflammasome[461], which are also associated with insulin resistance and hepatic steatosis.

In recent years, the high-fat, carbohydrate-restricted ketogenic diet (KD) has emerged as an effective non-pharmacological intervention for the treatment of NAFLD and other metabolic disorders in obese subjects[462]. The KD lowers insulinemia and causes a metabolic shift in which fatty acid oxidation and ketone production are significantly increased[462]. These effects are compatible with an anti-steatotic effect of KD as they promote the disposal of fatty acids

entering the liver, limiting the availability of substrate for TAG synthesis. In fact, the induction of ketogenesis has been shown to prevent diet-induced fatty liver injury and hyperglycemia[463]. Additionally, because inflammation plays a key role in the physiopathology of obesity-induced insulin resistance and T2D, the anti-inflammatory effect of the KD[464] has also been directly linked to reduced hepatic steatosis and improved whole-body glycemic control[462]. However, what remains undetermined is how the KD-induced metabolic shift affects the liver content of DAG and ceramides, as well as PKCε activity and hepatic insulin sensitivity. Importantly, the ability of the liver to synthesize glycogen in response to insulin in the fed state is crucial to curtail hepatic glucose output and to maintain proper whole-body glycemic control[465]. In this context, we hypothesize that, despite providing an abundant source of dietary fat, the KD lowers DAG and ceramides levels and prevents the impairment of insulin signaling caused by these lipids in hepatocytes. To test this hypothesis, we measured TAG content, fatty acid oxidation, insulin signalling, insulin-stimulated glycogen synthesis, DAG and ceramides content, total and membrane-associated PKCε levels, as well as the expression of SREBP1c and ChREBP and inflammatory genes in livers of rats exposed for 8 weeks to either an obesogenic (high-fat, sucrose-enriched diet) or a KD. Here, we provide evidence that the anti-steatotic and insulin sensitizing effects of the KD are associated with reduced DAG content, PKCε activity, and the expression of lipogenic and inflammatory genes, despite markedly increased hepatic accumulation of ceramides.

6.3 Materials and Methods

Reagents – Fatty acid (FA)-free bovine serum albumin (BSA), glycogen, palmitic acid, beta-hydroxybutyrate (βHB) assay kit (cat # MAK041), and N-Acetyl-D-sphingosine were obtained

from Sigma (St. Louis, MO, USA). Diolein was from Nu-check (Elysian, MN, USA). Human insulin (Humulin R) was purchased from Eli Lilly Inc. (Toronto, ON, Canada). The insulin ELISA kit and Luminata Forte were from Millipore (Billerica, MA, USA). The RNeasy Kit was from Qiagen Inc. (Toronto, ON, Canada) and the DNase from Thermo Fisher Scientific (Waltham, Massachusetts, USA). D-[U-^{14}C] glucose and [1-^{14}C] palmitic acid were from GE Healthcare Radiochemicals (Quebec City, QC, Canada). The reverse phase column (C18 5µm 250 x 4.6mm) was from Restek (Bellefonte, PA, USA). The subcellular protein fractionation Kit was from Thermo Fisher (Cambridge, MA, USA). The PKCε antibody (cat # 2683), AKT (cat # 9272), P-AKT (cat # 9271), GSK3α/β (cat # 5676), P-GSK3α/β (cat # 9331) and β-actin (cat# 4967) were purchased from Cell Signalling Technology Inc. (Beverly, MA, USA).

Animals – Male albino rats from the Wistar strain (Envigo, Indianapolis, IN, USA) weighing 200 – 250 g (initial weight) were maintained in a 23^{o}C room with a fixed 12h light/12h dark cycle. The animals were fed for 8 weeks *ad libitum* one of the following diets: standard chow (SC, 27.0%, 13.0%, and 60.0% of calories provided by protein (casein), fat, and carbohydrates, respectively, energy density = 3.43 kcal/g), a high-fat, sucrose-enriched diet (HFS, 20.0%, 60.0%, and 20.0% of calories provided by protein [casein], fat [lard/soybean oil], and carbohydrates [sucrose], respectively, energy density = 5.24 kcal/g) or a ketogenic diet (KD, 20.0%, 80.0%, and 0.0% of calories provided by protein (casein), fat (lard/soybean oil), and carbohydrates, respectively, energy density = 6.14 kcal/g). The standard rat chow diet (cat # 5012) was purchased from TestDiet (Richmond, IN, USA). The HFS and KD (cat # D12492 and D03022101, respectively) were purchased from Research Diets Inc. (New Brunswick, NJ, USA).

Ethics approval – The investigators understand the ethical principles under which the journal operates and that their work complies with this animal ethics checklist. The protocol containing all animal procedures described in this study was specifically approved by the Committee on the Ethics of Animal Experiments of York University (York University Animal Care Committee, YUACC, permit number: 2021-03 and performed strictly in accordance with the YUACC guidelines. All tissue extraction procedures were performed under ketamine/xylazine anesthesia (90 mg and 10 mg/100 g B.W., respectively), and all efforts were made to minimize suffering. Upon completion of tissue extraction, all animals were decapitated. All experiments in this study were carried out in compliance with the ARRIVE guidelines. The investigators understand the ethical principles under which the journal operates and that their work complies with this animal ethics checklist.

Liver morphology – Morphological analysis of liver samples was performed using light microscopy as described previously [466]. Briefly, ~50 mg of liver tissue was collected from each animal and fixed in 4% paraformaldehyde, 0.1 M phosphate-buffered saline (PBS), pH 7.4, for 24h at 4^{o}C. Following fixation, liver samples were washed three times in PBS and stored at 4°C in 70% ethanol. Samples were then embedded in paraffin blocks, sectioned (thickness 3 μm), and stained with hematoxylin and eosin. Digital images of tissue sections were captured with a Nikon Eclipse microscope (Nikon Canada, Mississauga, ON, Canada) under 40x magnification.

Glucose monitoring, determination of βHB, glucose, and insulin in the plasma – Blood from all animals was collected in the fed state between 09:00 and 10:00 by saphenous vein bleeding. Plasma glucose was measured using the Contour Next one meter blood glucose monitoring system by Ascensia Diabetes Care US (Parsippany, NJ, USA). Insulin and βHB were measured

using commercially available kits listed in the reagents section. All procedures were performed according to instructions provided by the manufacturers of the kits.

Incubation of liver slices and determination of glycogen synthesis and glycogen content – All animals were anesthetized with a single intraperitoneal injection of ketamine/xylazine (90 mg and 10 mg/100 g B.W., respectively). Subsequently, the liver was quickly extracted. Three sets of liver strips (18 – 22 mg) were immediately placed in plastic scintillation vials containing 2 ml of pre-gassed [30 min with O_2:CO_2-95:5 % (vol/vol)] Krebs-Ringer bicarbonate (KRB) buffer containing 4% fat-free BSA and 6 mM glucose. The vials were sealed with rubber stoppers and gasification was continued during the entire 1h pre-incubation period. For the determination of glycogen synthesis, one set of liver strips was transferred to vials containing 2 ml of the same KRB buffer plus D-[U-^{14}C]glucose (0.2 µCi/ml) and incubated under continuous gasification for one additional hour either in the absence (basal) or presence of insulin (100 nM). Immediately after incubation, liver strips were quickly washed in ice-cold PBS, blotted on filter paper, frozen (N_2), and digested in 0.5 ml of KOH 1M at 70^{o}C for 1h. Subsequently, glycogen was precipitated overnight (-20^{o}C) with 100% ethanol, resuspended in 0.5 ml of water, and its radioactivity was determined using a scintillation counter. For the determination of glycogen content, an aliquot (100 µl) of the digested liver sample was used. To the digested tissue, 10% (v/v) of acetic acid 17M and 500 µl of acetate buffer (pH 4.8) with amyloglucosidase (0.5 mg/ml) were added, and the solution was incubated overnight. On the following day, the solution was neutralized with 1/16 (v/v) of NaOH (5N), mixed with 1 ml of ATP-TRA buffer, and vortexed. Lastly, 1 ml of the solution was placed in a cuvette and absorbance (λ= 340 nm) was determined spectrophotometrically[467].

Measurement of palmitate oxidation – Palmitate oxidation was measured by assessing the production of $^{14}CO_2$ from [1-^{14}C]palmitic acid. The flasks where liver slices were incubated contained 2 ml of KRB buffer plus 0.2 mM of cold palmitic acid previously complexed with fatty acid-free BSA and [1-^{14}C]palmitic acid (0.2 µCi/ml). The slices were incubated under continuous gasification for 1h and the vials had a centered isolated well containing a loosely folded piece of filter paper moistened with 0.2 ml of 2-phenylethylamine/methanol (1:1, vol/vol). After the 1h incubation-period, liver slices were quickly removed and the media were acidified with 0.2 ml of H_2SO_4 (5N), and the flasks were maintained sealed at 37°C for an additional 1h for collection of the $^{14}CO_2$ released. Subsequently, the filter papers were carefully removed and transferred to scintillation vials for radioactivity counting[433].

Determination of DAG, TAG, and ceramides contents – The ultra-high-pressure liquid chromatography system (UHPLC-UV, Nexera X2, Shimadzu, Kyoto, Japan) was used to measure total amounts of DAG, TAG, and ceramides[433] in lipid samples extracted using the Folch's method[468]. Briefly, 50 mg of liver tissue was homogenized in 200 µl of chloroform:methanol (MeOH) [2:1 vol/vol], dried overnight under nitrogen gas, and resuspended in 100 µl of 2-propanol-hexane (ProHex, 5:4 vol/vol) prior to chromatographic analysis. Quantification was performed using the UHPLC-UV detection machine. Sample volumes (50µl) were injected automatically into a reverse phase column (C18 5 µm 250 x 4.6 mm). The chromatography conditions were set to 40°C for 20 min using a gradient of MeOH and ProHex:100% of MeOH from 0 to 10 min, followed by 50% of MeOH and 50% of ProHex for 10 min, maintained with isocratic elution for 10 min. Diolein (0.25 µg/µl) and Triolein (0.25 µg/µl) were also dissolved in ProHex and quantified to obtain a standard curve[413]. To analyse total ceramide content, a small volume of the lipid extract obtained after chloroform extraction

was transferred into new pre-weighed eppendorfs as previously described[414]. The organic phase was hydrolyzed in 1M KOH at 90°C for 60 min. The sphingosine liberated from ceramides was analyzed by means of UHPLC by mixing it with 15 µl OPA reagent and allowing it to derivatize for 20 min at room temperature. The calibration curve was prepared using N-Acetyl-D-sphingosine as a standard. The samples were reconstituted in 100 µl of chloroform-methanol-acetic acid-water (50:37.5:3.5:2 vol/vol/vol/vol) and run through a porous silica column (ARC-18 1.8µm 100 x 2.1mm). Elution was conducted with heptane-isopropyl ether-acetic acid (60:40:3 vol/vol/vol) at a gradient from 0 to 10% in 30 min at a flow rate of 0.8 ml/min followed by isocratic elution with acetonitrile: deionized distilled water (90:10, vol/vol) and a flow rate of 1 ml/min[240]. Subsequently, the column was equilibrated with chloroform-methanol-acetic acid-water (50:37.5:3.5:2 vol/vol/vol/vol) for 10 min at the same flow rate.

Western blot Analysis – Liver samples were immediately washed in ice-cold PBS, snap frozen in liquid $N_{2,}$ and stored in -80°C. Approximately 20 mg of the frozen samples were homogenized in 350 µl of lysis buffer containing 135 mM NaCl, 1 mM $MgCl_2$, 2.7 mM KCl, 20 mM Tris, 1% Triton X-100, 10% Glycerol, protease inhibitor (1:100) (cOmplete ULTRA Tablets), and phosphatase inhibitor (1:100) (PhosStop). Sample homogenates were then centrifuged (16,000 g for 10 min at 4°C) and the supernatant was collected and transferred to a separate microtube. An aliquot was taken for determination of protein concentration, which was measured using the Bradford method. Finally, the samples were diluted 1:1 in 2x Laemmli buffer, heated at 95°C for 5 min, and subjected to SDS-PAGE. Samples were probed with antibodies for total AKT, P-AKT (Ser_{473}), total GSK3αβ, P-GSK3αβ (Ser_{21}), and β-Actin (loading control). The developed blots were scanned and quantified using ImageJ software by

National Institutes of Health and the Laboratory for Optical and Computational Instrumentation (LOCI, University of Wisconsin).

Tissue fractionation and Western blotting analysis of PKCε content and its cellular localization – PKCε protein levels were determined in the cytosolic and membrane fractions by immunoblotting [433]. Liver homogenates (50 mg) were used to obtain the cytoplasmic and membrane protein fractions using a subcellular protein fractionation kit from Thermo Fisher Scientific (Waltham, MA, USA). The separated fractions were then collected, and respective aliquots were used to measure the protein content by the Bradford method. Samples were then diluted 1:1 (vol/vol) with 2x Laemmli sample buffer, heated to 95°C for 5 min, and subjected to SDS-PAGE. A PKCε-specific antibody (1:2,000 dilution) was used to determine its subcellular localization.

Quantitative PCR analysis – Total RNA was isolated from liver samples using the using Trizol™ (Thermo Fisher Scientific, Waltham, MA, USA). Primer sequences for the following genes: cluster of differentiation 40 (*Cd40*), ceramide synthases 1, 2, 4, 5, and 6 (*CerS 1, 2, 4, 5, and 6*), carbohydrate response element-binding protein (*Chrebp*), diacylglycerol acyltransferase 2 (*Dgat2*), death receptor FAS (*Fas*), fatty acid synthase (*Fasn*), fibroblast growth factor 21 (*Fgf21*), interleukin 6 (*Il-6*), nuclear factor kappa-beta (*Nf-kb*), phosphoenolpyruvate carboxykinase (*Pepck*), peroxisome proliferator-activated receptor-gamma co-activator-1α (PGC-1α), sterol regulatory element-binding protein-1c (*Srebp-1c*), TATA-box-binding protein (*Tbp*), toll-like receptor 4 (*Tlr4*), and tumor necrosis factor α (*Tnf-α)* were designed using the software PrimerQuest (IDT) based on probe sequences available at the Affymetrix database (NetAffx™ Analysis Center, http://www.affymetrix.com/analysis) for each

given gene. Real-time PCR reactions were carried out as previously described[469] and the amplification conditions were as follows: 95°C (10 min); 40 cycles of 95°C (15 s), 60°C (60 s) using the CFX96 Real-time system from Bio-Rad. All genes were normalized to the *Tbp* gene with relative differences in expression between treatment groups determined using the ΔΔCt method[470] expressed as relative to the SC control group. Table 1 shows Primer sequences used.

Statistical Analyses – Data were expressed as Mean ± SD. Statistical analyses were performed by using One-way ANOVA with Bonferroni multiple comparison post-hoc test as indicated in the figure legends. Parametric tests selected for statistical significance were based on normality tests (the D'Agostino & Pearson test and the Kolmogorov-Smirnov test) performed on the data. The GraphPad Prism software version 9.4.1 was used for all statistical analyses and for the preparation of all graphs. The level of significance was set to $p<0.05$.

Table 6.1: Primer sequences for qPCR analysis.

Genes	Forward	Reverse
Cd40	AGATTATCCCGGTCACAACAC	TCTGAGATGCGACTCTCTTTACC
CerS1	CTCCGTGCTCTTCTTCGATAAT	ACAAACGGTCCCTGCTTT
CerS2	CCTAGATCTCACTGCCTCCTAT	CAGAACTAGTTGCCCTTCTACTC
CerS4	GCCTCCAGCATTGTGGATATT	GAAGGGAAACAGATCACCAGTC
CerS5	GCCATCGGAATCAGGAC	GCCAGCATGTCGGATGT
CerS6	GTTCGGAGCATTCAACGCTG	CTGAGTCGTGAAGACAGAGG
Chrebp	CGACACTCACCCGCCTCTTC	TTGTTCAGCCGAATCTTGTC
Dgat2	AGACCAAATTCGGCCTTCCAGAGA	TTTGCAGTCATTCCTTCCAGGAGC
Fas	AAGGCATCACCATAGCTACAGCCT	TATGCTTCTCACAGTGGCCACACA
Fasn	CCCAGTGTGACCAAGCACGCC	GCGCTGGAGCACAAGGAACGC
Fgf21	GGTACACATTGTATCCGTCCTT	CAACAACCAGATGGAACTCTCTA
Il-6	TGGCAACCTTAGTGCTCATT	TGTCTGCTCCAGCTTGTTAC
Nf-κb	TCCAGCTGCTATTGGATTACAC	GGGATGCGATACCTTAATGAC

Pepck	CTCACCTCTGGCCAAGATTGGTA	GTTGCAGGCCCAGTTGTTGA
Pgc-1α	ACCGTAAATCTGCGGGATGATGGA	ATTCTCAAGAGCAGCGAAAGCGTC
Srebp-1c	GGACCACAGAAAGGTGGAAT	GGCAGTTGATGTAGAGGCTAAG
Tbp	TACAGGTGGCAGCATGAATGACA	AACCAACAATCACCAGCAGCAGTG
Tlr4	ACCTAAGGAGAGGAGGCTAAG	GGTAACTGCAGCACACTACA
Tnfα	GGGACAGTGACCTGGACTGT	TTCGGAAAGCCCATTTGAGT

6.4 Results

Energy intake, body weight, and adiposity – Food was provided *ad libitum* and the animals adjusted food intake to compensate for the differences in energy density of the diets. As such, total energy intake during the feeding period did not differ among the groups (data not shown). However, at the end of the 8-week dietary intervention period, the HFS-fed and KD-fed groups gained significantly more body weight (BW) than SC-fed rats (Figure 6.1 A). Similarly, the subcutaneous inguinal (Sc Ing) and epididymal (Epid) fat masses were significantly higher in HFS- (2.3-fold) and KD-fed (1.3-fold) rats than SC-fed rats (Figure 6.2 B). Despite no significant differences in BW between HFS and KD animals, the SC Ing and Epid fat pads of KD-fed rats displayed significantly lower masses (~25%) than HFS-fed rats (Figure 6.1 B). Thus, despite providing 80% of its calories from fat, in the absence of carbohydrates the KD caused less adipose tissue expansion than the HFS diet that provided 60% of its calories from fat.

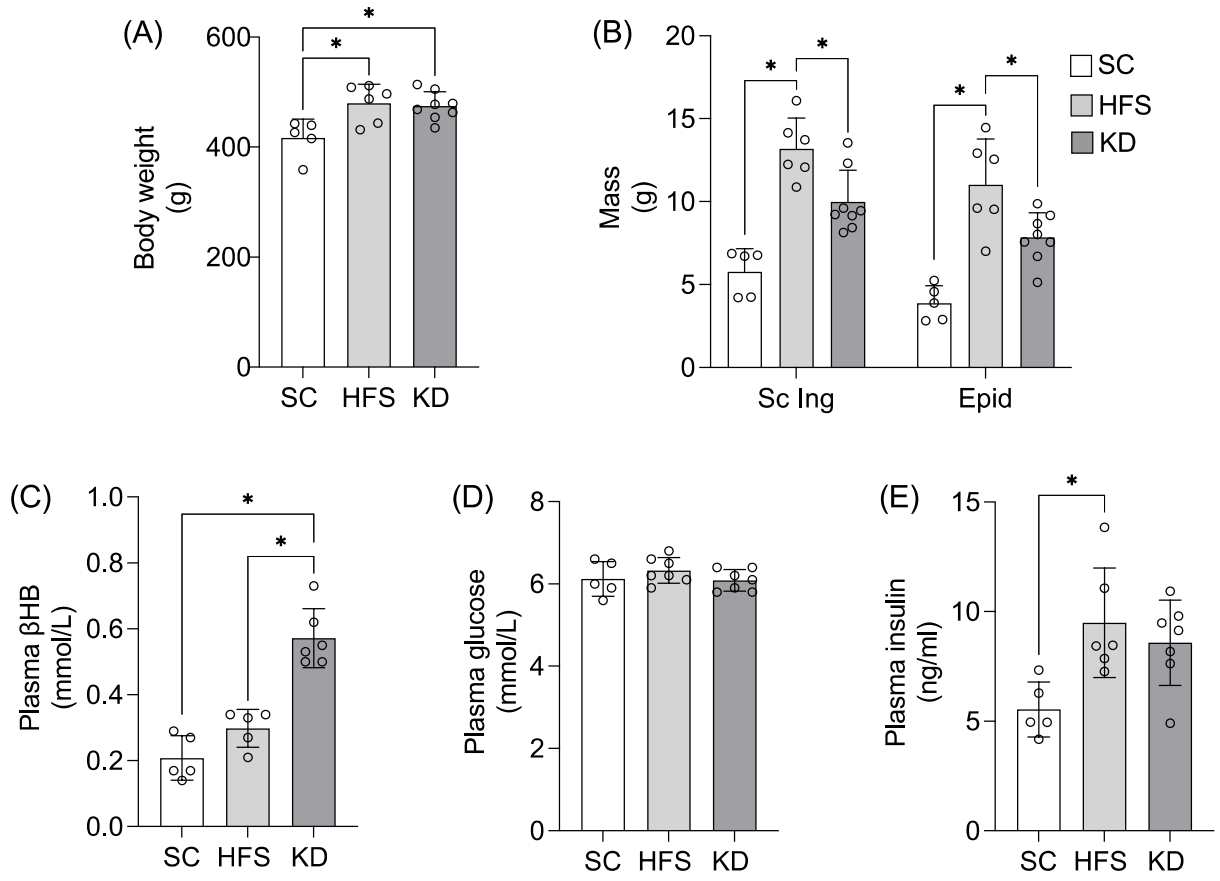

Figure 6.1: HFS and KD increase body weight (A), adiposity (B), **β**HB (C), glycemia (D), and insulinemia (E). However, adiposity was lower in KD- than HFS-fed rats. βHB, plasma glucose and insulin were measured in the fed state. Mean ± SD. *p<0.05, One-way ANOVA, n=5-8.

Plasma levels of βHB, glucose, and insulin **–** In the fed state, plasma βHB levels were ~2.7- and 1.9-fold higher in KD-fed than SC- and HFS-fed rats, respectively (Figure 6.1 C). Plasma glucose did not differ among the groups (Figure 6.1 D), whereas plasma insulin was significantly higher (~1.71fold) in HFS-fed rats than SC-fed rats (Figure 6.1 E). The KD-fed also displayed higher values (~1.5-fold) of plasma insulin than SC-fed rats, although it did not reach statistical significance (Figure 6.1 E).

Liver morphology, DAG, and TAG contents, Dgat mRNA expression, and palmitate oxidation – Light microscopy images of hematoxylin and eosin (H&E) staining of liver sections revealed that the HFS diet increased lipid droplets in hepatocytes, whereas the KD did not (Figure 6.2 A). In fact, the TAG content in livers of HFS-fed rats was 2.21- and 1.67-fold higher than SC- and KD-fed rats (Figure 6.2 B). This was also accompanied by DAG levels in livers of rats fed the HFS diet that were ~1.5-fold higher than SC-fed rats, whereas in KD-fed animals DAG levels did not differ from those of SC-fed rats (Figure 6.2 C). This was in line with mRNA expression of hepatic acyl CoA:diacylglycerol acyltransferase 2 (*Dgat2*), a key enzyme in TAG synthesis, being ~4-fold higher in HFS- than SC-fed rats (Figure 6.2 D). Even though *Dgat2* mRNA levels in KD-fed rats was 2.18-fold higher than SC-fed counterparts, it was still significantly lower (45%) than HFS animals (Figure 6.2 D). Additionally, rates of palmitate oxidation in liver tissue of HFS-fed and KD-fed rats were 1.94- and 2.30-fold higher than the rates detected in liver samples from SC-fed animals (Figure 6.2 E), respectively.

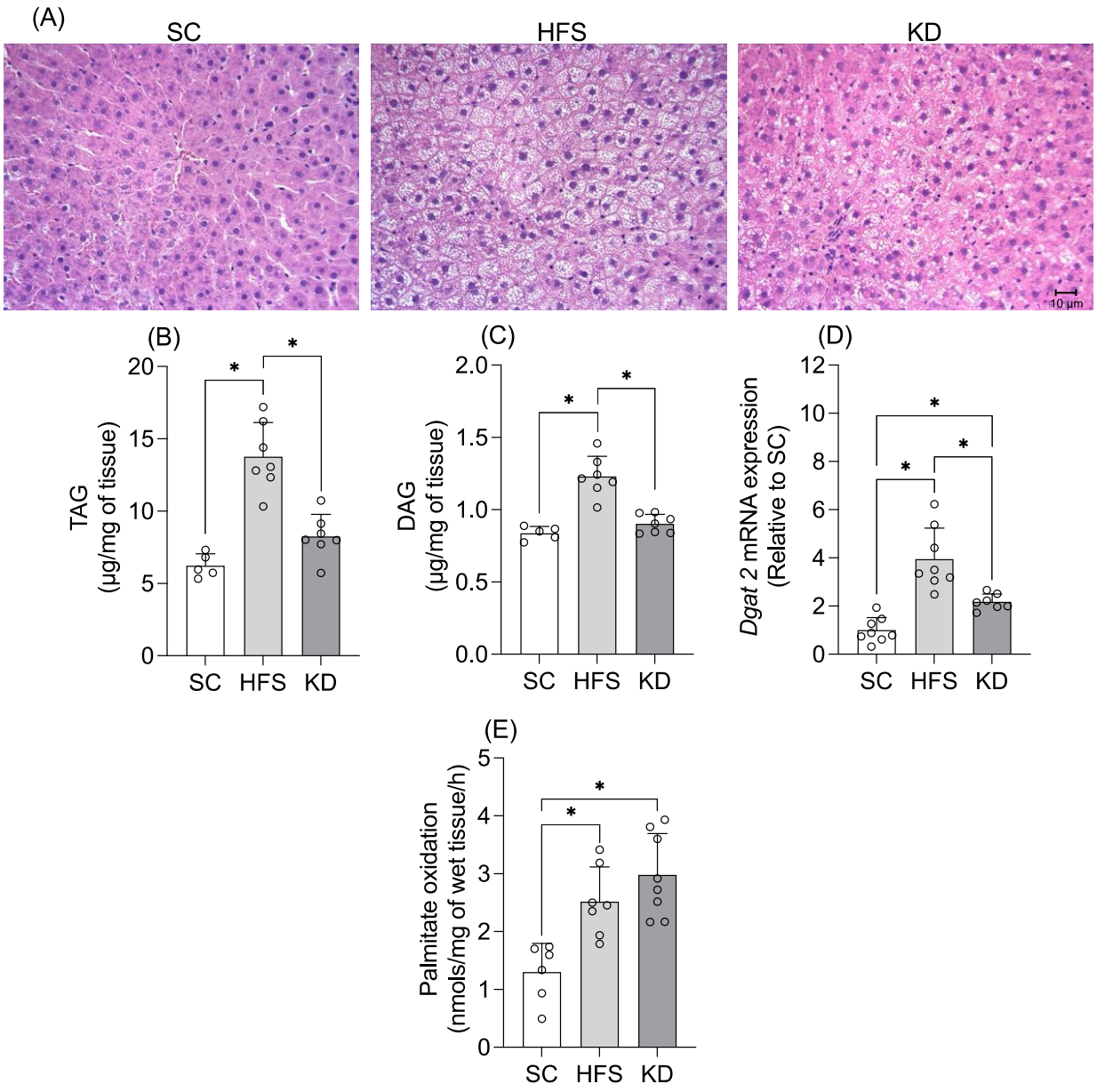

Figure 6.2: Contents of TAG (A and B) and DAG (C), as well as the mRNA of Dgat2 (D) increase in the liver of HFS-fed rats, but not in KD-fed rats in comparison to SC. Rates of palmitate oxidation (E) similarly increased by HFS and KD. Panel A shows representative Images of hematoxylin and eosin staining of liver sections (40x magnification, 10 µm scale). Mean ± SD. *p<0.05, One-way ANOVA, n=5-8.

mRNA expression of genes involved in mitochondrial biogenesis and the regulation of glucose and fat metabolism in the liver – Quantitative PCR analysis revealed that the KD increased liver mRNA expression of *Pgc1α* (Figure 6.3 A), *Pepck* (Figure 6.3 B), and *Fgf21* (Figure 6.3 C) by 3.34-, 8.26-, and 1.64-fold, respectively, when compared to SC-fed rats (Figure 6.3 A-C). Conversely, the KD reduced liver *Fasn* mRNA expression by 66% and 78% in comparison to SC and HFS rats, respectively (Figure 6.3 D). Furthermore, the mRNA expression of *Srbp1c* was slightly elevated by the HFS diet in comparison to SC and KD, but it did not reach statistical difference. Thus, *Srbp-1c* mRNA remained unaltered irrespective of the diet (Figure 6.3 E). The HFS diet significantly elevated the mRNA expression of *Chrebp* by ~3.6-fold, whereas the KD maintained *Chrebp* expression at the same level of SC-fed rats (Figure 6.3 F). These gene expression data are consistent with KD exerting an anti-steatotic effect by reducing lipogenesis and promoting mitochondrial biogenesis and fatty acid oxidation in hepatocytes.

Content of ceramides and mRNA expression of ceramide synthases (CerS) in the liver – Interestingly, we found that HFS and KD markedly increased ceramides by 2.35- and 4.63-fold, respectively, in comparison to SC-fed rats (Figure 6.4 A). Additionally, ceramides content in the livers of KD-fed rats were significantly higher (~2-fold) than in HFS rats (Figure 6.4 A). Further analyses of mRNA expression for *CerS* 1, 2, 4, 5, and 6 revealed that the HFS and KD affected liver expressions of these enzymes in a distinct manner. In fact, the HFS diet significantly increase mRNA expression of *CerS1* and *CerS2* by ~3-fold (Figure 6.4 B) and ~43.5-fold (Figure 6.4 C), respectively, whereas the KD did not affect mRNA expression of *CerS1* (Figure 6.4 B), although it significantly elevated the expression of *CerS2* by ~38-fold (Figure 6.4 C). Also, the HFS diet did not significantly affect the liver expression of *CerS4* (Figure 6.4 D) and

CerS6 (Figure 6.5 F) when compared to the SC diet. However, the KD significantly reduced liver mRNA expression of *CerS4* by 63% (Figure 6.4 D) and *CerS6* by 70% (Figure 6.4 F) when compared to HFS diet. Finally, the liver expression of *CerS5* did not differ among the diets (Figure 6.4 E).

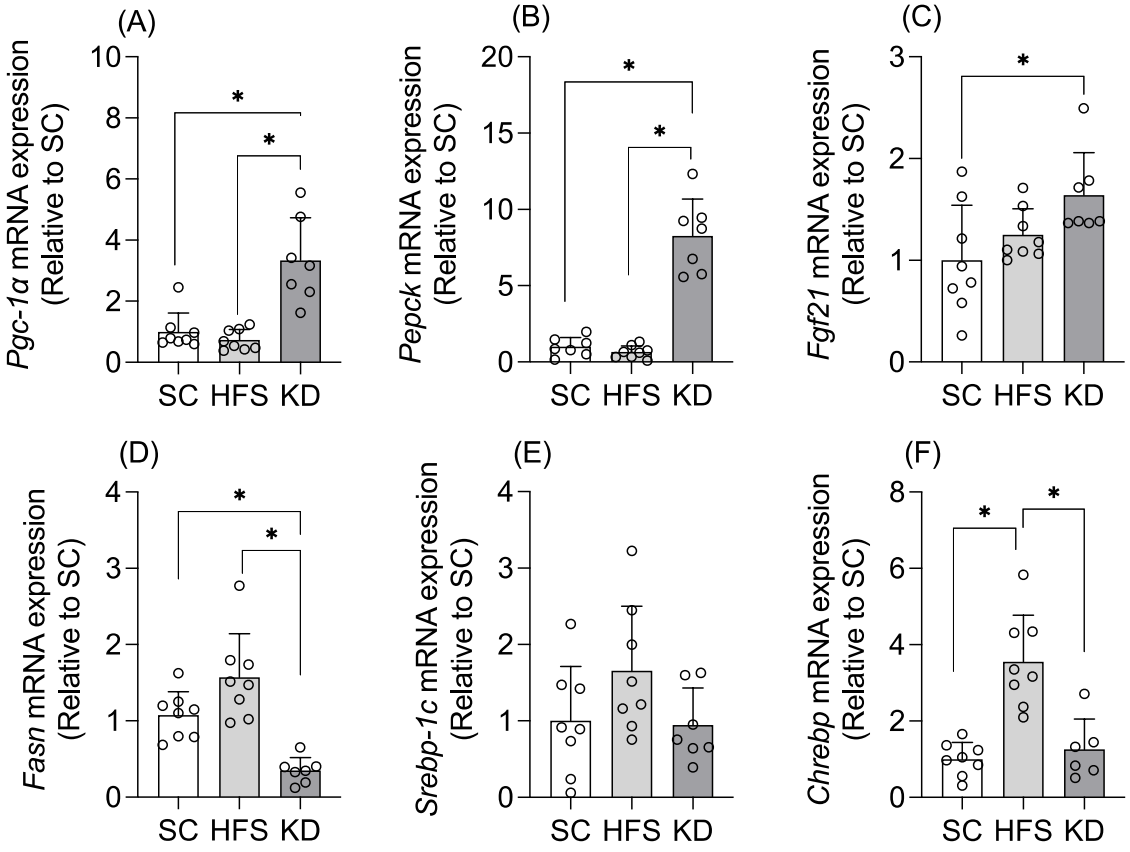

Figure 6.3: The hepatic mRNA expressions of Pgc-1α (A), Pepck (B), and Fgf21 (C) are increased, whereas the mRNA expression of Fasn (D) was downregulated by KD in comparison to SC and HFS diets. Contrary to the HFS diet, the KD maintained unaltered liver mRNA expressions of Srebp-1c (E) and Chrebp (F). Mean ± SD. *p<0.05 One-way ANOVA, n=7-8.

Total PKCε content and its cellular localization in the liver – Total PKCε levels remained unaltered irrespective of the diet (Figure 6.5 A). Because PKC activation requires translocation

from the cytoplasm to the membrane[471,472], we measured PKCε content in the membrane (Memb) and cytoplasmic (Cyto) fractions in liver. Although not statistically significant, HFS feeding increased the Memb:Cyto PKCε ratio by 1.37-fold, whereas the KD reduced this ratio by 40% in comparison to SC (Figure 6.5 B). However, livers from KD-fed rats displayed a significantly lower (60%) PKCε Memb:Cyto ratio than HFS rats (Figure 6.5 B). Thus, these data provide evidence that the KD maintained low levels of hepatic PKCε activity.

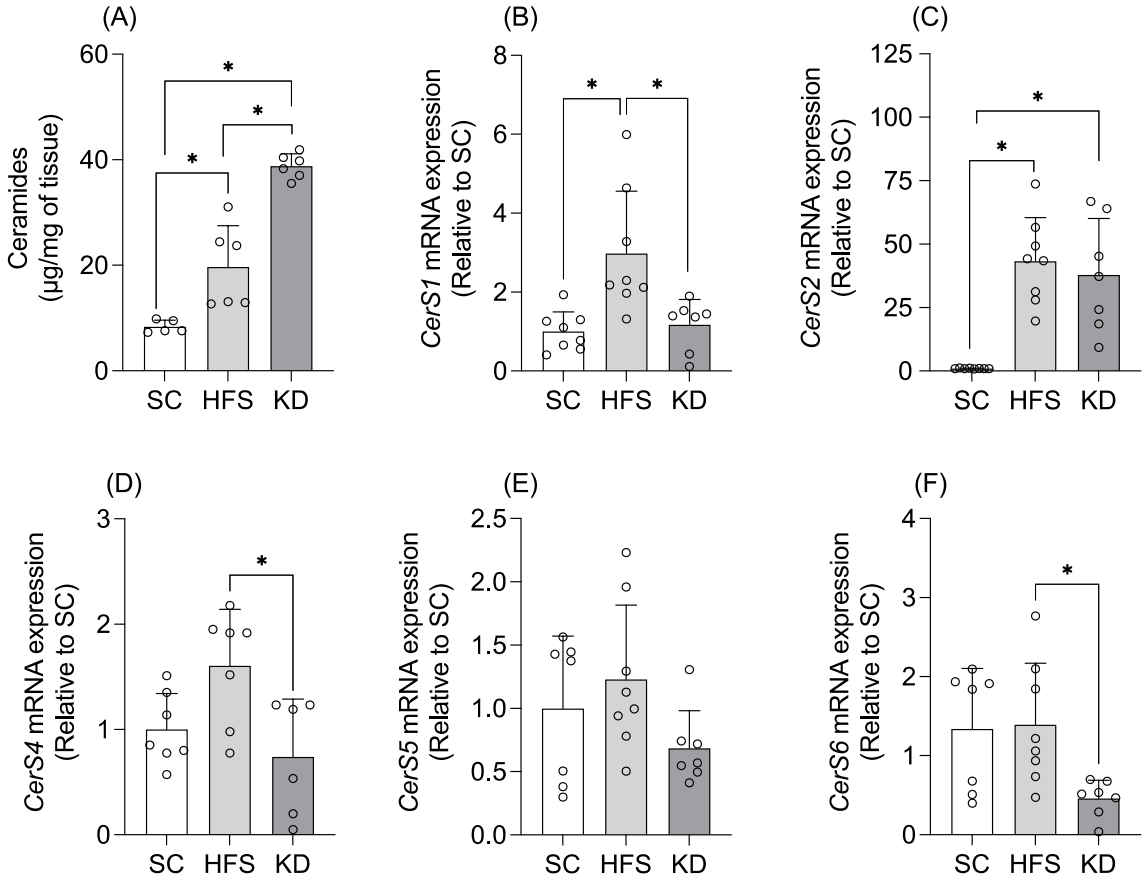

Figure 6.4: HFS and KD increase ceramides content (A), but distinctly regulate the expression of ceramide synthase (CerS) enzymes 1 (B), 2 (C), 4 (D), 5 (E), and 6 (F) in the liver. mRNA

expression data presented relative to standard chow (SC)-fed rats. Mean ± SD. *p<0.05 One-way ANOVA, n=5-8.

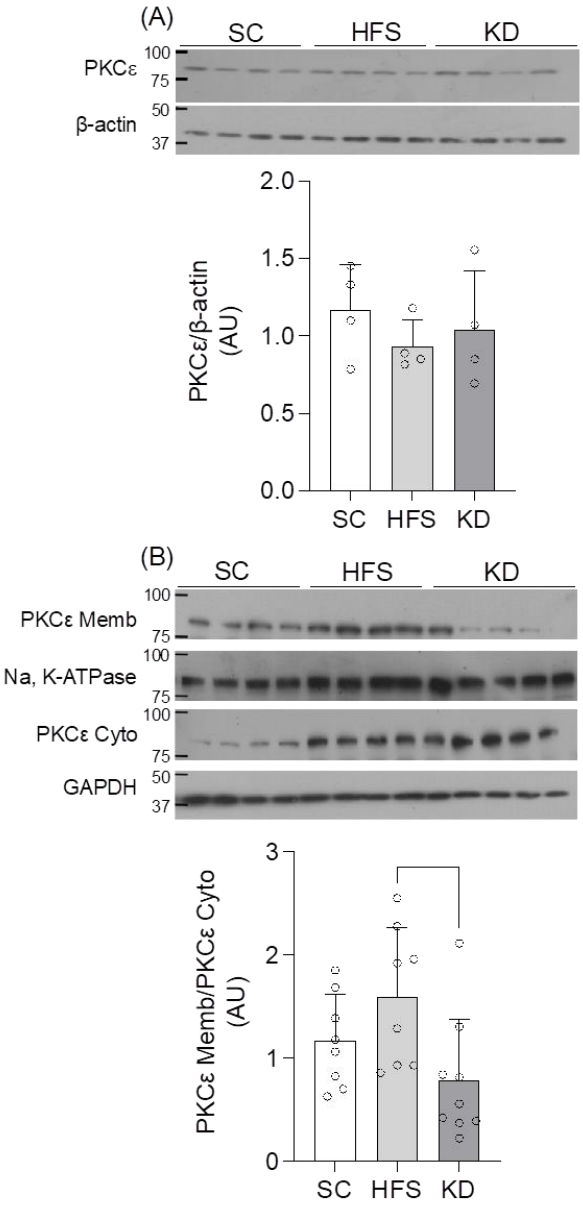

Figure 6.5: HFS and KD do not affect total cellular PKCε levels (A), but the translocation/activity of this kinase is significantly lower in KD-fed rats (B). Representative

blots and densitometric analyses of levels in membrane (Memb) and cytoplasmic (Cyto) cellular fractions were corrected by loading controls Na, K-ATPase and GAPDH, respectively. AU = arbitrary units. Mean ± SD. *p<0.05, One-way ANOVA, n=4 for total protein, n=8-9 for fractionated protein.

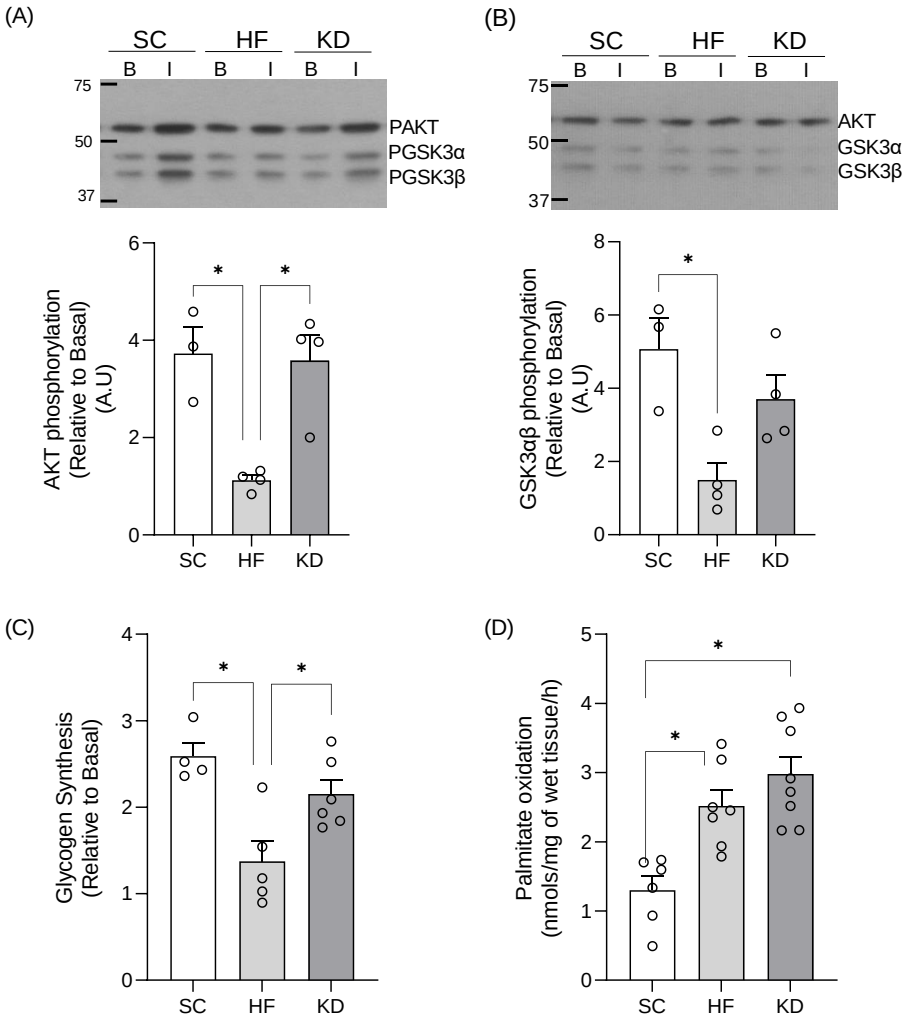

Figure 6.6: The HFS diet caused impairment of insulin signaling and glycogen synthesis, whereas the KD maintained hepatic cells responsive to insulin intact. Representative blots and densitometric analyses for AKT (A) and GSK3αβ (B) phosphorylation under basal (B) and

insulin (I, 100 nM)-stimulated conditions, as well as rates of glycogen synthesis (C) and total glycogen content (D) in incubated liver slices from SC-, HFS-, and KD-fed rats. Mean ± SD. *p<0.05, One-way ANOVA, n=3-6.

Insulin signaling and glycogen synthesis in incubated liver samples – Insulin-stimulated AKT phosphorylation in livers of HFS-fed animals was impaired by ~70% in comparison to SC- and KD-fed animals (Figure 6.6 A). Consistent with impaired AKT phosphorylation, insulin-stimulated GSK3αβ phosphorylation (Figure 6.6 B) and glycogen synthesis (Figure 6.6 C) were reduced by 70% and 47%, respectively, in livers of rats fed the HFS diet in comparison to SC-fed animals. The KD neither affected insulin-stimulated AKT nor GSK3αβ phosphorylations (Figure 6.6 A and B); therefore, the ability of hepatocytes to promote glycogen synthesis in response to insulin was preserved in KD-fed rats (Figure 6.6 C). No significant differences were detected for total liver glycogen content among the three dietary interventions (Figure 6.6 D).

mRNA expression of genes involved in inflammation – As expected, the HFS diet significantly elevated the liver mRNA expression of key inflammatory genes such as *Tnf-α* (Figure 6.7 A), *Nf-kb* (Figure 6.7 B), *Tlr4* (Figure 6.7 C), and *Il-6* (Figure 6.7 D) by 3.0-, 2.26-, 3.27-, and 2.38-fold, respectively, in comparison to SC-fed rats. The mRNA expressions of *Cd40* (Figure 6.7 E) and *Fas* (Figure 6.7 F) were not significantly affected by the HFS diet. When comparing the mRNA expression of inflammatory genes between the livers of KD-fed and SC-fed rats, no significant differences were detected (Figure 6.7 A-F). Thus, whereas the HFS diet exerted a pro-inflammatory effect, the KD and SC maintained a low hepatic inflammatory profile.

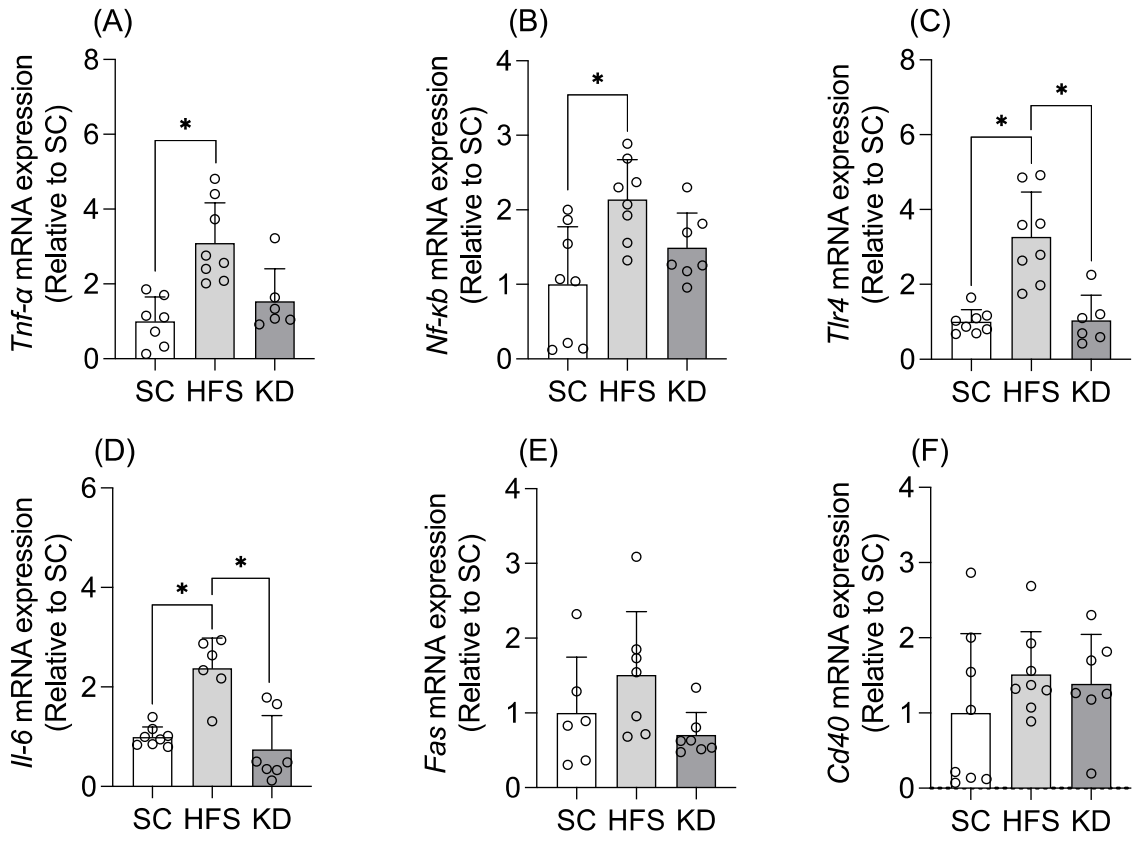

Figure 6.7: The HFS diet promoted inflammation, whereas the KD exerted an anti-inflammatory effect in the liver. *Tnf-α* (A), *Nf-κb* (B), *Tlr4* (C), and *Il-6* (D) liver mRNA expressions were significantly upregulated by HFS diet in comparison to SC and KD, whereas *Nf-κb* (E) and *Fas* (F) mRNA expressions did not differ among the diets. Mean ± SD. *p<0.05, One-way ANOVA, n=6-8.

6.5 Discussion

The main finding of this study was that despite providing 80% of its calories from fat, the KD maintained low levels of liver TAG content and preserved the ability of hepatocytes to respond to insulin and promote glycogen synthesis. These effects were accompanied by low levels of hepatic DAG accumulation and *Dgat2* mRNA expression, which also coincided with reduced

levels of membrane-bound PKCε. This latter effect of KD is consistent with low PKCε activity and maintenance of insulin signaling in hepatocytes[457]. However, we originally hypothesized that both DAG and ceramides would be reduced as a consequence of KD shifting metabolism towards fatty acid oxidation and ketone production, leaving less substrate available for the synthesis of these potentially deleterious lipid intermediates. Indeed, the KD significantly enhanced fatty acid oxidation, increased circulating βHB, and kept DAG and TAG at low levels in the liver. What is at odds with our original hypothesis is the fact that ceramides were markedly higher in KD than even the steatogenic HFS diet. This was surprising because elevated levels of ceramides has been associated with induction of AKT dephosphorylation via PP2A activation and impairment of translocation of this kinase from the cytoplasm towards the plasma membrane[459], leading to the development of insulin resistance. Interestingly, whereas in livers of HFS-fed rats insulin-stimulated phosphorylation of AKT and its downstream target GSK3αβ were markedly impaired, in livers of KD-fed rats insulin-stimulated AKT and GSK3αβ phosphorylations were intact, and so was the ability of hepatocytes to promote glycogen synthesis in response to insulin. Therefore, the KD-induced elevation in ceramides did not translate into impairment of insulin signaling and regulation of glucose metabolism in hepatocytes.

To further investigate why elevated ceramides did not lead to hepatic insulin resistance, we measured the mRNA expression of *CerS 1*, *2*, *4*, *5*, and *6*, which are enzymes that produce dihydroceramides, and determine much of the diversity in the cellular sphingolipid pool[461]. Ceramides vary in acyl-chain lengths between C14:0 and C30:0. Long-chain (C16-18) and very long-chain (C20-26) ceramides exert distinct effects in the liver, with the former generally being harmful and the later beneficial[473]. In this context, increased *CerS6* expression has been shown

to cause insulin resistance, whereas *CerS6* deficiency reduced C16:0 ceramides and protected mice from diet-induced obesity and glucose intolerance[350]. In this study, we found that the livers of rats fed a KD had a much lower level of *CerS6* mRNA expression than the steatotic and insulin-resistant HFS-fed rats, which is consistent with maintenance of hepatic insulin action in KD-fed animals. We have also found that *CerS1* and *CerS4* mRNA expression were significantly lower in KD- than HFS-fed rats, and that *CerS2* was equally elevated in both groups of rats. Importantly, *CerS2* has been reported to be the dominant isoform in the liver and preferentially produces very long-chain ceramides[474]. Moreover, mice with haploinsufficiency of *CerS2* display reduced levels of very long-chain ceramides and increased long-chain C16:0 ceramides in the liver, rendering the mice susceptible to steatohepatitis and insulin resistance[474]. Even though in this study we did not measure specific types of ceramides, it is plausible that the elevation of *CerS2* expression along with a marked reduction in *CerS6* expression shifted the production of ceramides predominately towards very long-chain ceramide species in KD-fed rats. In this scenario, the large increase in total ceramides in the liver of KD-fed rats ultimately led to a protective effective against hepatic steatosis and insulin resistance. Conversely, in HFS-fed rats, the elevated expression of *CerS1* and *CerS4* along with sustained *CerS5* and *CerS6* expression likely offset the increase in *CerS2*, leading to the accumulation of predominately harmful long-chain ceramides that created in these animals an environment conducive to steatosis and insulin resistance in the liver. Future studies are required to assess the production and distribution of various species of ceramides (long- and very-long chain) in the liver under conditions of KD feeding.

Consistent with the reduced hepatic content of glycerolipids and maintenance of insulin signaling were the increases in mRNA expressions of *Pgc-1α* and *Fgf21* in the livers of KD-fed

rats. This is supported by observations that PGC-1α is critical for the induction of β-oxidation and ketogenesis, as well as for the maintenance of insulin signaling in the liver[475]. In fact, mice deficient in liver PGC-1α displayed reduced capacity to oxidize fatty acids and subsequently developed steatosis[476–478]. Also, the administration of FGF21 to diet-induced obese and *ob/ob* mice increased fat utilization, reduced hepatic steatosis, and improved glycemic control in these animals[479]. The liver is the main source of circulating FGF21[480], and the actions of this hormone in hepatocytes require PGC-1α[481]. FGF21 has been reported to enhance gluconeogenesis, fatty acid oxidation, and ketogenesis[480], which are metabolic adaptations we did observe in KD-fed rats. Previous studies have also shown that feeding mice a KD induces hepatic expression and circulating levels of *Fgf21*, whereas knock-down of this hormone in the liver caused steatosis and reduced serum ketones in KD-fed mice[482]. Importantly, the KD used in this study was devoid of carbohydrates and the animals relied essentially on gluconeogenesis for the maintenance of glycemia. Indeed, KD-fed rats displayed a marked elevation in hepatic *Pepck* expression along with an increase in TCA cycle flux that shifted substrate away from DNL. The latter effect being in line with our findings that *Fasn* mRNA expression in the livers of KD-fed rats was significantly reduced in comparison to SC- and HFS-fed rats. Moreover, SREBP1c and ChREBP, the two main transcription factors that regulate DNL[450], did not have their mRNA expressions altered by KD. In contrast, the steatotic and insulin-resistant HFS-fed rats displayed much higher levels of *Fasn* and *Chrebp* mRNA expression in the liver than KD-fed rats.

The harmful effects that diet-induced obesity causes to liver function has also been, at least in part, attributed to the induction of systemic inflammation as fat mass expands[483]. In fact, inflammation has been linked to impairment of insulin signaling and the development of hepatic steatosis[484]. Two cytokines, TNF-α and IL-6, and other mediators of inflammation such as

TLR4 and NF-κB have been identified as key players in obesity-induced hepatic insulin resistance and NAFLD[483]. It has been previously reported that the KD exerts an anti-inflammatory effect via βHB-mediated blockage of palmitate-, ceramide-, and sphingosine-induced NLRP3 inflammasome activation in mouse bone marrow-derived macrophages[464]. βHB has also been shown to inhibit the processing of IL-1β in response to TLR4 agonism[464]. In KD-fed rats, the levels of βHB in the serum were 2.7- and 1.9-fold higher than in SC- and HFS-fed rats, respectively. This likely contributed to prevent potential deleterious ceramide-mediated inflammatory effects in the livers of KD-fed rats. Indeed, this is consistent with our observations that the hepatic mRNA expression of *Tnfα, Nf-kb, Tlr4,* and *Il-6* were all much lower in KD-fed rats than in HFS-fed counterparts.

In summary, despite having a higher fat content than the HFS diet, the carbohydrate-free KD did not cause hepatic steatosis and preserved the ability of hepatocytes to promote glycogen synthesis in response to insulin. This was compatible with a metabolic shift that led to a reduction in hepatic DAG content and PKCε activity, although at odds with a marked increase in the liver content of ceramides caused by the KD. However, by increasing the expression of *CerS2* and suppressing *CerS6* expression, the KD likely promoted the production of potentially beneficial very long-chain ceramides as opposed to harmful long-chain ceramides. The KD also enhanced the expression of *Pgc-1α, Pepck,* and *Fgf21,* downregulated *Fasn* and *Chrebp,* and shifted substrate away from DNL. Finally, the KD exerted an anti-inflammatory effect by downregulating the expression of *Tnfα, Nf-kb, Tlr4, and Il-6* in the liver. Thus, through multiple mechanisms the KD was able to exert an anti-steatogenic and insulin-sensitizing effect in the liver.

Authors Contribution: *Shailee Jani*: Acquisition or analysis or interpretation of data for the work; Drafting the work or revising it critically for important intellectual content; Final approval of the version to be published; Agreement to be accountable for all aspects of the work. *Daniel Da Eira*: Acquisition or analysis or interpretation of data for the work; Drafting the work or revising it critically for important intellectual content; Final approval of the version to be published; Agreement to be accountable for all aspects of the work. *Mateja Stefanovic*: Acquisition or analysis or interpretation of data for the work; Final approval of the version to be published; Agreement to be accountable for all aspects of the work. *Rolando Ceddia*: Conception or design of the work; Acquisition or analysis or interpretation of data for the work; Drafting the work or revising it critically for important intellectual content; Final approval of the version to be published; Agreement to be accountable for all aspects of the work.

Grants: This research was funded by a Discovery Grant from the Natural Science and Engineering Research Council of Canada (NSERC) and by infrastructure grants from the Canada Foundation for Innovation (CFI) and the Ontario Research Fund (ORF) awarded to RBC. DDE was funded by NSERC Alexander Graham Bell Canada graduate scholarship-Doctoral.

Disclosures: The authors state no conflict or duality of interest with regards to this work.

Data Availability Statement: All data supporting the results are included within the figures revealing their range and distribution.

Chapter 7 Summary

In this dissertation, we aimed to develop an understanding of integrated mechanisms that are involved in the pathophysiology of insulin resistance, concentrating on the two primary insulin target tissues, skeletal muscle, and the liver, specifically in the setting of diet-induced obesity.

It is widely accepted that an impairment in the insulin mediated glucose disposal in skeletal muscles leads to a reduction in the uptake of glucose from the blood to be stored in the form of glycogen. This elevates whole-body blood glucose levels leading to insulin resistance and eventually T2D. However, the molecular mechanisms underlying the relationship between obesity and skeletal muscle insulin resistance are not completely understood. The pathogenesis of obesity-induced insulin resistance in skeletal muscles has been assumed to be caused by a number of mechanisms, including excessive intramyocellular lipid accumulation, mitochondrial dysfunction, increased levels of inflammatory cytokines, and increased oxidative stress. Moreover, it is possible that the mechanisms driving diet-induced insulin resistance differ depending on the fibre type composition of different skeletal muscles. Skeletal muscle is a heterogeneous tissue consisting of three general phenotypes, which include oxidative type I myofibers (type I), these are myofibers that have higher concentrations of mitochondria, greater oxidative phosphorylation capacity, and capillary density compared to type II fibers. While type II fibers are subdivided into oxidative/glycolytic type IIa myofibers (IIa), and glycolytic type IIx myofibers (IIx)[97]. Several studies have found a positive correlations between type I myofibers and whole-body insulin sensitivity as well as greater insulin-stimulated glucose uptake in type I myofibers[115,272]. These studies also show increased insulin-stimulated glucose uptake in type I myofibers compared to type II myofibers in rodent studies. Additionally, Albers et al. have demonstrated that human type I myofibers had superior glucose absorption, phosphorylation and

oxidation, and glycogen production capabilities than type II myofibers[485]. Therefore, the first part of my thesis investigated if an obesogenic diet displayed a muscle fiber type-specific adaptation and if it was dependent on biological sex.

For the first study, in chapter 4, we investigated the effects of chronic high fat sucrose enriched feeding on in skeletal muscle in male Wistar rats. We studied three muscles based on their oxidative capacities, Sol (highly oxidative muscle rich in Type 1 fibers) [408], EDL (mixed muscle, rich in Type I and IIa fibers) [408], and Epit muscles (highly glycolytic, rich in Type IIa and IIb fibers) [409]. The HFS diet caused the animals to significantly gain weight and also have significantly increased whole-body fat oxidation. However, much to our surprise all muscles, regardless of their fiber-type developed insulin resistance under these conditions of overnutrition. Further, based on our hypothesis we expected that with the consumption of a HFS diet skeletal muscles rich in type I fibers oxidize more fat and therefore have reduced the availability of substrate to form lipid intermediates. Skeletal muscles that were rich in type IIb/x fibers have limited capacity to oxidize fat; therefore, the susceptibility of these cells to lipotoxicity would be increased under conditions of chronically elevated fatty acid abundance. However, fatty acid oxidation was enhanced regardless of fiber type distribution under a HFS diet and intercellular accumulation of DAG and ceramides displayed a fiber-type specific pattern. In relation to insulin resistance, lipotoxicity links both DAG and ceramide accumulation in skeletal muscle and the impairment of glycemic control[486]. Based on the theory, lipid intermediates are generated when there is an excessive inflow of FA into the skeletal muscle that overwhelms the use of FA via pathways such as β-oxidation and triacylglycerol synthesis. The DAG-induced and ceramide-induced insulin resistance involves the activation/translocation of protein kinase C (PKC), which, in turn, impairs the insulin signalling cascade and glucose

uptake and glycogen synthesis. However, there is a slight discord as to which PKC isoform is affected via DAG-induced insulin resistance[487]. Research conducted by Yu et al. and Griffin et al. identified PKC-theta (PKCθ) as the isoform that was activated post DAG accumulation in lipid infusion experiments on Wistar rats[488,489]. Also, human studies conducted by Itani et al. identified alterations in PKC-beta II (PKCβII) and PKC-delta (PKCδ)[490]. Conversely another study, used muscle biopsies to identify a correlation between DAG accumulation and PKCθ in insulin sensitivity in lean, obese and obese-diabetic human subjects. Therefore, involvement of DAG-induced PKC activation is well established, but the specific PKC isoform is yet to be identified[491]. Our findings on the lipotoxicity hypothesis, provided novel evidence that muscles with high capacity to oxidize fat (Sol and EDL) accumulated more DAG, TAG, and ceramides. However, these muscles were as vulnerable to developing insulin resistance as the Epit muscle with much lower ability to oxidize fat under conditions of HFS diet-induced obesity. As expected, the accumulation of excess lipotoxic metabolites (DAG and ceramides) activated protein kinase C (PKC) in male rats. We found that the total contents of two most prominent PKC isoforms (PKCδ and PKCθ) were much lower in Sol than in EDL and Epit muscles. However, analysis of the cytosolic and membrane fractions, revealed that the translocation of both PKCδ and PKCθ were markedly elevated in Sol muscles, whereas in EDL, only PKCδ translocation was increased by HFS diet. Conversely, in Epit muscles, translocation of both PKC isoforms was reduced. These findings were consistent with the fact that HFS feeding increased DAG and ceramides in Sol and EDL, but not in Epit muscles. Thus, obesity-induced insulin resistance was not necessarily determined by dysfunctional metabolic alterations in lipid metabolism within skeletal muscles. This is particularly relevant if one considers that even though skeletal muscles handle lipids in a fiber-type specific manner, insulin resistance

manifests in all muscles. Therefore, lipotoxicity may affect insulin signalling and glucose metabolism in oxidative muscles, whereas in glycolytic muscles elevated circulating inflammatory cytokines may have been the primary determinants of insulin sensitivity. It has been widely accepted that there is an association between increased weight gain and increased inflammation. To test this hypothesis, we also measured, circulating levels of inflammatory cytokines and corticosterone, as well as the expression of their receptors and *Nf-κb* in skeletal muscles of rats chronically exposed to the obesogenic diet. Indeed, we found that highly glycolytic Epit muscle was the only one that increased the expression of inflammatory cytokines (*Cd40, Fas, Tlr, and 11β-Hsd1*) and glucocorticoid signalling in male rats fed a HFS diet. Interestingly none of these variables were altered in highly oxidative, Sol muscle. Suggesting that the Epit muscle elicited a significant pro-inflammatory response under obesogenic conditions, which likely played a preponderant role in driving insulin resistance in this glycolytic muscle chronically exposed to the HFS diet.

Overall, as represented in **Figure 7.1**, our findings provide novel evidence why insulin resistance similarly develops in oxidative and glycolytic muscles of HFS-fed rats, despite major differences in their fat oxidizing capacity. Thus, while overconsumption of lipids appears to be an important factor that leads to disruption of insulin signalling and glucose metabolism in oxidative muscles (Sol and EDL muscles), in highly glycolytic muscles it is the activation of inflammatory pathways and upregulation of glucocorticoid signalling that was associated to the induction of impaired insulin sensitivity under conditions of chronic HFS feeding in male rats.

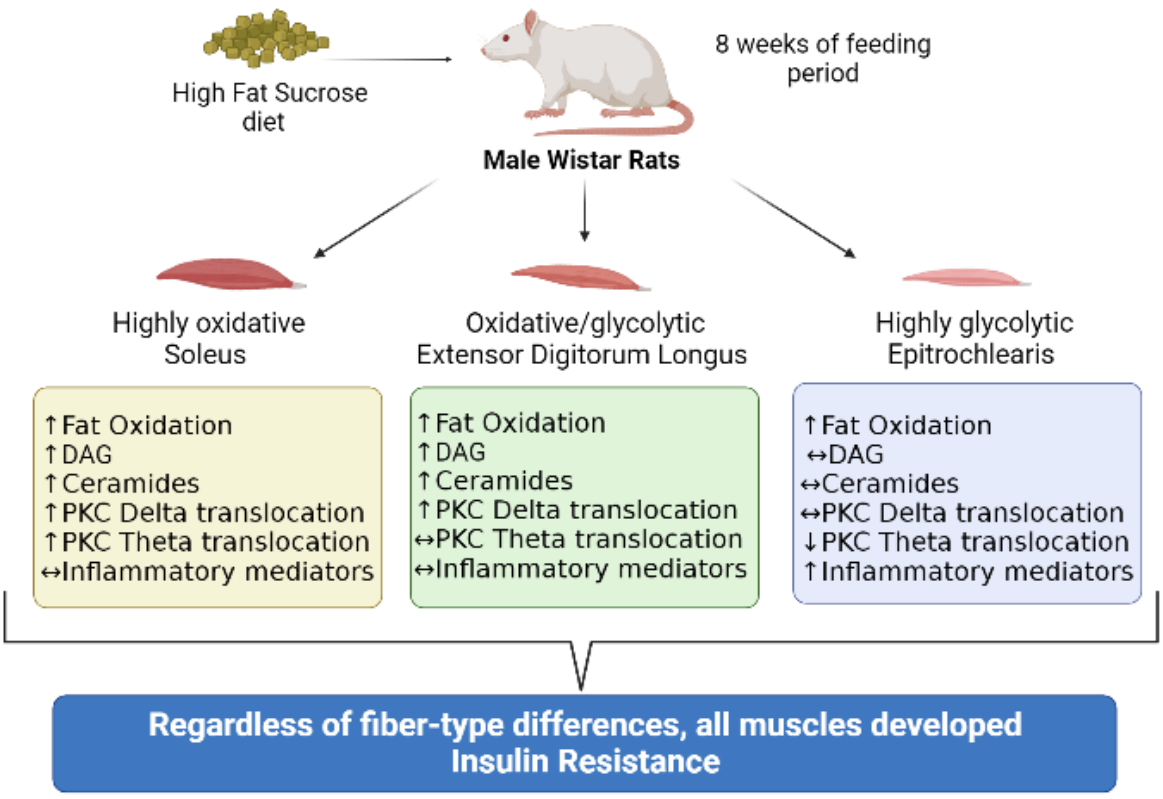

Figure 7.1: Schematic summary of the effects of a high fat sucrose enriched diet on skeletal muscle in male rats. Image generated using BioRender.

Several studies in rodent models have reported gender dimorphism in the development of obesity-associated to palatable hypercaloric and hyperlipidic diet with similar characteristics to diets usually consumed by humans. These studies have unanimously reported that females showed a greater susceptibility to weight gain as compared to men on the same diet[492,493]. However, females seemed to be more protected from obesity-associated disorders, such as hypertension[492] and sucrose-induced insulin resistance[494]. These differences could be observed because men have lower fat mass than women, making them less susceptible to dysfunctional metabolic alterations caused by lipotoxicity. Indeed, it has been reported that women are less prone to fatty acid-induced peripheral insulin resistance than men [264]. This was based on the

observation that acutely increased levels of circulating non-esterified fatty acids (NEFA) inhibited peripheral tissue insulin sensitivity in men, but not in women [264]. However, based on our knowledge, no sex differences have been reported regarding the contribution of specific peripheral organs (*e.g.* liver and skeletal muscle) to NEFA-induced insulin resistance in men versus women.

Hence, taking into account the reported role of accumulation of excess lipotoxic metabolites (DAG and ceramides) and pro-inflammatory markers in the development of obesity-associated insulin sensitivity impairment, the aim of the next study was to investigate whether there were gender differences found in development of high-fat sucrose enriched obesogenic diet-induced insulin resistance in rat skeletal muscle and if so, whether this happened in a fiber-type specific manner.

Similar to the male study, in chapter 5, female rats were fed a SC and a HFS diet for a span of 8 weeks in order to see the effects of an obesogenic diet. Despite consuming equivalent calories to a SC diet, female rats fed a HFS significantly gained body weight as well as an increase in their fat mass and muscle mass. But more importantly, the diet led to hyperglycemia and hyper insulinemia, effects that indicated the development of whole-body insulin resistance. This disparity with other published work[495], probed us further to understand the effects of the diet on skeletal muscles. Therefore, we studied Sol, EDL, and Epit in order to have muscles with different fiber-types and found, the obesogenic HFS diet significantly enhanced rates of fatty acid oxidation and displayed marked impairments in insulin-stimulated phosphorylation of the master regulator, AKT_{Thr308}, as well as impaired insulin-stimulated glycogen synthesis, glucose oxidation and lactate production in all muscles from female rats fed the obesogenic diet. Further, to understand the extent of the involvement of ectopic lipid accumulation, on lipid-induced

insulin resistance in the skeletal muscle we measured TAG, DAG and ceramide content using high-pressure liquid chromatography. In female rats the HFS diet-induced obesity and led to a significant elevation in intramuscular TAG and DAG contents without any alteration in ceramides levels in insulin-resistant female oxidative and glycolytic muscles. In addition, we also observed that the total levels of PKCδ in all muscles studied were not affected by feeding the HFS diet; however, total PKCθ content was significantly reduced in Sol and EDL, whereas in the highly glycolytic, Epit muscles it remained unaltered. Importantly, analysis of the cytosolic versus membrane fractions revealed that in Sol and EDL female muscles the translocation of PKCθ was significantly elevated by the HFS diet. This latter finding was similar to what we had previously reported for male Sol and EDL muscles in which insulin resistance was accompanied by elevated PKCδ and PKCθ translocation upon HFS feeding. However, in female Epit both PKC isoforms were reduced by HFS feeding. Thus, in both males and females the mechanism underlying HFS diet-induced insulin resistance in Epit muscles appears to be independent of DAG-induced PKC activation. Moreover, a pro-inflammatory response was observed in skeletal muscles of rats fed a HFS diet. In fact, muscles rich in type IIa and type IIb fibers (EDL and Epit) displayed a marked increase in the mRNA expression of *Tlr4, Il-6, Nf-κb,* and *Fas*, whereas in female Sol muscles (rich in type I fibers) these markers of inflammation did not differ from SC-fed rats. In this context, both male and female Epit muscle elicited a significant pro-inflammatory response under obesogenic conditions, which likely played a preponderant role in driving insulin resistance in this glycolytic muscle chronically exposed to the HFS diet.

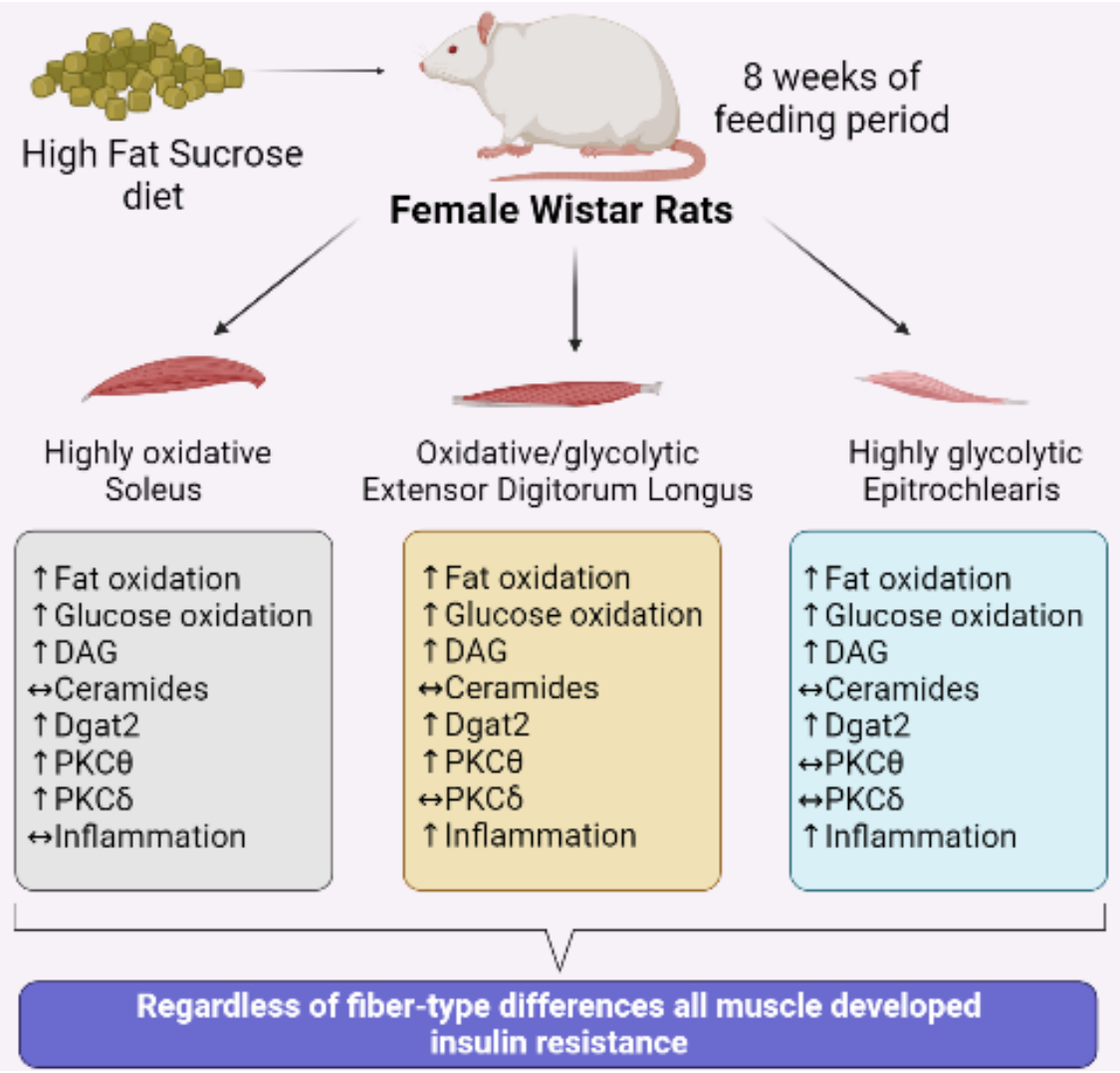

Figure 7.2: Effects of a high fat sucrose enriched diet on skeletal muscle in female rats. Image generated using BioRender.

Altogether, our findings provide novel evidence why insulin resistance similarly develops in oxidative and glycolytic muscles of HFS-fed rats, despite major differences in fat oxidative capacity among them. Thus, while overconsumption of lipids appears to be an important factor that can be lead to the disruption of insulin signalling and glucose metabolism in oxidative muscles (Sol and EDL muscles), in highly glycolytic muscles it is the activation of

inflammatory pathways and upregulation of glucocorticoid signalling that seem to be mainly responsible for the induction of insulin resistance under conditions of chronic HFS feeding in male rats. Our research on female rats shows that inflammation and DAG-induced PKC activation are the primary factors associated with insulin resistance in oxidative and glycolytic skeletal muscles in obese individuals who consume the HFS diet. However, none of the muscles studied displayed changes in ceramides content, despite increasing Tlr4 expression in response to HFS feeding. Because ceramide levels remained unaltered in Epit muscles from both males and females fed a H|FS diet, DAG buildup and inflammation were the factors that likely drove the development of insulin resistance. Thus, distinct fibre type-specific pathways, independent of gender, appeared to control insulin resistance in skeletal muscles. Overall, these studies help elucidate the sexual dimorphism in molecular mechanisms controlling insulin resistance in the skeletal muscles under conditions of diet-induced obesity.

More often than not, comorbidities such as non-alcoholic fatty liver disease (NAFLD), atherosclerosis, type 2 diabetes (T2D) and a cluster of metabolic and cardiovascular risk factors coexist. Many tissues, including the liver, skeletal muscle, and adipocytes, manifest resistance to insulin simultaneously, but the severity of insulin resistance may differ among these various tissues. In addition to skeletal muscles, the liver is considered a critical modulator of whole body lipid and carbohydrate metabolism and hence a crucial regulator insulin sensitivity[465]. Recently, weight loss via the use of ketogenic diet (KD) has gained popularity as a means to reverses NAFLD and manage insulin resistance. This is particularly interesting since the KD is a predominantly fat rich diet that would lead to an increase in circulating NEFA, the main substrate for synthesis of intrahepatic triglycerides (IHTG). To explore the underlying mechanism, and understand metabolic adaptations in response to specific macronutrients in the

liver, in chapter 6, we fed male Wistar rats 3 different diets: Standard chow (SC) low fat-high carbohydrate diet (27% protein, 13% fat and 60% carbohydrate), typical obesogenic High fat sucrose enriched diet (60% fat, 20% protein, and 20% carbohydrate (100% sucrose)) and Ketogenic diet (KD) devoid of carbohydrates (80% fat and 20% protein).

In chapter 6 we demonstrated that animals given a HFS diet developed obesity, insulin resistance and fatty livers after feeding for 8 weeks. Rats that consumed a zero-carbohydrate (KD) indicated significantly reduced adiposity and intrahepatic lipid accumulation. These animals also improved insulin sensitivity and glucose intolerance; despite being fed a diet with a very high fat (80%) content. Our study demonstrated that animals given *ad libitum* access to a HFS diet and KD accumulated more visceral and subcutaneous fat than animals receiving SC. This occurred despite both groups of animals consuming identical amounts of calories[437]. However, the consumption of the HFS diet greatly decreased insulin sensitivity and glucose intolerance as demonstrated by the GTT. While, the KD indicated improved blood glucose clearance in these rats provided additional evidence that chronic fat consumption is an effective tool against insulin resistance.

As we expected fat oxidation was enhanced in HFS-fed animals and more so in rats that were fed an 80% fat diet (KD). Indicating that, the beneficial effects of KD on fatty livers may be the result downregulation of lipogenesis and/or a simultaneous upregulation of β-oxidation indicated by the upregulated *Pgc1α* expression. *Pgc1α* directly increased transcription of the *Pepck* the rate-controlling enzyme of gluconeogenesis[496], that helps maintain blood glucose levels[497]. The KD markedly upregulated *Pgc1α* gene expression compared to rats fed either a SC diet or a HFS diet, indicating that the improvements observed in overall glucose tolerance could, at least partially, be attributed to reduction in gluconeogenesis. Here, we also attempted

to understand the changes in their expression levels of major transcriptional regulators such as Carbohydrate-responsive element-binding protein (ChREBP) and Sterol regulatory element binding protein -1c (SREBP-1c) that induce key lipogenic enzymes to promote lipogenesis in the liver in response to the different diets. We found that *Chrebp* expression levels were significantly upregulated with the consumption of HFS diet in comparison to SC and KD-fed animals, while *srbp1c* gene expression remained unchanged with diet indicating that macronutrient changes may exert an effect on hepatic lipid metabolism.

Hepatic steatosis is strongly associated with hepatic insulin resistance particularly when the former is induced by HFS feeding[498]. Typically, intrahepatic lipid accumulation is the product of DNL and esterification of FFA into triglycerides. In addition, in our study, HFS feeding lead to a significant increase in the levels of intrahepatic TAG accumulation, an effect that was ameliorated by consuming a carbohydrate-free diet. We further investigated effects of the diet on intermediary lipids such as DAG and ceramides. HPLC analysis indicated a significant increase in the hepatic DAG content in animals fed a HFS diet but not in KD fed animals as compared to control animals.

In sync with the DAG and TAG content, quantitative PCR analysis revealed that the mRNA levels of DGAT were also elevated for HFS-fed animals in comparison to SC-fed and KD-fed animals. On further investigating the mRNA gene expression of the four main mammalian ceramide synthesizing enzymes present in the liver (cersyn1, cersyn2, cersyn4, and cersyn6), we observed that with HFS feeding the liver had an elevated mRNA expression of cersyn1 in the liver which can play a role in the pathogenesis of insulin resistance, similar to studies comparing obese insulin resistant and insulin sensitive subjects. In direct contrast, mRNA levels for *cersyn4*, and *cersyn6* were downregulated with KD. Deletions of which are known to alleviate

insulin resistance caused by a HFD. Next, we investigated the link between hepatic intracellular glycerolipid accumulation and hepatic insulin resistance and the activation of PKCε, which was the predominant PKC isoform activated in liver following high fat feeding [499,500]. Multiple studies have suggested the involvement of PKCε in mediating lipid-induced dysregulation of insulin signaling and glycogen metabolism and thereby the development of hepatic insulin resistance Despite having similar levels of total PKCε, consistent with what literature suggests we observed an elevation in the PKCε translocation with HFS feeding. In response to the KD this effect was attenuated. In addition, HFS feeding for 8 weeks dramatically decreased AKT and GSK3αβ phosphorylation in the liver. In contrast, KD significantly augmented phosphorylation of these two proteins, suggesting improvements in hepatic insulin sensitivity in these animals. In addition, we also provide novel evidence that KD in fact does not alter rates of glycogen synthesis under basal and insulin-stimulated conditions.

In summary, the study provides a comprehensive analysis of the effects of a carbohydrate-free KD in regulating hepatic fuel metabolism under conditions of diet-induced obesity. Here, we provide novel evidence indicating that hepatic glycogen synthesis is reduced following chronic HFS feeding but maintained by consuming a KD. These findings might have important implications for understanding the multiple mechanisms by which obesity promotes the development of hepatic insulin resistance and NAFLD. In addition, our data also suggest that reversing hepatic insulin resistance through eliminating/limiting carbohydrate might be an effective way of preventing the development of NAFLD and normalizing hepatic glucose and lipid metabolism.

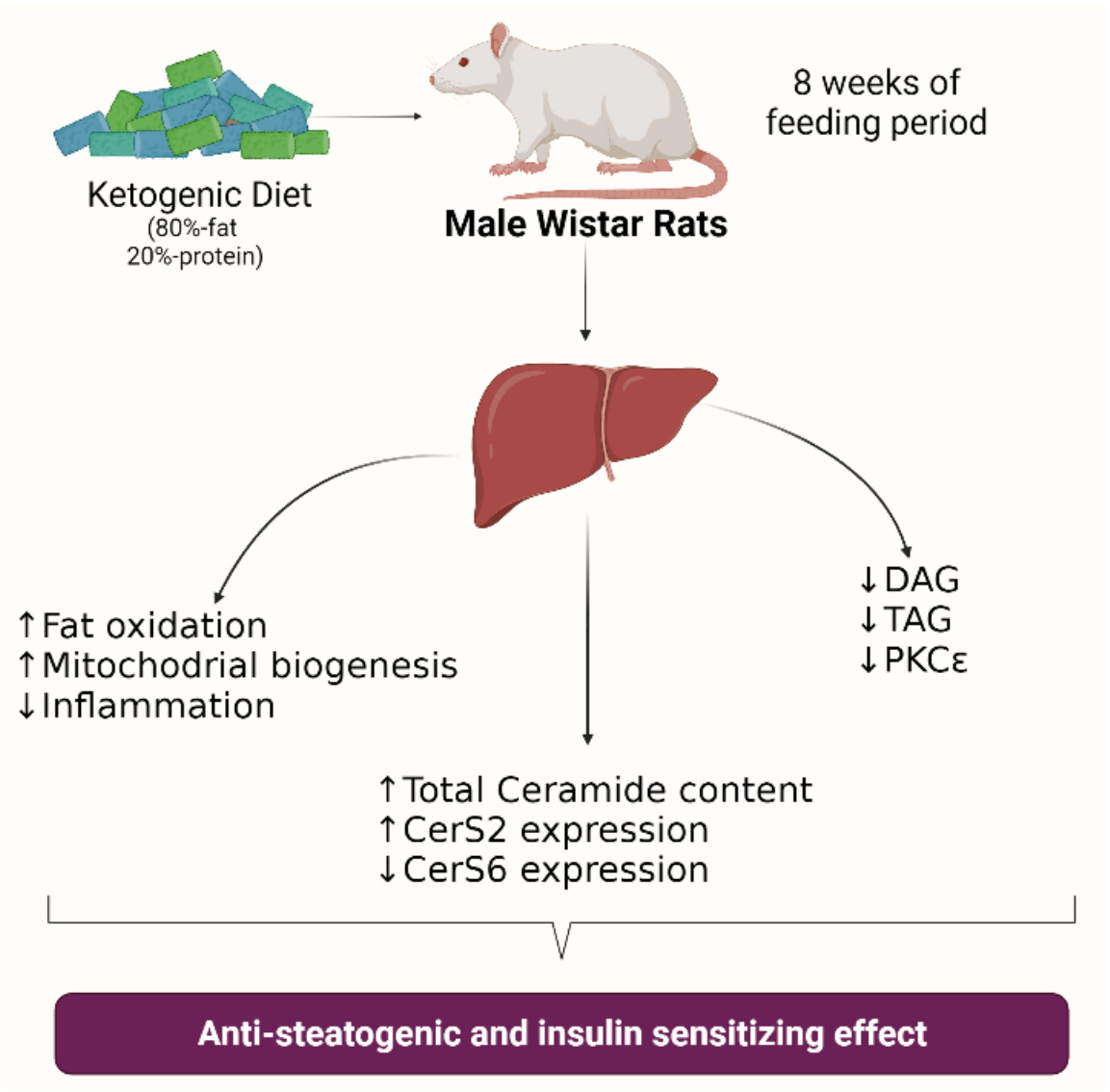

Figure 7.3: Effects of a ketogenic diet in male rat liver. Image generated using BioRender.

Therefore, **the overall findings from this dissertation** elucidates a high fat sucrose enriched diet leads to development of insulin resistance in all the muscles despite their fiber-type differences in both male and female rats. However, the mechanisms that affect insulin signalling, glucose and lipid metabolism in these oxidative and glycolytic skeletal muscles are different. Highly oxidative muscles from male rats tend to develop insulin resistance that can be

associated to elevated intramyocellular accumulation of lipids such as DAG and ceramides, while in addition to the intermediary fatty acid accumulation, inflammation seems to be a cause for the impairment in insulin sensitivity in highly glycolytic muscles. However, HFS diet-induced obesity led to a significant elevation in intramuscular DAG and TAG contents without any alteration in ceramides levels in insulin-resistant female oxidative and glycolytic muscles, indicating sexual dimorphism. We also show that the KD improved hepatic insulin sensitivity and decreased DAG and TAG contents despite an increase in ceramide concentrations. The KD also enhanced the expression of *Pgc-1α, Pepck,* and *Fgf21*, downregulated *Fasn* and *Chrebp,* and shifted substrate away from DNL. Finally, similar to previously published work the KD exerted an anti-inflammatory effect by downregulating the expression of *Tnfα, Nf-kb, Tlr4, and Il-6* in the liver. All together, the factors linking insulin resistance to obesity, T2D and dysfunctional metabolic conditions such as NAFLD are not precisely defined yet, and rather propose an integrative model.

Chapter 8 Limitation of the study

For this dissertation all experiments were carefully thought through and performed with utmost care, however, some limitations exist.

In Chapter 4, we attempted to identify key differences in mechanisms used by skeletal muscles with distinct fiber-types under the influence of a high fat, high sucrose diet. More importantly, we looked at how the diet altered the accumulation of lipid intermediates such as TAG, DAG, and ceramides, as well as cytoplasmic and membrane fractions of PKCθ/δ. Activation of PKC was assessed based on its translocation from the cytoplasm to the membrane. The membrane

and cytoplasmic PKC densities were normalized with commonly used marker proteins (Na,K-ATPase for the membrane fraction and GAPDH for the cytosol fraction) and then the ratio of marker-normalized PKC densities reported. However, these are not ideal, marker proteins for our project since, both Na,K-ATPase and GAPDH proteins have been shown to be regulated by high-fat feeding and PKC itself[501–503], which may have negatively affected the results. We even analysed our results on PKC localization without normalizing them with Na,K-ATPase and GAPDH and found that the numbers did not change much. However, since we were requested by a reviewer for chapter 4, we normalized our PKCθ/δ/ε localization with Na,K-ATPase and GAPDH and have presented results similarly for chapter 5 and 6 as well.

For chapter 4 and 5 we indicate that the intramuscular accumulation fatty acids beyond their storage capacity may lead to insulin desensitisation through the generation of toxic lipid intermediates such as DAG and ceramides. Various studies have suggested that ectopic accumulation of ceramides in often lead to the development of insulin resistance through inhibition of protein kinase B (PKB/AKT)[357]. This inhibition is said to take place via two distinct pathways: either involving the action of atypical protein kinase C (PKCζ) isoforms, and the second dependent on protein phosphatase-2A (PP2A). Therefore, in order to completely understand the extent of ceramides involvement in causing impairment in the insulin signal transduction, it would have been interesting to see if PKCζ was activated. This would be especially important for Epit muscle in male rats, where DAG and ceramide levels do not seem to change but the muscle develops insulin resistance. We analysed the DAG mediated PKCδ/θ pathway but overlooked the ceramide mediated PKCζ pathway. Although total ceramide content did not change with the diet, but an understanding of how the diet impacted total PKCζ content or if there were changes to its localization would have been interesting to note. Similarly, we

noted that all muscles in female rats did not have any changes in their ceramide accumulation in response to the HFS diet. But we did not assess levels of PKCζ. Since, it has now become clear that PKCδ/θ in skeletal muscle, and PKCε in liver relay DAG-induced insulin resistance in these tissues. We are unable to make similar claims about the implication of PKCζ in mediating the deleterious effects of ceramides in muscle and liver.

In addition to the downstream protein target for total ceramides, research is now suggesting that the focus may need to be on the nature of ceramide species involved rather than the total ceramide in IMCL. Recent studies on, rodent models studies have identified C16:0 and C18:0 ceramides as the ceramide species that is linked to the pathophysiology of hepatic insulin resistance[350,474]. Similarly, C24 ceramides synthesized by cersyn2 are known to protect against insulin resistance in mice liver[343,351,389]. While, interestingly, Bergman et al. did not find significant changes in total ceramide, but found C18:0 ceramide to be associated with impaired insulin sensitivity in skeletal muscles of obese individuals, diabetic individuals as well as endurance-trained athletes[249]. De La Maza et al., also found a link between ceramide species C20:1, C22:0 and C22:1, and glucose intolerance when comparing male human subjects. They did not find any association between total ceramide content, and glucose intolerance[504]. To add further complication it is still unclear if there is a single or a set of ceramide species that are linked to development of IR[343]. In chapter 6, we observed that the ketogenic diet had an overall positive, anti-steatotic and insulin sensitizing effect on the liver. However, we saw a significant increase in the total ceramide content with the ketogenic diet**.** The separation and quantification of several endogenous long-chain and very-long-chain ceramide species using mass spectrometry post our chromatographic run could have helped us with a complete breakdown of the specific species that were up or down regulated. Using this analytical lipidomic technique

we would have been able to demonstrate exactly how the ketogenic diet may have an increased total ceramide content but accumulation of specific deleterious species such as C18 and C16 may have been down regulated with the diet. However, we could not conduct mass spectrometry analysis in our study because the facility at York was not operational. Hence, we completed our study by measuring the quantitative mRNA expression of the main mammalian ceramide synthesizing enzymes present in the liver (cersyn1, cersyn2, cersyn4, and cersyn6). This was an indirect approach that we had to take.

Finally, the standard chow that was used in the dissertation was comprised of 27% protein, 13% fat and 60% carbohydrate. This diet had a slightly higher percentage of protein to the typical obesogenic High fat sucrose enriched diet (60% fat, 20% protein, and 20% carbohydrate (100% sucrose)) and the Ketogenic diet (KD) (80% fat and 20% protein) used in the study. Despite, the focus of the dissertation being on fat and the carbohydrate content of the diet, attention to standardizing protein content must be made in the future studies. Therefore a diet with 20% protein, 13% fat and 67% carbohydrate can then be used to address differences in different compositions of the diet based only on the fat and carbohydrate content.

Chapter 9 Future directions

Studies that look at subcellular localization of PKC isoforms almost exclusively use Na,K-ATPase as the membrane fraction marker, and GAPDH as the cytosolic marker for Western blot analysis[285,330], making it an important aspect of the analysis. However, in future, techniques such as Ponceau staining or Coomassie Blue can be used to visualize total protein in each lane and then be quantified using ImageJ software, to normalize western blots in order to minimize

experimental error. This can help avoid the use of marker proteins such as Na,K-ATPase and GAPDH, that are known to get altered by high fat diet in skeletal muscles.

Ceramides in literature have been long known to promote insulin resistance (IR), induce inflammation and causing oxidative stress, ultimately altering muscle/liver function. We observed that under a HFS diet, male muscles accumulate ceramides in a distinct fiber-type manner, but female rats showed no alterations to their ceramide accumulation regardless of the diet. However, both male and female rats developed if insulin resistance. In chapter 6, we observed that with a HFS diet, ceramide accumulation was increased in liver, but interestingly with a ketogenic diet the ceramide accumulation was increased even more as compared to livers from rats fed a SC diet and a HFS diet. Hence, our overall observations from the dissertation point out that ceramides having a distinct characteristic and cannot be generalized with other lipid moieties such as DAG. In addition, the latest research in the field also suggests that even within a particular lipid intermediate, its localization as well as the stereo-isomer species of the lipid class may be important in determining its potency in impairing insulin sensitivity[246,249]. Taking this into consideration, it is not surprising that we observed skeletal muscle IR without an increase in total ceramide accumulation or improved insulin sensitivity in the liver but increased total ceramide content[231] . However, the approach used by us is limited to total ceramide and are unable to provide data on individual ceramide species. A future study using electrospray ionization tandem mass spectrometry (ESI-MS/MS) can help resolve some of these limitations. ESI-MS/MS have been used often in the field of lipidomics in order to make the validation and optimization of measuring multiple metabolites simultaneously. As a step further on our research on the specific IMCL species related mechanisms of insulin resistance, a mixed approach with reverse-phase liquid chromatography followed by ESI-MS/MS technique could

be of interest to attain for the simultaneous measurement of multiple ceramide species in both muscles and liver tissue samples. Furthermore, a thorough investigation with the knockdown of individual CerS would be a valuable addition to the work published so far. By knocking down CerS2 or CerS6, two of the most prominent ceramide-synthesizing enzymes in the liver, would allow us to tease out the specific role of each synthase enzyme under the HFS and KD conditions. |In this context, we would expect that knocking out CerS6 would lower the production of the deleterious C16:0-C18:0 ceramides species in the livers of HFS-fed rats. This would prevent the steatotic effect of the HFS diet. Conversely, the elimination of CerS6 in KD-fed mice would prevent the antisteatotic effect of this dietary intervention.

In addition to identifying the specific ceramide species in the impairment of the insulin-stimulated glucose uptake, a more thorough investigation of the mechanism by which ceramide impairs the signalling cascade would be interesting addition to the understanding we have so far. Moreover, conducting experiments on localization and activation of PKC-zeta (PKC-ζ) like we did for PKCδ and PKCθ would help understand the mechanism used by ceramides to inhibit AKT and thereby the signalling cascade. Further, to establish the role of DAG and ceramide induced PKC activation, PKC inhibitors can be used. In fact, a phase IIa clinical trial showed that bryostatin-1-mediated activation of PKCε could result in improved hepatic function in the first 24 weeks. Effects that were reproduced by knocking out PKCε in mice that indicated improved glucose tolerance[506]. In addition, PKCθ inhibition has been associated to increased levels of AKT phosphorylation in other rodent models[228]. Therefore, we hypothesize that a study incorporating a commercially available PKC inhibitor such as Sotrastaurin with the HFS diet could help identify the role of PKC activation in inducing insulin resistance.

Overall, despite providing novel ideas about the molecular pathogenesis of insulin resistance in the dissertation, there are still multiple aspects of the research that remain unanswered and should be addressed in future to provide new therapeutic targets for the treatment and possible prevention of type 2 diabetes and other metabolic conditions.

References

1. Calle EE, Thun MJ. Obesity and cancer. *Oncogene*. 2004;23(38):6365-6378.
2. Kahn SE, Hull RL, Utzschneider KM. Mechanisms linking obesity to insulin resistance and type 2 diabetes. *Nature*. 2006;444(7121):840-846.
3. Kleinridders A, Ferris HA, Cai W, Kahn CR. Insulin action in brain regulates systemic metabolism and brain function. *Diabetes*. 2014;63(7):2232-2243.
4. Klein S, Sheard NF, Pi-Sunyer X, et al. Weight management through lifestyle modification for the prevention and management of type 2 diabetes: Rationale and strategies. A statement of the American Diabetes Association, the North American Association for the Study of Obesity, and the American So. *Am J Clin Nutr*. 2004;80(2):257-263.
5. Spiegelman BM, Flier JS, Israel B, Medical D. Obesity and Energy Balance. 2001;104:531-543.
6. Montague, Carl. O'Rahilly S. Causes and Consequences of Visceral Adiposity. *Diabetes Journals*. 2000;(49):883-888.
7. Petersen KF, Dufour S, Befroy D, Lehrke M, Hendler RE, Shulman GI. Reversal of nonalcoholic hepatic steatosis, hepatic insulin resistance, and hyperglycemia by moderate weight reduction in patients with type 2 diabetes. *Diabetes*. 2005;54(3):603-608.
8. Schwingshackl L, Hoffmann G. Comparison of the long-term effects of high-fat v. low-fat diet consumption on cardiometabolic risk factors in subjects with abnormal glucose metabolism: A systematic review and meta-analysis. *Br J Nutr*. 2014;111(12):2047-2058.
9. Pinho RA, Sepa-Kishi DM, Bikopoulos G, et al. High-fat diet induces skeletal muscle oxidative stress in a fiber type-dependent manner in rats. *Free Radic Biol Med*. 2017;110(July):381-389.
10. Fargion S, Dongiovanni P, Guzzo A, Colombo S, Valenti L, Fracanzani AL. Insulin and insulin resistance. *Aliment Pharmacol Ther Suppl*. 2005;22(2):61-63.
11. MacLean PS, Bergouignan A, Cornier MA, Jackman MR. Biology's response to dieting: The impetus for weight regain. *Am J Physiol - Regul Integr Comp Physiol*. 2011;301(3).
12. Lackey DE, Olefsky JM. Regulation of metabolism by the innate immune system. *Nat Rev Endocrinol*. 2016;12(1):15-20.
13. Poirier P, Giles TD, Bray GA, et al. Obesity and Cardiovascular Disease: Pathophysiology, Evaluation, and Effect of Weight Loss An Update of the 1997 American Heart Association Scientific Statement on Obesity and Heart Disease From the Obesity Committee of the Council on Nutrition, Physical Activity, and Metabolism. 2006.
14. Omer H, Rothman-Kabir Y. Diabetes. *Parent Vigilant Care*. 2018:118-123.

15. Ye J. Role of Insulin in the Pathogenesis of Free Fatty Acid-Induced Insulin Resistance in Skeletal Muscle. *Endocrine, Metab Immune Disord Targets*. 2012;7(1):65-74.

16. Di Cesare M, Bentham J, Stevens GA, et al. Trends in adult body-mass index in 200 countries from 1975 to 2014: A pooled analysis of 1698 population-based measurement studies with 19.2 million participants. *Lancet*. 2016;387(10026):1377-1396.

17. Facts F, Diabetes ON. centers for disease control and prevention. National Diabetes Fact Sheet. *Nj*. 2011;07470:973-696.

18. US Department of Health and Human Services. National Diabetes Statistics Report, 2020. *Natl Diabetes Stat Rep*. 2020:2.

19. Wild. Estimates for the year 2000 and projections for 2030. *World Health*. 2004;27(5):1047-1053.

20. Wilmot E, Idris I. Early onset type 2 diabetes: Risk factors, clinical impact and management. *Ther Adv Chronic Dis*. 2014;5(6):234-244.

21. Sinaiko AR, Jacobs DR, Steinberger J, et al. Insulin resistance syndrome in childhood: Associations of the euglycemic insulin clamp and fasting insulin with fatness and other risk factors. *J Pediatr*. 2001;139(5):700-707.

22. Koistinen HA, Zierath JR. Regulation of glucose transport in human skeletal muscle. *Ann Med*. 2002;34(6):410-418.

23. DeFronzo RA, Jacot E, Jequier E, Maeder E, Wahren J, Felber JP. The effect of insulin on the disposal of intravenous glucose. Results from indirect calorimetry and hepatic and femoral venous catheterization. *Diabetes*. 1981;30(12):1000-1007.

24. L R. Energy metabolism in the liver. *Compr Physiol*. 2014;4(1):177-197.

25. RS S. Role of the liver in glucose homeostasis. *Diabetes Care*. 1980;3(2):261-265.

26. Samuel VT, Shulman GI. The pathogenesis of insulin resistance: Integrating signaling pathways and substrate flux. *J Clin Invest*. 2016;126(1):12-22.

27. Gual P, Le Marchand-Brustel Y, Tanti JF. Positive and negative regulation of insulin signaling through IRS-1 phosphorylation. *Biochimie*. 2005;87(1 SPEC. ISS.):99-109.

28. Boucher J, Kleinridders A, Kahn CR. Insulin Receptor Signaling in Normal. *Cold Spring Harb Perspect Biol 2014*. 2014;6:a009191.

29. Haeusler RA, Mcgraw TE, Accili D, Medicine C, Surgery C. Biochemical and cellular properties of insulin receptor signalling. *Nat Rev Mol Cell Biol*. 2019;19(1):31-44.

30. Valverde AM, Lorenzo M, Pons S, White MF, Benito M. Insulin receptor substrate (IRS) proteins IRS-1 and IRS-2 differential signaling in the insulin/insulin-like growth factor-I pathways in fetal brown adipocytes. *Mol Endocrinol*. 1998;12(5):688-697.

31. Huang C, Wu M, Du J, Liu D, Chan C. Systematic modeling for the insulin signaling network mediated by IRS1 and IRS2. *J Theor Biol*. 2014;355:40-52.

32. Doria A, Patti M-E, Kahn CR. The emerging genetic architecture of T2DM. 2013;18(9):1199-1216.

33. J. R. Zierath1 AKHW-H. *Insulin Action and Insulin Resistance in Human Skeletal Muscle*.; 2000.

34. Shepherd PR, Withers DJ, Siddle K. *Phosphoinositide 3-Kinase : The Key Switch Mechanism in Insulin Signalling*. Vol 333.; 1998.

35. Bart VanhaesebroeckSally J. LeeversGeorge Panayotouet al. Phosphoinositide3kinases a conserved family of signaltransducerd.

36. Donnelly R, Reed MJ, Azhar S, Reaven GM. Expression of the major isoenzyme of protein kinase-c in skeletal muscle, npkc theta, varies with muscle type and in response to fructose-induced insulin resistance. *Endocrinology*. 1994;135(6):2369-2374.

37. Brozinick JT, Roberts BR, Dohm GL. *Defective Signaling Through Akt-2 and-3 But Not Akt-1 in Insulin-Resistant Human Skeletal Muscle Potential Role in Insulin Resistance*.; 2003.

38. Leto D, Saltiel AR. Regulation of glucose transport by insulin: traffic control of GLUT4. *Nat Rev Mol Cell Biol*. 2012;13(6):383-396.

39. Thong FSL, Dugani CB, Klip A. Turning signals on and off: GLUT4 traffic in the insulin-signaling highway. *Physiology (Bethesda)*. 2005;20(4):271-284.

40. EJ H, BB D. Role of glycogen synthase kinase-3 in insulin resistance and type 2 diabetes. *Curr Drug Targets*. 2006;7(11):1435-1441.

41. J. Henriksen E. Dysregulation of Glycogen Synthase Kinase-3 in Skeletal Muscle and the Etiology of Insulin Resistance and Type 2 Diabetes. *Curr Diabetes Rev*. 2010;6(5):285-293.

42. Lawrence JC, Roach PJ. New Insights Into the Role and Mechanism of Glycogen Synthase Activation by Insulin. *Diabetes*. 1997;46(4):541-547.

43. Jope RS, Johnson GVW. The glamour and gloom of glycogen synthase kinase-3. *Trends Biochem Sci*. 2004;29(2):95-102.

44. Ceddia RB. The role of AMP-activated protein kinase in regulating white adipose tissue metabolism. *Mol Cell Endocrinol*. 2013;366(2):194-203.

45. Thong FSL, Dugani CB, Klip A. Turning signals on and off: GLUT4 traffic in the insulin-signaling highway. *Physiology*. 2005;(4):271-284.

46. Ciaraldi TP, Mudaliar S, Barzin A, et al. Skeletal muscle GLUT1 transporter protein expression and basal leg glucose uptake are reduced in type 2 diabetes. *J Clin Endocrinol Metab*. 2005;90(1):352-358.

47. salway metabolism at a glance - Google Search. https://www.google.com/search?q=salway+metabolism+at+a+glance&rlz=1C1GCEA_enCA750CA750&oq=salway+metabolism+at+a+&aqs=chrome.1.69i57j0i22i30.6560j0j15

&sourceid=chrome&ie=UTF-8. Accessed October 19, 2021.

48. Tirone TA, Brunicardi FC. Overview of glucose regulation. *World J Surg*. 2001;25(4):461-467.

49. Savage DB, Petersen KF, Shulman GI. Mechanisms of insulin resistance in humans and possible links with inflammation. *Hypertension*. 2005;45(5):828-833.

50. Hatting M, Tavares CDJ, Sharabi K, Rines AK, Puigserver P. Insulin regulation of gluconeogenesis.

51. Ferrer JC, Favre C, Gomis RR, et al. Control of glycogen deposition. *FEBS Lett*. 2003;546(1):127-132.

52. Graham TE. Glycogen: An overview of possible regulatory roles of the proteins associated with the granule. *Appl Physiol Nutr Metab*. 2009;34(3):488-492.

53. Nielsen J, Farup J, Rahbek SK, De Paoli FV, Vissing K. Enhanced glycogen storage of a subcellular hot spot in human skeletal muscle during early recovery from eccentric contractions. *PLoS One*. 2015;10(5).

54. Knuiman P, Hopman MTE, Mensink M. Glycogen availability and skeletal muscle adaptations with endurance and resistance exercise. *Nutr Metab*. 2015;12(1).

55. Creer A, Gallagher P, Slivka D, Jemiolo B, Fink W, Trappe S. Influence of muscle glycogen availability on ERK1/2 and Akt signaling after resistance exercise in human skeletal muscle. *J Appl Physiol*. 2005;99(3):950-956.

56. Griffin TM, Humphries KM, Kinter M, Lim HY, Szweda LI. Nutrient sensing and utilization: Getting to the heart of metabolic flexibility. *Biochimie*. 2016;124:74-83.

57. Sugden MC, Holness MJ. Mechanisms underlying regulation of the expression and activities of the mammalian pyruvate dehydrogenase kinases. *Arch Physiol Biochem*. 2006;112(3):139-149.

58. Egan B, Zierath JR. Exercise Metabolism and the Molecular Regulation of Skeletal Muscle Adaptation. *Cell Metab*. 2013;17(2):162-184.

59. Patel MS, Nemeria NS, Furey W, Jordan F. The Pyruvate Dehydrogenase Complexes: Structure-based Function and Regulation. *J Biol Chem*. 2014;289(24):16615.

60. Biensø RS, Knudsen JG, Brandt N, Pedersen PA, Pilegaard H. Effects of IL-6 on pyruvate dehydrogenase regulation in mouse skeletal muscle. *Pflugers Arch Eur J Physiol*. 2014;466(8):1647-1657.

61. Guevara EL, Yang L, Birkaya B, et al. Global view of cognate kinase activation by the human pyruvate dehydrogenase complex. *Sci Reports 2017 71*. 2017;7(1):1-11.

62. Zhang S, Hulver MW, McMillan RP, Cline MA, Gilbert ER. The pivotal role of pyruvate dehydrogenase kinases in metabolic flexibility. *Nutr Metab*. 2014;11(1):1-9.

63. Wu P, Inskeep K, Bowker-K I N L E Y MM, Popov KM, Harris RA. *Mechanism*

Responsible for Inactivation of Skeletal Muscle Pyruvate Dehydrogenase Complex in Starvation and Diabetes. Vol 48.; 1999.

64. Constantin-Teodosiu D. Regulation of Muscle Pyruvate Dehydrogenase Complex in Insulin Resistance: Effects of Exercise and Dichloroacetate. 2013.

65. Patel MS, Nemeria NS, Furey W, Jordan F. The pyruvate dehydrogenase complexes: Structure-based function and regulation. *J Biol Chem*. 2014;289(24):16615-16623.

66. Svensson K, Dent JR, Tahvilian S, et al. Defining the contribution of skeletal muscle pyruvate dehydrogenase 1 to exercise performance and insulin action. *Am J Physiol Endocrinol Metab*. 2018;315:1034-1045.

67. Lund J, Aas V, Tingstad RH, Van Hees A, Nikolić N. Utilization of lactic acid in human myotubes and interplay with glucose and fatty acid metabolism. *Sci Reports 2018 81*. 2018;8(1):1-14.

68. Sola-Penna M. Metabolic regulation by lactate. *IUBMB Life*. 2008;60(9):605-608.

69. Melkonian EA, Schury MP. Biochemistry, Anaerobic Glycolysis. *StatPearls*. August 2021.

70. Péronnet F, Aguilaniu B. [Physiological significance and interpretation of plasma lactate concentration and pH in clinical exercise testing]. *Rev Mal Respir*. 2014;31(6):525-551.

71. Granchi C, Bertini S, Macchia M, Minutolo F. Inhibitors of lactate dehydrogenase isoforms and their therapeutic potentials. *Curr Med Chem*. 2010;17(7):672-697.

72. Peek CB, Levine DC, Cedernaes J, et al. Circadian Clock Interaction with HIF1α Mediates Oxygenic Metabolism and Anaerobic Glycolysis in Skeletal Muscle. *Cell Metab*. 2017;25(1):86-92.

73. Juel G, Halestrap AP. Lactate transport in skeletal muscle - role and regulation of the monocarboxylate transporter. *J Physiol*. 1999;517 (Pt 3)(Pt 3):633-642.

74. Juraschek SP, Shantha GPS, Chu AY, et al. Lactate and Risk of Incident Diabetes in a Case-Cohort of the Atherosclerosis Risk in Communities (ARIC) Study. *PLoS One*. 2013;8(1).

75. Nalbandian M, Radak Z, Takeda M. Lactate Metabolism and Satellite Cell Fate. *Front Physiol*. 2020;11.

76. Gladden LB. Lactate metabolism: A new paradigm for the third millennium. *J Physiol*. 2004;558(1):5-30.

77. Rawat D, Chhonker SK, Naik RA, Mehrotra A, Trigun SK, Koiri RK. Lactate as a signaling molecule: Journey from dead end product of glycolysis to tumor survival. *Front Biosci - Landmark*. 2019;24(2):366-381.

78. Kitaoka Y, Takeda K, Tamura Y, Hatta H. Lactate administration increases mRNA expression of PGC-1α and UCP3 in mouse skeletal muscle. *Appl Physiol Nutr Metab*. 2016;41(6):695-698.

79. Hoshino D, Tamura Y, Masuda H, Matsunaga Y, Hatta H. Effects of decreased lactate accumulation after dichloroacetate administration on exercise training-induced mitochondrial adaptations in mouse skeletal muscle. *Physiol Rep*. 2015;3(9).

80. Percival ME, Martin BJ, Gillen JB, et al. Sodium bicarbonate ingestion augments the increase in PGC-1α mRNA expression during recovery from intense interval exercise in human skeletal muscle. *J Appl Physiol*. 2015;119(11):1303-1312.

81. Takahashi K, Kitaoka Y, Matsunaga Y, Hatta H. Effects of lactate administration on mitochondrial enzyme activity and monocarboxylate transporters in mouse skeletal muscle. *Physiol Rep*. 2019;7(17).

82. Shirai T, Uemichi K, Hidaka Y, Kitaoka Y, Takemasa T. Effect of lactate administration on mouse skeletal muscle under calorie restriction. *Curr Res Physiol*. 2021;4(May):202-208.

83. Brooks GA. The Science and Translation of Lactate Shuttle Theory. *Cell Metab*. 2018;27(4):757-785.

84. Glancy B, Kane DA, Kavazis AN, Goodwin ML, Willis WT, Gladden LB. Mitochondrial lactate metabolism: history and implications for exercise and disease. *J Physiol*. 2021;599(3):863-888.

85. CS C, YB K, FN L, JM Z, BB K, JH Y. Lactate induces insulin resistance in skeletal muscle by suppressing glycolysis and impairing insulin signaling. *Am J Physiol Endocrinol Metab*. 2002;283(2).

86. Qvisth V, Hagström-Toft E, Moberg E, Sjöberg S, Bolinder J. Lactate release from adipose tissue and skeletal muscle in vivo: defective insulin regulation in insulin-resistant obese women. *Am J Physiol Endocrinol Metab*. 2007;292.

87. Poretsky L. Principles of diabetes mellitus. *Princ Diabetes Mellit*. 2010:1-887.

88. Shulman GI. Cellular mechanisms of insulin resistance Find the latest version : Cellular mechanisms of insulin resistance. *J Clin Invest*. 2000;106(2):171-176.

89. Abdul-Ghani MA, DeFronzo RA. Pathogenesis of insulin resistance in skeletal muscle. *J Biomed Biotechnol*. 2010;2010:476279.

90. Thiebaud D, Jacot E, DeFronzo RA, Maeder E, Jequier E, Felber JP. The effect of graded doses of insulin on total glucose uptake, glucose oxidation, and glucose storage in man. *Diabetes*. 1982;31(11):957-963.

91. Bokhari S, Emerson P, Israelian Z, Gupta A, Meyer C. Metabolic fate of plasma glucose during hyperglycemia in impaired glucose tolerance: Evidence for further early defects in the pathogenesis of type 2 diabetes. *Am J Physiol - Endocrinol Metab*. 2009;296(3).

92. Rose AJ, Richter EA. Skeletal muscle glucose uptake during exercise: How is it regulated? *Physiology*. 2005;(4):260-270.

93. Cline GW, Petersen KF, Krssak M, et al. Impaired Glucose Transport as a Cause of

Decreased Insulin-Stimulated Muscle Glycogen Synthesis in Type 2 Diabetes. *N Engl J Med*. 1999;341(4):240-246.

94. Rothman DL, Magnusson I, Cline G, et al. Decreased muscle glucose transport/phosphorylation is an early defect in the pathogenesis of non-insulin-dependent diabetes mellitus. *Natl Acad Sci*. 1995;92:983-987.

95. Petersen KF, Hendler R, Price T, et al. 13C/31P NMR studies on the mechanism of insulin resistance in obesity. *Diabetes*. 1998;47(3):381-386.

96. Rothman DL, Shulman RG, Shulman GI. 31P nuclear magnetic resonance measurements of muscle glucose-6-phosphate: Evidence for reduced insulin-dependent muscle glucose transport or phosphorylation activity in non-insulin-dependent diabetes mellitus. *J Clin Invest*. 1992;89(4):1069-1075.

97. Schiaffino S, Reggiani C. Fiber types in Mammalian skeletal muscles. *Physiol Rev*. 2011;91(4):1447-1531.

98. Plowman S, Smith D. *Exercise Physiology for Health Fitness and Performance*.; 2013.

99. Wang YX, Zhang CL, Yu RT, et al. Regulation of muscle fiber type and running endurance by PPARδ. *PLoS Biol*. 2004;2(10).

100. Fisher G, Windham ST, Griffin P, Warren JL, Gower BA, Hunter GR. Associations of human skeletal muscle fiber type and insulin sensitivity, blood lipids, and vascular hemodynamics in a cohort of premenopausal women. *Eur J Appl Physiol*. 2017;117(7):1413-1422.

101. Andruchov O, Andruchova O, Wang Y, Galler S. Kinetic properties of myosin heavy chain isoforms in mouse skeletal muscle: Comparison with rat, rabbit, and human and correlation with amino acid sequence. *Am J Physiol - Cell Physiol*. 2004;287(6 56-6):1725-1732.

102. Human Skeletal Muscle Fiber Type Classifications. 1997.

103. Essén B, Jansson E, Henriksson J, Taylor AW, Saltin B. Metabolic Characteristics of Fibre Types in Human Skeletal Muscle. *Acta Physiol Scand*. 1975;95(2):153-165.

104. Cartee GD, Arias EB, Yu CS, Pataky MW. Novel single skeletal muscle fiber analysis reveals a fiber type-selective effect of acute exercise on glucose uptake. 2023;(10):818-824.

105. Pataky MW, Wang H, Yu CS, et al. High-Fat Diet-Induced Insulin Resistance in Single Skeletal Muscle Fibers is Fiber Type Selective. *Sci Rep*. 2017;(September):1-11.

106. Blaauw B, Schiaffino S, Reggiani C. Mechanisms modulating skeletal muscle phenotype. *Compr Physiol*. 2013;3(4):1645-1687.

107. Schiaffino S, Reggiani C. Fiber Types In Mammalian Skeletal Muscles. *Physiol Rev*. 2011;91:1447-1531.

108. James DE, Zorzano A, Boni-Schnetzler M, et al. Intrinsic differences of insulin receptor

kinase activity in red and white muscle. *J Biol Chem*. 1986;261(32):14939-14944.

109. Bonen A, Tan MH, Watson-Wright WM. Insulin binding and glucose uptake differences in rodent skeletal muscles. *Diabetes*. 1981;30(8):702-704.

110. Pette D, Peuker H, Staron RS. The impact of biochemical methods for single muscle fibre analysis. *Acta Physiol Scand*. 1999;166(4):261-277.

111. He J, Watkins S, Kelley DE. Skeletal Muscle Lipid Content and Oxidative Enzyme Activity in Relation to Muscle Fiber Type in Type 2 Diabetes and Obesity. *Diabetes*. 2001;50(4):817-823.

112. James DE, Jenkins AB, Kraegen EW. Heterogeneity of insulin action in individual muscles in vivo: Euglycemic clamp studies in rats. *Am J Physiol - Endocrinol Metab*. 1985;11(5).

113. Henriksen EJ, Bourey RE, Rodnick KJ, Koranyi L, Permutt MA, Holloszy JO. Glucose transporter protein content and glucose transport capacity in rat skeletal muscles. *Am J Physiol - Endocrinol Metab*. 1990;259(4 22-4).

114. Nyholm B, Qu Z, Kaal A, et al. Evidence of an increased number of type IIb muscle fibers in insulin-resistant first-degree relatives of patients with NIDDM. *Diabetes*. 1997;46(11):1822-1828.

115. Stuart CA, Mccurry MP, Marino A, et al. Slow-Twitch Fiber Proportion in Skeletal Muscle Correlates With Insulin Responsiveness. *J Clin Endocrinol Metab*. 2013;98(5):2027-2036.

116. Lumeng CN, Saltiel AR. Inflammatory links between obesity and metabolic disease. *J Clin Invest*. 2011;121(6):2111-2117.

117. Chawla A, Nguyen KD, Goh YPS. Macrophage-mediated inflammation in metabolic disease. *Nat Rev Immunol*. 2011;11(11):738-749.

118. I K, M C, A B-Z. Obesity, Bioactive Lipids, and Adipose Tissue Inflammation in Insulin Resistance. *Nutrients*. 2020;12(5).

119. Perreault M, Marette A. Targeted disruption of inducible nitric oxide synthase protects against obesity-linked insulin resistance in muscle. *Nat Med*. 2001;7(10):1138-1143.

120. Lappas M, Yee K, Permezel M, Rice GE. Sulfasalazine and BAY 11-7082 interfere with the nuclear factor-κB and IκB kinase pathway to regulate the release of proinflammatory cytokines from human adipose tissue and skeletal muscle in vitro. *Endocrinology*. 2005;146(3):1491-1497.

121. Saghizadeh M, Ong JM, Garvey WT, Henry RR, Kern PA. The expression of TNFα by human muscle: Relationship to insulin resistance. *J Clin Invest*. 1996;97(4):1111-1116.

122. Yamaguchi K, Ura N, Murakami H, et al. Olmesartan Ameliorates Insulin Sensitivity by Modulating Tumor Necrosis Factor-α and Cyclic AMP in Skeletal Muscle. *Hypertens Res 2005 289*. 2005;28(9):773-778.

123. T. Barry Levine ABL. Metabolic Syndrome and Cardiovascular Disease. https://books.google.ca/books?id=sl4KJOgnHj4C&pg=PT399&lpg=PT399&dq=Togashi+N,+Ura+N,+Higashiura+K,+Murakami+H,+Shimamoto+K.+The+contribution+of+skeletal+muscle+tumor+necrosis+factor-alpha+to+insulin+resistance+and+hypertension+in+fructose-fed+rats.+J+Hyp. Accessed February 15, 2022.

124. Steinberg GR, Michell BJ, van Denderen BJW, et al. Tumor necrosis factor alpha-induced skeletal muscle insulin resistance involves suppression of AMP-kinase signaling. *Cell Metab*. 2006;4(6):465-474.

125. Uysal KT, Wiesbrock SM, Marino MW, Hotamisligil GS. Protection from obesity-induced insulin resistance in mice lacking TNF-alpha function. *Nature*. 1997;389(6651):610-614.

126. Togashi N, Ura N, Higashiura K, Murakami H, Shimamoto K. Effect of TNF-alpha--converting enzyme inhibitor on insulin resistance in fructose-fed rats. *Hypertens (Dallas, Tex 1979)*. 2002;39(2 Pt 2):578-580.

127. Bouzakri K, Zierath JR. MAP4K4 gene silencing in human skeletal muscle prevents tumor necrosis factor-alpha-induced insulin resistance. *J Biol Chem*. 2007;282(11):7783-7789.

128. Rask-Madsen C, Domínguez H, Ihlemann N, Hermann T, Køber L, Torp-Pedersen C. Tumor Necrosis Factor-α Inhibits Insulin's Stimulating Effect on Glucose Uptake and Endothelium-Dependent Vasodilation in Humans. *Circulation*. 2003;108(15):1815-1821.

129. Borst SE, Lee Y, Conover CF, Shek EW, Bagby GJ. Neutralization of tumor necrosis factor-α reverses insulin resistance in skeletal muscle but not adipose tissue. *Am J Physiol - Endocrinol Metab*. 2004;287(5 50-5).

130. I N-V, S F-V, DK K, R V-B, L G-G, M L. Insulin resistance associated to obesity: the link TNF-alpha. *Arch Physiol Biochem*. 2008;114(3):183-194.

131. Pedersen BK, Febbraio MA, Mooney RA. Interleukin-6 does/does not have a beneficial role in insulin sensitivity and glucose homeostasis. *J Appl Physiol*. 2007;102(2):814-819.

132. Weigert C, Hennige AM, Lehmann R, et al. Direct Cross-talk of Interleukin-6 and Insulin Signal Transduction via Insulin Receptor Substrate-1 in Skeletal Muscle Cells *. *J Biol Chem*. 2006;281(11):7060-7067.

133. Kim JH, Bachmann RA, Chen J. Interleukin-6 and insulin resistance. *Vitam Horm*. 2009;80(C):613-633.

134. HJ K, T H, SY P, et al. Differential effects of interleukin-6 and -10 on skeletal muscle and liver insulin action in vivo. *Diabetes*. 2004;53(4):1060-1067.

135. López-Soriano J, Chiellini C, Maffei M, Grimaldi PA, Argilés JM. Roles of skeletal muscle and peroxisome proliferator-activated receptors in the development and treatment of obesity. *Endocr Rev*. 2006;27(3):318-329.

136. Steensberg A, Fischer CP, Sacchetti M, et al. Acute interleukin-6 administration does not impair muscle glucose uptake or whole-body glucose disposal in healthy humans. *J Physiol*. 2003;548(Pt 2):631.

137. Rotter V, Nagaev I, Smith U. Interleukin-6 (IL-6) induces insulin resistance in 3T3-L1 adipocytes and is, like IL-8 and tumor necrosis factor-alpha, overexpressed in human fat cells from insulin-resistant subjects. *J Biol Chem*. 2003;278(46):45777-45784.

138. Pedersen BK, Febbraio MA, Mooney RA. Interleukin-6 does/does not have a beneficial role in insulin sensitivity and glucose homeostasis. *J Appl Physiol*. 2007;102(2):814-819.

139. Jin X, Zimmers TA, Perez EA, Pierce RH, Zhang Z, Koniaris LG. Paradoxical effects of short- and long-term interleukin-6 exposure on liver injury and repair. *Hepatology*. 2006;43(3):474-484.

140. Frost RA, Nystrom GJ, Lang CH. Multiple Toll-like receptor ligands induce an IL-6 transcriptional response in skeletal myocytes. *Am J Physiol - Regul Integr Comp Physiol*. 2006;290(3).

141. Tschöp M, Thomas G. Fat fuels insulin resistance through Toll-like receptors. *Nat Med*. 2006;12(12):1359-1361.

142. Francaux M. Toll-like receptor signalling induced by endurance exercise. *Appl Physiol Nutr Metab*. 2009;34(3):454-458.

143. Reyna SM, Ghosh S, Tantiwong P, et al. Elevated Toll-Like Receptor 4 Expression and Signaling in Muscle From Insulin-Resistant Subjects. *Diabetes*. 2008;57(10):2595.

144. Halliwell B. Free Radicals and Other Reactive Species in Disease. *Encycl Life Sci*. 2005:1-7.

145. Furukawa S, Fujita T, Shimabukuro M, et al. Increased oxidative stress in obesity and its impact on metabolic syndrome. *J Clin Invest*. 2004;114(12):1752-1761.

146. Fisher-Wellman KH, Neufer PD. Linking mitochondrial bioenergetics to insulin resistance via redox biology. *Trends Endocrinol Metab*. 2012;23(3):142-153.

147. Loh K, Deng H, Fukushima A, et al. Reactive oxygen species enhance insulin sensitivity. *Cell Metab*. 2009;10(4):260-272.

148. Espinosa A, Campos C, Díaz-Vegas A, et al. Insulin-dependent H2O2 production is higher in muscle fibers of mice fed with a high-fat diet. *Int J Mol Sci*. 2013;14(8):15740-15754.

149. Anderson EJ, Lustig ME, Boyle KE, et al. Mitochondrial H2O2 emission and cellular redox state link excess fat intake to insulin resistance in both rodents and humans. *J Clin Invest*. 2009;119(3):573-581.

150. Di Meo S, Iossa S, Venditti P. Skeletal muscle insulin resistance: Role of mitochondria and other ROS sources. *J Endocrinol*. 2017;233(1):R15-R42.

151. JL E, ID G, BA M, GM G. Oxidative stress and stress-activated signaling pathways: a

unifying hypothesis of type 2 diabetes. *Endocr Rev*. 2002;23(5):599-622.

152. Meo S Di, Iossa S, Venditti P. Improvement of obesity-linked skeletal muscle insulin resistance by strength and endurance training. *J Endocrinol*. 2017;234(3):R159-R181.

153. Fridlyand LE, Philipson LH. Reactive species and early manifestation of insulin resistance in type 2 diabetes. *Diabetes Obes Metab*. 2006;8(2):136-145.

154. Barazzoni R, Zanetti M, Gortan Cappellari G, et al. Fatty acids acutely enhance insulin-induced oxidative stress and cause insulin resistance by increasing mitochondrial reactive oxygen species (ROS) generation and nuclear factor-κB inhibitor (IκB)-nuclear factor-κB (NFκB) activation in rat muscle, in the . *Diabetologia*. 2012;55(3):773-782.

155. Harrell CS, Gillespie CF, Neigh GN. Energetic stress: The reciprocal relationship between energy availability and the stress response. *Physiol Behav*. 2016;166:43-55.

156. Sharma AK, Shi X, Isales CM, McGee-Lawrence ME. Endogenous Glucocorticoid Signaling in the Regulation of Bone and Marrow Adiposity: Lessons from Metabolism and Cross Talk in Other Tissues. *Curr Osteoporos Rep*. 2019;17(6):438-445.

157. Loerz C, Maser E. The cortisol-activating enzyme 11β-hydroxysteroid dehydrogenase type 1 in skeletal muscle in the pathogenesis of the metabolic syndrome. *J Steroid Biochem Mol Biol*. 2017;174:65-71.

158. Morton NM, Seckl JR. 11beta-hydroxysteroid dehydrogenase type 1 and obesity. *Front Horm Res*. 2008;36:146-164.

159. SA M, LL G, C S, et al. Regulation of lipid metabolism by glucocorticoids and 11β-HSD1 in skeletal muscle. *Endocrinology*. 2013;154(7):2374-2384.

160. Weinstein SP, Paquin T, Pritsker A, Haber RS. Glucocorticoid-induced insulin resistance: Dexamethasone inhibits the activation of glucose transport in rat skeletal muscle by both insulin- and non-insulin-related stimuli. *Diabetes*. 1995;44(4):441-445.

161. Ruzzin J, Wagman AS, Jensen J. Glucocorticoid-induced insulin resistance in skeletal muscles: defects in insulin signalling and the effects of a selective glycogen synthase kinase-3 inhibitor. *Diabetologia*. 2005;48(10):2119-2130.

162. G D, B L, M P-B, et al. Effects of glucocorticoid excess on the sensitivity of glucose transport and metabolism to insulin in rat skeletal muscle. *Biochem J*. 1997;321 (Pt 3)(Pt 3):707-712.

163. Beaupere C, Liboz A, Fève B, Blondeau B, Guillemain G. Molecular mechanisms of glucocorticoid-induced insulin resistance. *Int J Mol Sci*. 2021;22(2):1-30.

164. Li YL, Yao YX, Zhao YM, Di YQ, Zhao XF. The steroid hormone 20-hydroxyecdysone counteracts insulin signaling via insulin receptor dephosphorylation. *J Biol Chem*. 2021;296.

165. DH van R, DM O, M D. Novel insights into glucocorticoid-mediated diabetogenic effects: towards expansion of therapeutic options? *Eur J Clin Invest*. 2009;39(2):81-93.

166. Rasmussen BB, Wolfe RR. Regulation of fatty acid oxidation in skeletal muscle. *Annu Rev Nutr*. 1999;19:463-484.

167. Lundsgaard AM, Fritzen AM, Kiens B. Molecular Regulation of Fatty Acid Oxidation in Skeletal Muscle during Aerobic Exercise. *Trends Endocrinol Metab*. 2018;29(1):18-30.

168. BALTZAN MA, ANDRES R, CADER G, ZIERLER KL. Heterogeneity of forearm metabolism with special reference to free fatty acids. *J Clin Invest*. 1962;41:116-125.

169. ANDRES R, CADER G, ZIERLER KL. The quantitatively minor role of carbohydrate in oxidative metabolism by skeletal muscle in intact man in the basal state; measurements of oxygen and glucose uptake and carbon dioxide and lactate production in the forearm. *J Clin Invest*. 1956;35(6):671-682.

170. Tancredi R, … GD-TJH, 1976 undefined. Free fatty acid metabolism in the forearm at rest: muscle uptake and adipose tissue release of free fatty acids. *europepmc.org*.

171. Ruderman, Neil B., Asish K. Saha, Demetrios Vavvas and LAW. Malonyl-CoA, fuel sensing, and insulin resistance _ Enhanced Reader.pdf.

172. Ruderman NB, Saha AK, Vavvas D, Heydrick SJ, Kurowski TG. Lipid abnormalities in muscle of insulin-resistant rodents: The malonyl CoA hypothesis. *Ann N Y Acad Sci*. 1997;827:221-230.

173. Holloway GP, Benton CR, Mullen KL, et al. In obese rat muscle transport of palmitate is increased and is channeled to triacylglycerol storage despite an increase in mitochondrial palmitate oxidation. *Am J Physiol Endocrinol Metab*. 2009;296:738-747.

174. Kelley DE, Goodpaster B, Wing RR, Simoneau J, Simoneau J-A. Skeletal muscle fatty acid metabolism in association with insulin resistance, obesity, and weight loss. 1999.

175. Goodpaster BH, Wolf D. Skeletal muscle lipid accumulation in obesity, insulin resistance, and type 2 diabetes. *Pediatr Diabetes*. 2004;5(4):219-226.

176. Tracey TJ, Steyn FJ, Wolvetang EJ, Ngo ST. Neuronal Lipid Metabolism: Multiple Pathways Driving Functional Outcomes in Health and Disease. *Front Mol Neurosci*. 2018;11(January):1-25.

177. Rekhi UR, Omar M, Alexiou M, et al. Endothelial Cell CD36 Reduces Atherosclerosis and Controls Systemic Metabolism. *Front Cardiovasc Med*. 2021;8(November):1-14.

178. Goldberg IJ, Eckel RH, Abumrad NA. Regulation of fatty acid uptake into tissues: Lipoprotein lipase- And CD36-mediated pathways. *J Lipid Res*. 2009;50(SUPPL.).

179. Pownall H, Moore K. Commentary on fatty acid wars: The diffusionists versus the translocatists. *Arterioscler Thromb Vasc Biol*. 2014;34(5):8-9.

180. Li J, Wang X, Zhang T, et al. A review on phospholipids and their main applications in drug delivery systems. *Asian J Pharm Sci*. 2014;10(2):81-98.

181. DP K, JF G, A B, JJ L. Long-chain fatty acid uptake and FAT/CD36 translocation in heart and skeletal muscle. *Biochim Biophys Acta*. 2005;1736(3):163-180.

182. Coe N, Smith A, Frohnert B, … PW-J of B, 1999 undefined. The fatty acid transport protein (FATP1) is a very long chain acyl-CoA synthetase. *ASBMB*.

183. Ruan H, Diabetes HP-, 2001 undefined. Overexpression of 1-acyl-glycerol-3-phosphate acyltransferase-α enhances lipid storage in cellular models of adipose tissue and skeletal muscle. *Am Diabetes Assoc*. 2016.

184. Schneider H, Staudacher S, … MP-A of biochemistry, 2014 undefined. Protein mediated fatty acid uptake: synergy between CD36/FAT-facilitated transport and acyl-CoA synthetase-driven metabolism. *Elsevier*.

185. Schwenk RW, Holloway GP, Luiken JJFP, Bonen A, Glatz JFC. Fatty acid transport across the cell membrane: Regulation by fatty acid transporters. *Prostaglandins Leukot Essent Fat Acids*. 2010;82(4-6):149-154.

186. Abumrad N, Coburn C, Ibrahimi A. Membrane proteins implicated in long-chain fatty acid uptake by mammalian cells: CD36, FATP and FABPm. *Biochim Biophys Acta - Mol Cell Biol Lipids*. 1999;1441(1):4-13.

187. Jang C, Oh SF, Wada S, et al. A branched-chain amino acid metabolite drives vascular fatty acid transport and causes insulin resistance. *Nat Med*. 2016;22(4):421-426.

188. Longo N, Frigeni M, Pasquali M. Carnitine transport and fatty acid oxidation. *Biochim Biophys Acta - Mol Cell Res*. 2016;1863(10):2422-2435.

189. Mitchell RW, On NH, Del Bigio MR, Miller DW, Hatch GM. Fatty acid transport protein expression in human brain and potential role in fatty acid transport across human brain microvessel endothelial cells. *J Neurochem*. 2011;117(4):735-746.

190. Eyre NS, Cleland LG, Mayrhofer G. FAT/CD36 expression alone is insufficient to enhance cellular uptake of oleate. *Biochem Biophys Res Commun*. 2008;370(3):404-409.

191. Holloway GP, Chou CJ, Lally J, et al. Increasing skeletal muscle fatty acid transport protein 1 (FATP1) targets fatty acids to oxidation and does not predispose mice to diet-induced insulin resistance. *Diabetologia*. 2011;54(6):1457-1467.

192. Guitart M, Andreu AL, García-Arumi E, et al. FATP1 localizes to mitochondria and enhances pyruvate dehydrogenase activity in skeletal myotubes. *Mitochondrion*. 2009;9(4):266-272.

193. Kim JK, Gimeno RE, Higashimori T, et al. Inactivation of fatty acid transport protein 1 prevents fat-induced insulin resistance in skeletal muscle. *J Clin Invest*. 2004;113(5):756-763.

194. Wu Q, Ortegon AM, Tsang B, Doege H, Feingold KR, Stahl A. FATP1 Is an Insulin-Sensitive Fatty Acid Transporter Involved in Diet-Induced Obesity. *Mol Cell Biol*. 2006;26(9):3455-3467.

195. Storch J, Thumser AEA. The fatty acid transport function of fatty acid-binding proteins. *Biochim Biophys Acta - Mol Cell Biol Lipids*. 2000;1486(1):28-44.

196. Zanotti G. Muscle fatty acid-binding protein. *Biochim Biophys Acta*. 1999;1441(2-3):94-105.

197. Ring A, Pohl J, Völkl A, Stremmel W. Evidence for vesicles that mediate long-chain fatty acid uptake by human microvascular endothelial cells. *J Lipid Res*. 2002;43(12):2095-2104.

198. Brinkmann JFF, Abumrad NA, Ibrahimi A, Van der Vusse GJ, Glatz JFC. New insights into long-chain fatty acid uptake by heart muscle: A crucial role for fatty acid translocase/CD36. *Biochem J*. 2002;367(3):561-570.

199. Stremmel W, Pohl J, Ring A, Herrmann T. A new concept of cellular uptake and intracellular trafficking of long-chain fatty acids. *Lipids*. 2001;36(9):981-989.

200. McGarry JD, Brown NF. The mitochondrial carnitine palmitoyltransferase system. From concept to molecular analysis. *Eur J Biochem*. 1997;244(1):1-14.

201. Hénique C, Mansouri A, Vavrova E, et al. Increasing mitochondrial muscle fatty acid oxidation induces skeletal muscle remodeling toward an oxidative phenotype. *FASEB J*. 2015;29(6):2473-2483.

202. Fillmore N, Abo Alrob O, Lopaschuk GD. Fatty Acid beta-Oxidation. July 2011.

203. Price ER. The physiology of lipid storage and use in reptiles. *Biol Rev*. 2017;92(3):1406-1426.

204. Seifert EL, Estey C, Xuan JY, Harper M-E. Electron transport chain-dependent and -independent mechanisms of mitochondrial H2O2 emission during long-chain fatty acid oxidation. *J Biol Chem*. 2010;285(8):5748-5758.

205. Graham P Holloway, Arend Bonen and LLS. Regulation of skeletal muscle mitochondrial fatty acid metabolism inlean and obese individuals.

206. Holland WL KT. Lipid mediators of insulin resistance. . Nutrition Review. https://www.google.com/search?q=Holland+WL%2C+Knotts+TA%2C+Chavez+JA+et+al.%3A+Lipid+mediators+of+insulin+resistance.+Nutr.+Rev.+65%2C+S39–S46+(2007).&rlz=1C1GCEA_enCA750CA750&oq=Holland+WL%2C+Knotts+TA%2C+Chavez+JA+et+al.%3A+Lipid+mediators+of+insulin+resistance.+Nutr.+Rev.+65%2C+S39–S46+(2007).&aqs=chrome..69i57.440j0j15&sourceid=chrome&ie=UTF-8. Published 2007. Accessed January 18, 2022.

207. Benton CR, Wright DC, Bonen A. PGC-1α-mediated regulation of gene expression and metabolism: Implications for nutrition and exercise prescriptions. *Appl Physiol Nutr Metab*. 2008;33(5):843-862.

208. Mootha VK, Lindgren CM, Eriksson KF et al.: PGC-1a-responsive genes involved in oxidative phosphorylation are coordinately downregulated in human diabetes. Nat. Genet. 34, 267–273 (2003). - Google Search. https://www.google.com/search?q=Mootha+VK%2C+Lindgren+CM%2C+Eriksson+KF+et+al.%3A+PGC-1a-

responsive+genes+involved+in+oxidative+phosphorylation+are+coordinately+downregulated+in+human+diabetes.+Nat.+Genet.+34%2C+267–273+(2003).&rlz=1C1GCEA_enCA750CA750&oq=Mootha+VK%2C+Lindgren+CM%2C+Eriksson+KF+et+al.%3A+PGC-1a-responsive+genes+involved+in+oxidative+phosphorylation+are+coordinately+downregulated+in+human+diabetes.+Nat.+Genet.+34%2C+267–273+(2003).&aqs=chrome..69i57.400j0j15&sourceid=chrome&ie=UTF-8. Accessed January 16, 2022.

209. Hancock CR, Han DH, Chen M, et al. High-fat diets cause insulin resistance despite an increase in muscle mitochondria. *Proc Natl Acad Sci U S A*. 2008;105(22):7815-7820.

210. Turner N, Bruce CR, Beale SM, et al. Excess Lipid Availability Increases Mitochondrial Fatty Acid Oxidative Capacity in Muscle Evidence Against a Role for Reduced Fatty Acid Oxidation in Lipid-Induced Insulin Resistance in Rodents. 2085.

211. BH G, J H, S W, DE K. Skeletal muscle lipid content and insulin resistance: evidence for a paradox in endurance-trained athletes. *J Clin Endocrinol Metab*. 2001;86(12):5755-5761.

212. Van Loon LJC, Koopman R, Manders R, Van Der Weegen W, Van Kranenburg GP, Keizer HA. Intramyocellular lipid content in type 2 diabetes patients compared with overweight sedentary men and highly trained endurance athletes. *Am J Physiol - Endocrinol Metab*. 2004;287(3 50-3).

213. Duncan SH, Lobley GE, Holtrop G, et al. SHORT COMMUNICATION Human colonic microbiota associated with diet , obesity and weight loss. 2008:1720-1724.

214. Amati F, Dubé JJ, Alvarez-Carnero E, et al. Skeletal muscle triglycerides, diacylglycerols, and ceramides in insulin resistance: Another paradox in endurance-trained athletes? *Diabetes*. 2011;60(10):2588-2597.

215. Kelley DE, Goodpaster BH, Storlien L. Muscle Triglyceride and Insulin Resistance. *Annu Rev Nutr*. 2002;22(1):325-346.

216. Turcotte LP, Kiens B, Richter EA. Saturation kinetics of palmitate uptake in perfused skeletal muscle. *FEBS Lett*. 1991;279(2):327-329.

217. Yang M, Nickels JT. MOGAT2: A New Therapeutic Target for Metabolic Syndrome. 2015;3:176-192.

218. Dircks L, Sul HS. Acyltransferases of de novo glycerophospholipid biosynthesis. *Prog Lipid Res*. 1999;38(5-6):461-479.

219. J C, J L, P B, Y S. Cloning and functional characterization of a mouse intestinal acyl-CoA:monoacylglycerol acyltransferase, MGAT2. *J Biol Chem*. 2003;278(16):13860-13866.

220. Hall AM, Kou K, Chen Z, et al. Evidence for regulated monoacylglycerol acyltransferase expression and activity in human liver. *J Lipid Res*. 2012;53(5):990.

221. H D, C N, L L, et al. Diacylglycerol acyltransferase 1 inhibition with AZD7687 alters lipid handling and hormone secretion in the gut with intolerable side effects: a randomized clinical trial. *Diabetes Obes Metab*. 2014;16(4):334-343.

222. Haas JT, Winter HS, Lim E, et al. DGAT1 mutation is linked to a congenital diarrheal disorder. *J Clin Invest*. 2012;122(12):4680-4684.

223. Lai N, Fealy CE, Kummitha CM, Cabras S, Kirwan JP, Hoppel CL. Mitochondrial Utilization of Competing Fuels Is Altered in Insulin Resistant Skeletal Muscle of Non-obese Rats (Goto-Kakizaki). *Front Physiol*. 2020;11.

224. Schmitz-Peiffer C, Biden TJ. Protein kinase C function in muscle, liver, and β-cells and its therapeutic implications for type 2 diabetes. *Diabetes*. 2008;57(7):1774-1783.

225. Donnelly R, Reed MJ, Azhar S, Reaven GM. Expression of the major isoenzyme of protein kinase-C in skeletal muscle, nPKC theta, varies with muscle type and in response to fructose-induced insulin resistance. *Endocrinology*. 1994;135(6):2369-2374.

226. Morino K, Petersen KF, Shulman GI. Molecular mechanisms of insulin resistance in humans and their potential links with mitochondrial dysfunction. *Diabetes*. 2006;55(SUPPL. 2).

227. K. D. Copps and M. F. White. Regulation of insulin sensitivity by serine/threonine phosphorylation of insulin receptor substrate proteins IRS1 and IRS2. *Bone*. 2012;55(10):2565–2582.

228. Szendroedi J, Yoshimura T, Phielix E, et al. Role of diacylglycerol activation of PKCθ in lipid-induced muscle insulin resistance in humans. *Proc Natl Acad Sci U S A*. 2014;111(26):9597-9602.

229. Dubé JJ, Amati F, Toledo FGS, et al. Effects of weight loss and exercise on insulin resistance, and intramyocellular triacylglycerol, diacylglycerol and ceramide. *Diabetologia*. 2011;54:1147-1156.

230. S J, D DE, I H, et al. Distinct mechanisms involving diacylglycerol, ceramides, and inflammation underlie insulin resistance in oxidative and glycolytic muscles from high fat-fed rats. *Sci Rep*. 2021;11(1).

231. Kitessa SM, Abeywardena MY. Lipid-induced insulin resistance in skeletal muscle: The chase for the culprit goes from total intramuscular fat to lipid intermediates, and finally to species of lipid intermediates. *Nutrients*. 2016;8(8).

232. Merrill AH. De novo sphingolipid biosynthesis: A necessary, but dangerous, pathway. *J Biol Chem*. 2002;277(29):25843-25846.

233. Hanada K. Intracellular trafficking of ceramide by ceramide transfer protein. *Proc Japan Acad Ser B Phys Biol Sci*. 2010;86(4):426-437.

234. Hanada K. Serine palmitoyltransferase, a key enzyme of sphingolipid metabolism. *Biochim Biophys Acta - Mol Cell Biol Lipids*. 2003;1632(1-3):16-30.

235. Mullen TD, Hannun YA, Obeid LM. Ceramide synthases at the centre of sphingolipid metabolism and biology. *Biochem J*. 2012;441(3):789-802.

236. Luberto C, Hassler DF, Signorelli P, et al. Inhibition of tumor necrosis factor-induced cell death in MCF7 by a novel inhibitor of neutral sphingomyelinase. *J Biol Chem*. 2002;277(43):41128-41139.

237. Lin T, Genestier L, Pinkoski MJ, et al. Role of acidic sphingomyelinase in Fas/CD95-mediated cell death. *J Biol Chem*. 2000;275(12):8657-8663.

238. Gianfrancesco MA, Paquot N, Piette J, Legrand-Poels S. Lipid bilayer stress in obesity-linked inflammatory and metabolic disorders. *Biochem Pharmacol*. 2018;153(December 2017):168-183.

239. Phaniendra A, Jestadi DB, Periyasamy L. Free Radicals: Properties, Sources, Targets, and Their Implication in Various Diseases. *Indian J Clin Biochem*. 2015;30(1):11-26.

240. Dobrzyń A, Górski J. Ceramides and sphingomyelins in skeletal muscles of the rat: Content and composition. Effect of prolonged exercise. *Am J Physiol - Endocrinol Metab*. 2002;282(2 45-2):277-285.

241. Kolak M, Westerbacka J, Velagapudi VR, et al. Adipose tissue inflammation and increased ceramide content characterize subjects with high liver fat content independent of obesity. *Diabetes*. 2007;56(8):1960-1968.

242. Neeland IJ, Singh S, McGuire DK, et al. Relation of plasma ceramides to visceral adiposity, insulin resistance and the development of type 2 diabetes mellitus: the Dallas Heart Study. *Diabetologia*. 2018;61(12):2570-2579.

243. Chew W, Torta F, Ji S, et al. Large-scale lipidomics identifies associations between plasma sphingolipids and T2DM incidence. *ncbi.nlm.nih.gov*.

244. Hilvo M, Salonurmi T, Havulinna AS, et al. Ceramide stearic to palmitic acid ratio predicts incident diabetes. *Diabetologia*. 2018;61(6):1424-1434.

245. Klein R, Hammad S, Baker N, Metabolism KH-, 2014 undefined. Decreased plasma levels of select very long chain ceramide species are associated with the development of nephropathy in type 1 diabetes. *Elsevier*.

246. Apostolopoulou M, Gordillo R, … CK-D, 2018 undefined. Specific hepatic sphingolipids relate to insulin resistance, oxidative stress, and inflammation in nonalcoholic steatohepatitis. *Am Diabetes Assoc*. 2018.

247. Wasilewska N, Bobrus-Chociej A, Harasim-Symbor E, et al. Increased serum concentration of ceramides in obese children with nonalcoholic fatty liver disease. *Lipids Health Dis*. 2018;17(1).

248. Abu-Farha M, Sokolowska E, Blachnio-Zabielska A. The Role of Ceramides in Insulin Resistance. *Front Endocrinol | www.frontiersin.org*. 2019;1:577.

249. Bergman BC, Brozinick JT, Strauss A, et al. Muscle sphingolipids during rest and

exercise: a C18:0 signature for insulin resistance in humans. *Diabetologia*. 2016;59(4):785-798.

250. Turpin-Nolan SM, Hammerschmidt P, Chen W, et al. CerS1-Derived C18:0 Ceramide in Skeletal Muscle Promotes Obesity-Induced Insulin Resistance. *Cell Rep*. 2019;26(1):1-10.e7.

251. Boon J, Hoy A, Stark R, Brown R, Diabetes RM-, 2013 undefined. Ceramides contained in LDL are elevated in type 2 diabetes and promote inflammation and skeletal muscle insulin resistance. *Am Diabetes Assoc*.

252. Diabetes CS-P-, 2010 undefined. Targeting ceramide synthesis to reverse insulin resistance. *Am Diabetes Assoc*. 2010.

253. Ussher J, Koves T, Cadete V, Diabetes LZ-, 2010 undefined. Inhibition of de novo ceramide synthesis reverses diet-induced insulin resistance and enhances whole-body oxygen consumption. *Am Diabetes Assoc*. 2010.

254. Kautzky-Willer A, Harreiter J, reviews GP-E, 2016 undefined. Sex and gender differences in risk, pathophysiology and complications of type 2 diabetes mellitus. *academic.oup.com*.

255. Qiu J, Bosch MA, Meza C, et al. Estradiol protects proopiomelanocortin neurons against insulin resistance. *Endocrinology*. 2018;159(2):647-664.

256. Abe T, Kearns C, Medicine TF-BJ of S, 2003 undefined. Sex differences in whole body skeletal muscle mass measured by magnetic resonance imaging and its distribution in young Japanese adults. *bjsm.bmj.com*.

257. Karastergiou K, Smith SR, Greenberg AS, Fried SK. Sex differences in human adipose tissues - The biology of pear shape. *Biol Sex Differ*. 2012;3(1).

258. Bredella M, Ghomi R, Thomas B, … MT-, 2010 undefined. Comparison of DXA and CT in the assessment of body composition in premenopausal women with obesity and anorexia nervosa. *Wiley Online Libr*.

259. Mauvais-Jarvis F, Clegg D, reviews AH-E, 2013 undefined. The role of estrogens in control of energy balance and glucose homeostasis. *academic.oup.com*.

260. Abate N, Burns D, Peshock R, … AG-J of lipid, 1994 undefined. Estimation of adipose tissue mass by magnetic resonance imaging: validation against dissection in human cadavers. *ASBMB*.

261. Wajchenberg BL. Subcutaneous and visceral adipose tissue: Their relation to the metabolic syndrome. *Endocr Rev*. 2000;21(6):697-738.

262. Mittendorfer B. Sexual Dimorphism in Human Lipid Metabolism. *J Nutr*. 2005;135(4):681-686.

263. Brahe LK, Astrup A, Larsen LH. Can We Prevent Obesity-Related Metabolic Diseases by Dietary Modulation of the Gut Microbiota? *Adv Nutr An Int Rev J*. 2016.

264. Frias JP, Macaraeg GB, Ofrecio J, Yu JG, Olefsky JM, Kruszynska YT. Decreased susceptibility to fatty acid-induced peripheral tissue insulin resistance in women. *Diabetes*. 2001;50(6):1344-1350.

265. Macotela Y, Boucher J, Tran TT, Kahn CR. Sex and depot differences in adipocyte insulin sensitivity and glucose. *Diabetes*. 2009;58(4):803-812.

266. Turgeon JL, Carr MC, Maki PM, Mendelsohn ME, Wise PM. Complex actions of sex steroids in adipose tissue, the cardiovascular system, and brain: Insights from basic science and clinical studies. *Endocr Rev*. 2006;27(6):575-605.

267. Karakelides H, Irving B, Short K, Diabetes PO-, 2010 undefined. Age, obesity, and sex effects on insulin sensitivity and skeletal muscle mitochondrial function. *Am Diabetes Assoc*. 2010;59(1):89-97.

268. Roepstorff C, Thiele M, … TH-TJ of, 2006 undefined. Higher skeletal muscle α2AMPK activation and lower energy charge and fat oxidation in men than in women during submaximal exercise. *Wiley Online Libr*. 2006;574(1):125-138.

269. Steffensen CH, Roepstorff C, Madsen M, Kiens B. Myocellular triacylglycerol breakdown in females but not in males during exercise. *Am J Physiol - Endocrinol Metab*. 2002;282(3 45-3).

270. Maher AC, Fu MH, Isfort RJ, Varbanov AR, Qu XA, Tarnopolsky MA. Sex differences in global mRNA content of human skeletal muscle. *PLoS One*. 2009;4(7).

271. Welle S, Tawil R, Thornton CA. Sex-related differences in gene expression in human skeletal muscle. *PLoS One*. 2008;3(1).

272. Oberbach A, Bossenz Y, Lehmann S, … JN-D, 2006 undefined. Altered fiber distribution and fiber-specific glycolytic and oxidative enzyme activity in skeletal muscle of patients with type 2 diabetes. *Am Diabetes Assoc*. 2006;29(4):895-900.

273. Mårin P, Andersson B, Krotkiewski M, Björntorp P. Muscle fiber composition and capillary density in women and men with NIDDM. *Diabetes Care*. 1994;17(5):382-386.

274. Lillioja S, Young AA, Culter CL, et al. Skeletal muscle capillary density and fiber type are possible determinants of in vivo insulin resistance in man. *J Clin Invest*. 1987;80(2):415-424.

275. Jensen CB, Storgaard H, Madsbad S, Richter EA, Vaag AA. Altered Skeletal Muscle Fiber Composition and Size Precede Whole-Body Insulin Resistance in Young Men with Low Birth Weight. *J Clin Endocrinol Metab*. 2007;92(4):1530-1534.

276. Lillioja S, Young AA, Culter CL, et al. Skeletal muscle capillary density and fiber type are possible determinants of in vivo insulin resistance in man. *J Clin Invest*. 1987;80(2):415-424.

277. Karpe F, Dickmann J, Diabetes KF-, 2011 undefined. Fatty acids, obesity, and insulin resistance: time for a reevaluation. *Am Diabetes Assoc*. 2011;60(10):2441-2449.

278. Browning JD, Baxter J, Satapati S, Burgess SC. The effect of short-term fasting on liver and skeletal muscle lipid, glucose, and energy metabolism in healthy women and men. *J Lipid Res*. 2012;53(3):577-586.

279. Merimee TJ, Misbin RI, Pulkkinen AJ. Sex variations in free fatty acids and ketones during fasting: Evidence for a role of glucagon. *J Clin Endocrinol Metab*. 1978;46(3):414-419.

280. Nielsen S, Guo ZK, Albu JB, Klein S, O'Brien PC, Jensen MD. Energy expenditure, sex, and endogenous fuel availability in humans. *J Clin Invest*. 2003;111(7):981-988.

281. Binnert C, Koistinen HA, Martin G, et al. Fatty acid transport protein-1 mRNA expression in skeletal muscle and in adipose tissue in humans. *Am J Physiol - Endocrinol Metab*. 2000;279(5 42-5).

282. Tarnopolsky MA. Sex differences in exercise metabolism and the role of 17-beta estradiol. *Med Sci Sports Exerc*. 2008;40(4):648-654.

283. Fu MHH, Maher AC, Hamadeh MJ, Ye C, Tarnopolsky MA. Exercise, sex, menstrual cycle phase, and 17β-estradiol influence metabolism-related genes in human skeletal muscle. *Physiol Genomics*. 2009;40(1):34-47.

284. McFarlan JT, Yoshida Y, Jain SS, et al. In Vivo, Fatty Acid Translocase (CD36) Critically Regulates Skeletal Muscle Fuel Selection, Exercise Performance, and Training-induced Adaptation of Fatty Acid Oxidation. *J Biol Chem*. 2012;287(28):23502.

285. Bergman BC, Hunerdosse DM, Kerege A, Playdon MC, Perreault L. Localisation and composition of skeletal muscle diacylglycerol predicts insulin resistance in humans. *Diabetologia*. 2012;55(4):1140-1150.

286. Tarnopolsky MA, Rennie CD, Robertshaw HA, Fedak-Tarnopolsky SN, Devries MC, Hamadeh MJ. Influence of endurance exercise training and sex on intramyocellular lipid and mitochondrial ultrastructure, substrate use, and mitochondrial enzyme activity. *Am J Physiol - Regul Integr Comp Physiol*. 2007;292(3).

287. Devries MC, Lowther SA, Glover AW, Hamadeh MJ, Tarnopolsky MA. IMCL area density, but not IMCL utilization, is higher in women during moderate-intensity endurance exercise, compared with men. *Am J Physiol - Regul Integr Comp Physiol*. 2007;293(6).

288. Peters SJ, Samjoo IA, Devries MC, et al. Perilipin family (PLIN) proteins in human skeletal muscle: the effect of sex, obesity, and endurance training. *cdnsciencepub.com*. 2012;37(4):724-735.

289. Covington JD, Galgani JE, Moro C, et al. Skeletal muscle perilipin 3 and coatomer proteins are increased following exercise and are associated with fat oxidation. *PLoS One*. 2014;9(3).

290. J J, YC L. Regulation of muscle glycogen synthase phosphorylation and kinetic properties by insulin, exercise, adrenaline and role in insulin resistance. *Arch Physiol*

Biochem. 2009;115(1):13-21.

291. J R, Y I, JC Y, et al. Regulation of hepatic fasting response by PPARgamma coactivator-1alpha (PGC-1): requirement for hepatocyte nuclear factor 4alpha in gluconeogenesis. *Proc Natl Acad Sci U S A*. 2003;100(7):4012-4017.

292. T U, M K. Autophagy in the liver: functions in health and disease. *Nat Rev Gastroenterol Hepatol*. 2017;14(3):170-184.

293. Schwarz JM, Linfoot P, Dare D, Aghajanian K. Hepatic de novo lipogenesis in normoinsulinemic and hyperinsulinemic subjects consuming high-fat, low-carbohydrate and low-fat, high-carbohydrate isoenergetic diets. *Am J Clin Nutr*. 2003;77(1):43-50.

294. Benhamed F, Denechaud P-D, Lemoine M, et al. The lipogenic transcription factor ChREBP dissociates hepatic steatosis from insulin resistance in mice and humans. *J Clin Invest*. 2012;122.

295. Horton JD, Goldstein JL, Brown MS. SREBPs: activators of the complete program of cholesterol and fatty acid synthesis in the liver. *J Clin Invest*. 2002;109(9):1125.

296. Wang Y, Viscarra J, Kim S-J, Su HS. Transcriptional regulation of hepatic lipogenesis. 2015.

297. Shimano H, Shimomura I, Hammer RE, et al. Elevated levels of SREBP-2 and cholesterol synthesis in livers of mice homozygous for a targeted disruption of the SREBP-1 gene. *J Clin Invest*. 1997;100(8):2115.

298. Mueckler M, Thorens B. The SLC2 (GLUT) family of membrane transporters. *Mol Aspects Med*. 2013;34(2-3):121-138.

299. Arden C, Tudhope SJ, Petrie JL, et al. Fructose 2, 6-bisphosphate is essential for glucose-regulated gene transcription of glucose-6-phosphatase and other ChREBP target genes in hepatocytes. *Biochem J*. 2012;443(1):111-123.

300. Iizuka K, Bruick RK, Liang G, Horton JD, Uyeda K. Deficiency of carbohydrate response element-binding protein (ChREBP) reduces lipogenesis as well as glycolysis. *Proc Natl Acad Sci U S A*. 2004;101(19):7281-7286.

301. R D, F B, I H, et al. Liver-specific inhibition of ChREBP improves hepatic steatosis and insulin resistance in ob/ob mice. *Diabetes*. 2006;55(8):2159-2170.

302. Iizuka K, Miller B, Uyeda K. Deficiency of carbohydrate-activated transcription factor ChREBP prevents obesity and improves plasma glucose control in leptin-deficient (ob/ob) mice. *Am J Physiol - Endocrinol Metab*. 2006;291(2).

303. P P, AM O, LA V. Molecular mechanisms of steatosis in nonalcoholic fatty liver disease. *Nutr Hosp*. 2011;26(3):441-450.

304. Yaskolka Meir A, Tene L, Cohen N, et al. Intrahepatic fat, abdominal adipose tissues, and metabolic state: magnetic resonance imaging study. *Diabetes Metab Res Rev*. 2017;33(5).

305. Masuoka H, Academy NC-A of the new Y, 2013 undefined. Nonalcoholic fatty liver

disease: an emerging threat to obese and diabetic individuals. *Wiley Online Libr*. 2013;1281(1):106-122.

306. Parekh S, Anania FA. Abnormal Lipid and Glucose Metabolism in Obesity: Implications for Nonalcoholic Fatty Liver Disease. *Gastroenterology*. 2007;132(6):2191-2207.

307. Gaggini M, Morelli M, Buzzigoli E, Defronzo RA, Bugianesi E, Gastaldelli A. Non-alcoholic fatty liver disease (NAFLD) and its connection with insulin resistance, dyslipidemia, atherosclerosis and coronary heart disease. *mdpi.com*. 2013;5(5):1544-1560.

308. Kotronen A, Juurinen L, … AH-D, 2008 undefined. Liver fat is increased in type 2 diabetic patients and underestimated by serum alanine aminotransferase compared with equally obese nondiabetic subjects. *Am Diabetes Assoc*. 2008;31(1):165-169.

309. Day CP, James OFW. Steatohepatitis: A tale of two "Hits"? *Gastroenterology*. 1998;114(4 I):842-845.

310. H T, AR M. Insulin resistance, inflammation, and non-alcoholic fatty liver disease. *Trends Endocrinol Metab*. 2008;19(10):371-379.

311. Roth CL, Elfers CT, Figlewicz DP, et al. Vitamin D deficiency in obese rats exacerbates nonalcoholic fatty liver disease and increases hepatic resistin and toll-like receptor activation. *Hepatology*. 2012;55(4):1103-1111.

312. Brunt EM. Grading and staging the histopathological lesions of chronic hepatitis: The Knodell histology activity index and beyond. *Hepatology*. 2000;31(1):241-246.

313. Garbow JR, Doherty JM, Schugar RC, et al. Hepatic steatosis, inflammation, and ER stress in mice maintained long term on a very low-carbohydrate ketogenic diet. *Am J Physiol - Gastrointest Liver Physiol*. 2011;300(6):G956.

314. Hellerstein MK. De novo lipogenesis in humans: Metabolic and regulatory aspects. *Eur J Clin Nutr*. 1999;53:s53-s65.

315. Softic S, Cohen DE, Kahn CR. Role of Dietary Fructose and Hepatic De Novo Lipogenesis in Fatty Liver Disease. *Dig Dis Sci*. 2016;61(5):1282-1293.

316. Cintra DE, Ropelle ER, Vitto MF, et al. RETRACTED: Reversion of hepatic steatosis by exercise training in obese mice: the role of sterol regulatory element-binding protein-1c. *Life Sci*. 2012;91(11-12):395-401.

317. Knebel B, Haas J, Hartwig S, et al. Liver-specific expression of transcriptionally active srebp-1c is associated with fatty liver and increased visceral fat mass. *PLoS One*. 2012;7(2).

318. B K, J H, S H, et al. Liver-specific expression of transcriptionally active SREBP-1c is associated with fatty liver and increased visceral fat mass. *PLoS One*. 2012;7(2).

319. Méndez-Sánchez N, Arrese M, Zamora-Valdés D, Uribe M. Current concepts in the pathogenesis of nonalcoholic fatty liver disease. *Liver Int*. 2007;27(4):423-433.

320. Samuel V, Liu Z, Qu X, Elder B, … SB-J of B, 2004 undefined. Mechanism of hepatic insulin resistance in non-alcoholic fatty liver disease. *ASBMB*.

321. Nagai Y, Yonemitsu S, Erion D, Iwasaki T, metabolism RS-C, 2009 undefined. The role of peroxisome proliferator-activated receptor γ coactivator-1 β in the pathogenesis of fructose-induced insulin resistance. *Elsevier*.

322. YOON S, … YM-JJ of, 2000 undefined. Accumulation of diacylglycerol induced by CCl_4-derived radicals in rat liver membrane and its inhibition with radical trapping reagent: FT-IR spectroscopic and HPLC. *eprints.lib.hokudai.ac.jp*. 2000;47(4):135-144.

323. Nakajima T, research OY-J of radiation, 1999 undefined. Mechanism of radiation-induced diacylglycerol production in primary cultured rat hepatocytes. *ieeexplore.ieee.org*. 1999;40:135-144.

324. Yen C-LE, Stone SJ, Koliwad S, Harris C, Farese R V., Jr. DGAT enzymes and triacylglycerol biosynthesis. *J Lipid Res*. 2008;49(11):2283.

325. Finck BN, Hall AM. Does diacylglycerol accumulation in fatty liver disease cause hepatic insulin resistance? *Biomed Res Int*. 2015;2015.

326. YJ L, EH K, JE K, et al. Nuclear receptor PPARγ-regulated monoacylglycerol O-acyltransferase 1 (MGAT1) expression is responsible for the lipid accumulation in diet-induced hepatic steatosis. *Proc Natl Acad Sci U S A*. 2012;109(34):13656-13661.

327. Lutkewitte AJ, McCommis KS, Schweitzer GG, et al. Hepatic monoacylglycerol acyltransferase 1 is induced by prolonged food deprivation to modulate the hepatic fasting response. *J Lipid Res*. 2019;60(3):528.

328. Hall AM, Soufi N, Chambers KT, et al. Abrogating Monoacylglycerol Acyltransferase Activity in Liver Improves Glucose Tolerance and Hepatic Insulin Signaling in Obese Mice. *Diabetes*. 2014;63(7):2284-2296.

329. Cao J, Zhou Y, Peng H, et al. Targeting Acyl-CoA:Diacylglycerol Acyltransferase 1 (DGAT1) with Small Molecule Inhibitors for the Treatment of Metabolic Diseases. *J Biol Chem*. 2011;286(48):41838.

330. Abulizi A, Vatner DF, Ye Z, et al. Membrane-bound sn-1,2-diacylglycerols explain the dissociation of hepatic insulin resistance from hepatic steatosis in MTTP knockout mice. *J Lipid Res*. 2020;61(12):1565-1576.

331. Camporez J, Kanda S, … MP-J of lipid, 2015 undefined. ApoA5 knockdown improves whole-body insulin sensitivity in high-fat-fed mice by reducing ectopic lipid content. *ASBMB*.

332. Perry R, Samuel V, Petersen K, Nature GS-, 2014 undefined. The role of hepatic lipids in hepatic insulin resistance and type 2 diabetes. *nature.com*.

333. Matam Vijay-Kumar, Jesse D. Aitken, Frederic A. Carvalho1, Tyler C. Cullender S, Mwangi, Shanthi Srinivasan, Shanthi V. Sitaraman, Rob Knight, Ruth E. Ley A, Gewirtz AT. Metabolic Syndrome and Altered Gut Microbiota in Mice Lacking Toll-Like

Receptor 5. *Science (80-)*. 2010;328(5975)(April):228-231.

334. Kumashiro N, Erion DM, Zhang D, et al. Cellular mechanism of insulin resistance in nonalcoholic fatty liver disease. *Proc Natl Acad Sci U S A*. 2011;108(39):16381-16385.

335. Magkos F, Su X, Bradley D, Fabbrini E, Gastroenterology CC-, 2012 undefined. Intrahepatic diacylglycerol content is associated with hepatic insulin resistance in obese subjects. *Elsevier*.

336. Luukkonen P, Zhou Y, Sädevirta S, … ML-J of, 2016 undefined. Hepatic ceramides dissociate steatosis and insulin resistance in patients with non-alcoholic fatty liver disease. *Elsevier*.

337. ter Horst KW, Gilijamse PW, Versteeg RI, et al. Hepatic Diacylglycerol-Associated Protein Kinase Cε Translocation Links Hepatic Steatosis to Hepatic Insulin Resistance in Humans. *Cell Rep*. 2017;19(10):1997-2004.

338. Perry R, Kim T, Zhang X, Lee H, metabolism DP-C, 2013 undefined. Reversal of hypertriglyceridemia, fatty liver disease, and insulin resistance by a liver-targeted mitochondrial uncoupler. *Elsevier*.

339. Horst K Ter, Gilijamse P, reports RV-C, 2017 undefined. Hepatic diacylglycerol-associated protein kinase Cε translocation links hepatic steatosis to hepatic insulin resistance in humans. *Elsevier*.

340. Samuel V, Liu Z, … AW-TJ of, 2007 undefined. Inhibition of protein kinase Cε prevents hepatic insulin resistance in nonalcoholic fatty liver disease. *Am Soc Clin Investig*.

341. Petersen M, … AM-TJ of, 2016 undefined. Insulin receptor Thr1160 phosphorylation mediates lipid-induced hepatic insulin resistance. *Am Soc Clin Investig*.

342. Kumashiro N, Erion D, … DZ-P of the, 2011 undefined. Cellular mechanism of insulin resistance in nonalcoholic fatty liver disease. *Natl Acad Sci*.

343. Montgomery M, Brown S, … XL-… et BA (BBA, 2016 undefined. Regulation of glucose homeostasis and insulin action by ceramide acyl-chain length: A beneficial role for very long-chain sphingolipid species. *Elsevier*.

344. Montgomery MK, Hallahan NL, Brown SH, et al. Mouse strain-dependent variation in obesity and glucose homeostasis in response to high-fat feeding. *Diabetologia*. 2013;56(5):1129-1139.

345. Galbo T, Perry R, … MJ-P of the, 2013 undefined. Saturated and unsaturated fat induce hepatic insulin resistance independently of TLR-4 signaling and ceramide synthesis in vivo. *Natl Acad Sci*. 2013.

346. Camporez J, Jornayvaz F, Lee H, … SK-, 2013 undefined. Cellular mechanism by which estradiol protects female ovariectomized mice from high-fat diet-induced hepatic and muscle insulin resistance. *academic.oup.com*.

347. Tao H, Zhang Y, Zeng X, Shulman G, medicine SJ-N, 2014 undefined. Niclosamide

ethanolamine improves blood glycemic control and reduces hepatic steatosis in mice. *ncbi.nlm.nih.gov*.

348. Jornayvaz F, … AB-P of the, 2011 undefined. Hepatic insulin resistance in mice with hepatic overexpression of diacylglycerol acyltransferase 2. *Natl Acad Sci*. 2011;108(14).

349. Kurek K, Piotrowska DM, Wiesiołek-Kurek P, et al. Inhibition of ceramide de novo synthesis reduces liver lipid accumulation in rats with nonalcoholic fatty liver disease. *Liver Int*. 2014;34(7):1074-1083.

350. Turpin S, Nicholls H, Willmes D, metabolism AM-C, 2014 undefined. Obesity-induced CerS6-dependent C16: 0 ceramide production promotes weight gain and glucose intolerance. *Elsevier*.

351. Siddique MM, Li Y, Wang L, et al. Ablation of Dihydroceramide Desaturase 1, a Therapeutic Target for the Treatment of Metabolic Diseases, Simultaneously Stimulates Anabolic and Catabolic Signaling. *Mol Cell Biol*. 2013;33(11):2353-2369.

352. Hla T, metabolism RK-C, 2014 undefined. C16: 0-ceramide signals insulin resistance. *Elsevier*.

353. Turner N, Kowalski GM, Leslie SJ, et al. Distinct patterns of tissue-specific lipid accumulation during the induction of insulin resistance in mice by high-fat feeding. *Diabetologia*. 2013;56(7):1638-1648.

354. Salinas M, López-Valdaliso R, … DM-M and C, 2000 undefined. Inhibition of PKB/Akt1 by C2-ceramide involves activation of ceramide-activated protein phosphatase in PC12 cells. *Elsevier*.

355. Zhou H, Summers S, … MB-J of B, 1998 undefined. Inhibition of Akt kinase by cell-permeable ceramide and its implications for ceramide-induced apoptosis. *ASBMB*.

356. Galbo T, Perry R, Nishimura E, … VS-A (Albany, 2013 undefined. PP2A inhibition results in hepatic insulin resistance despite Akt2 activation. *ncbi.nlm.nih.gov*.

357. Schubert K, Scheid M, Chemistry VD-J of B, 2000 undefined. Ceramide inhibits protein kinase B/Akt by promoting dephosphorylation of serine 473. *ASBMB*.

358. Ingebritsen TS, Cohen P. Protein phosphatases: Properties and role in cellular regulation. *Science (80-)*. 1983;221(4608):331-338.

359. Kawaguchi T, Takenoshita M, Kabashima T, Uyeda K. Glucose and cAMP regulate the L-type pyruvate kinase gene by phosphorylation/dephosphorylation of the carbohydrate response element binding protein. *Proc Natl Acad Sci U S A*. 2001;98(24):13710-13715.

360. Xia J, Holland W, Kusminski C, Sun K, metabolism AS-C, 2015 undefined. Targeted induction of ceramide degradation leads to improved systemic metabolism and reduced hepatic steatosis. *Elsevier*.

361. Vandanmagsar B, Youm Y, Ravussin A, medicine JG-N, 2011 undefined. The NLRP3 inflammasome instigates obesity-induced inflammation and insulin resistance.

nature.com.

362. Yancy WS, Olsen MK, Guyton JR, Bakst RP, Westman EC. A low-carbohydrate, ketogenic diet versus a low-fat diet to treat obesity and hyperlipidemia. *ACC Curr J Rev*. 2004;13(8):18-19.

363. Yancy WS, Jr, Foy M, Chalecki AM, Vernon MC, Westman EC. A low-carbohydrate, ketogenic diet to treat type 2 diabetes. *Nutr Metab (Lond)*. 2005;2:34.

364. Arora SK, McFarlane SI. The case for low carbohydrate diets in diabetes management. *Nutr Metab*. 2005;2.

365. Manninen AH. Metabolic Effects of the Very-Low-Carbohydrate Diets: Misunderstood "Villains" of Human Metabolism. *J Int Soc Sports Nutr*. 2004;1(2):7.

366. Geisler CE, Renquist BJ. Hepatic lipid accumulation: Cause and consequence of dysregulated glucoregulatory hormones. *J Endocrinol*. 2017;234(1):R1-R21.

367. Tinguely D, Gross J, Kosinski C. Efficacy of Ketogenic Diets on Type 2 Diabetes: a Systematic Review. *Curr Diab Rep*. 2021;21(9):32.

368. T F, GD L, GA M. Pathways and control of ketone body metabolism: on the fringe of lipid biochemistry. *Prostaglandins Leukot Essent Fatty Acids*. 2004;70(3):243-251.

369. Malhi MS, Duerson F, Salabei JK, Okonoboh P. Starvation Ketoacidosis Induced by Ketogenic Diet and Consumption of Ketone Supplement. *Cureus*. June 2021.

370. D B, S E, L W, D L, R H, R W. The ketogenic diet in disease and development. *Int J Dev Neurosci*. 2018;68:53-58.

371. NJ J, HZ W, M N, J R. Effects of Ketone Bodies on Brain Metabolism and Function in Neurodegenerative Diseases. *Int J Mol Sci*. 2020;21(22):1-17.

372. Zammit VA. Regulation of Hepatic Fatty Acid Oxidation and Ketogenesis. *Proc Nutr Soc*. 1983;42(2):289-302.

373. McGarry JD, Foster DW. Ketogenesis and its regulation. *Am J Med*. 1976;61(1):9-13.

374. JD M, DW F. Regulation of hepatic fatty acid oxidation and ketone body production. *Annu Rev Biochem*. 1980;49:395-420.

375. Balasse EO, Féry F. Ketone body production and disposal: Effects of fasting, diabetes, and exercise. *Diabetes Metab Rev*. 1989;5(3):247-270.

376. Mitchell GA, Kassovska-Bratinova S, Boukaftane Y, et al. Medical aspects of ketone body metabolism. *Clin Investig Med*. 1995;18(3):193-216.

377. Traylor DA, Gorissen SHM, Phillips SM. Perspective: Protein Requirements and Optimal Intakes in Aging: Are We Ready to Recommend More Than the Recommended Daily Allowance? *Adv Nutr*. 2018;9(3):171.

378. Newman JC, Verdin E. Ketone bodies as signaling metabolites. *Trends Endocrinol*

Metab. 2014;25(1):42-52.

379. JC N, E V. β-hydroxybutyrate: much more than a metabolite. *Diabetes Res Clin Pract*. 2014;106(2):173-181.

380. Berg J, Tymoczko J, Stryer L. Lipids and Cell Membranes. *Biochemistry*. 2002:319-344.

381. Biochemistry - NCBI Bookshelf. https://www.ncbi.nlm.nih.gov/books/NBK21154/. Accessed October 2, 2021.

382. T F, XQ S, GA M, et al. Enzymes of ketone body utilization in human tissues: protein and messenger RNA levels of succinyl-coenzyme A (CoA):3-ketoacid CoA transferase and mitochondrial and cytosolic acetoacetyl-CoA thiolases. *Pediatr Res*. 1997;42(4):498-502.

383. Grandl G, Straub L, Rudigier C, et al. Short-term feeding of a ketogenic diet induces more severe hepatic insulin resistance than an obesogenic high-fat diet. *J Physiol*. 2018;596(19):4597-4609.

384. Klein KR, Walker CP, McFerren AL, Huffman H, Frohlich F, Buse JB. Carbohydrate intake prior to oral glucose tolerance testing. *J Endocr Soc*. 2021;5(5).

385. N D, T M, JM P, et al. Adaptive changes in amino acid metabolism permit normal longevity in mice consuming a low-carbohydrate ketogenic diet. *Biochim Biophys Acta*. 2015;1852(10 Pt A):2056-2065.

386. AM H, WC K, PW M, et al. Effects of a ketogenic diet on adipose tissue, liver, and serum biomarkers in sedentary rats and rats that exercised via resisted voluntary wheel running. *Am J Physiol Regul Integr Comp Physiol*. 2016;311(2):R337-R351.

387. FR J, MJ J, HY L, et al. A high-fat, ketogenic diet causes hepatic insulin resistance in mice, despite increasing energy expenditure and preventing weight gain. *Am J Physiol Endocrinol Metab*. 2010;299(5).

388. Fukazawa A, Koike A, Karasawa T, Tsutsui M, Kondo S, Terada S. Effects of a Ketogenic Diet Containing Medium-Chain Triglycerides and Endurance Training on Metabolic Enzyme Adaptations in Rat Skeletal Muscle. *Nutrients*. 2020;12(5).

389. Samuel VT, Shulman GI. The pathogenesis of insulin resistance: integrating signaling pathways and substrate flux. *J Clin Invest*. 2016;126(1):12-22.

390. Samuel VT, Shulman GI. Nonalcoholic Fatty Liver Disease as a Nexus of Metabolic and Hepatic Diseases. *Cell Metab*. 2018;27(1):22-41.

391. Elia M. Organ and Tissue Contribution to Metabolic Rate. In: Tucker JMK& HN, ed. *Energy Metabolism: Tissue Determinants and Cellular Corollaries*. New York: Raven Press; 1992:61-79.

392. Jornayvaz FR, Samuel VT, Shulman GI. The role of muscle insulin resistance in the pathogenesis of atherogenic dyslipidemia and nonalcoholic fatty liver disease associated with the metabolic syndrome. *Annu Rev Nutr*. 2010;30:273-290.

393. Shulman GI, Rothman DL, Jue T, Stein P, DeFronzo RA, Shulman RG. Quantitation of muscle glycogen synthesis in normal subjects and subjects with non-insulin-dependent diabetes by 13C nuclear magnetic resonance spectroscopy. *N Engl J Med*. 1990;322(4):223-228.

394. Holland WL, Knotts TA, Chavez JA, Wang L-P, Hoehn KL, Summers SA. Lipid mediators of insulin resistance. *Nutr Rev*. 2007;65(6 Pt 2):S39-46.

395. Dresner A, Laurent D, Marcucci M, et al. Effects of free fatty acids on glucose transport and IRS-1-associated phosphatidylinositol 3-kinase activity. *J Clin Invest*. 1999;103(2):253-259.

396. Mogensen M, Sahlin K, Fernström M, et al. Mitochondrial respiration is decreased in skeletal muscle of patients with type 2 diabetes. *Diabetes*. 2007;56(6):1592-1599.

397. Petersen KF, Dufour S, Befroy D, Garcia R, Shulman GI. Impaired mitochondrial activity in the insulin-resistant offspring of patients with type 2 diabetes. *N Engl J Med*. 2004;350(7):664-671.

398. Szendroedi J, Schmid AI, Chmelik M, et al. Muscle mitochondrial ATP synthesis and glucose transport/phosphorylation in type 2 diabetes. *PLoS Med*. 2007;4(5):e154.

399. Tornatore L, Thotakura AK, Bennett J, Moretti M, Franzoso G. The nuclear factor kappa B signaling pathway: integrating metabolism with inflammation. *Trends Cell Biol*. 2012;22(11):557-566.

400. Fazakerley DJ, Krycer JR, Kearney AL, Hocking SL, James DE. Muscle and adipose tissue insulin resistance: Malady without mechanism? *J Lipid Res*. 2019;60(10):1720-1732.

401. Pinho RA, Sepa-Kishi DM, Bikopoulos G, et al. High-fat diet induces skeletal muscle oxidative stress in a fiber type-dependent manner in rats. *Free Radic Biol Med*. 2017;110.

402. Stojanovska L, Rosella G, Proietto J. Evolution of dexamethasone-induced insulin resistance in rats. *Am J Physiol*. 1990;258(5 Pt 1):E748-56.

403. Guillaume-Gentil C, Rohner-Jeanrenaud F, Abramo F, Bestetti GE, Rossi GL, Jeanrenaud B. Abnormal regulation of the hypothalamo-pituitary-adrenal axis in the genetically obese fa/fa rat. *Endocrinology*. 1990;126(4):1873-1879.

404. Freedman MR, Horwitz BA, Stern JS. Effect of adrenalectomy and glucocorticoid replacement on development of obesity. *Am J Physiol*. 1986;250(4 Pt 2):R595-607.

405. Kusunoki M, Cooney GJ, Hara T, Storlien LH. Amelioration of high-fat feeding-induced insulin resistance in skeletal muscle with the antiglucocorticoid RU486. *Diabetes*. 1995;44(6):718-720.

406. du Sert NP, Ahluwalia A, Alam S, et al. Reporting animal research: Explanation and elaboration for the arrive guidelines 2.0. *PLoS Biol*. 2020;18(7):e3000411.

407. Araujo RL, Andrade BM, Padrón AS, et al. High-fat diet increases thyrotropin and

oxygen consumption without altering circulating 3,5,3′-triiodothyronine (T 3) and thyroxine in rats: The role of iodothyronine deiodinases, reverse T 3 production, and whole-body fat oxidation. *Endocrinology*. 2010;151(7):3460-3469.

408. Ariano MA, Armstrong RB, Edgerton VR. Hindlimb muscle fiber populations of five mammals. *J Histochem Cytochem*. 1973;21(1):51-55.

409. Nesher R, Karl IE, Kaiser KE, Kipnis DM. Epitrochlearis muscle. I. Mechanical performance, energetics, and fiber composition. *Am J Physiol - Endocrinol Metab*. 1980;2(6).

410. Fediuc S, Gaidhu MP, Ceddia RB. Inhibition of insulin-stimulated glycogen synthesis by 5-aminoimidasole-4-carboxamide-1-beta-d-ribofuranoside-induced adenosine 5'-monophosphate-activated protein kinase activation: interactions with Akt, glycogen synthase kinase 3-3alpha/beta, and glycog. *Endocrinology*. 2006;147(11):5170-5177.

411. Vitzel KF, Bikopoulos G, Hung S, et al. Chronic treatment with the AMP-kinase activator AICAR increases glycogen storage and fatty acid oxidation in skeletal muscles but does not reduce hyperglucagonemia and hyperglycemia in insulin deficient rats. *PLoS One*. 2013;8(4):e62190.

412. Folch J, Lees M, Sloane Stanley GH. A simple method for the isolation and purification of total lipides from animal tissues. *J Biol Chem*. 1957;226(1):497-509.

413. Carvalho MS, Mendonça MA, Pinho DMM, Resck IS, Suarez PAZ. Chromatographic analyses of fatty acid methyl esters by HPLC-UV and GC-FID. *J Braz Chem Soc*. 2012;23(4):763-769.

414. Błachnio-Zabielska A, Baranowski M, Zabielski P, Górski J. Effect of exercise duration on the key pathways of ceramide metabolism in rat skeletal muscles. *J Cell Biochem*. 2008;105(3):776-784.

415. Kolczynska K, Loza-Valdes A, Hawro I, Sumara G. Diacylglycerol-evoked activation of PKC and PKD isoforms in regulation of glucose and lipid metabolism: A review. *Lipids Health Dis*. 2020;19(1).

416. Osada S, Mizuno K, Saido TC, Suzuki K, Kuroki T, Ohno S. A new member of the protein kinase C family, nPKC theta, predominantly expressed in skeletal muscle. *Mol Cell Biol*. 1992;12(9):3930-3938.

417. Itani SI, Zhou Q, Pories WJ, MacDonald KG, Dohm GL. Involvement of protein kinase C in human skeletal muscle insulin resistance and obesity. *Diabetes*. 2000;49(8):1353-1358.

418. Li M, Vienberg SG, Bezy O, O'Neill BT, Kahn CR. Role of PKCδ in insulin sensitivity and skeletal muscle metabolism. *Diabetes*. 2015;64(12):4023-4032.

419. Yu C, Chen Y, Cline GW, et al. Mechanism by which fatty acids inhibit insulin activation of insulin receptor substrate-1 (IRS-1)-associated phosphatidylinositol 3-kinase activity in muscle. *J Biol Chem*. 2002;277(52):50230-50236.

420. N M, A A, N I. New perspectives on PKCtheta, a member of the novel subfamily of protein kinase C. *Stem Cells*. 1998;16(3):178-192.

421. Holland WL, Bikman BT, Wang LP, et al. Lipid-induced insulin resistance mediated by the proinflammatory receptor TLR4 requires saturated fatty acid-induced ceramide biosynthesis in mice. *J Clin Invest*. 2011;121(5):1858-1870.

422. Naito Y, Tamai S, Shingu K, et al. Responses of plasma adrenocorticotropic hormone, cortisol, and cytokines during and after upper abdominal surgery. *Anesthesiology*. 1992;77(3):426-431.

423. Burén J, Lai YC, Lundgren M, Eriksson JW, Jensen J. Insulin action and signalling in fat and muscle from dexamethasone-treated rats. *Arch Biochem Biophys*. 2008;474(1):91-101.

424. Surwit RS, Feinglos MN, Livingston EG, Kuhn CM, McCubbin JA. Behavioral manipulation of the diabetic phenotype in ob/ob mice. *Diabetes*. 1984;33(7):616-618.

425. Pascoe WS, Smythe GA, Storlien LH. Enhanced responses to stress induced by fat-feeding in rats: relationship between hypothalamic noradrenaline and blood glucose. *Brain Res*. 1991;550(2):192-196.

426. Beaudry JL, D'souza AM, Teich T, Tsushima R, Riddell MC. Exogenous glucocorticoids and a high-fat diet cause severe hyperglycemia and hyperinsulinemia and limit islet glucose responsiveness in young male Sprague-Dawley rats. *Endocrinology*. 2013;154(9):3197-3208.

427. Shimomura Y, Bray GA, Lee M. Adrenalectomy and steroid treatment in obese (ob/ob) and diabetic (db/db) mice. *Horm Metab Res = Horm und Stoffwechselforsch = Horm métabolisme*. 1987;19(7):295-299.

428. Rasool S, Geetha T, Broderick TL, Babu JR. High fat with high sucrose diet leads to obesity and induces myodegeneration. *Front Physiol*. 2018;9(SEP).

429. Lundsgaard AM, Kiens B. Gender differences in skeletal muscle substrate metabolism - molecular mechanisms and insulin sensitivity. *Front Endocrinol (Lausanne)*. 2014;5(NOV).

430. Clausen JO, Borch-Johnsen K, Ibsen H, et al. Insulin sensitivity index, acute insulin response, and glucose effectiveness in a population-based sample of 380 young healthy Caucasians. Analysis of the impact of gender, body fat, physical fitness, and life-style factors. *J Clin Invest*. 1996;98(5):1195-1209.

431. Defronzo RA, Tripathy D. Skeletal Muscle Insulin Resistance Is the Primary Defect in Type 2 Diabetes. 2009.

432. Sokolowska E, Blachnio-Zabielska A. The Role of Ceramides in Insulin Resistance. *Front Endocrinol (Lausanne)*. 2019;10.

433. Jani S, Da Eira D, Hadday I, et al. Distinct mechanisms involving diacylglycerol, ceramides, and inflammation underlie insulin resistance in oxidative and glycolytic

muscles from high fat-fed rats. *Sci Rep*. 2021;11(1).

434. Høeg L, Roepstorff C, Thiele M, Richter EA, Wojtaszewski JFP, Kiens B. Higher intramuscular triacylglycerol in women does not impair insulin sensitivity and proximal insulin signaling. *J Appl Physiol*. 2009;107(3):824-831.

435. Sepa-Kishi DM, Katsnelson G, Bikopoulos G, Iqbal A, Ceddia RB. Cold acclimation reduces hepatic protein Kinase B and AMP-activated protein kinase phosphorylation and increases gluconeogenesis in rats. *Physiol Rep*. 2018;6(5).

436. Jani S, Da Eira D, Stefanovic M, Ceddia RB. The ketogenic diet prevents steatosis and insulin resistance by reducing lipogenesis, diacylglycerol accumulation and protein kinase C activity in male rat liver. *J Physiol*. 2022;600(18):4137-4151.

437. So M, Gaidhu MP, Maghdoori B, Ceddia RB. Analysis of time-dependent adaptations in whole-body energy balance in obesity induced by high-fat diet in rats. *Lipids Health Dis*. 2011;10(1):99.

438. Wu M V., Bikopoulos G, Hung S, Ceddia RB. Thermogenic capacity is antagonistically regulated in classical brown and white subcutaneous fat depots by high fat diet and endurance training in rats: Impact on whole-body energy expenditure. *J Biol Chem*. 2014;289(49):34129-34140.

439. Da Eira D, Jani S, Ceddia RB. An obesogenic diet impairs uncoupled substrate oxidation and promotes whitening of the brown adipose tissue in rats. *J Physiol*. 2023;601(1):69-82.

440. Yu C, Chen Y, Cline GW, et al. Mechanism by which fatty acids inhibit insulin activation of insulin receptor substrate-1 (IRS-1)-associated phosphatidylinositol 3-kinase activity in muscle. *J Biol Chem*. 2002;277(52):50230-50236.

441. Broussard JL, Perreault L, Macias E, et al. Sex Differences in Insulin Sensitivity are Related to Muscle Tissue Acylcarnitine But Not Subcellular Lipid Distribution. *Obesity (Silver Spring)*. 2021;29(3):550-561.

442. Chen G, Harwood JL, Lemieux MJ, Stone SJ, Weselake RJ. Acyl-CoA:diacylglycerol acyltransferase: Properties, physiological roles, metabolic engineering and intentional control. *Prog Lipid Res*. 2022;88.

443. Choi CS, Kim YB, Lee FN, Zabolotny JM, Kahn BB, Youn JH. Lactate induces insulin resistance in skeletal muscle by suppressing glycolysis and impairing insulin signaling. *Am J Physiol Endocrinol Metab*. 2002;283(2).

444. Maschari D, Saxena G, Law TD, Walsh E, Campbell MC, Consitt LA. Lactate-induced lactylation in skeletal muscle is associated with insulin resistance in humans. *Front Physiol*. 2022;13.

445. Kelley DE, Goodpaster B, Wing RR, Simoneau JA. Skeletal muscle fatty acid metabolism in association with insulin resistance, obesity, and weight loss. *Am J Physiol - Endocrinol Metab*. 1999;277(6 40-6).

446. PJ R, PB G, CN H, EA N. The glucose fatty-acid cycle. Its role in insulin sensitivity and the metabolic disturbances of diabetes mellitus. *Lancet (London, England)*. 1963;1(7285):785-789.

447. Song JD, Alves TC, Befroy DE, et al. Dissociation of Muscle Insulin Resistance from Alterations in Mitochondrial Substrate Preference. *Cell Metab*. 2020;32(5):726-735.e5.

448. Fabbrini E, Sullivan S, Klein S. Obesity and nonalcoholic fatty liver disease: Biochemical, metabolic, and clinical implications. *Hepatology*. 2010;51(2):679-689.

449. Angulo P. Medical progress: Nonalcoholic fatty liver disease. *N Engl J Med*. 2002;346(16):1221-1231.

450. Ipsen DH, Lykkesfeldt J, Tveden-Nyborg P. Molecular mechanisms of hepatic lipid accumulation in non-alcoholic fatty liver disease. *Cell Mol Life Sci*. 2018;75(18):3313-3327.

451. Fujii H, Kawada N. The Role of Insulin Resistance and Diabetes in Nonalcoholic Fatty Liver Disease. *Int J Mol Sci*. 2020;21(11).

452. Donnelly KL, Smith CI, Schwarzenberg SJ, Jessurun J, Boldt MD, Parks EJ. Sources of fatty acids stored in liver and secreted via lipoproteins in patients with nonalcoholic fatty liver disease. *J Clin Invest*. 2005;115(5):1343-1351.

453. Yki-Järvinen H, Luukkonen PK, Hodson L, Moore JB. Dietary carbohydrates and fats in nonalcoholic fatty liver disease. *Nat Rev Gastroenterol Hepatol*. 2021;18(11):770-786.

454. Kawano Y, Cohen DE. Mechanisms of hepatic triglyceride accumulation in non-alcoholic fatty liver disease. *J Gastroenterol*. 2013;48(4):434-441.

455. Friedman SL, Neuschwander-Tetri BA, Rinella M, Sanyal AJ. Mechanisms of NAFLD development and therapeutic strategies. *Nat Med*. 2018;24(7):908-922.

456. Samuel VT, Liu ZX, Qu X, et al. Mechanism of hepatic insulin resistance in non-alcoholic fatty liver disease. *J Biol Chem*. 2004;279(31):32345-32353.

457. Samuel VT, Liu ZX, Wang A, et al. Inhibition of protein kinase Cepsilon prevents hepatic insulin resistance in nonalcoholic fatty liver disease. *J Clin Invest*. 2007;117(3):739-745.

458. Raddatz K, Turner N, Frangioudakis G, et al. Time-dependent effects of Prkce deletion on glucose homeostasis and hepatic lipid metabolism on dietary lipid oversupply in mice. *Diabetologia*. 2011;54(6):1447-1456.

459. Petersen MC, Shulman GI. Roles of Diacylglycerols and Ceramides in Hepatic Insulin Resistance. *Trends Pharmacol Sci*. 2017;38(7):649-665.

460. Xia JY, Holland WL, Kusminski CM, et al. Targeted Induction of Ceramide Degradation Leads to Improved Systemic Metabolism and Reduced Hepatic Steatosis. *Cell Metab*. 2015;22(2):266-278.

461. Chaurasia B, Summers SA. Ceramides - Lipotoxic Inducers of Metabolic Disorders.

Trends Endocrinol Metab. 2015;26(10):538-550.

462. Watanabe M, Tozzi R, Risi R, et al. Beneficial effects of the ketogenic diet on nonalcoholic fatty liver disease: A comprehensive review of the literature. *Obes Rev*. 2020;21(8).

463. Cotter DG, Patti GJ, Crawford PA. Ketogenesis prevents diet-induced fatty liver injury and hyperglycemia The Journal of Clinical Investigation. *J Clin Invest*. 2014;124(12).

464. Youm Y-H, Nguyen KY, Grant RW, et al. The ketone metabolite β-hydroxybutyrate blocks NLRP3 inflammasome–mediated inflammatory disease. *Nat Med*. 2015;21(3):263-269.

465. Jones JG. Hepatic glucose and lipid metabolism. *Diabetologia*. 2016;59(6):1098-1103.

466. Sepa-Kishi DM, Jani S, Da Eira D, Ceddia RB. Cold acclimation enhances UCP1 content, lipolysis, and triacylglycerol resynthesis, but not mitochondrial uncoupling and fat oxidation, in rat white adipocytes. *Am J Physiol - Cell Physiol*. 2019;316(3):C365.

467. Sepa-Kishi DM, Sotoudeh-Nia Y, Iqbal A, Bikopoulos G, Ceddia RB. Cold acclimation causes fiber type-specific responses in glucose and fat metabolism in rat skeletal muscles. *Sci Rep*. 2017;7(1).

468. Folch J, Lees M, Sloane Stanley G. A Simple method for the isolation and purification of total lipides from animal tissues. 1987;55(5):999-1033.

469. Da Eira D, Jani S, Ceddia RB. Obesogenic and Ketogenic Diets Distinctly Regulate the SARS-CoV-2 Entry Proteins ACE2 and TMPRSS2 and the Renin-Angiotensin System in Rat Lung and Heart Tissues. *Nutrients*. 2021;13(10).

470. Livak KJ, Schmittgen TD. Analysis of Relative Gene Expression Data Using Real-Time Quantitative PCR and the 2−ΔΔCT Method. *Methods*. 2001;25(4):402-408.

471. Kumashiro N, Erion DM, Zhang D, et al. Cellular mechanism of insulin resistance in nonalcoholic fatty liver disease. *Natl Acad Sci*. 2011;108(39):16381-16385.

472. Petersen MC, Madiraju AK, Gassaway BM, et al. Insulin receptor Thr1160 phosphorylation mediates lipid-induced hepatic insulin resistance. *J Clin Invest*. 2016;126(11):4361-4371.

473. Tippetts TS, Holland WL, Summers SA. Cholesterol - the devil you know; ceramide - the devil you don't. *Trends Pharmacol Sci*. 2021;42(12):1082-1095.

474. Raichur S, Wang ST, Chan PW, et al. CerS2 haploinsufficiency inhibits β-oxidation and confers susceptibility to diet-induced steatohepatitis and insulin resistance. *Cell Metab*. 2014;20(4):687-695.

475. Estall JL, Kahn M, Cooper MP, et al. Sensitivity of lipid metabolism and insulin signaling to genetic alterations in hepatic peroxisome proliferator-activated receptor-gamma coactivator-1alpha expression. *Diabetes*. 2009;58(7):1499-1508.

476. Estall JL, Kahn M, Cooper MP, et al. Sensitivity of lipid metabolism and insulin

signaling to genetic alterations in hepatic peroxisome proliferator-activated receptor-gamma coactivator-1alpha expression. *Diabetes*. 2009;58(7):1499-1508.

477. Haase TN, Ringholm S, Leick L, et al. Role of PGC-1α in exercise and fasting-induced adaptations in mouse liver. *Am J Physiol Regul Integr Comp Physiol*. 2011;301(5):R1501-9.

478. Leone TC, Lehman JJ, Finck BN, et al. PGC-1α Deficiency Causes Multi-System Energy Metabolic Derangements: Muscle Dysfunction, Abnormal Weight Control and Hepatic Steatosis. Vidal-Puig A, ed. *PLoS Biol*. 2005;3(4):e101.

479. Coskun T, Bina HA, Schneider MA, et al. Fibroblast growth factor 21 corrects obesity in mice. *Endocrinology*. 2008;149(12):6018-6027.

480. Cantó C, Auwerx J. Cell biology. FGF21 takes a fat bite. *Science*. 2012;336(6082):675-676.

481. Potthoff MJ, Inagaki T, Satapati S, Ding X, He T, Goetz R. FGF21 induces PGC-1 ⎵ and regulates carbohydrate and fatty acid metabolism during the adaptive. 2009;106(26).

482. Badman MK, Pissios P, Kennedy AR, Koukos G, Flier JS, Maratos-Flier E. Hepatic Fibroblast Growth Factor 21 Is Regulated by PPARalpha and Is a Key Mediator of Hepatic Lipid Metabolism in Ketotic States. *Cell Metab*. 2007;5(6):426-437.

483. Luo Y, Lin H. Inflammation initiates a vicious cycle between obesity and nonalcoholic fatty liver disease. *Immunity, Inflamm Dis*. 2021;9(1):59-73.

484. Asrih M, Jornayvaz FR. Inflammation as a potential link between nonalcoholic fatty liver disease and insulin resistance. *J Endocrinol*. 2013;218(3):R25-R36.

485. Albers PH, Pedersen AJT, Birk JB, et al. Human Muscle Fiber Type-Specific Insulin Signaling: Impact of Obesity and Type 2 Diabetes. *Diabetes*. 2015;64:485-497.

486. Roger Unger. Genetic and Clinical Implications of. *Am J Psychiatry*. 1986:863-870.

487. Kitessa SM, Abeywardena MY, Vogel S. Lipid-Induced Insulin Resistance in Skeletal Muscle: The Chase for the Culprit Goes from Total Intramuscular Fat to Lipid Intermediates, and Finally to Species of Lipid Intermediates. 2016.

488. Yu C, Chen Y, Cline GW, et al. Mechanism by which fatty acids inhibit insulin activation of insulin receptor substrate-1 (IRS-1)-associated phosphatidylinositol 3-kinase activity in muscle. *J Biol Chem*. 2002;277(52):50230-50236.

489. Griffin ME, Marcucci MJ, Cline GW, et al. Free fatty acid-induced insulin resistance is associated with activation of protein kinase C θ and alterations in the insulin signaling cascade. *Diabetes*. 2000;48(6):1270-1274.

490. Itani SI, Ruderman NB, Schmieder F, Boden G. Lipid-induced insulin resistance in human muscle is associated with changes in diacylglycerol, protein kinase C, and IκB-α. *Diabetes*. 2002;51(7):2005-2011.

491. Lam YY, Hatzinikolas G, Weir JM, et al. Insulin-stimulated glucose uptake and pathways

regulating energy metabolism in skeletal muscle cells: The effects of subcutaneous and visceral fat, and long-chain saturated, n-3 and n-6 polyunsaturated fatty acids. *Biochim Biophys Acta - Mol Cell Biol Lipids*. 2011;1811(7-8):468-475.

492. Coatmellec-Taglioni G, Dausse JP, Giudicelli Y, Ribière C. Sexual Dimorphism in Cafeteria Diet-Induced Hypertension Is Associated with Gender-Related Difference in Renal Leptin Receptor Down-Regulation. *J Pharmacol Exp Ther*. 2003;305(1):362-367.

493. Lladó I, Rodríguez-Cuenca S, Pujol E, et al. Gender effects on adrenergic receptor expression and lipolysis in white adipose tissue of rats. *Obes Res*. 2002;10(4):296-305.

494. Horton TJ, Gayles EC, Prach PA, Koppenhafer TA, Pagliassotti MJ. Female rats do not develop sucrose-induced insulin resistance. *Am J Physiol - Regul Integr Comp Physiol*. 1997;272(5 41-5).

495. Hevener A, Reichart D, Janez A, Olefsky J. Female rats do not exhibit free fatty acid-induced insulin resistance. *Diabetes*. 2002;51(6):1907-1912.

496. Yoon JC, Puigserver P, Chen G, et al. Control of hepatic gluconeogenesis through the transcriptional coactivator PGC-1. 2001:131-138.

497. She P, Burgess SC, Shiota M, et al. Mechanisms by which liver-specific PEPCK knockout mice preserve euglycemia during starvation. *Diabetes*. 2003;52(7):1649-1654.

498. Perry RJ, Samuel VT, Petersen KF, Shulman GI. The role of hepatic lipids in hepatic insulin resistance and type 2 diabetes. *Nature*. 2014;510(7503):84-91.

499. Vatner DF, Majumdar SK, Kumashiro N, et al. Insulin-independent regulation of hepatic triglyceride synthesis by fatty acids. *Natl Acad Sci*. 2015;112(4):1143-1148.

500. Gassaway BM, Petersen MC, Surovtseva Y V., et al. PKCe contributes to lipid-induced insulin resistance through cross talk with p70S6K and through previously unknown regulators of insulin signaling. *Proc Natl Acad Sci U S A*. 2020;115(38):E8996-E9005.

501. Galuska D, Kotova O, Barrès R, Chibalina D, Benziane B, Chibalin A V. Altered expression and insulin-induced trafficking of Na-K-ATPase in rat skeletal muscle: effects of high-fat diet and exercise Chibalin AV. Altered expression and insulin-induced trafficking of Na-K-ATPase in rat skeletal muscle: effects of high-fat diet and exercise. *Am J Physiol Endocrinol Metab*. 2009;297:38-49.

502. Fan X, Yao H, Liu X, et al. High-Fat Diet Alters the Expression of Reference Genes in Male Mice. *Front Nutr*. 2020;7:249.

503. Feschenko MS, Sweadner KJ. Conformation-dependent phosphorylation of Na,K-ATPase by protein kinase A and protein kinase C. *J Biol Chem*. 1994;269(48):30436-30444.

504. de la Maza MP, Rodriguez JM, Hirsch S, Leiva L, Barrera G, Bunout D. Skeletal muscle ceramide species in men with abdominal obesity. *J Nutr Health Aging*. 2015;19(4):389-396.

505. Kawano T, Inokuchi J, Eto M, Murata M, Kang J. Activators and Inhibitors of Protein

Kinase C (PKC): Their Applications in Clinical Trials. 2021:1-27.

506. Brandon AE, Liao BM, Diakanastasis B, et al. Short Article Protein Kinase C Epsilon Deletion in Adipose Tissue , but Not in Liver , Improves Glucose Tolerance Short Article Protein Kinase C Epsilon Deletion in Adipose Tissue , but Not in Liver , Improves Glucose Tolerance. *Cell Metab*. 2019;29(1):183-191.e7.

507. Nassir F, Rector RS, Hammoud GM, Ibdah JA. Pathogenesis and prevention of hepatic steatosis. *Gastroenterol Hepatol*. 2015;11(3):167-175.

Appendix A - Experimental Methods in Detail

a) Lysis Buffer for Homogenization

Concentration	Reagent	Molecular Weight
135mmol/L	NaCl	58.44
1mmol/L	MgCl2	203.3
2.7mmol/L	KCl	74.55
20mmol/L	Tris (pH 8)	121.14
1%	Triton	-
10%	Glycerol	-
Aliquoted and stored at -20°C		
Protease (cOmplete ULTRA Tablets) and phosphatase (PhoStop) inhibitors added immediately prior to use		

b) Laemmli Sample Buffer (2x)

Per 1mL-950µl of 2x Laemmli sample buffer (Bio-Rad, Cat#161-0737) and 50µl β-Mercaptoethanol stored at room temperature. Used to dilute the protein sample followed by boiling for 5min at 95°C.

c) Preparation of Tissue Lysates

Remove frozen tissue sample from -80°C freezer and keep on dry ice. Carefully weigh out desired sample (~ 25mg for liver or ~ 25mg for muscles) (avoid thawing out the rest of the tissue sample) and add to 250µl of lysis buffer containing both protease & phosphatase inhibitors. Using a homogenizer, thoroughly homogenize the sample. Next sonicate the samples for 3 seconds each at a pulse of 40, making sure the lysate samples are constantly on ice. Centrifuge the tissue lysate for 10min @ 12,000rpm (4°C). Transfer the supernatant into a fresh micro tube. Protein concentration is then determined using Bradford method, for which one aliquot needs to be removed. Another aliquot is removed to be diluted with 2x lammeli buffer (1 to 1 v/v) for western blot analysis and the remaining lysate is stored at -80°C. The diluted lysates for western blot purposes is heated for 5 min at 95°C and is prepared for use.

d) Buffers for Western Blotting

- 10x Electrophoresis/Running Buffer (pH - 8.3)

30.34g Tris base

144g Glycine

10g SDS

Dissolve contents in 1L of ddH20 and store at room temperature.

- 1x Running Buffer (pH- 8.3)
  10% 10x Running buffer.

  90% ddH20

  Store at room temperature.

- 10x Transfer Buffer (pH- 8.3)
  30.3g Tris base

  144g Glycine

  Dissolve contents in 1L of ddH20 and store at room temperature.

- 1x Transfer Buffer (pH- 8.3)
  10% 10x Transfer buffer

  20% Methanol

  70% ddH20

  Mix solutions and store at -20°C prior to use as it has to be kept cool.

- 10x Wash Buffer
  60.57g Tris base

  87.66g Sodium Chloride (NaCl)

  Dissolve contents in 1L of ddH20, store at room temperature.

- 1x Wash Buffer
  10% 10x Wash buffer.

  90% ddH20

  500µl/L Tween-20

  500µl/L NP-40

  Mix solutions and store at room temperature.

- Blocking Buffer

  3% BSA (w/v: 1.5g/50mL)

  Dissolve in 1x Wash buffer, store at 4°C.

- Antibody (Ab) Buffer 1° Ab and 2°Ab (1:2000-1:4000 dilution)

  1°Ab - 1 part blocking buffer + 1 part wash buffer + 0.02% NaAzide (stock in ddH20)

  2°Ab - 1 part blocking buffer + 1 part wash buffer (NO NaAzide).

- SDS Gel preparation Buffers
  - Resolving gel Tris Buffer (1.5M) (pH-8.8)

    90.86g/500mL of ddH20
  - Stacking gel Tris Buffer (0.5M) (pH-6.8)

    30.3g/500mL of ddH20
  - 10% APS Solution

    10% (w/v) Ammoniumperoxide Sulfate in ddH20 and store at -20°C
  - 10% SDS Solution

    10% (w/v) Sodium dodecylsulfate in ddH20 and store at room temperature

e) Western Blotting

Running samples

1. Remove lysate samples out of -80° freezer and place on ice.
2. Place gels into cassettes and add the cassette to tank ensuring red and black terminals of cassette correspond with red and black markings on the tank respectively and fill it up with 1x running buffer.
3. Vortex the lysates when thawed.
4. Take out combs from gel and pipette 7µl Bio-Rad protein ladder.
5. Add samples into each well according to Bradford values (25 mg/well/sample).
6. Ensure positive and negative electrodes are matched (black to black, red to red)
7. Turn on the voltage for 90V for 10min, and then turn it up to 110V for ~1.5hrs or until dye runs off the gel.
8. In the meantime prepare 1x transfer buffer and place in the -20°C freezer until ready for transfer.

Transferring the Gel onto a membrane

1. Fill glass dish with 250 ml cold 1x transfer buffer.
2. Activate membranes in by submerging them in methanol for 30 seconds, followed by rinsing with ddH2O for 2min and eventually equilibrating the membranes in 1x transfer buffer. Also cut out equal sized filter papers and prepare the appropriate number of foam pads.
3. Once the run has completed, remove the gels from tank and soak in transfer buffer. Gently detach the gels from the glass plates. Cut off the stacking gel portion of the gel. Loosen gel from the glass plate with scraper while keeping it emerged in the buffer.
4. In the deep glass dish, place the black sandwich side of the cassette on the bottom and place two sponge pads followed by 2 filter papers on top. Roll out the air bubbles using a rolling pin.
5. Cautiously place gel on top of filter paper with the ladder on the right side and roll out the bubbles.
6. Now place the activated membrane on top of the gel and tease out any bubbles.
7. Add 2 more filter papers on top of the gel and membrane and roll out any bubbles.
8. Add one sponge pad and roll out any bubbles.
9. Carefully close sandwich (sponge pad, 2 filter papers, gel, membrane, 2 filter papers and sponge pad) and place into transfer tank. With black side of the sandwich matching the back side of the tank and red matching the red.
10. Place ice pack near the black side in order to keep buffer cold. Close the lid ensuring positive and negative electrodes are matched (black to black, red to red).
11. Surround transfer tank with ice to keep cold or place in the cold room. Transfer can be done at 120 V for 2 hours or at 40V overnight. If possible, check on the temperature throughout transfer time to ensure no overheating.

Probing the membranes

1. Prepare containers with about 10 mL of 1x blocking buffer for each membrane.
2. Once transfer has finished, remove the cassettes immediately from the transfer apparatus and quickly place membranes in containers with blocking buffer.
3. Allow the membranes to sit in the blocking buffer for at least 1hr at room temperature on an orbital shaker.
4. Pour out blocking buffer and add 5 mL of desired 1°Ab. 5. Incubate overnight on shaker at 4°C or for 2 hrs at room temperature.
5. Remove 1°Ab and replace the containers with 1x wash buffer. Wash the membranes 4x at 15 min intervals with 10mL of wash buffer to get rid of any unbound Ab.
6. After washing add 7 mL of 2° Ab and allow membranes to sit on orbital shaker for 1hr at room temperature.
7. Remove 2°Ab and wash membranes 3x at 15 min intervals with 10mL of 1x wash buffer to get rid of any unbound 2°Ab. Membranes are now ready to be developed.

Developing the membrane

1. For each membrane, use 3mL chemiluminescence (Millipore Immobilon Western Chemiluminescent HRP substrate) to the container and incubate for 3 minutes.
2. Carefully align the membranes on the radiography cassette.
3. In the darkroom, expose film for desired time.
4. Place film in developer for a few seconds until signal appears. Rinse with water to stop the reaction, and place in fixer solution. Ensure ample fixing time. 5. Rinse with water and allow drying.

f) Buffers for tissue incubation

Stock solutions for Krebs Ringer Bicarbonate (KRB) Buffer Note:

Quantity Reagent/Molarity	Concentration	Reagent	Molecular Weight
0.9 g in 100 mL	0.154 M	NaCl	58.44
610 mg in 50 mL	0.154 M	CaCl2	110.99
575 mg in 50 mL	0.154 M	KCl	74.55
1.055g in 50ml	0.154 M	KH2PO4	136.09
927mg in 50ml	0.154M	MgSO4	120.30
650mg in 50ml	0.154M	NaHCO3 *	84.01
*Gasify NaHCO3 with carbogen (95% O2/5% CO2) for 1h after preparation. Stock solutions can be stored at 4°C			

For 100ml of KRB buffer:

Quantity Reagent/Molarity	Concentration	Reagent
78.6ml	0.154 M	NaCl
2.32ml	0.11 M	CaCl2
3.08ml	0.154 M	KCl
0.768ml	0.154 M	KH2PO4
0.768ml	0.154M	MgSO4
16.1ml	0.154M	NaHCO3
100mg	5.5mM	Glucose
715mg	30mM	Hepes
Gasify with carbogen (95% O2/5% CO2) for 45 min after preparation.		
pH the gasified KRB buffer to 7.4 using 10N NaOH		
Then add fatty acid free BSA (Sigma Cat# A3803) to the solution at a concentration of 3.5% (35mg/ml).		

For glycogen synthesis and glycogen content assays, take the required amount of KRB Buffer and add radiolabelled D-[14C] (hot) glucose at a concentration of 0.2 µCi/ml.

Or for Palmitate oxidation assay, take the required amount of KRB Buffer and add radiolabelled D-[14C] (hot) palmitic acid at a concentration of 0.2 µCi/ml and 200 uM for cold palmitate.

g) Incubation of muscle strips/liver slices for Glycogen Synthesis & Glycogen Content

1. Fill pre-incubation scintillation vials with 2ml of KRB-BSA buffer & place in the water bath at 37°C.
2. For the actual experimental scintillation vials fill basal vials with 2ml of KRB-BSA containing 0.2 µCi/ml D-[14C] glucose.
3. Add insulin (100nM) to the remaining KRB-BSA containing D-[14C]glucose.
4. Ensure that all vials are capped with rubber stoppers and continuously gasified with carbogen (95% O2/5% CO2) at a steady rate.
5. Extract a slice of liver or strip if muscle weighing ~ 20mg (along the edges of the organ) being careful not to inflict damage to the tissue. (Make sure to keep it moist at all times with ice cold PBS).
6. Gently place the slice into the pre-incubation scintillation vial and allow it to shake with gentle agitation in the water bath for 1h. Subsequently, the slice is transferred to a second vial (basal or insulin stimulated in the presence of D-[14C] glucose) and incubated for another hour.
7. At the end of the second hour, remove the slice from the vial and immediately dip in liquid nitrogen to discontinue the reaction.
8. Place the frozen slice in 500µl of 1N KOH for digestion for 30min @ 90°C.
9. Vortex the sample and then extract 100µl for glycogen content assay and freeze at -80°C and the store the rest for glycogen synthesis assays at -20°C.

Glycogen Synthesis Reagents

- 1N KOH
  5.61g KOH make final volume to 100ml using ddH2O

- 25 mg/ml Glycogen Carrier
  Add 625 mg Glycogen Carrier (Sigma Aldrich cat #G8751-5G) in 25 ml water and store at -20°C

- Saturated Na2SO4
  Dissolve powdered Na2So4 in ddH2O until precipitation forms. Precipitate formation is a sign of saturation.

- Cold Ethanol
  Place 100% Ethanol in a 50ml falcon tube. Leave in -20°C freezer.

Glycogen Synthesis Assay (Incorporation of D-[14C] glucose into Glycogen)

1. Use the 400µl extract meant for glycogen synthesis and place in a 2ml Eppendorf
2. Add 100µl of carrier glycogen (25mg/ml) to each sample.
3. Add 80µl of saturated Na2SO4 to each sample
4. Add 1.2ml of cold ethanol
5. Gently vortex each sample for 30 sec and incubate at -20°C overnight to allow precipitation.
6. On the next day, centrifuge the samples for 20min @ 3000rpm for proper precipitation to occur.
7. Discard the resultant supernatant by dabbing on to kim wipes.
8. Dissolve the pellet in 500µl of ddH20.
9. Extract 400µl of sample and add to 5ml of scintillation fluid (ECOLITE+ liquid scintillation cocktail (MP Biomedicals Cat #01882475)) for counting.
10. Correct readings for tissue weight.

Glycogen Content Reagents

Note: Adjust volumes accordingly depending on number of samples.

- Acetate Buffer (0.2M, pH 4.8)
  480µl Acetic Acid (98%)
  975mg Sodium Acetate
  Make final volume to 100ml using ddH20.
  Adjust pH to 4.8 and store at 0-4°C.

- Amyloglucosidase Solution
  1mg Amyloglucosidase Enzyme Protein Powder
  1ml 0.2M Acetate Buffer

- 1N KOH (pH off the scale) 5.61g KOH
  Make final volume to 100ml using ddH2O.

- Triethanolamine (TRA) Buffer
  (0.3M TRA; 4.05mM MgSO4; 1N KOH, pH 7.5)
  5.6g Triethanolamine
  100mg MgSO4
  12ml 1N KOH
  Make final volume to 100ml using ddH2O. Store at 0-4°C

- Ammonium Sulfate (3.2M)
  4.23g (NH4)2SO4
  Make final volume to 10ml with ddH2O.

- Hexokinase/G6PDH Suspension 500U (based on HK units – 125U/mg of protein.
  Re-suspend the lyophilized enzyme in 2ml of 3.2M Ammonium Sulfate (~ 250U/ml).

- ATP-TRA Buffer (1mM ATP; 0.9mM NADP; 5ug/ml HK/G6PDH)
  6mg ATP
  8mg NADP
  10ml TRA Buffer
  50µl HK/G6PDH Suspension
  Note: Solution is stable for one week at 0-4°C.

h) Glycogen Content Assay

1. Thaw the eppindorf with 100µl sample meant for glycogen content assay.
2. Add 10% (v/v) of acetic acid 17.5M to digested tissue (maintains pH between 4-5, ideally 4.8 which is optimum for hydrolysis of glycogen by amyloglucosidase.
3. Add 500µl of acetate buffer (4.8 pH) with amyloglucosidase (0.5mg/ml).
4. Incubate for 2h at 40°C with shaking or on bench overnight.
5. Neutralize the solution with 1/16 (v/v) of NaOH (5N). pH should now be 7.37 @ 25°C.
6. Centrifuge for 5min @ 3000rpm.
7. Extract 400µl of the digested supernatant & add 1ml of ATP-TRA Buffer.
8. Incubate for 30min on the bench.
9. Gently vortex and extract 1ml and dispense into a plastic cuvette.
10. Read the OD at 340nm. Note: (OD x 8.89) = umol of glucosyl units.
11. Correct readings for tissue weight.

i) Palmitate Oxidation Assay

Complexation of Palmitic Acid

1. Prepare 30mL of KRB Buffer (without glucose)
2. Add 3.75g FA-free BSA (Sigma Cat# A3803) to get a 12.5% solution
3. Heat to 50°C in water bath
4. Take 1600mg palmitic acid (Sigma Cat# P-5585) to put into a 2mL eppendorf
5. Dissolve palmitic acid by slowly adding 100µl NaOH (10N) and vortexing vigorously
6. Add palmitic acid into preheated medium while constantly stirring otherwise it will precipitate/coagulate.
7. Pour into falcon tube, protected from light
8. Incubate in 50°C water bath for overnight while shaking at 150-200rpm

9. After the incubation period, filter solution to get chunks out using a 10mL syringe and sterile strainer
10. pH to 7.4, measure concentration using a spectrophotometer Aliquot solution and store at -20°C

Incorporation of [1-14C] Palmitic acid into 14CO2

1. Following extraction, weigh tissues (~20mg muscle strips or liver slices) and place into scintillation vial containing 2mls of KRBS Ringer buffer for the purposes of preincubation.
2. Gasify each vial for 1 hour and incubate at 37°C to make sure the tissue remains live
3. After 1 hour, carefully remove the muscle strip/liver slice and ass it to another scintillation vial with 2ml of radiolabelled buffer (3.5% BSA containing [1- 14C] palmitic acid and 200 µM non-labelled palmitate). Make sure to gasify the vials at 37°C.
4. On completion of the hour add 200µl (1:1, vol/vol) 2-phenylethylamine/methanol onto loosely folded filter paper placed inside a 1.5ml Eppendorf and add it to the vial.
5. Gasify each scintillation vial and incubate for 1 hour at 37°C
6. After 1 hour, add 200µl of H2SO4 (5N) to acidify media. Incubate for 1 hour at 37°C
7. 10. Collect filter papers and transfer to corresponding scintillation vial containing 10mL of ECOLITE+ liquid scintillation cocktail (MP Biomedicals Cat #01882475) and place in scintillation counter for radioactivity counting and finally correct for tissue weight

j) High Pressure Liquid Chromatography

Lipid Extraction using Folch's Method

1. Take frozen tissue samples out of the -80°C freezer and measure out approx. (150 mg of Sol, 125 mg of EDL, 100 mg of Epit and 50 mg of liver)
2. Resuspend the above-mentioned tissues in cholorform:methanol (2:1 vol:vol)
3. Vortex the cells for 30 s followed by 2 rounds of homogenization
4. Spin the samples at 3000 x g for 5 min at 4°C
5. Transfer 300 µl of the upper cholorform phase into a new Eppendorf tubes
6. Allow the tubes to evaporate overnight inside the fumehood
7. Resuspend in 100 µl of 2-propanol-hexane 5:4 (v/v) (PrHex) and use for HPLC analysis

High Pressure Liquid Chromatography for MAG DAG TAG content

1. Quantification was performed using UV detection in an ultra high-pressure liquid chromatography system (UHPLC-UV) (Nexera X2, Shimadzu, Kyoto, Japan).
2. 50 µl sample volumes were injected automatically into a reverse phase column (C18 5µm 250 x 4.6mm; Restek, Bellefonte, USA). The chromatography conditions were set to 40 °C for 20 min using a gradient of methanol (MeOH) and PrHex: 100% of MeOH from 0 min

until 10 min, followed by 50% of MeOH and 50% of PrHex for 10 min, maintained with isocratic elution for 10 min.
3. 0.25 µg/µl Triololein, Diolein, and Monoolein (Nu-check, Elysian, USA) were also dissolved in PrHex and quantified to obtain a standard curve.

Ceramide content:

1. Quantification was performed using UV detection in an ultra high-pressure liquid chromatography system (UHPLC-UV) (Nexera X2, Shimadzu, Kyoto, Japan).
2. 50 µl sample volume of the lipid extract obtained after chloroform extraction was transferred into new pre-weighed eppendorfs. The organic phase was then hydrolyzed in 1M KOH at 90 °C for 60 min and then mixed with15µl OPA reagent for 20 min at room temperature. The samples were reconstituted in 100 µl of chloroform-methanol-acetic acid-water (50:37.5:3.5:2 vol/vol/vol/vol) and run through a porous silica column (ARC-18 1.8 µm 100 x 2.1 mm). Elution was conducted with heptane-isopropyl ether-acetic acid (60:40:3 vol/vol/vol) at a gradient from 0 to 10 % in 30 min at a flow rate of 0.8 ml/min followed by isocratic elution with acetonitrile: deionized distilled water (90:10, vol/vol) and a flow rate of 1 ml/min[240].
3. The calibration curve was prepared using N-Acetyl-D-sphingosine as a standard

k) Lactate Assay

1. Lactate Determination using the Biovision Lactate Colorimetric/Fluorimetric Assay Kit (Cat. # K607-100) 1. Thaw the frozen media samples to be analyzed for lactate production
2. Rinse 10-kDa molecular weight spin filters in 2 ml Eppendorf tubes using ddH2O and centrifuge at 13, 000 RPM for 5 min
3. Discard the ddH2O from the filters and allow them to dry
4. Add 100 µl of the sample to the filter and spin at 13, 000 RPM for 5 min at 4°C
5. Following deproteination of the sample, remove the filter and extract the sample from the bottom of the Eppendorf.
6. Using the Lactate Assay Kit, mix 990 µl of the Lactate Assay Buffer with 10 µl of the Lactate Standard to produce the Assay Standard
7. Load 2, 4, 6, 8 and 10 µl of the Assay Standard into a 96-well plate and bring total volume to 50 µl with Lactate Assay buffer.
8. Load 2-50 µl of sample and bring total volume to 50µl with Lactate Assay Buffer
9. Add 46 µl of Lactate Assay Buffer, 2 µl of resuspended Lactate Enzyme and 2 µl of the Lactate Probe per well
10. Mix reaction mixes well and incubate the 96-well plate for 30 min in the dark
11. Read the plate at 570nm in a plate reader

l) Measuring Circulating Insulin by ELISA

1. Fast the animals for 14-16 hr then obtain a blood sample from the saphenous vein.
2. Always keep blood on ice.
3. Centrifuge the blood at for 10min @ 13,000rpm (4°C)
4. Extract the plasma (supernatant) and place into another labeled eppendorf. Store at -80°C until you are ready to run the ELISA.
5. When ready to assay, pre-warm all reagents of the EMD Millipore ELISA kit (Cat. # EZRMI-13K) to room temperature. 6. Dilute the provided 10X wash buffer by 10-fold.
6. Determine the number of samples to be assayed and place any extra microtiter strips in 2-8°C. 8. Place the microtiter strips that you will be using in a plate holder and wash 3 times with 300µl of diluted wash buffer.
7. Remove buffer from wells by tapping lightly onto an absorbent surface DO NOT let the wells dry completely.
8. Add 10µl of assay buffer to each blank & sample wells.
9. Add 10µl of Matrix solution to blank, standard, and control wells.
10. Add 10µl of 0.2, 0.5, 1, 2, 5 and 10 ng/mL insulin standards in ascending order.
11. Add 10µl of quality control 1 & 2 into their own wells.
12. Add 10µl of sample into the remaining wells.
13. Add 80µl of detection antibody to all wells
14. Seal the plate and incubate at room temperature for 2h on an orbital shaker
15. Remove plate sealer and tap onto an absorbent surface to empty contents.
16. Reaction Mix Assay Buffer 46µl Triglyceride Probe 2µl Enzyme Mix 2µl
17. Wash the plate 3 times with 300µl of wash buffer by decanting after each wash.
18. Add 100 µl of enzyme solution to each well. Seal with plate sealer and incubate for 30min at moderate speed on an orbital shaker.
19. Remove the seal and decant the contents.
20. Wash 6 times using diluted wash buffer making sure to decant contents after each wash.
21. Add 100 µl of substrate solution to each well. Cover with plate sealer and shake for 20 min on orbital shaker.
22. Add 100µl of stop solution to each well and mix well by hand. Ensure there are no bubbles and read using a plate reader at 450 and 590nm. Record absorbance.
23. Calculate insulin concentrations as outlined in the manual.

m) Glucose Tolerance Test

1. Fast rodents overnight (12-16 hours)
2. Calculate the amount of 30% glucose solution required for each rat based on their individual weight. Use the following formula to calculate the volume of solution required to inject each rodent with: {Weight of rodent in kg x (1.75 g/Kg of body weight of glucose/0.30.

3. Prepare the 30% glucose solution, mix D-glucose (MW=180.16) with Physiological Saline. Place ready made solution in a 50ml falcon tube. Then heat the solution to 37 ºC in water bath.
4. Bleeds will occur. These times are as follows:
5. Time 0, Time 15 min, Time 30 min, Time 60 min, and Time 120 min.
6. Collect basal glucose readings for all animals prior to injecting glucose.
7. Inject rat with glucose solution into peritoneal cavity and start the timer.
8. Collect blood after 15, 30, 60, and 120 min after glucose injection. Make sure to record blood glucose values immediately after each time point and graph the results.

Appendix B: Supplementary figures

Figure B1: Uncropped, original western blots for figure 4.5 in chapter 4 indicating higher levels of PKCδ (A) and PKCθ (B) in EDL and Epit than in Sol muscles.

Total PKCδ in all muscles

SOL EDL Epit

β-actin to normalize PKCθ in all muscles

SOL EDL Epit

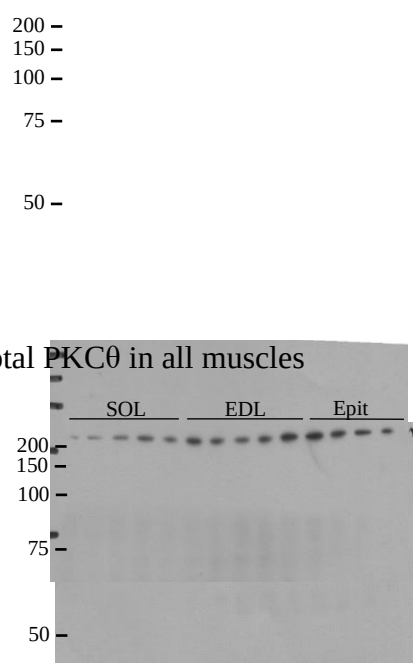

Total PKCθ in all muscles

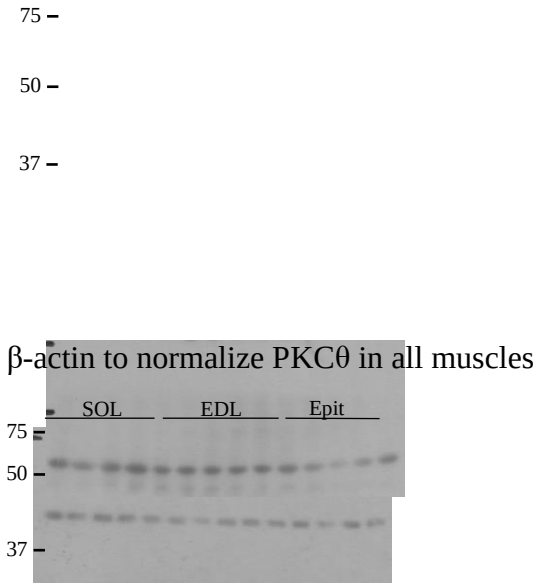

β-actin to normalize PKCθ in all muscles

Figure B2: Uncropped, original western blot images for figure 4.6 in chapter 4 indicating Distinct effects HFS diet on PKC translocation towards the membrane in Sol, EDL, and Epit muscles. Representative blots and densitometric analyses of PKCδ, Na,K-ATPase, and GAPDH (A–C) and PKCθ, Na,K-ATPase, and GAPDH (D–F) levels in membrane (Memb) and cytoplasmic (Cyto) cellular fractions.

(A) Cytoplasmic PKCδ in Soleus muscle

Membrane PKCδ in Soleus muscle

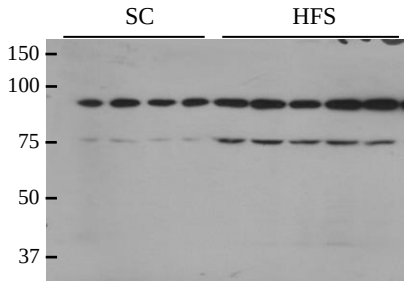

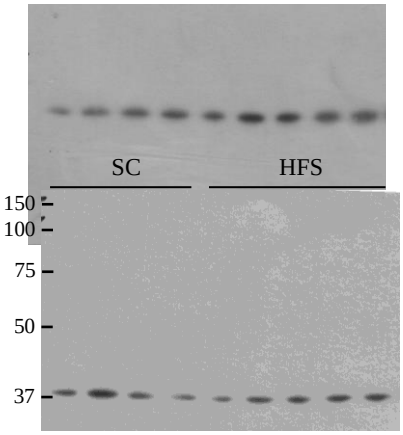

GAPDH to normalize

Na,K-ATPase to normalize

PKCδ in Sol cytoplasm

PKCδ in Sol membrane

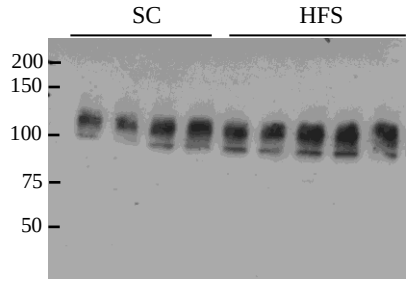

(B) Cytoplasmic PKCδ in EDL muscle

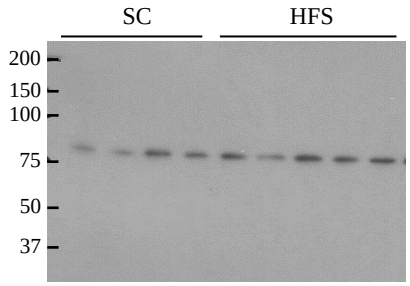

GAPDH to normalize
PKCδ in EDL cytoplasm

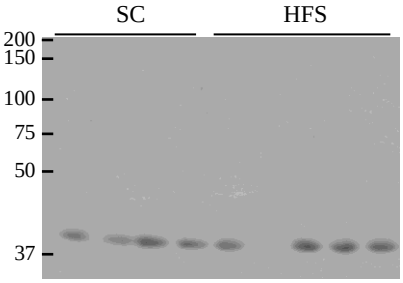

Membrane PKCδ in EDL muscle

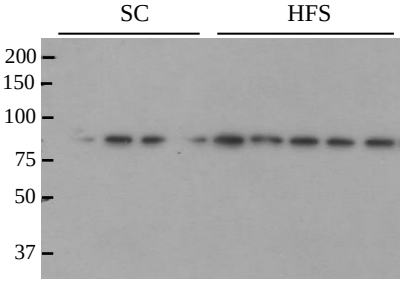

Na,K-ATPase to normalize
PKCδ in EDL membrane

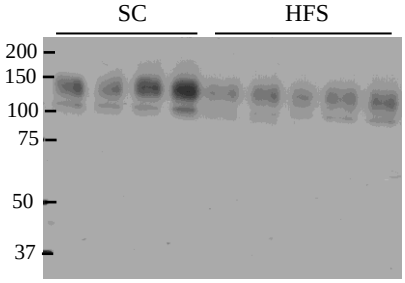

(C) Cytoplasmic PKCδ in Epit muscle

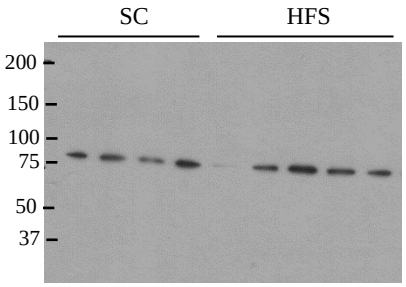

Membrane PKCδ in Epit muscle

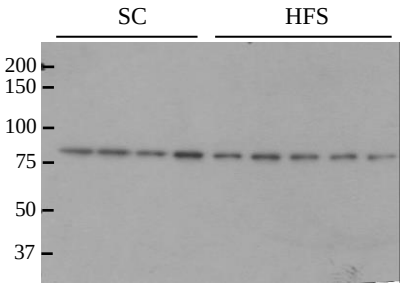

GAPDH to normalize
PKCδ in Epit cytoplasm

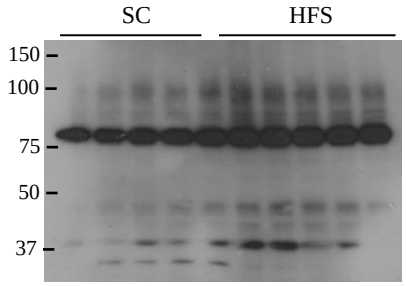

Na,K-ATPase to normalize
PKCδ in Epit membrane

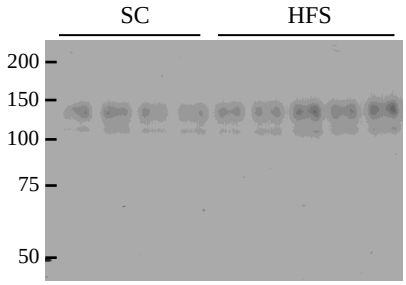

(D) Cytoplasmic PKCθ in Soleus muscle

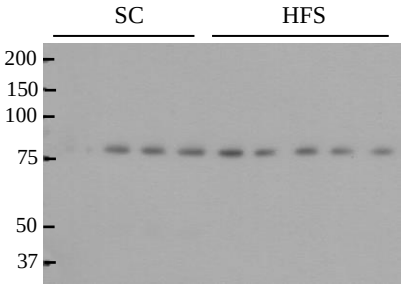

GAPDH to normalize
PKCθ in Sol cytoplasm

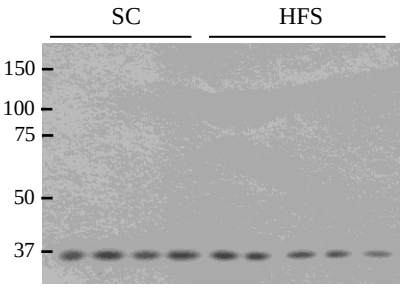

Membrane PKCθ in Soleus muscle

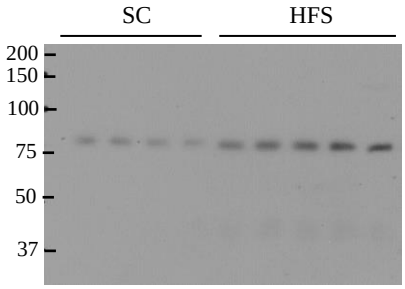

Na,K-ATPase to normalize
PKCθ in Sol membrane

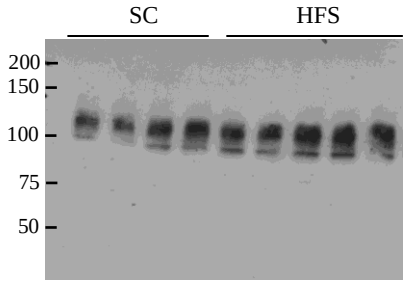

(E) Cytoplasmic PKCθ in EDL muscle

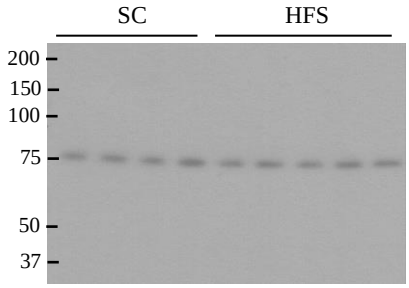

GAPDH to normalize
PKCθ in EDL cytoplasm

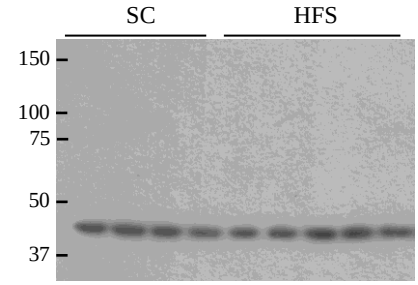

Membrane PKCθ in EDL muscle

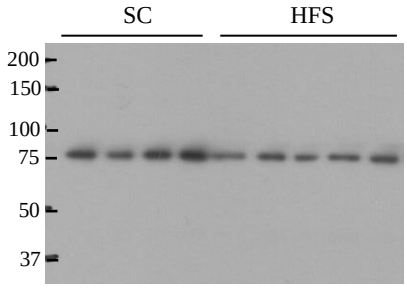

Na,K-ATPase to normalize
PKCθ in EDL membrane

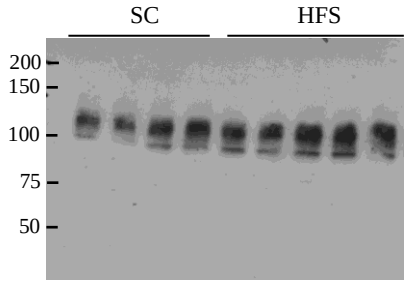

(F) Cytoplasmic PKCθ in Epit muscle

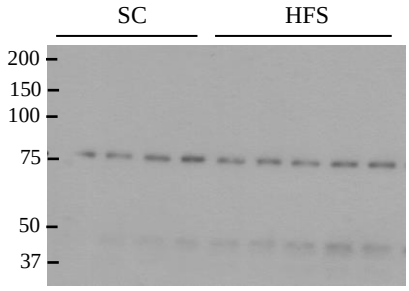

Membrane PKCθ in Epit muscle

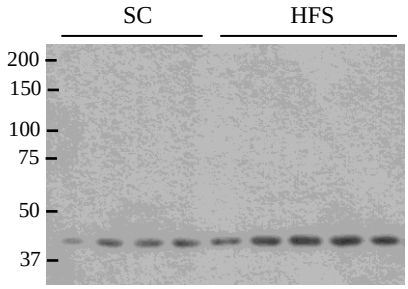

GAPDH to normalize
PKCθ in Epit cytoplasm

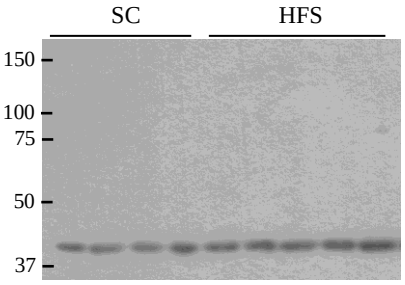

Na,K-ATPase to normalize
PKCθ in Epit membrane

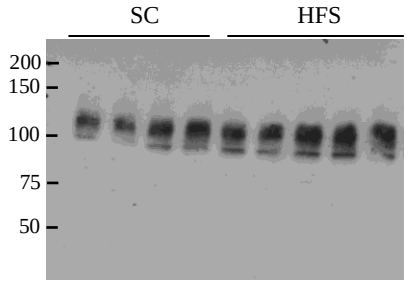

Figure B3: Uncropped, original western blots for figure 5.1 in chapter 5. HFS diet causes impairment of insulin-induced AKT_{Thr308} phosphorylation in oxidative and glycolytic muscles under basal (B) and insulin-stimulated (I) conditions. AKT phosphorylation (A-C)) in Sol, EDL, and Epit, respectively. *p<0.05, Two-way ANOVA, n-6-11 for AKT. Mean ± SD.

(A) Phospho-AKT in Sol muscle

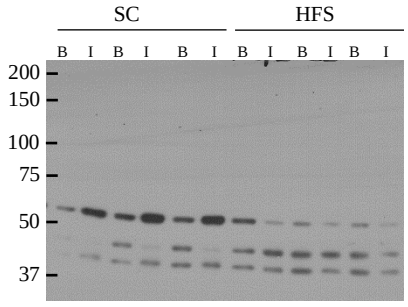

Total AKT in Sol muscle

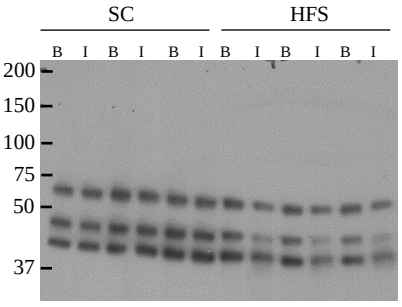

(B) Phospho-AKT in EDL muscle

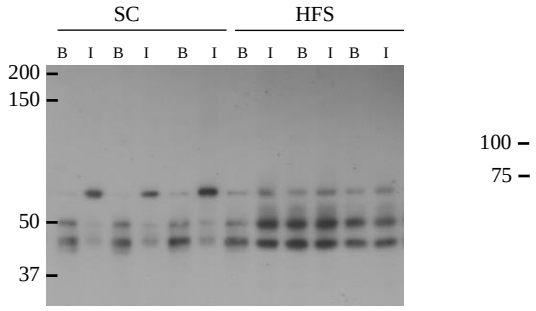

Total AKT in EDL muscle

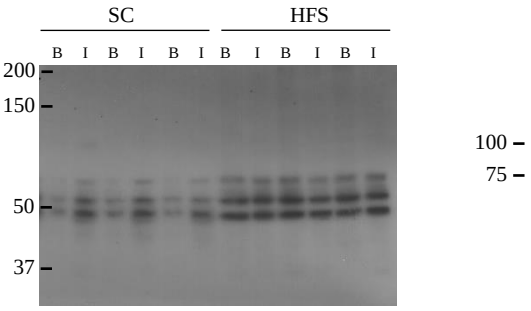

(C) Phospho-AKT in Epit muscle

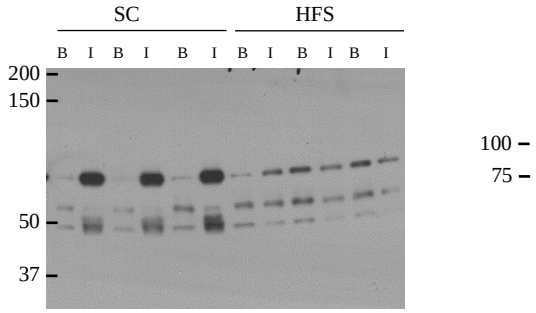

Total AKT in Epit muscle

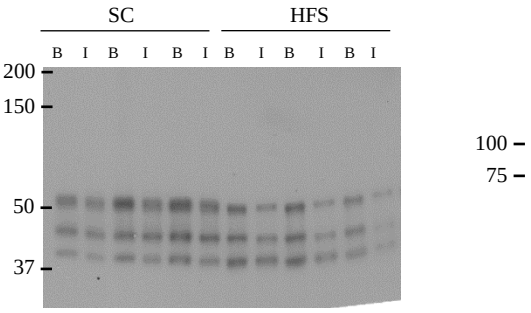

Figure B4: Uncropped, original western blots for figure 5.5 in chapter 5: The HFS diet does not alter total PKCδ and PKCθ protein levels in oxidative and glycolytic muscles. PKCδ and PKCθ normalized by β-actin in Sol (A), EDL (B) and Epit (C). *$p<0.05$ vs.SC (t-test), n=6-7. Mean ± SD.

(A) Total PKCδ in Sol muscle

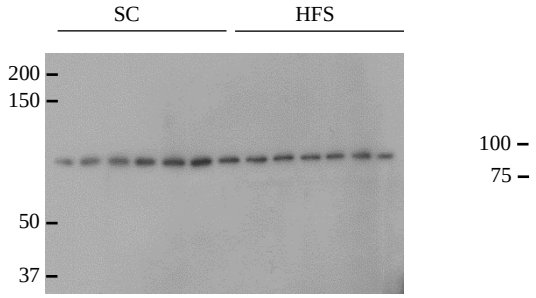

Total PKCθ in Sol muscle

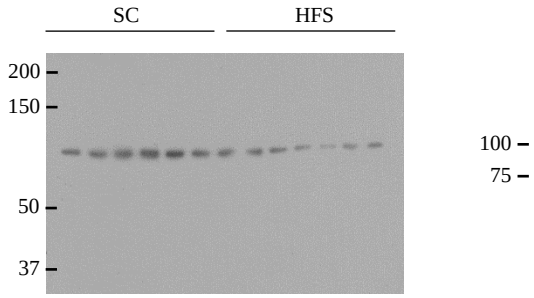

β-actin to normalize for total PKCδ and PKCθ in Sol muscle

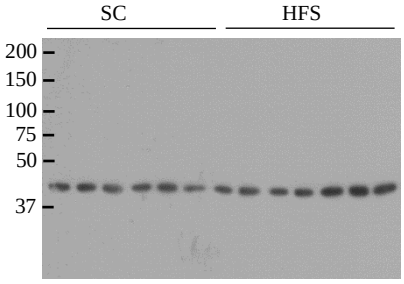

(B) Total PKCδ in EDL muscle

SC HFS

Total PKCθ in EDL muscle

SC HFS

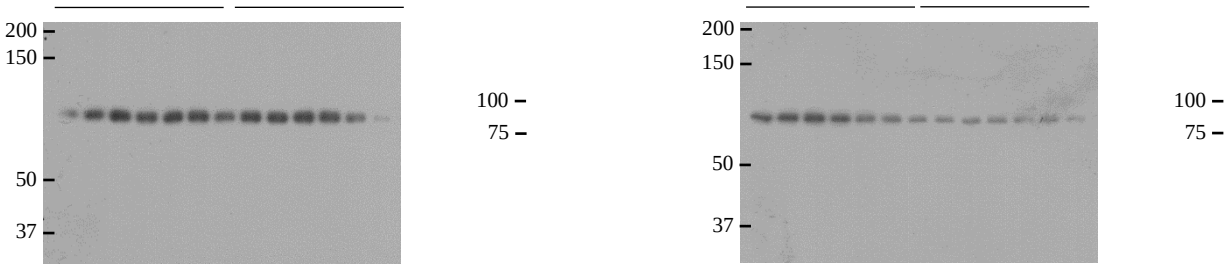

β-actin to normalize for total PKCδ and PKCθ in EDL muscle

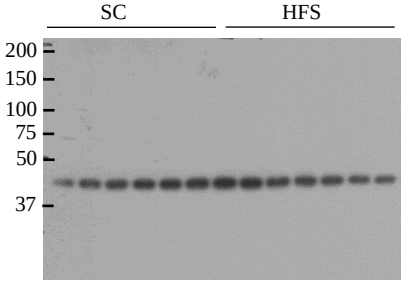

(C) Total PKCδ in Epit muscle

Total PKCθ in Epit muscle

SC HFS

SC HFS

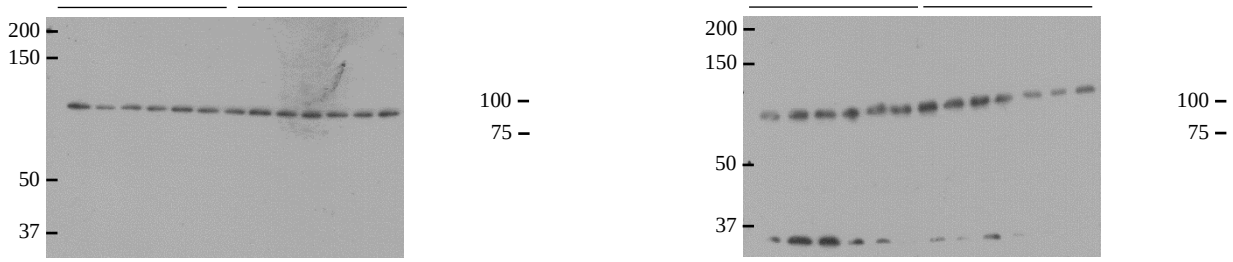

β-actin to normalize for total PKCδ and PKCθ in Epit muscle

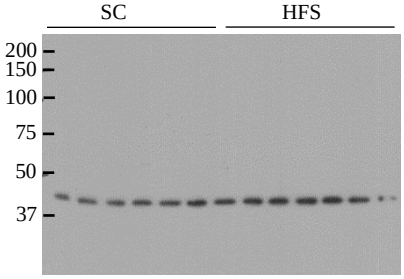

Figure B5: Uncropped, original western blots for figure 5.6 in chapter 5: The HFS diet distinctly affects membrane-bound PKC levels in oxidative and glycolytic muscles. Representative blots and densitometric analyses of PKCδ (A-C) and PKCθ (D-F) levels in membrane (Mem) and cytoplasmic (Cyto) cellular fractions in Sol, EDL, and Epit muscles, respectively. *p<0.05, t-test, n=6 for Sol and EDL, n=4 and 5 for Epit. Mean ± SD.

(A) Cytoplasmic PKCδ in Soleus muscle Membrane PKCδ in Soleus muscle

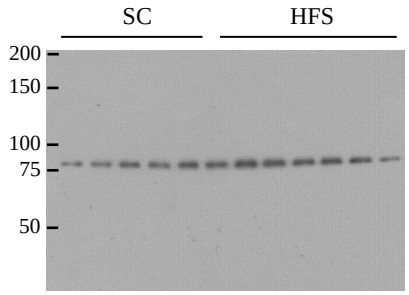

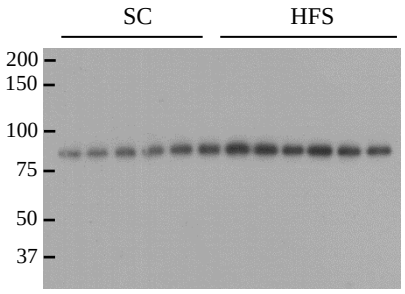

(D) Cytoplasmic PKCθ in Soleus muscle

Membrane PKCθ in Soleus muscle

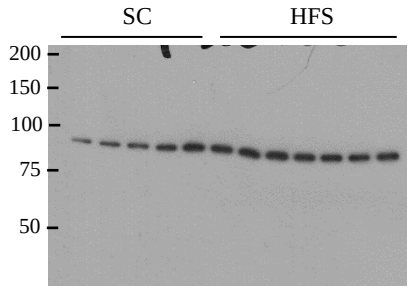

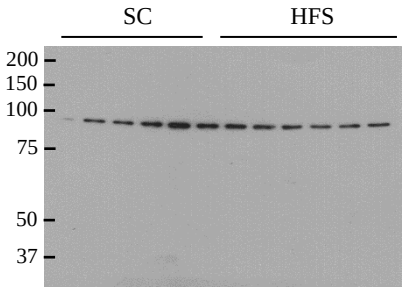

GAPDH to normalize
PKCδ and PKCθ in Sol cytoplasm

Na,K-ATPase to normalize
PKCδ and PKCθ in Sol membrane

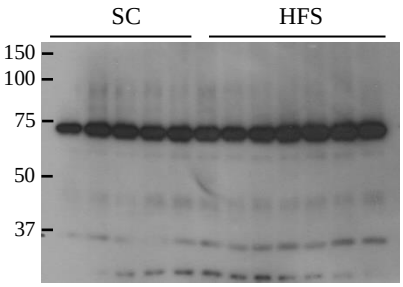

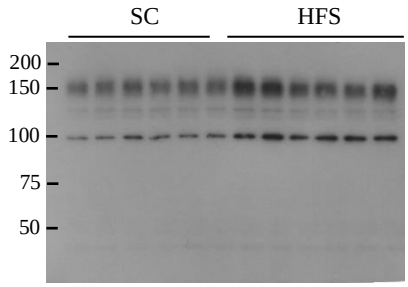

(B) Cytoplasmic PKCδ in EDL muscle

Membrane PKCδ in EDL muscle

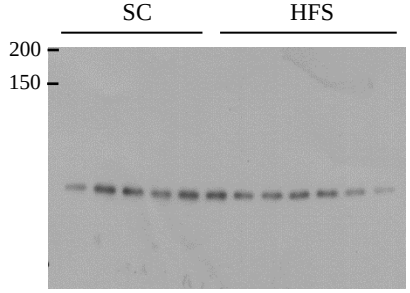

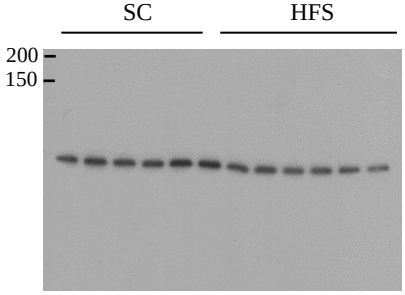

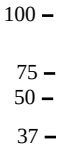

(E) Cytoplasmic PKCθ in EDL muscle

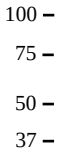

Membrane PKCθ in EDL muscle

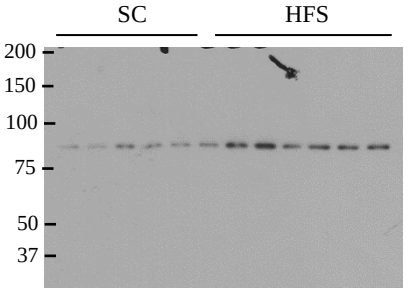

GAPDH to normalize
PKCδ and PKCθ in EDL cytoplasm

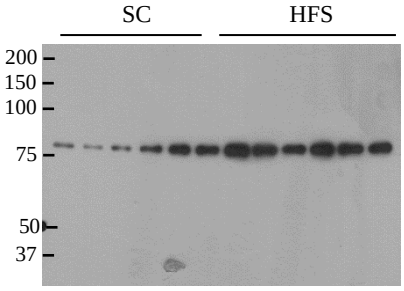

Na,K-ATPase to normalize
PKCδ and PKCθ in EDL membrane

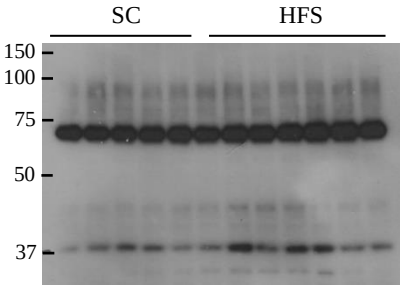

(C) Cytoplasmic PKCδ in Epit muscle

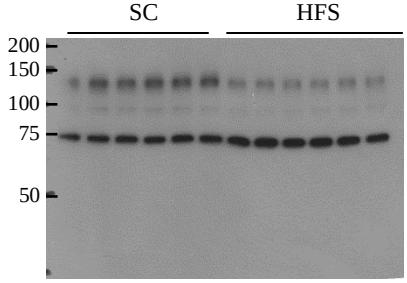

Membrane PKCδ in Epit muscle

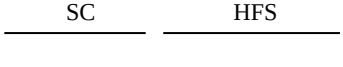

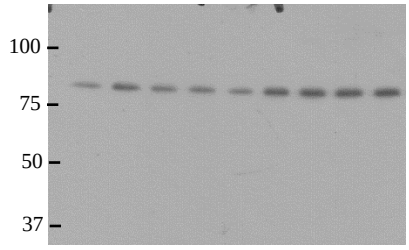

(F) Cytoplasmic PKCθ in Epit muscle

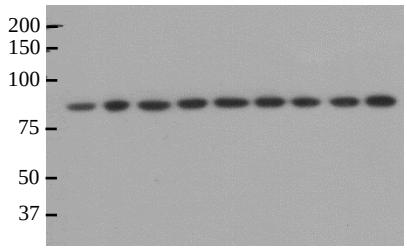

Membrane PKCθ in Epit muscle

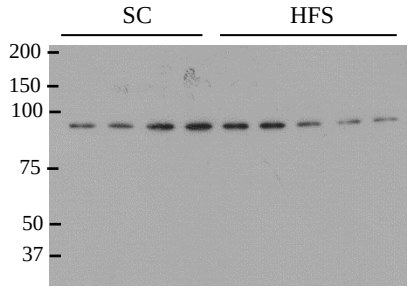

GAPDH to normalize
PKCδ and PKCθ in Epit cytoplasm

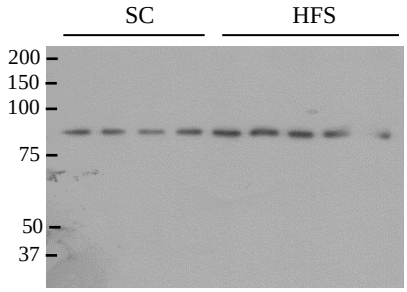

Na**,**K-ATPase to normalize
PKCδ and PKCθ in Epit membrane

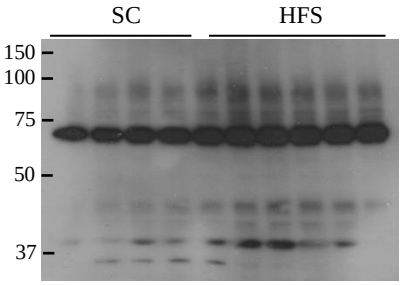

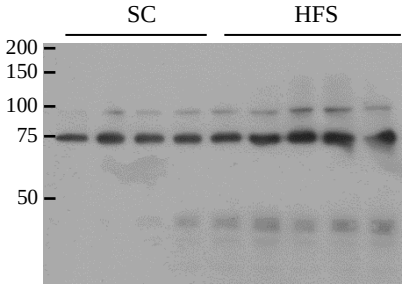

Figure B6: Uncropped, original western blots for figure 6.5 in chapter 6. HFS and KD do not affect total cellular PKCε levels (A), but the translocation/activity of this kinase is significantly lower in KD-fed rats (B). Representative blots and densitometric analyses of levels in membrane (Memb) and cytoplasmic (Cyto) cellular fractions were corrected by loading controls Na,K-ATPase and GAPDH, respectively.

(A) Total PKCε in Liver

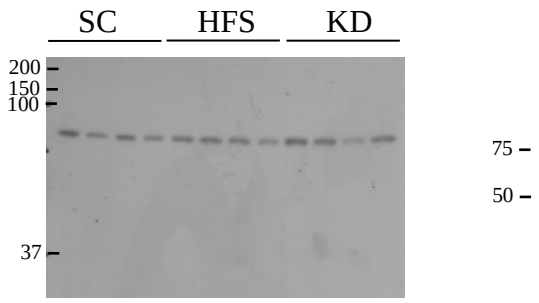

β-actin to normalize in PKCε Liver

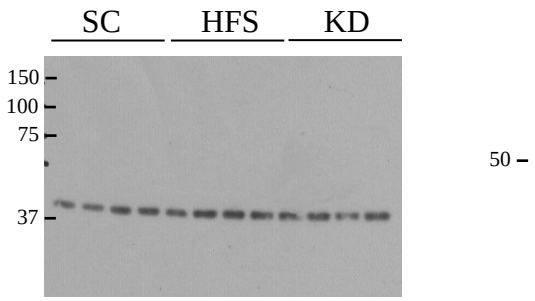

(B) Cytoplasmic PKCε in Liver membrane

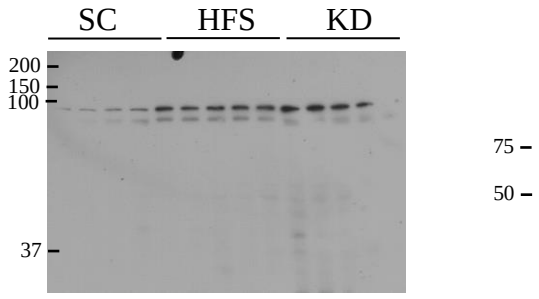

Membrane PKCε in Liver

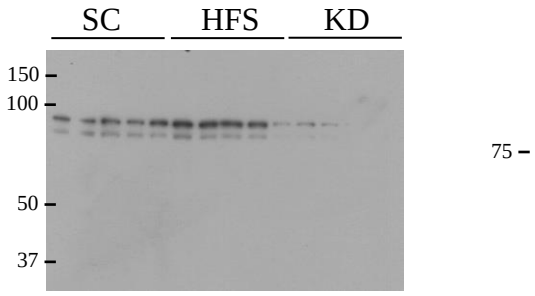

GAPDH to normalize Cytoplasmic PKCε in Liver

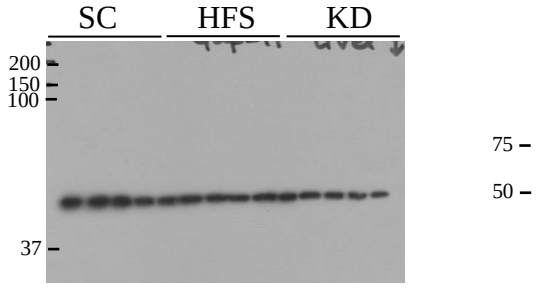

Na,K-ATPase to normalize PKCε in Liver membrane fraction

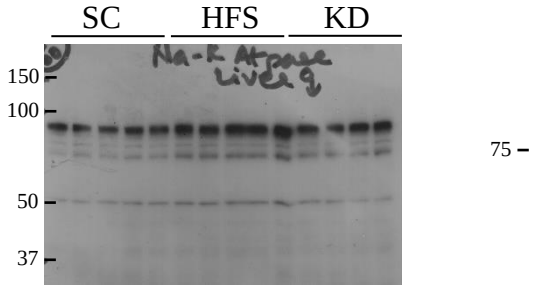

Figure B7: Uncropped, original western blots for figure 6.6 from chapter 6. The HFS diet causes impairment of insulin signaling and glycogen synthesis, whereas the KD maintains hepatic cells responsive to insulin intact. Representative blots and densitometric analyses for AKT (A) and GSK3 αβ (B) phosphorylations under basal (B) and insulin (I, 100 nM)-stimulated conditions.

(A) & (B): PAKT and PGSK3αβ

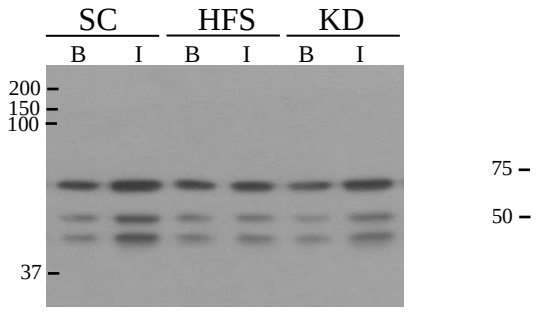

Total AKT and GSK3 αβ

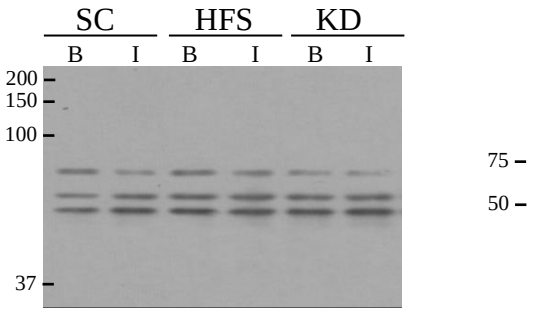

Appendix C: Additional Contributions

I made the following contributions during my doctoral tenure but are not included in my dissertation:

1. Sepa-Kishi DM, Jani S, Da Eira D, Ceddia RB. Cold acclimation enhances UCP1 content, lipolysis, and triacylglycerol resynthesis, but not mitochondrial uncoupling and fat

oxidation, in rat white adipocytes. Am J Physiol Cell Physiol. 2019 Mar 1;316(3):C365-C376. doi: 10.1152/ajpcell.00122.2018. Epub 2019 Jan 9. PMID: 30624981; PMCID: PMC6457102.

2. Song E, Da Eira D, Jani S, Sepa-Kishi D, Vu V, Hunter H, Lai M, Wheeler MB, Ceddia RB, Sweeney G. Cardiac Autophagy Deficiency Attenuates ANP Production and Disrupts Myocardial-Adipose Cross Talk, Leading to Increased Fat Accumulation and Metabolic Dysfunction. Diabetes. 2021 Jan;70(1):51-61. doi: 10.2337/db19-0762. Epub 2020 Oct 12. PMID: 33046483.

3. Da Eira D, Jani S, Sung H, Sweeney G, Ceddia RB. Effects of the adiponectin mimetic compound ALY688 on glucose and fat metabolism in visceral and subcutaneous rat adipocytes. Adipocyte. 2020 Dec;9(1):550-562. doi: 10.1080/21623945.2020.1817230. PMID: 32897149; PMCID: PMC7714433.

4. Da Eira D, Jani S, Ceddia RB. Obesogenic and Ketogenic Diets Distinctly Regulate the SARS-CoV-2 Entry Proteins ACE2 and TMPRSS2 and the Renin-Angiotensin System in Rat Lung and Heart Tissues. Nutrients. 2021 Sep 25;13(10):3357. doi: 10.3390/nu13103357. PMID: 34684358; PMCID: PMC8541329.

5. Da Eira D, Jani S, Stefanovic M, Ceddia RB. Obesogenic versus ketogenic diets in the regulation of the renin-angiotensin system in rat white and brown adipose tissues. Nutrition. 2023 Jan;105:111862. doi: 10.1016/j.nut.2022.111862. Epub 2022 Oct 10. PMID: 36356378.

6. Da Eira D, Jani S, Ceddia RB. An obesogenic diet impairs uncoupled substrate oxidation and promotes whitening of the brown adipose tissue in rats. J Physiol. 2023 Jan;601(1):69-82. doi: 10.1113/JP283721. Epub 2022 Dec 11. PMID: 36419345.